Technical Report Documentation Page

1. Report No. FHWA/TX-07/0-1895-1	2. Government Accession No.	3. Recipient's Catalog No.
4. Title and Subtitle **Evaluation of Serviceability Requirements for Load Rating Prestressed Concrete Bridges**		5. Report Date January 2007 6. Performing Organization Code
7. Author(s) **Sharon L. Wood, Michael J. Hagenberger, Bryan E. Heller, and Patrick J. Wagener**		8. Performing Organization Report No. 1895-1
9. Performing Organization Name and Address Center for Transportation Research The University of Texas at Austin 3208 Red River, Suite 200 Austin, TX 78705-2650		10. Work Unit No. (TRAIS) 11. Contract or Grant No. Research Project 0-1895
12. Sponsoring Agency Name and Address Texas Department of Transportation Research and Technology Implementation Office P.O. Box 5080 Austin, TX 78763-5080		13. Type of Report and Period Covered Research Report (9/1999 - 8/2002) 14. Sponsoring Agency Code

15. Supplementary Notes

Project performed in cooperation with the Texas Department of Transportation and the Federal Highway Administration.

16. Abstract

Within Texas, the procedures in the AASHTO Manual for Condition Evaluation of Bridges (MCEB) are used to determine the load rating of existing structures. A large number of prestressed concrete bridges that were constructed in the 1950s and 1960s have load ratings that fall below the minimum design vehicle specified in the MCEB. The load ratings for this group of are typically controlled by the serviceability limit state criterion related to the tensile stress in the concrete. A low load rating implies that these bridges have experienced damage under service loads. However, observations made by TxDOT personnel during routine inspections indicate that the condition of these bridges is very good, and that there are generally no signs of deterioration.

Based on the results of the diagnostic load tests and laboratory fatigue tests, it was concluded that the tensile stress criterion in the MCEB should not be used to evaluate existing prestressed concrete bridges. The calculated tensile stress in the concrete is not a reliable indicator of the stresses induced in the strand due to live load. Conservative guidelines for considering the fatigue limit state explicitly in the load rating process were developed.

17. Key Words	18. Distribution Statement
fatigue life, flexural cracks, load rating, prestressed concrete bridges, serviceability limit states	No restrictions. This document is available to the public through the National Technical Information Service, Springfield, Virginia 22161; www.ntis.gov.

19. Security Classif. (of report)	20. Security Classif. (of this page)	21. No. of pages	22. Price
Unclassified	Unclassified	200	

Evaluation of Serviceability Requirements for Load Rating Prestressed Concrete Bridges

Sharon L. Wood
Michael J. Hagenberger
Bryan E. Heller
Patrick J. Wagener

CTR Research Report:	1895-1
Report Date:	January 2007
Research Project:	0-1895
Research Project Title:	Evaluate the Effect of Using $12\sqrt{f_c'}$ to Load Rate Prestressed Concrete Bridges
Sponsoring Agency:	Texas Department of Transportation
Performing Agency:	Center for Transportation Research at the University of Texas at Austin

Project performed in cooperation with the Texas Department of Transportation and the Federal Highway Administration.

Center for Transportation Research
The University of Texas at Austin
3208 Red River
Austin, TX 78705

www.utexas.edu/research/ctr

Disclaimers

Author's Disclaimer: The contents of this report reflect the views of the authors, who are responsible for the facts and the accuracy of the data presented herein. The contents do not necessarily reflect the official view or policies of the Federal Highway Administration or the Texas Department of Transportation (TxDOT). This report does not constitute a standard, specification, or regulation.

Patent Disclaimer: There was no invention or discovery conceived or first actually reduced to practice in the course of or under this contract, including any art, method, process, machine manufacture, design or composition of matter, or any new useful improvement thereof, or any variety of plant, which is or may be patentable under the patent laws of the United States of America or any foreign country.

Notice: The United States Government and the State of Texas do not endorse products or manufacturers. If trade or manufacturers' names appear herein, it is solely because they are considered essential to the object of this report.

Engineering Disclaimer

THIS REPORT IS NOT INTENDED FOR CONSTRUCTION, BIDDING, OR PERMIT PURPOSES.

Sharon L. Wood, Texas P.E. #83804
Research Supervisor

Acknowledgments

This research project was funded by the Texas Department of Transportation (TxDOT) under Project No. 0-1895. The support of the project director, Jon H. Kilgore (SAT), and program coordinator, Keith Ramsey (BRG), are greatly appreciated. Michael E. Kreger served as Research Supervisor for the early stages of this project.

Products

Research Product P1, proposed revisions to TxDOT load rating specifications for prestressed concrete bridges for inventory and operating-levels of service, is included in Chapter 7 of this research report. Research Product P2, load rating procedures for prestressed concrete bridges, is included in Chapter 9 of this research report.

TABLE OF CONTENTS

LIST OF FIGURES

LIST OF TABLES

SUMMARY

Within Texas, the procedures in the AASHTO Manual for Condition Evaluation of Bridges (MCEB) are used to determine the load rating of existing structures. A large number of prestressed concrete bridges that were constructed in the 1950s and 1960s have load ratings that fall below the minimum design vehicle specified in the MCEB. The load ratings for this group of are typically controlled by the serviceability limit state criterion related to the tensile stress in the concrete. A low load rating implies that these bridges have experienced damage under service loads. However, observations made by TxDOT personnel during routine inspections indicate that the condition of these bridges is very good, and that there are generally no signs of deterioration.

Based on the results of the diagnostic load tests and laboratory fatigue tests, it was concluded that the tensile stress criterion in the MCEB should not be used to evaluate existing prestressed concrete bridges. The calculated tensile stress in the concrete is not a reliable indicator of the stresses induced in the strand due to live load. Conservative guidelines for considering the fatigue limit state explicitly in the load rating process were developed.

CHAPTER 1
Introduction

Within Texas, the procedures in the AASHTO Manual for Condition Evaluation of Bridges (MCEB) are used to determine the load rating of existing structures. A large number of prestressed concrete bridges that were constructed in the 1950s and 1960s have load ratings that fall below the minimum design vehicle specified in the MCEB. The direct consequences of the reduced load ratings range from increasing the frequency of structural inspections and posting of maximum permissible loads to strengthening or replacing the bridge. Indirect consequences include loss of trucking routes and increased traffic congestion due to bridge closures and construction. Therefore, it is critical that the techniques used to evaluate existing bridges maintain an acceptable level of safety, without being overly conservative.

The load ratings for this group of prestressed concrete bridges are typically controlled by the serviceability limit state criterion in the MCEB related to the tensile stress in the concrete. A low load rating implies that these bridges have experienced damage due to daily vehicular traffic. However, observations made by TxDOT personnel during routine inspections indicate that the condition of these bridges is very good, and that there are generally no signs of deterioration.

The discrepancy between the conditions implied by the load ratings and those observed in the field implies that the tensile stress serviceability limit state in the MCEB is conservative. The MCEB specifies a limiting tensile stress of $6\sqrt{f_c'}$ for the inventory-level load rating, where f_c' is the specified compressive strength of the concrete and the tensile stress is calculated assuming that the composite cross section is uncracked.

In an effort to improve the load ratings of these older prestressed concrete bridges, TxDOT has increased the concrete tensile stress limit when evaluating the serviceability limit state criterion. A limiting tensile stress of $7.5\sqrt{f_c'}$ is most commonly used, but occasionally limiting tensile stresses as high as $12\sqrt{f_c'}$ have been selected. These values correspond to the upper limits of computed extreme fiber stress at service loads in the precompressed tensile zone for Class U (uncracked) and Class T (transition from uncracked to cracked) prestressed concrete members, respectively, in the ACI Building Code (ACI 318, 2005).

ACI Committee 215 (1974) reports that the strengths of concrete in compression, tension, and flexure are reduced under fatigue loading. The strength corresponding to a fatigue life of ten million cycles is approximately 55% of the static strength. Given the differences between the predominately

static live load in buildings and cyclic live load applied to bridges, the possible consequences of increasing the limiting tensile stress on the fatigue limit state should be evaluated for prestressed concrete bridges.

1.1 RESEARCH OBJECTIVES

The primary objectives of this investigation were to evaluate the appropriateness of using these elevated tensile stress limits when calculating the inventory-level load rating of older prestressed concrete bridges and to determine if the fatigue limit state should be included explicitly in the load rating process.

1.2 FATIGUE RESPONSE OF PRESTRESSED CONCRETE BEAMS

Prestressed concrete beams are typically designed such that flexural cracks do not form under the specified live load. The AASHTO Standard Specifications limit the maximum tensile stress in the precompressed tensile zone to $6\sqrt{f_c'}$ under service loads for beams with bonded reinforcement that are not exposed to severe environmental conditions, such as coastal zones. Under these conditions, the fatigue characteristics of the prestressing steel is not likely to influence the fatigue life of the beam (ACI 215, 1974), and the fatigue limit state is not considered explicitly in the design. The AASHTO LRFD Specifications adopt a similar approach and state that fatigue need not be considered if the extreme fiber tensile stress due to a serviceability limit state is less than $6\sqrt{f_c'}$ for prestressed concrete girders that are subjected to not worse than moderate corrosion conditions. The fact that no structural problems attributable to fatigue failures of the prestressed concrete beams have been reported in North America (ACI 215, 1974) confirms the merit of this approach for design.

This same approach has been adopted for evaluating existing structures in the MCEB, and the limiting stress used to determine the inventory-level rating is also $6\sqrt{f_c'}$. The reason that the older prestressed concrete bridges fail the criterion for tensile stress in the concrete is that the design vehicle has changed with time. Many of the bridges were designed to resist H-20 vehicles and some were designed to resist H-15 vehicles. Due to this higher than anticipated level of live load, the calculated tensile stresses in the concrete often exceed $6\sqrt{f_c'}$.

Under these circumstances, flexural cracks are expected to be present and the fatigue life of the girders will be controlled by the fatigue life of the strand. The results of previous experimental investigations are summarized in the following sections. Axial fatigue tests of prestressing strand in air are discussed in Section 1.2.1 and bending fatigue tests of prestressed concrete beams are presented in Section 1.2.2.

1.2.1 Axial Fatigue Response of Prestressing Strand

A database of more than 650 finite-life fatigue tests of prestressing strands was assembled from three sources:

(1) Paulson et al. (1983) compiled the results of nearly 400 fatigue tests reported in the literature and more than 40 tests conducted at Ferguson Structural Engineering Laboratory.

(2) Heller (2003) documented the results of more than 200 tests conducted by VSL Corporation to certify strand used to construct cable-stay bridges around the world.

(3) Heller (2003) and Bean (2006) conducted approximately 20 tests in Ferguson Structural Engineering Laboratory to characterize the strand used in this investigation and the cable-stay specimens tested in Project 1401.

The data from all sources are plotted in Figure 1.1. The levels of applied axial tensile stress varied from 22 to 106 ksi, with the majority of the tests conducted between 40 and 70 ksi.

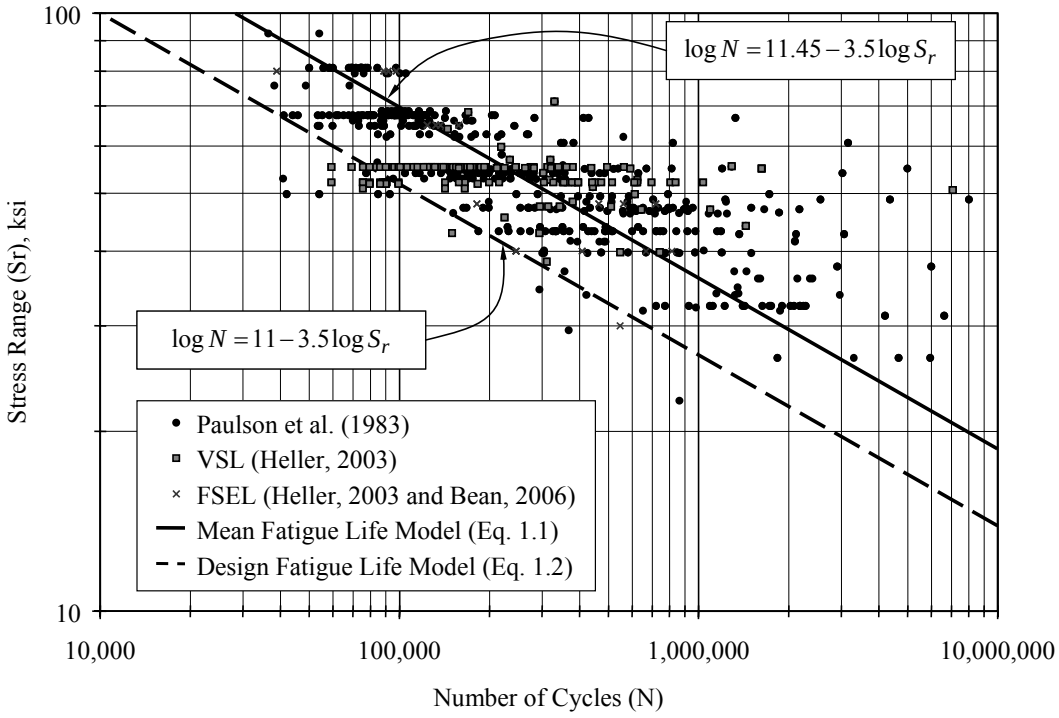

Figure 1.1 Fatigue Life Models for Prestressing Strand Developed by Paulson et al. (1983)

Paulson et al. (1983) also developed two fatigue life models to represent the prestressing strand. These models are also shown in Figure 1.1. The first model represents the mean number of cycles that the strand experienced when subjected to cyclic loading at a constant stress range:

$$\log N = 11.45 - 3.5 \log S_r \tag{1.1}$$

where

N = number of loading cycles at failure
S_r = stress range in the strand, ksi

Due to the variability of the measured data, Paulson, et al. (1983) also proposed a model for design purposes which corresponds to the 2.5% fractile at a confidence level of 95%.

$$\log N = 11 - 3.5 \log S_r \tag{1.2}$$

As shown in Figure 1.2, the fatigue model corresponding to AASHTO Detail Category B is more conservative than the design model proposed by Paulson et al. for stress ranges less than 60 ksi. However, no data are available to confirm the presence of a threshold stress.

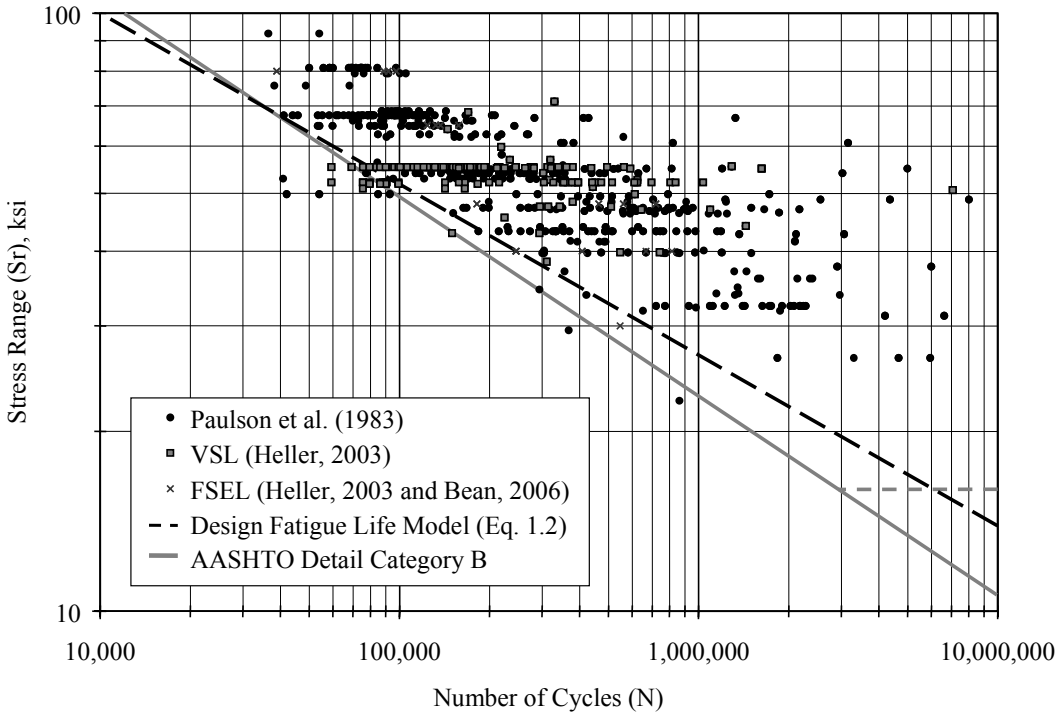

Figure 1.2 Comparison of Measured Response of Prestressing Strand and Fatigue Model Corresponding to AASHTO Detail Category B

1.2.2 Bending Fatigue Response of Prestressed Concrete Beams

Data from 78 fatigue tests of prestressed concrete beams are plotted in Figure 1.3. The beams have been divided into two groups:

(1) Fifty five beams with straight strands tested by Abeles, Brown, and Hu (1974), Muller and Dux (1994), Norby and Venuti (1957), Overman (1984), Ozel and Ardaman (1956), Ozel and Diniz (1958), Rabbat et al. (1978), and Warner and Hulsbos (1966).

(2) Twenty three beams with depressed strands tested by Muller and Dux (1994), Overman (1984), Ozel (1962), Rabbat et al. (1978), and Roller et al. (1995).

The sizes of the test specimens ranged from small-scale (4.5-in. by 6-in. rectangular cross sections) to 54-in. deep bulb-tee sections with a 9½-in. topping slab. Two tendon profiles were used among the beams with depressed strands (Figure 1.4).

All beams were tested at levels of applied load that generated flexural cracks in the precompressed tension zone of the concrete. The fatigue life was taken as the number of loading cycles corresponding to the first wire break, although many of the beams sustained more loading cycles. The stress ranges in the strand correspond to those reported by the researchers. No finite-life fatigue data are available for stress ranges less than 10 ksi.

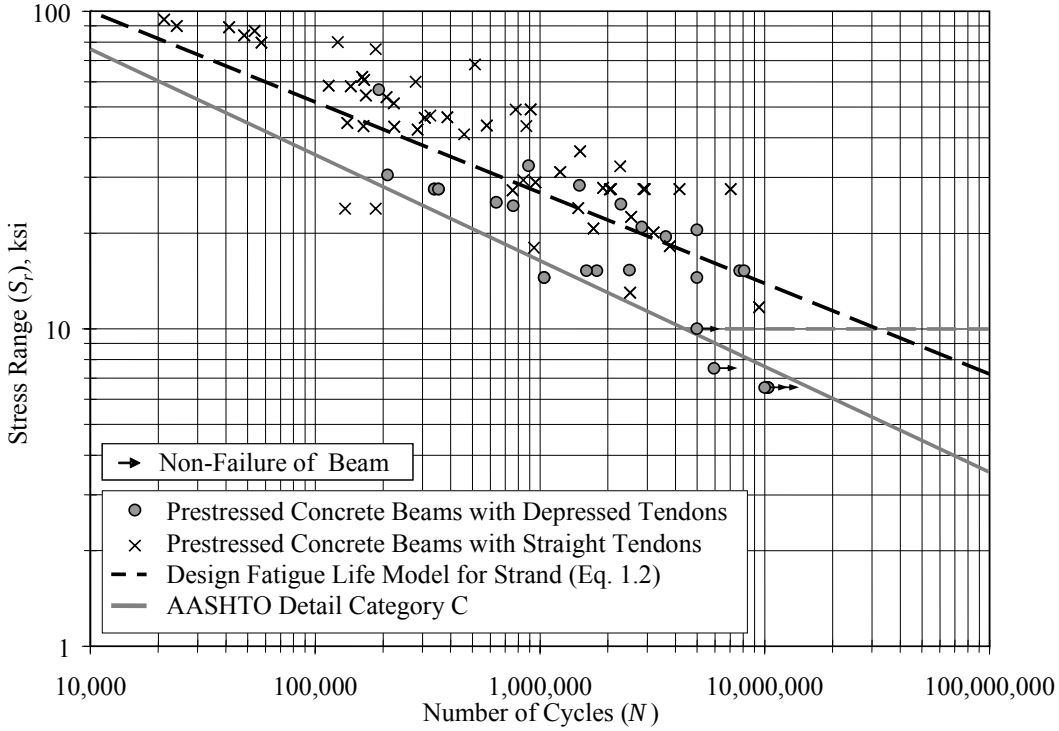

Figure 1.3 Fatigue Response of Prestressed Beams

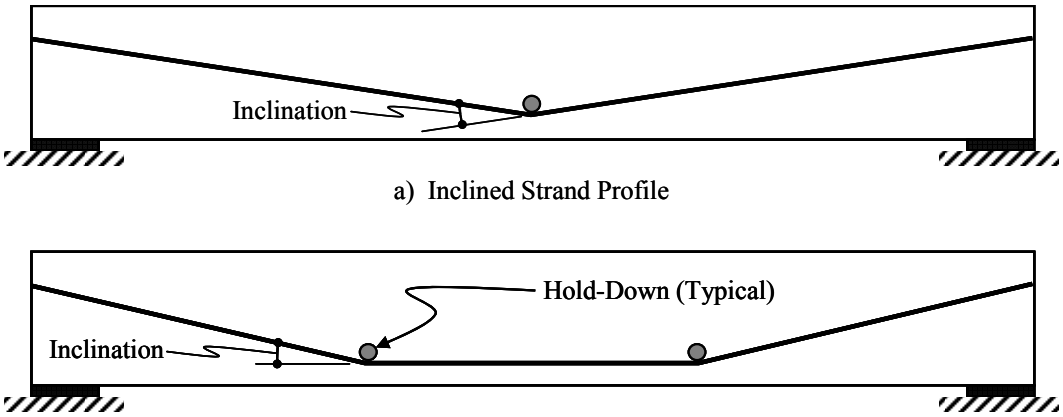

Figure 1.4 Strand Profiles for Beams with Depressed Tendons

The measured response of the beams is compared with the design fatigue life model for strand proposed by Paulson et al. (1983) in Figure 1.3. The model is representative of the mean fatigue life of the beams. The fatigue model corresponding to AASHTO Detail Category C provides a reasonable lower bound to the measured response.

1.3 SCOPE OF INVESTIGATION

TxDOT (2002) provided the research team with a list of thirty bridges for which at least one span failed to meet the tensile stress criterion in the MCEB. Five bridges from this list were selected for detailed investigation. All bridges studied were two-lane, simply-supported, highway bridges composed of prestressed concrete beams and a composite, cast-in-place deck. A total of eight spans from the five bridges were inspected, instrumented, and load tested.

The measured data collected during the diagnostic load tests were used to evaluate the live load response of the bridges. Data indicated the likely presence of flexural cracks and the actual distribution of live load among the girders. Laboratory fatigue tests were conducted on six, quarter-scale specimens. The variation in strand stress due to the fatigue loads varied from 7 to 48 ksi during the laboratory tests.

Based on the results of the diagnostic load tests and laboratory fatigue tests, it was concluded that the tensile stress criterion in the MCEB should not be used to evaluate existing prestressed concrete bridges because the calculated tensile stress in the concrete is not a reliable indicator of the stresses induced in the strand due to live load. Conservative guidelines for considering the fatigue limit state explicitly in the load rating process were developed.

Using this approach, it was concluded that one of the five bridges had an infinite fatigue life and that fatigue did not limit the design life of the remaining four bridges. Because each of the bridges

satisfied the flexural strength criterion in the MCEB, the limiting rating factors exceeded 1.0 for all five bridges, which is consistent with the observed condition of the bridges. In addition, posting of the bridges is not required.

This report contains nine chapters and two appendices. Chapter 2 is a description of the five bridges that were studied in detail during this investigation. Chapter 3 provides information about the diagnostic load testing program and a description of the measured data collected during the load tests. Chapter 4 provides the analysis and evaluation of the data collected during the load tests. Chapter 5 discusses the design of the fatigue test specimens and provides an overview of fatigue tests that were performed. Chapter 6 discusses the results of the fatigue tests. Chapter 7 relates the results of the inventory-level load ratings to stress range in the strand. Detailed analyses of the fatigue response of the bridges are discussed in Chapter 8, and recommended procedures for considering the fatigue limit state in the load rating process are presented in Chapter 9. The conclusions of this investigation are summarized in Chapter 10. Appendix A summarizes the live load distribution factors for the five bridges and the procedures used to approximate the nonlinear response of the composite girders are presented in Appendix B.

1.4 DESIGN SPECIFICATIONS

Throughout this report, references are frequently made to several specifications that are currently used by TxDOT for the design and evaluation of highway bridges. Because the recommendations are closely tied to these specifications, the edition of each specification is identified below for clarity. The abbreviations that will be used to identify these specifications are also noted.

- MCEB – AASTHO Manual for the Condition Evaluation of Bridges, 2nd Edition with 2003 Interim Revisions.
- AASHTO Standard Specifications – AASHTO Standard Specifications for Highway Bridges, 17th Edition with 2005 Errata.
- AASTHO LRFD Specifications – AASHTO LRFD Bridge Design Specifications, 3rd Edition with 2005 Interim Revisions.
- LRFR – AASHTO Manual for Condition Evaluation and Load and Resistance Factor Rating (LRFR) of Highway Bridges, 1st Edition with 2005 Interim Revisions.

CHAPTER 2
Prestressed Concrete Bridges

Diagnostic load tests were conducted on five prestressed concrete bridges during this project. General information about the geometry of the bridges, the material properties, and the cross-sectional properties is summarized in this chapter.

2.1 OVERVIEW OF BRIDGES

TxDOT (2002) provided the research team with a list of thirty prestressed concrete bridges in the Austin District that were constructed between 1946 and 1970 (Table 2.1). The length of the longest span in each bridge varied from 45 to 75 ft. The load ratings, calculated using standard TxDOT procedures, were controlled by the tensile stress criterion for all bridges on the list. The load ratings ranged from HS-11.6 to HS-27.7.

The research team conducted visual inspections of many of the candidate bridges and selected five for diagnostic load testing. Access for installing instruments and worker safety during the load tests were the primary criteria used to select the bridges. General information about the five bridges selected for load testing is summarized in Table 2.2. The names assigned to each bridge in Table 2.2 will be used throughout this report.

All five bridges selected for load testing were two-lane highway bridges and were constructed with prestressed concrete beams and a composite cast-in-place deck. End and intermediate concrete diaphragms were present in all bridges. All spans were simply-supported. Although the bridges were similar in layout and construction, their overall dimensions varied. The lengths of the spans varied between 40 ft and 75 ft, roadway widths varied between 24 ft and 28 ft-8 in., beam spacing varied between 6 ft-8 in. and 8 ft, and skew angles varied between 0° and 30° (Table 2.3 and Table 2.4).

As indicated in Table 2.3, the overall length of the bridges varied form 130 to 780 ft. It was not possible to instrument all spans. One span from the Lake LBJ and Willis Creek Bridges were tested, while two spans from the Chandler Creek, Lampasas River, and Wimberley Bridges were tested. The 40-ft spans on the Chandler Creek and Wimberley Bridges were not typical of the prestressed concrete bridges considered (Table 2.1) because the load ratings for these spans were controlled by the flexural strength, rather than the tensile stress criterion. However, the load ratings for the longer spans in these bridges were limited by the tensile stress criterion.

Brief descriptions of the five bridges are given in Sections 2.1.1 through 2.1.5. Additional information about the bridges is presented in Hagenberger (2004) and Wagoner (2002).

Table 2.1 Representative Prestressed Concrete Bridges in Austin District (TxDOT, 2002)

Bridge	Longest Span (ft)	Beam Spacing (ft)	Slab Thickness (in.)	f_c' (psi)		TxDOT Load Rating*			Girder Type	Year Completed
				Beam	Slab	Limiting Tensile Stress† $\left(\sqrt{f_c'}\right)$	Tensile Stress Criterion	Flexural Strength Criterion		
SH 95 @ Mustang Creek	50	8.00	7.25	5000	3000	7.5	HS-15.8	HS-17.8	B	1946
I-35 @ Redwood Road	65	6.00	6.00	5000	3000	7.5	HS-24.2	HS-27.6	C	1958
I-35 @ McCarty Lane	65	6.00	6.67	5000	3000	7.5	HS-20.7	HS-24.7	C	1958
I-35 @ Center Point Road	65	6.67	6.00	5000	3000	7.5	HS-20.7	HS-24.7	C	1958
I-35 @ Posey Road	65	6.67	6.00	5000	3000	7.5	HS-20.7	HS-24.7	C	1958
FM 12 @ Blanco River	60	6.92	6.25	5000	3000	7.5	HS-23.2	HS-27.4	C	1959
FM 972 @ Willis Creek	65	6.67	6.00	5000	3000	7.5	HS-16.4	HS-22.4	C	1961
I-35 @ FM2001	65	6.67	6.25	5000	3000	7.5	HS-20.0	HS-24.6	C	1961
I-35 @ Bunton Road	65	6.67	6.25	5000	3000	7.5	HS-18.5	HS-24.5	B	1961
I-35 @ Loop 150	65	6.00	6.00	5000	3000	7.5	HS-23.8	HS-27.4	C	1961
MoPac RR Overpass @ US-290	60	8.56	6.75	5000	3000	7.5	HS-21.8	HS-24.6	C	1961
US-290 @ Loop 275	45	7.25	6.25	5000	3000	7.5	HS-27.7	HS-27.9	B	1961
I-35 @ Yarrington Road	70	6.67	6.50	5000	3000	7.5	HS-22.4	HS-26.8	C	1962
Loop 343 @ IH-35 (NB&SB)	70	7.17	6.50	5000	3000	7.5	HS-25.7	HS-30.9	C	1962
US-183 @ IH-35 (NB)	70	7.17	6.50	5000	3000	7.5	HS-25.5	HS-30.9	C	1962
US-183 @ IH-35 (SB)	70	7.17	6.50	5000	3000	7.5	HS-25.5	HS-30.9	C	1962
FM 1431 @ LBJ Lake	65	8.00	7.25	5000	3000	7.5	HS-19.8	HS-25.4	C	1964
US-290 @ Yeager Creek	50	7.67	7.25	4700	3000	7.5	HS-19.7	HS-23.5	B	1964
US-290 @ Middle Creek	50	7.67	7.25	4700	3000	7.5	HS-19.7	HS-23.5	B	1964
US-281 @ Miller Creek (NB)	50	6.00	6.00	5000	3000	7.5	HS-27.1	HS-27.2	B	1964
US-281 @ Miller Creek (SB)	50	6.00	6.00	5000	3000	7.5	HS-27.1	HS-27.2	B	1964
I-35 @ Loop 418	75	8.67	7.75	5000	3000	12.0	HS-21.6	HS-24.8	C	1965
IH-35 WFR @ Chandler Creek	65	8.00	7.25	5000	3000	7.5	HS-20.9	HS-25.8	C	1965
I-35 @ Westinghouse Road	65	8.00	7.25	5000	3000	7.5	HS-21.1	HS-25.7	C	1965
IH-35 EFR @ Chandler Creek	60	8.00	7.25	5000	3000	7.5	HS-21.6	HS-23.4	C	1965
US-183 @ FM 969	70	7.00	7.00	5000	3000	7.5	HS-23.1	HS-28.2	C	1966
Bergrstrom Main @ SH 71	60	8.33	7.50	5000	3000	7.5	HS-18.6	HS-21.4	C	1968
US-290 @ Loop 360 (EB)	61	7.50	7.00	5000	3000	7.5	HS-17.2	HS-19.1	C	1969
US-290 @ Loop 360 (WB)	59	7.50	7.00	5000	3000	7.5	HS-19.7	HS-20.5	C	1969
FM 2657 @ Lampasas River	75	7.33	6.50	5100	3000	7.5	HS-11.6	HS-20.8	C	1970

* The governing load rating for the bridge corresponds to the longest span. In some cases, span length varied within the bridge.

† Value of tensile stress used in load rating calculations.

Table 2.2 General Bridge Information

Bridge Name	Year Completed	Location	Daily Traffic Volume*	% Truck Traffic*
Chandler Creek	1965	IH 35 @ Chandler Creek	7,951	25%
Lake LBJ	1964	FM 1431 @ Lake LBJ	8,300	5%
Lampasas River	1970	FM 2657 @ Lampasas River	2,100	12%
Willis Creek	1961	FM 972 @ Willis Creek	800	16%
Wimberley	1959	RM 12 @ Blanco River	10,200	5%

* Recorded by TxDOT between 1999 and 2000.

Table 2.3 Overall Dimensions of Bridges

Bridge Name	Overall Length	Roadway Width	Beam Length	Girder Type	No. of Spans	No. of Spans Tested	No. of Beams
Chandler Creek	140'	28'-0″	40'	B	2	1	4
			60'	C	1	1	
Lake LBJ	780'	28'-0″	65'	C	12	1	4
Lampasas River	600'	26'-0″	75'	C	8	2	4
Willis Creek	130'	24'-0″	65'	C	2	1	4
Wimberley	440'	28'-8″	40'	B	5	2	5
			60'	C	4	0	

Table 2.4 Geometry of Bridges

Bridge Name	Beam Spacing	Skew Angle	Slab Thickness	Curb*	Deck Overhang**
Chandler Creek	8'-0″	30°	7.25″	No	3'-2″
Lake LBJ	8'-0″	0°	7.25″	Yes	3'-7″
Lampasas River	7'-4″	0°	6.5″	No	3'-1½″
Willis Creek	6'-8″	0°	6″	Yes	3'-7″
Wimberley	6'-11″	22°	6.25″	Yes	2'-2¾″ (avg)

* Curb dimensions vary.

** Deck overhang is measured from centerline of exterior girder to exterior face of curb or slab. Average dimension is reported for Wimberley Bridge because overhang varies along the span.

2.1.1 Chandler Creek Bridge

The Chandler Creek Bridge (Figure 2.1) carries two lanes of the northbound I-35 access road over Chandler Creek in Round Rock, TX. The three-span bridge was constructed in 1965. The length of both end spans is 40 ft, while the length of the center span is 60 ft. The southern two spans were tested (Figure 2.2). Type B girders were used in the end spans and Type C girders were used in the center span. The bridge is skewed at an angle of 30°. The calculated load rating for this bridge is HS-21.6, and is limited by the center span.

Figure 2.1 Photograph of Chandler Creek Bridge

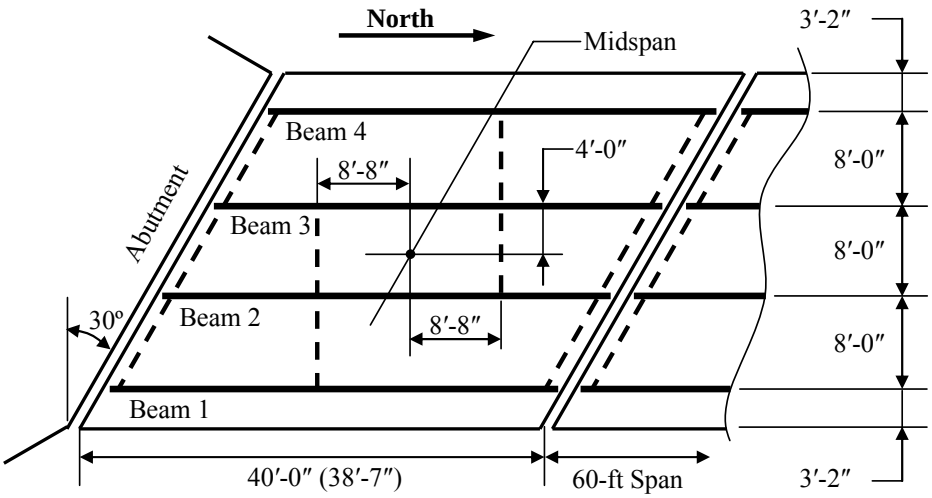

(a) Span 1 (40-ft Span)

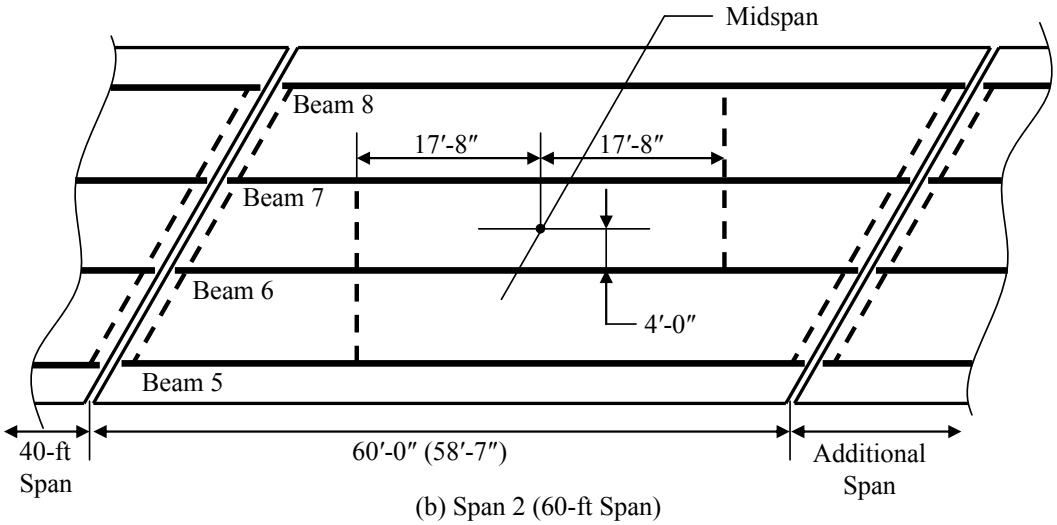

(b) Span 2 (60-ft Span)

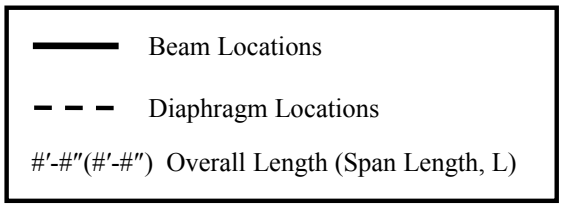

Figure 2.2 Plan of Chandler Creek Bridge

2.1.2 Lake LBJ Bridge

The Lake LBJ Bridge (Figure 2.3) carries both lanes of FM 1431 over Lake LBJ near Marble Falls, TX. The twelve-span bridge was constructed in 1964. The length of all spans is 65 ft. The end span at the east end of the bridge was tested (Figure 2.4). Type C girders were used in all spans and the cast-in-place slab included a curb. The calculated load rating for this bridge is HS-19.8.

Figure 2.3 Photograph of Lake LBJ Bridge

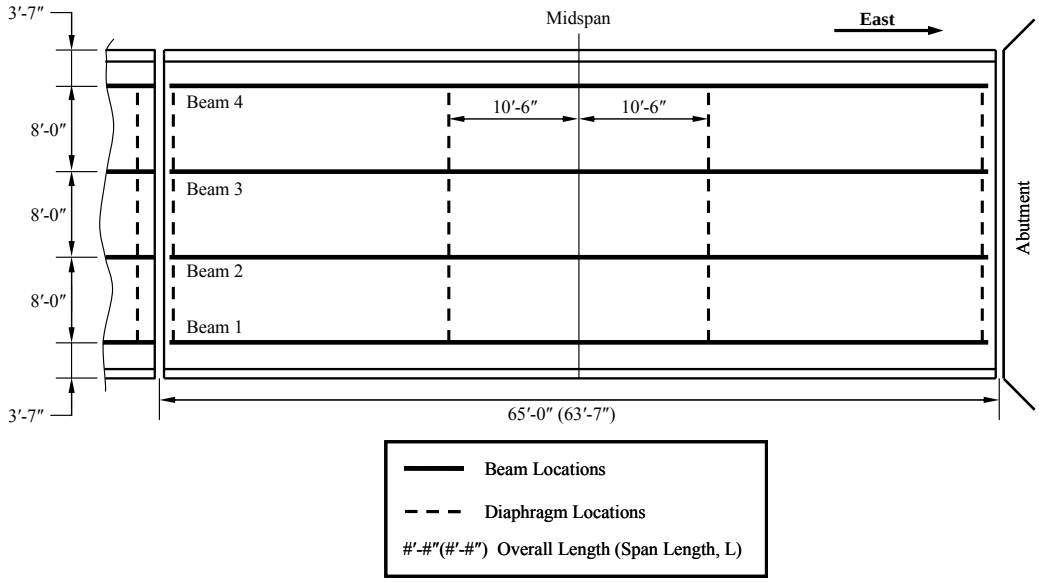

Figure 2.4 Plan of Lake LBJ Bridge

2.1.3 Lampasas River Bridge

The Lampasas River Bridge (Figure 2.5) carries both lanes of FM 2657 over the Lampasas River near Oakalla, TX. The eight-span bridge was constructed in 1970. Two, 75-ft spans near the center of the bridge were tested (Figure 2.6). Type C girders were used in all spans. The calculated load rating for this bridge is HS-11.6.

Figure 2.5 Photograph of Lampasas River Bridge

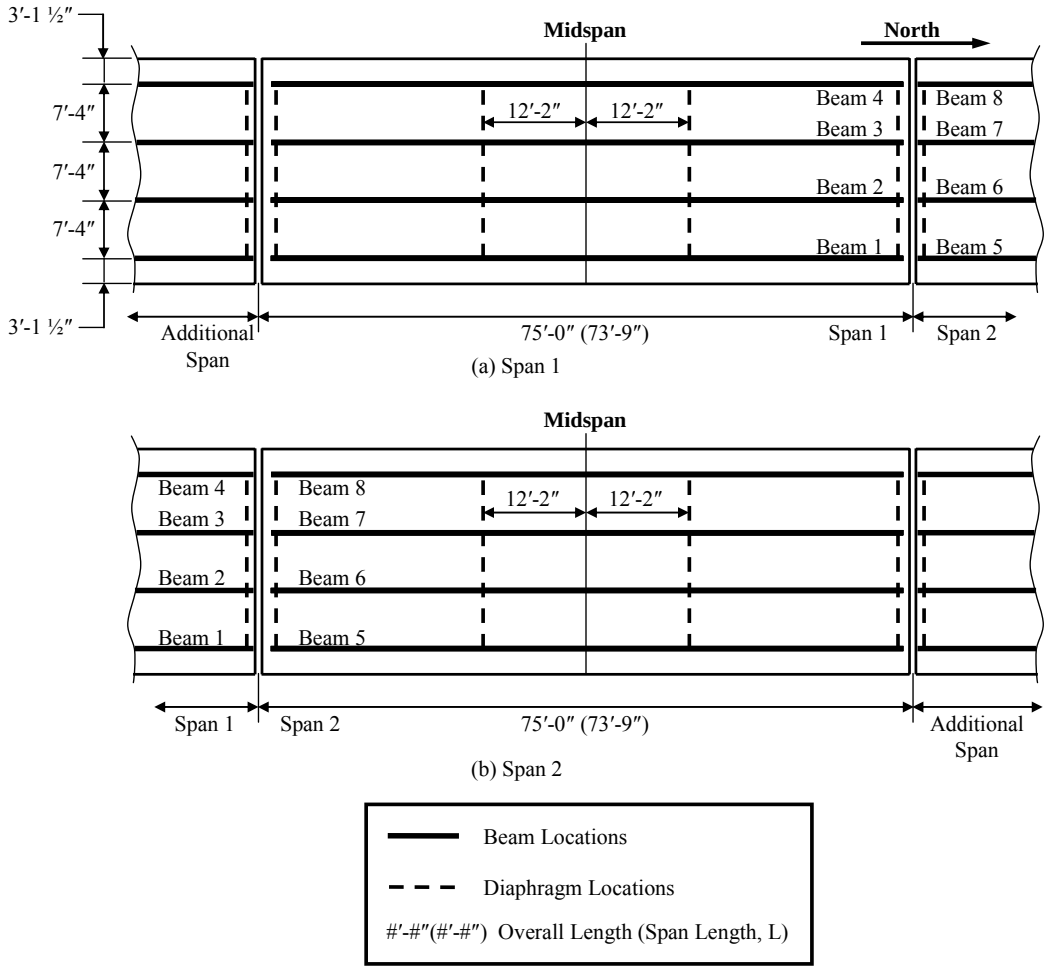

Figure 2.6 Plan of Lampasas River Bridge

2.1.4 Willis Creek Bridge

The Willis Creek Bridge (Figure 2.7) carries both lanes of FM 972 over Willis Creek near Keelersville, TX. The two-span bridge was constructed in 1961 and the west span was tested (Figure 2.8). Type C girders were used in both spans and the cast-in-place slab included a curb. The calculated load rating for this bridge is HS-16.4.

Figure 2.7 Photograph of Willis Creek Bridge

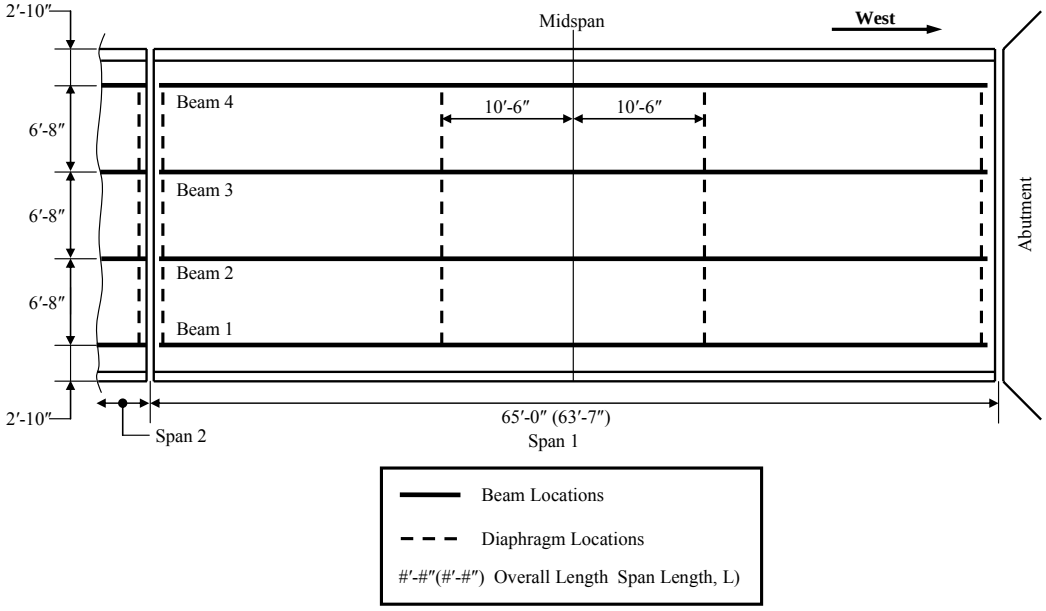

Figure 2.8 Plan of Willis Creek Bridge

2.1.5 Wimberley Bridge

The Wimberley Bridge (Figure 2.9) carries both lanes of RM 12 over the Blanco River near Wimberley, TX. The nine-span bridge is curved in plan, but straight prestressed girders were used. Therefore, each span is skewed with respect to the adjacent spans (Figure 2.10). Two 40-ft spans at the south end of the bridge were tested. The bridge was constructed in 1959. Five Type B girders were used in the 40-ft spans and five, Type C girders were used in the 60-ft spans. The cast-in-place slab included a curb. The calculated load rating for this bridge is HS-23.2, and is limited by the 60-ft spans.

Figure 2.9 Photograph of Wimberley Bridge

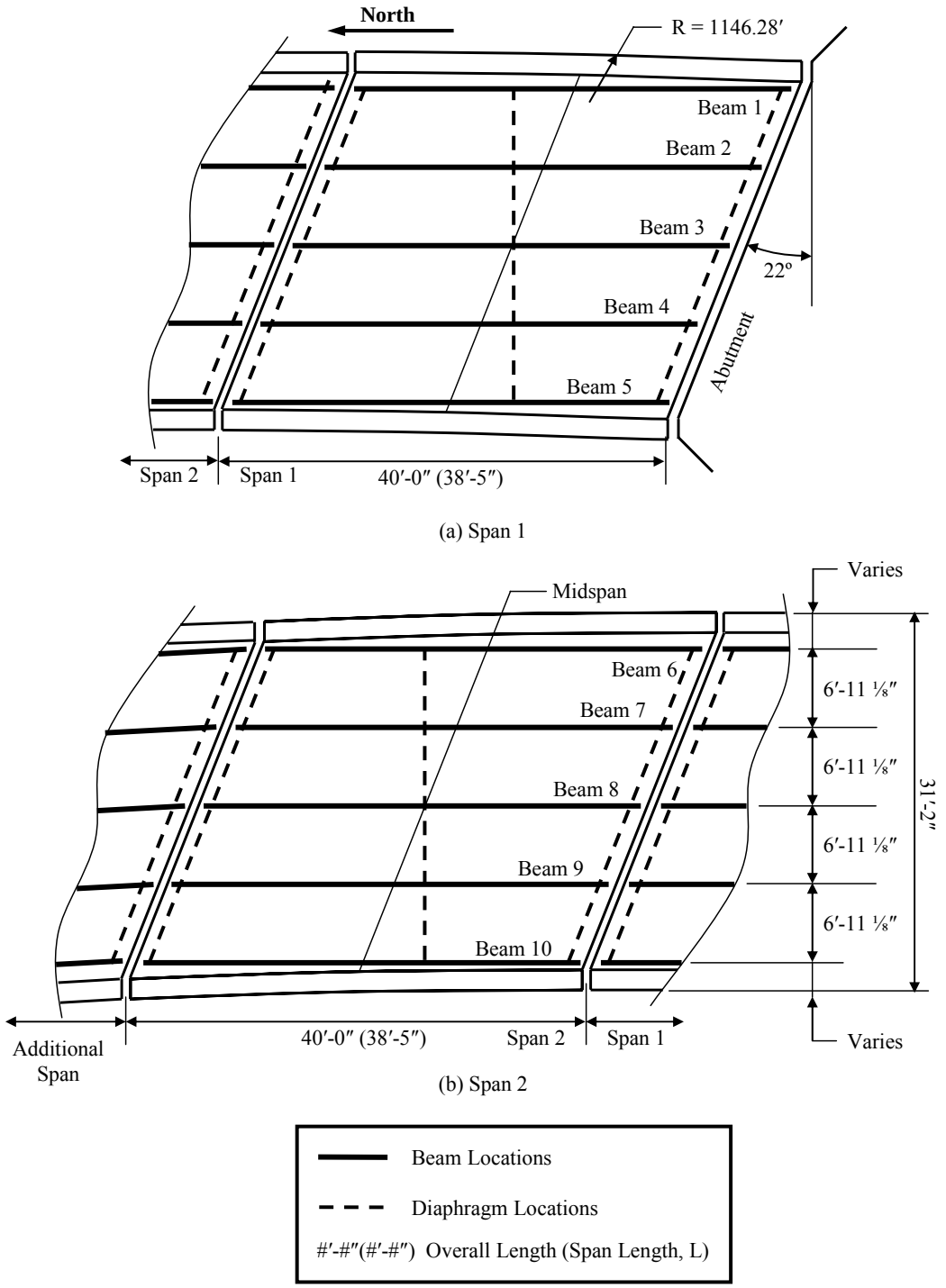

Figure 2.10 Plan of Wimberley Bridge

2.2 MATERIAL PROPERTIES

Material properties for the prestressing strand and concrete were specified on the structural drawings for each bridge. In addition, quality control records were available in the TxDOT archives for four of the five bridges. Available information about the prestressing strand is presented in Section 2.2.1 and available information about the concrete is presented in Section 2.2.2.

2.2.1 Prestressing Strand

Grade 250, stress-relieved strand was used in all the prestressed concrete beams. The older two bridges (Willis Creek and Wimberley) differed from the newer three bridges (Chandler Creek, Lake LBJ, and Lampasas River) in two ways (Table 2.5):

- 3/8-in. diameter strands were used to construct the beams in the older bridges, while 7/16-in. diameter strands were used to construct the beams in the newer bridges.
- Straight strands were used to construct the beams in the older bridges, while draped strands were used to construct the beams in the newer bridges.

In all cases, the arrangements of the strand were identical in the interior and exterior girders.

Table 2.5 Properties of Prestressing Strand

Bridge Name	f_{pu} (ksi)	f_{pi} (ksi)	Strand Diameter (in.)
Chandler Creek	250	175	7/16
Lake LBJ	250	175	7/16
Lampasas River	250	175	7/16
Willis Creek	250	175	3/8
Wimberley	250	175	3/8

2.2.2 Compressive Strength of Concrete

As discussed in Chapter 1, the load rating for many older prestressed concrete bridges in Texas is controlled by the concrete tensile stress criterion in the MCEB. TxDOT currently uses the specified concrete compressive strength in all calculations to establish the load rating. The actual concrete compressive strength is likely to be considerably higher than the specified value; therefore, available data are also presented.

(a) Specified Compressive Strength

Design calculations are based on the specified compressive strength of the concrete; however, the average measured strength of the concrete typically exceeds this value. Therefore, load rating calculations based on the specified compressive strength of the concrete are considered to be conservative. The specified concrete compressive strengths, f'_c, for the bridges considered in this study are summarized in Table 2.6.

Table 2.6 Specified Compressive Strength of Concrete

Bridge Name	Beam		Slab	Curb
	f'_{ci} (psi)	f'_c (psi)	f'_c (psi)	f'_c (psi)
Chandler Creek	4000	5000	3000	-
Lake LBJ	4000	5000	3000	3000
Lampasas River	4000	5000	3000	-
Willis Creek	4000	5000	3000	3000
Wimberley	4000	5000	3000	3000

(b) Construction Quality Control Records

The compressive strength of the concrete was measured during construction as part of the quality control process. These data were available in the TxDOT archives for the prestressed beams used to construct four of the five bridges and for the concrete used in the cast-in-place slab for the Chandler Creek Bridge. All results correspond to the measured compressive strength of 6x12-in. cylinders.

Measured compressive strengths for the concrete used to construct the prestressed beams were available at ages between 1 and 21 days. The average compressive strengths for each span at release of the prestressing and for the latest available record are summarized in Table 2.7. The compressive strengths based on the latest available record were between 50% and 75% higher than the specified compressive strengths.

Data from compressive strength tests of concrete from the Chandler Creek cast-in-place slab were available at ages between 3 and 28 days. The average compressive strength at 28 days is reported in Table 2.7, and was 75% higher than the specified compressive strength.

Quality control test records were not available for the prestressed beams in the Wimberley Bridge or the cast-in-place concrete used for the slabs and curbs in the Lake LBJ, Lampasas River, Willis Creek, of Wimberley Bridges.

Table 2.7 Concrete Compressive Strengths Reported in Quality Control Records

Bridge Name		Release		Latest Available Reports		
		No. of Tests	f'_c (psi)	Age* (days)	No. of Tests	f'_c (psi)
Chandler Creek	40-ft Span	19	5100	14	10	7400
	60-ft Span	2	5500	14	6	8700
	Slab	–	–	28	6	5300
Lake LBJ		30	5100	14	26	8000
Lampasas River		8	6000	10	2	8300
Willis Creek		4	5400	21	4	8600

* Age after placement of concrete.

The 28-day compressive strength of the concrete used to construct the girders was estimated using the ACI Committee 209 (1992) model:

$$f'_c(t) = \frac{t}{\alpha + \beta t} f'_c(28) \qquad (2.1)$$

where $f'_c(28)$ is the compressive strength of the concrete at 28 days, $f'_c(t)$ is the compressive strength of the concrete after t days, α is a constant that depends on the type of cement (Type I or Type III), and β is a constant that depends on the method of curing (moist or steam). The values of α and β were taken as 2.3 and 0.92, respectively for the prestressed concrete beams. These values correspond to Type III cement and moist curing.

The data from the quality control tests (Table 2.7) were used in Eq. 2.1 to estimate the 28-day strength. These estimates are summarized in Table 2.8. Conservative values were assumed in cases where data were not available. The compressive strength of the concrete at the time of release was assumed to be 5100 psi for the Wimberley Bridge.

2.3 CROSS-SECTIONAL PROPERTIES

The dimensions of the beams and slabs in the five bridges are given in Figure 2.11 through Figure 2.15 and the eccentricities of the prestressing strands are summarized in Table 2.9. The corresponding cross-sectional properties for the non-composite sections are summarized in Table 2.10. The design procedures in the AASHTO LFRD Specifications (Figure 2.16) were used to determine the effective flange widths for the interior and exterior beams (Table 2.11). The cross-sectional properties of the curbs are summarized in Table 2.12.

Table 2.8 Estimated 28-Day Compressive Strength of Concrete

Bridge Name		Estimated 28-Day Strength (psi)	
		Girder	Slab
Chandler Creek	40-ft Span	8000	5300
	60-ft Span	9400	5300
Lake LBJ		8700	4500*
Lampasas River		9500	4500*
Willis Creek		8900	4500*
Wimberley		8000*	4500*

* Assumed value.

Table 2.9 Eccentricity of Prestressing Strand

Bridge Name	**Eccentricity (in.)**		**Number of Strand**	**Number of Depressed Strand**
	e_{end}	e_{mid}		
Chandler Creek – 40-ft Span	8.40	11.90	16	4
Chandler Creek – 60-ft Span	9.07	13.07	30	6
Lake LBJ	5.74	12.40	36	8
Lampasas River	7.09	12.42	36	8
Willis Creek	8.02	8.02	44	0
Wimberley – 40-ft Span	8.14	8.14	34	0
Wimberley – 60-ft Span	8.02	8.02	44	0

Table 2.10 Cross-Sectional Properties for Non-Composite Beams

Bridge Name	Area ($in.^2$)	Moment of Inertia ($in.^4$)	Distance to Centroid	
			from Bottom (in.)	from Top (in.)
Chandler Creek – 40-ft Span	360	43,300	14.9	19.1
Chandler Creek – 60-ft Span	496	82,800	17.1	22.9
Lake LBJ	496	82,800	17.1	22.9
Lampasas River	496	82,800	17.1	22.9
Willis Creek	496	82,800	17.1	22.9
Wimberley – 40-ft Span	360	43,300	14.9	19.1
Wimberley – 60-ft Span	496	82,800	17.1	22.9

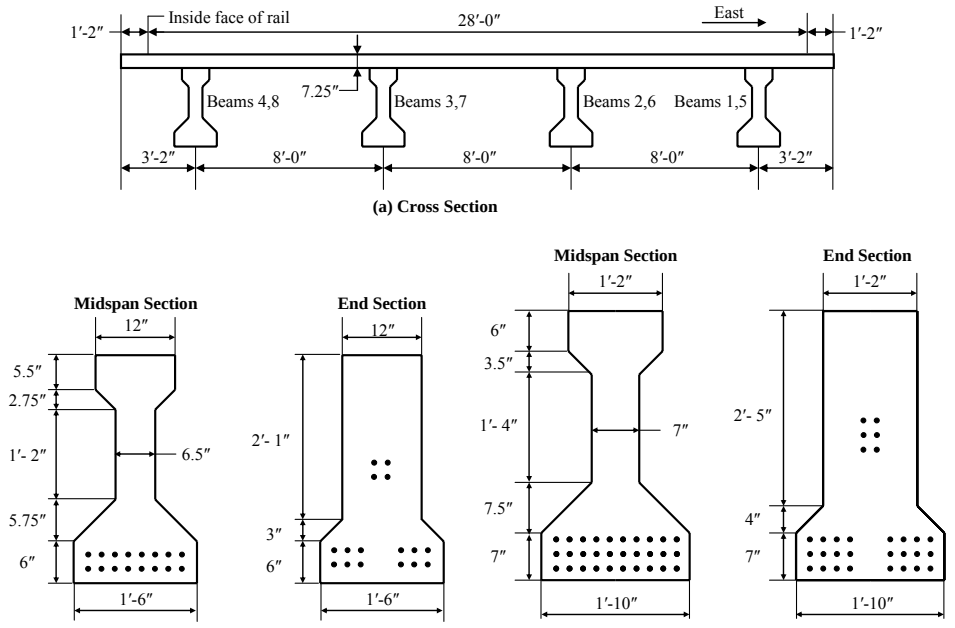

Figure 2.11 Cross Section and Beam Details for Chandler Creek Bridge

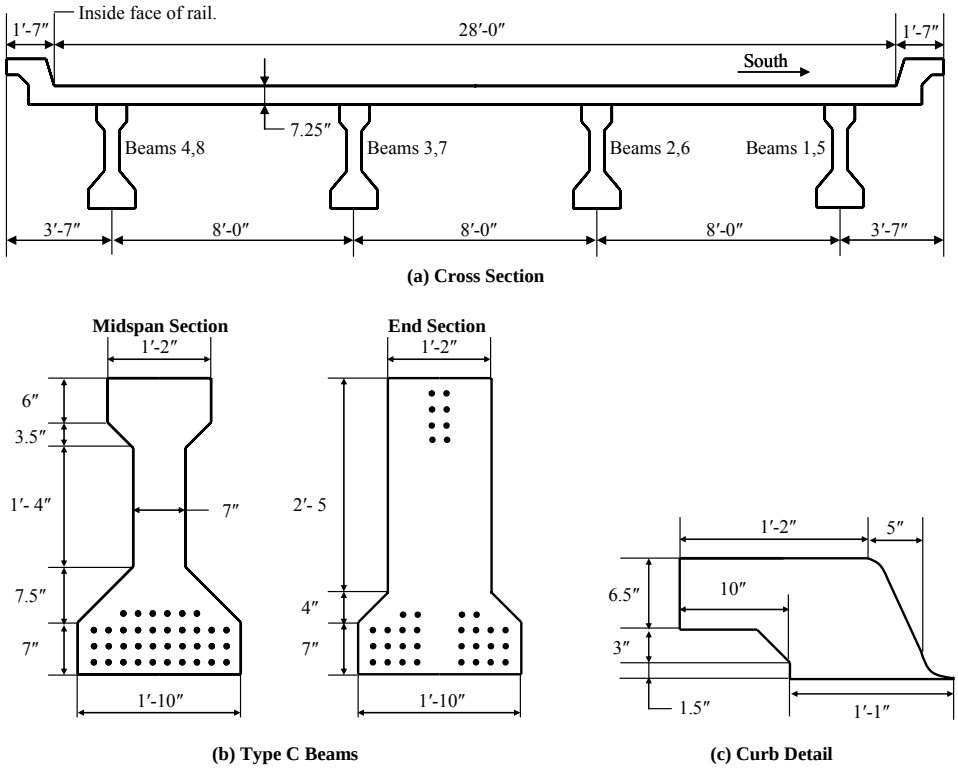

Figure 2.12 Cross Section, Beam, and Curb Details for Lake LBJ Bridge

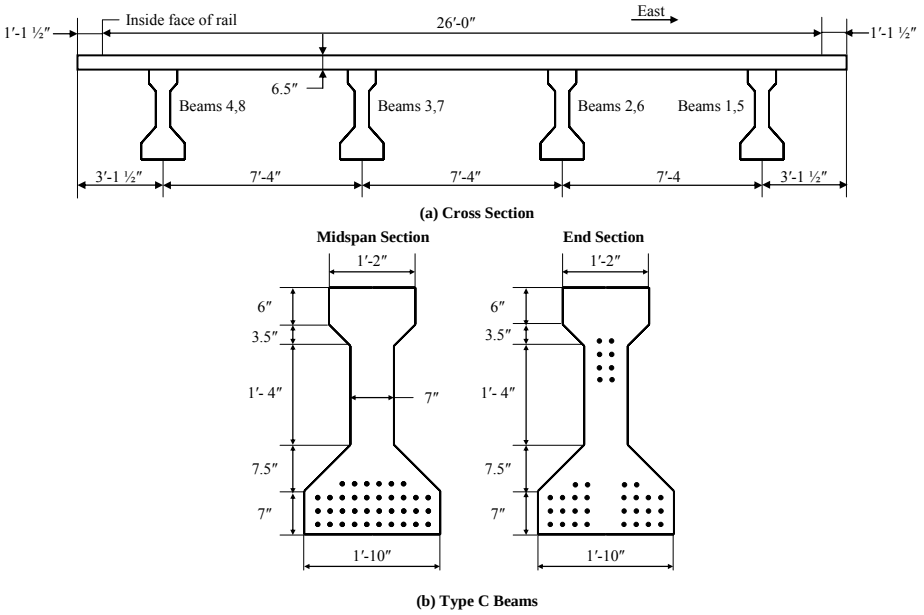

Figure 2.13 Cross Section and Beam Details for Lampasas River Bridge

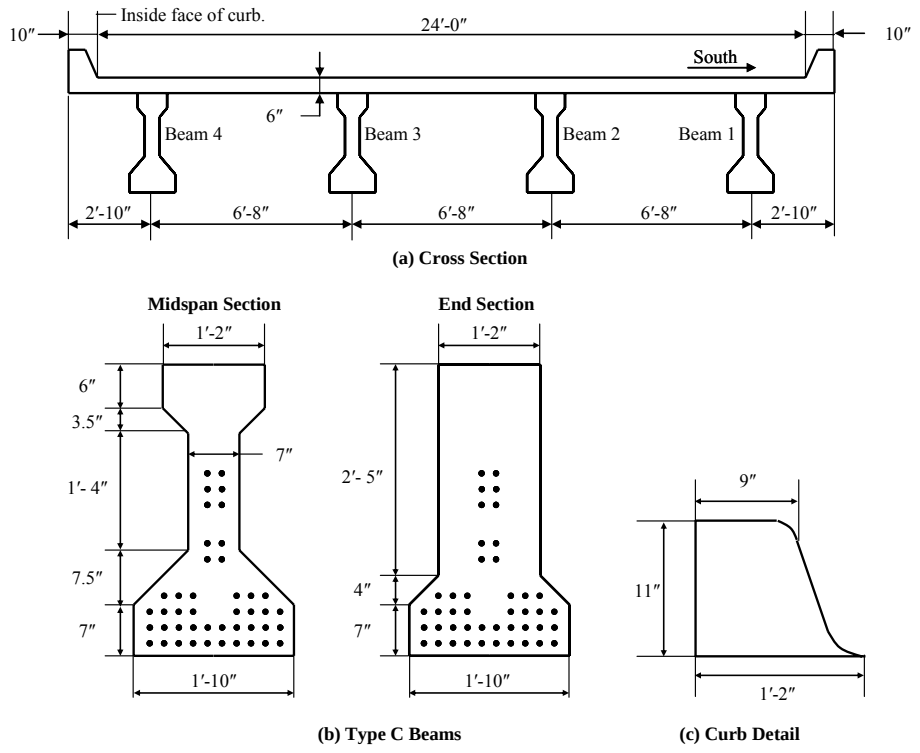

Figure 2.14 Cross Section, Beam, and Curb Details for Willis Creek Bridge

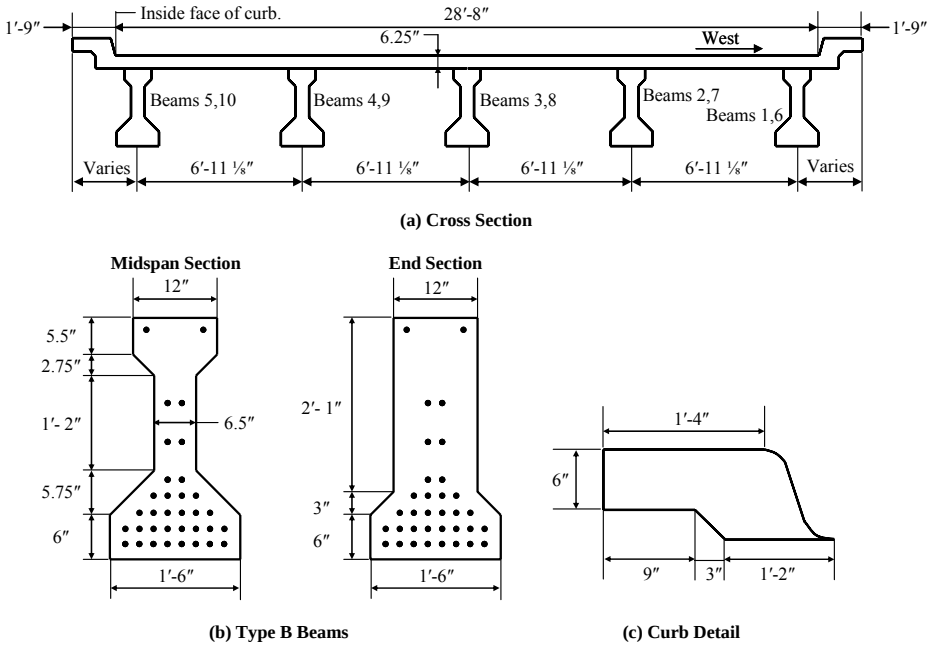

Figure 2.15 Cross Section, Beam and Curb Details for Wimberley Bridge

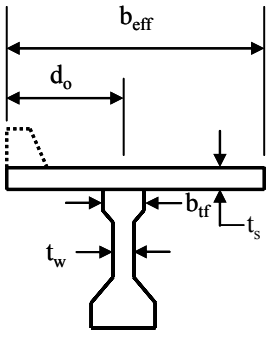

(a) Exterior Beam

b_{eff} = Effective flange width

For exterior beams, the effective flange width is the minimum of the following:

1. Minimum of $L/8 + d_o$ or $L/4$
2. Maximum of $6t_s + t_w/2 + d_o$ or $6t_s + b_{tf}/2 + d_o$
3. Maximum of $12t_s + t_w$ or $12t_s + b_{tf}/2$
4. Minimum of $S/2 + d_o$ or S

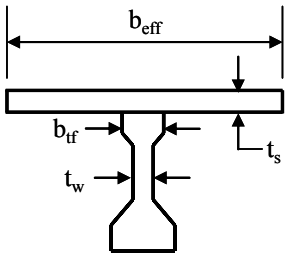

(b) Interior Beam

For interior beams, the effective flange width is the minimum of the following:

1. $L/4$
2. Maximum of $12t_s + t_w$ or $12t_s + b_{tf}/2$
3. S

Figure 2.16 Definition of Effective Flange Width (AASHTO LRFD)

Uncracked, transformed, composite cross-sectional properties were calculated using the geometric information summarized in Table 2.10, Table 2.11, and Table 2.12 for the beams, slabs, and curbs, respectively. Two values of the concrete compressive strengths were used: the specified compressive strengths and the estimated 28-day compressive strengths. The corresponding properties of the composite cross sections are summarized in Table 2.13.

Table 2.11 Effective Flange Widths Used to Calculate Properties of Composite Cross Section

Bridge Name	Interior Beam	Exterior Beam
	b_{eff} (in.)	b_{eff} (in.)
Chandler Creek – 40-ft Span	93.5	84.8
Chandler Creek – 60-ft Span	94.0	85.0
Lake LBJ	94.0	80.0
Lampasas River	85.0	80.0
Willis Creek	79.0	73.5
Wimberley – 40-ft Span	81.5	55.8
Wimberley – 60-ft Span	82.0	56.0

Table 2.12 Dimensions of Curbs

Bridge Name	Area (in.^{2})	Moment of Inertia (in.^{4})	Distance to Centroid* (in.)
Lake LBJ	158	1500	6.3
Willis Creek	99	1000	5.3
Wimberley	137	700	5.3

* Distance from top of slab to centroid of curb.

The modulus of elasticity, E_c, for concrete was calculated for each value of concrete compressive strength considered using Eq. 2.2 from ACI 318 (2005):

$$E_c = 57{,}000\sqrt{f'_c} \qquad (2.2)$$

where f'_c and E_c are expressed in units of psi. The modulus of elasticity of the prestressing strand was assumed to be 29,000 ksi.

The calculated properties of the composite cross sections are reported in Table 2.13. The results were not sensitive to the choice of concrete compressive strength.

Table 2.13 Cross-Sectional Properties for Composite Beams

(a) Specified Compressive Strength of Concrete*

Bridge Name		Interior Beam				Exterior Beam			
		Area ($in.^2$)	Moment of Inertia ($in.^4$)	Distance to Centroid		Area ($in.^2$)	Moment of Inertia ($in.^4$)	Distance to Centroid	
				from Bottom (in.)	from Top (in.)			from Bottom (in.)	from Top (in.)
Chandler Creek	40-ft Span	900	163,000	28.1	13.2	850	158,000	27.5	13.8
	60-ft Span	1040	279,000	30.3	16.9	990	269,000	29.6	17.7
Lake LBJ		1060	283,000	30.3	17.0	1090	331,000	31.8	15.4
Lampasas River		940	254,000	28.5	18.0	920	249,000	28.1	18.4
Willis Creek		880	233,000	27.7	18.4	940	269,000	29.2	16.8
Wimberley	40-ft Span	770	144,000	26.1	14.2	750	168,000	27.0	13.2
	60-ft Span	920	242,000	28.2	18.1	900	249,000	28.2	18.0

(b) Estimated 28-Day Compressive Strength of Concrete**

Bridge Name		Interior Beam				Exterior Beam			
		Area ($in.^2$)	Moment of Inertia ($in.^4$)	Distance to Centroid		Area ($in.^2$)	Moment of Inertia ($in.^4$)	Distance to Centroid	
				from Bottom (in.)	from Top (in.)			from Bottom (in.)	from Top (in.)
Chandler Creek	40-ft Span	920	164,00	28.4	12.9	870	159,000	27.9	13.4
	60-ft Span	1020	272,000	30.2	17.0	970	263,000	29.5	17.8
Lake LBJ		1000	270,000	29.8	16.5	1040	318,000	31.5	15.7
Lampasas River		890	241,000	28.0	18.5	870	235,000	27.6	18.9
Willis Creek		850	224,000	27.2	18.9	890	257,000	28.7	17.3
Wimberley	40-ft Span	760	141,000	26.0	14.3	740	165,00	26.9	13.3
	60-ft Span	900	237,000	28.1	18.2	880	244,00	28.1	18.1

* Values reported in Table 2.6.
** Values reported in Table 2.8.

CHAPTER 3
Diagnostic Load Tests

The diagnostic load tests of the five prestressed concrete bridges are summarized in this chapter. Loading vehicles and paths, instrumentation, and measured strain response are discussed in Sections 3.1, 3.2, and 0, respectively. More detailed information is provided in Hagenberger (2004) and Wagener (2002).

3.1 LOADING VEHICLES

Two standard, 10-yd^3 dump trucks were used as the loading vehicles for each of the diagnostic load tests (Figure 3.1). Dimensions and axle weights of the vehicles are given in Figure 3.2 and Table 3.1, respectively. Gross vehicle weights ranged from 40 to 50 kip.

Figure 3.1 Typical Vehicle Used for Diagnostic Load Tests

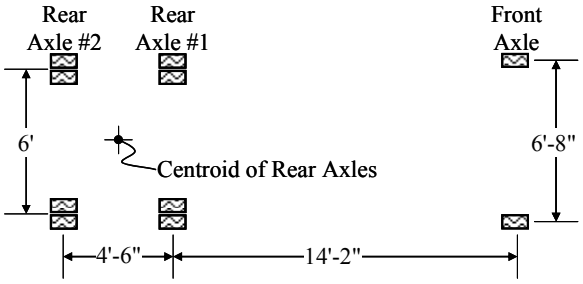

Figure 3.2 Dimensions of Loading Vehicles

Table 3.1 Weight of Loading Vehicles

Bridge Name	Truck ID	Axle Weight (kip)			Total Weight (kip)
		Front	Rear #1	Rear #2	
Chandler Creek	1	10.7	15.5	14.3	40.5
	2	11.1	15.0	14.0	40.1
Lake LBJ	1	12.7	18.0	18.0	48.7
	2	10.8	17.6	17.6	46.0
Lampasas River	1	10.9	17.2	17.2	45.3
	2	10.7	16.7	16.7	44.1
Willis Creek	1	12.6	18.6	17.9	49.1
	2	10.6	18.2	17.8	46.6
Wimberley	1	13.3	18.6	18.6	50.5
	2	9.9	18.0	18.0	45.9

Three different configurations of loading vehicles were used during the diagnostic tests: (1) single vehicle (Figure 3.3 and Figure 3.4), (2) two vehicles positioned side by side (Figure 3.5 and Figure 3.6), and (3) two vehicles positioned back to back (Figure 3.7 and Figure 3.8).

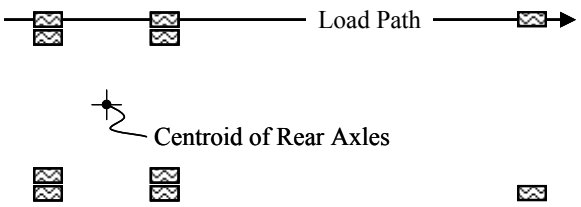

Figure 3.3 Configuration for Single Truck

Figure 3.4 Single Truck on Willis Creek Bridge

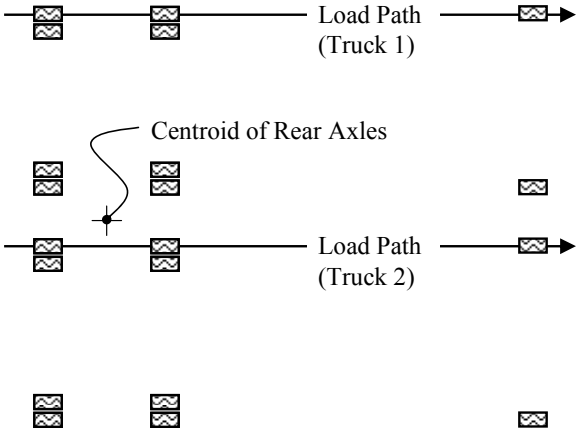

Figure 3.5 Configuration of Two Trucks Positioned Side by Side

Figure 3.6 Side-by-Side Trucks on Willis Creek Bridge

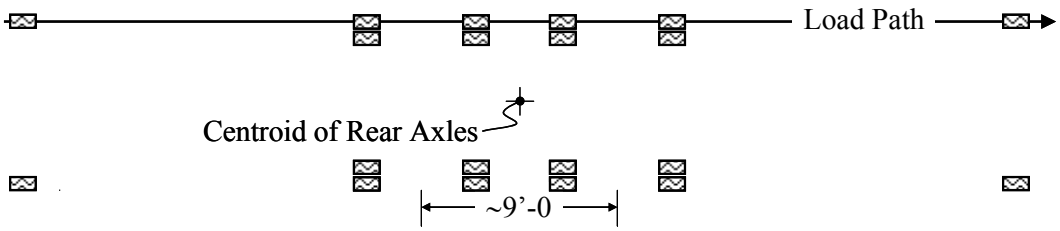

Figure 3.7 Configuration of Two Trucks Positioned Back to Back

Figure 3.8 Back-to-Back Trucks on Lampasas River Bridge

In order to obtain comprehensive information about the distribution of live load, several load paths were selected for each bridge. The loading vehicles were centered between adjacent prestressed concrete girders and centered over the interior girders (Figure 3.9 and Figure 3.10). Because the bridges were narrow, the loading vehicles were not centered within the traffic lanes.

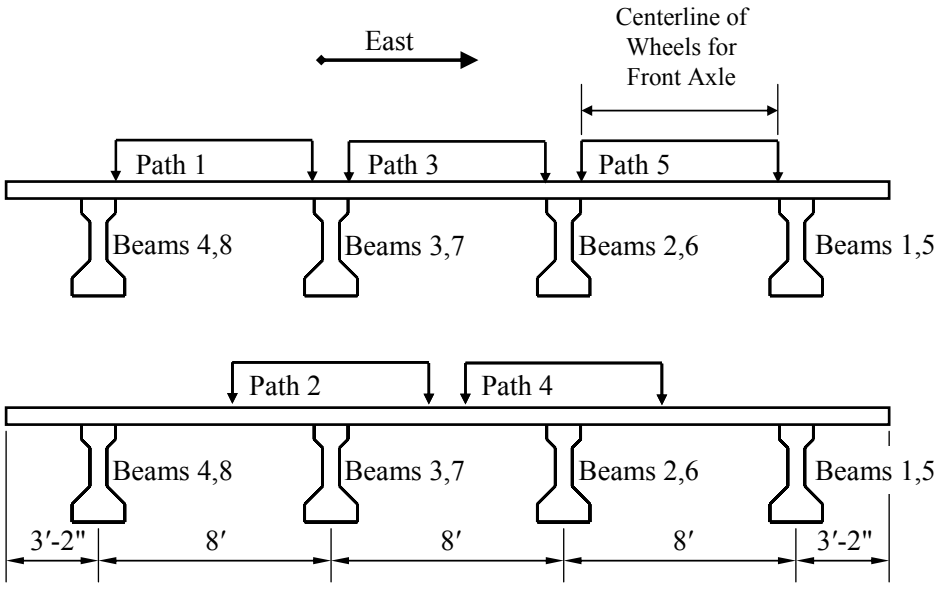

Figure 3.9 Load Paths for Chandler Creek Bridge

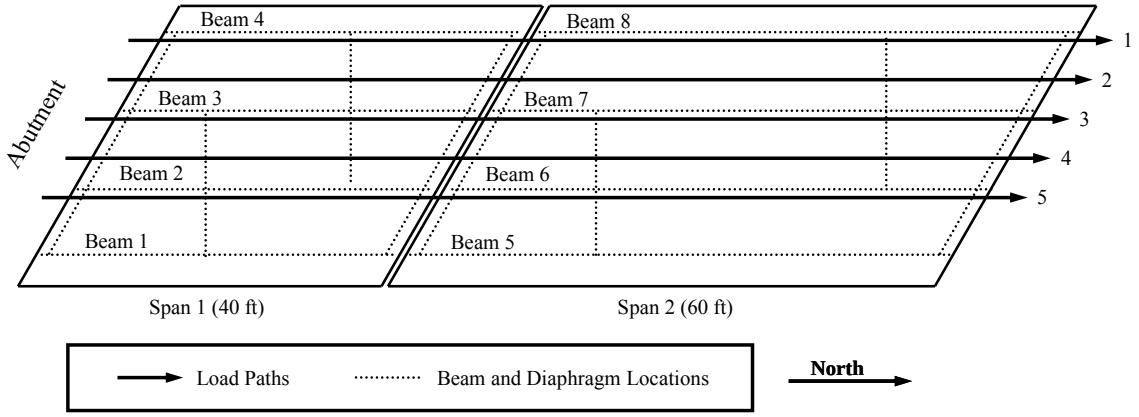

Figure 3.10 Plan View of Load Paths for Chandler Creek Bridge

Five load paths were selected for the Chandler Creek, Lake LBJ, Lampasas River, and Willis Creek Bridges, while seven load paths were selected for the Wimberley Bridge (Table 3.2). Between fifteen and twenty load tests were conducted on each bridge. In all cases, the loading vehicles crossed the bridge in the same direction. Where an instrumented span was adjacent to the abutment, the loading vehicles moved from the abutment onto the bridge.

The speed of the loading vehicles was between 5 and 10 mph. This was selected to limit the dynamic amplification as each axle entered the instrumented span.

Table 3.2 Overview of Diagnostic Load Tests

Bridge Name	Direction of Loading Vehicles	Number of Load Paths	Number of Test Runs			
			Total	Single Truck	Side by Side Trucks	Back to Back Trucks
Chandler Creek	Northbound	5	15	3	6	6
Lake LBJ	Westbound	5	15	3	5	7
Lampasas River	Northbound	5	16	3	4	9
Willis Creek	Eastbound	5	20	5	3	12
Wimberley	Northbound	7	17	7	4	6

3.2 INSTRUMENTATION

Strain gages were used to monitor the response of the bridges during the diagnostic load tests. For the Lake LBJ and Willis Creek Bridges, a single span was instrumented and strain gages were positioned at three locations along each girder (Table 3.3). Two spans were instrumented for the other three bridges. Strain gages were positioned at midspan of each girder and at the two quarter points between the midspans (Figure 3.11). All instruments were located based on the distance between the

centerlines of the supports for the girders. Therefore, the lines of instrumentation were skewed at the same angle as the bridge.

Table 3.3 Locations of Strain Gages

Bridge Name		1/4 *L*	1/2 *L*	3/4 *L*
Chandler Creek	Span 1 (40 ft)		✔	✔
	Span 2 (60 ft)	✔	✔	
Lake LBJ		✔	✔	✔
Lampasas River	Span 1		✔	✔
	Span 2	✔	✔	
Willis Creek		✔	✔	✔
Wimberley	Span 1		✔	✔
	Span 2	✔	✔	

Temperature compensating, 120-ohm, electrical resistance strain gages with a 2-in. gage length were used for all tests. The strain gages were attached to the surface of the prestressed concrete girders on the bottom of the bottom flange, side of the web, and side of the top flange (Figure 3.12). In some cases, the top gages were omitted in order to keep the total number of gages within the capacity of the 55-channel Campbell Scientific CR9000 data logger.

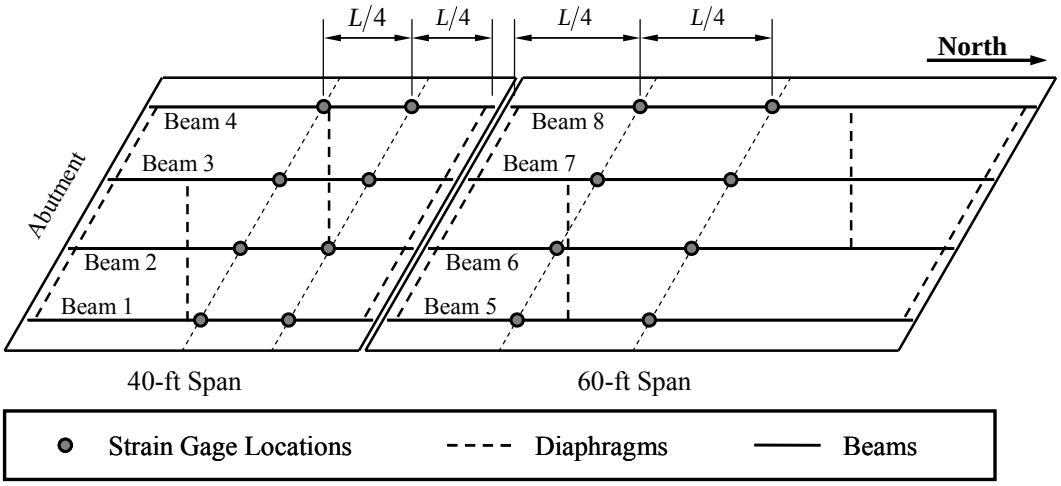

Figure 3.11 Instrumentation Plan for Chandler Creek Bridge

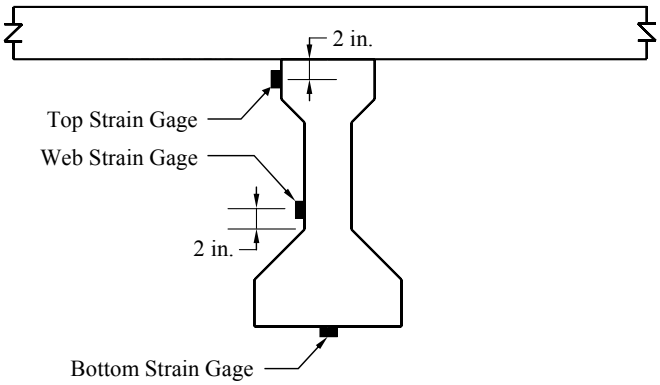

Figure 3.12 Approximate Gage Locations of Strain Gages

The instrumentation, cables, and data acquisition system are shown in place beneath a bridge in Figure 3.13, and a detailed view of the strain gage attached to the bottom flange is shown in Figure 3.14. The research team spent three to five days installing instrumentation and routing the cables in preparation for each diagnostic load test.

Figure 3.13 Instrumentation Used to Monitor Bridge Response during Diagnostic Load Tests

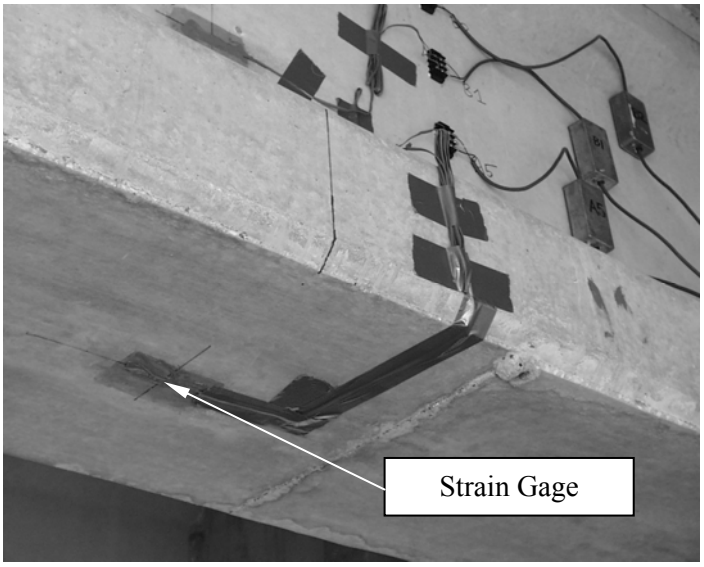

Figure 3.14 Strain Gage Attached to Bottom Flange of Prestressed Girder

3.3 MEASURED RESPONSE OF BRIDGES

Detailed information on the measured strain response of the bridges was reported by Wagener (2002). Sample strain histories from the Chandler Creek Bridge are shown in Figure 3.15 and Figure 3.16. The measured strain is expressed in units of microstrain, and positive values correspond to tensile strains. The position of the centroid of the rear axle is used to define the location of the loading vehicles within the span. Negative values indicate that the front axle of the loading vehicle is within the instrumented span, but the rear axles have not yet entered the span.

The shapes of the strain histories were similar for all bridges and all test runs; however, the amplitude of the strain response varied considerably depending on the transverse location of the loading vehicles. Tensile strains were measured from the gages on the bottom flange and web, while compressive strains were measured from the gages on the top flange. The maximum strains measured for each instrumented span are summarized in Table 3.4, Table 3.5, and Table 3.6.

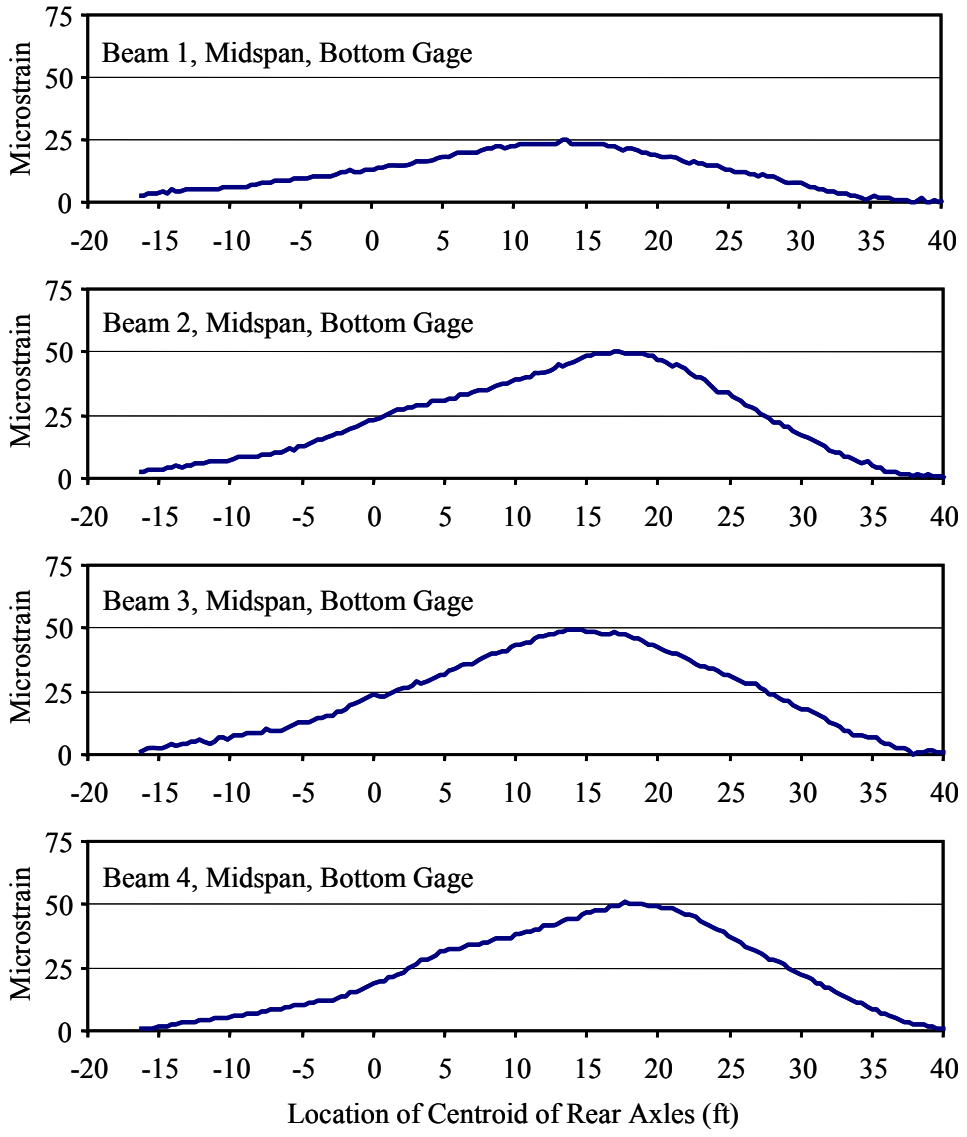

Figure 3.15 Chandler Creek Bridge (40-ft Span) – Side-by-Side Truck Configuration (Run 1)

Table 3.4 Maximum Tensile Strains Measured along Bottom Flange at Midspan

Bridge Name	Beam 1	Beam 2	Beam 3	Beam 4	Beam 5
	$(\mu\varepsilon)$	$(\mu\varepsilon)$	$(\mu\varepsilon)$	$(\mu\varepsilon)$	$(\mu\varepsilon)$
Chandler Creek (40-ft Span)	66	52	51	61	—
Chandler Creek (60-ft Span)	86	68	63	84	—
Lake LBJ	71	88	104	105	—
Lampasas River (Span 1)	89	92	108	139	—
Lampasas River (Span 2)	83	84	97	131	—
Willis Creek	101	87	91	117	—
Wimberley (Span 1)	76	68	65	61	73
Wimberley (Span 2)	76	63	69	66	78

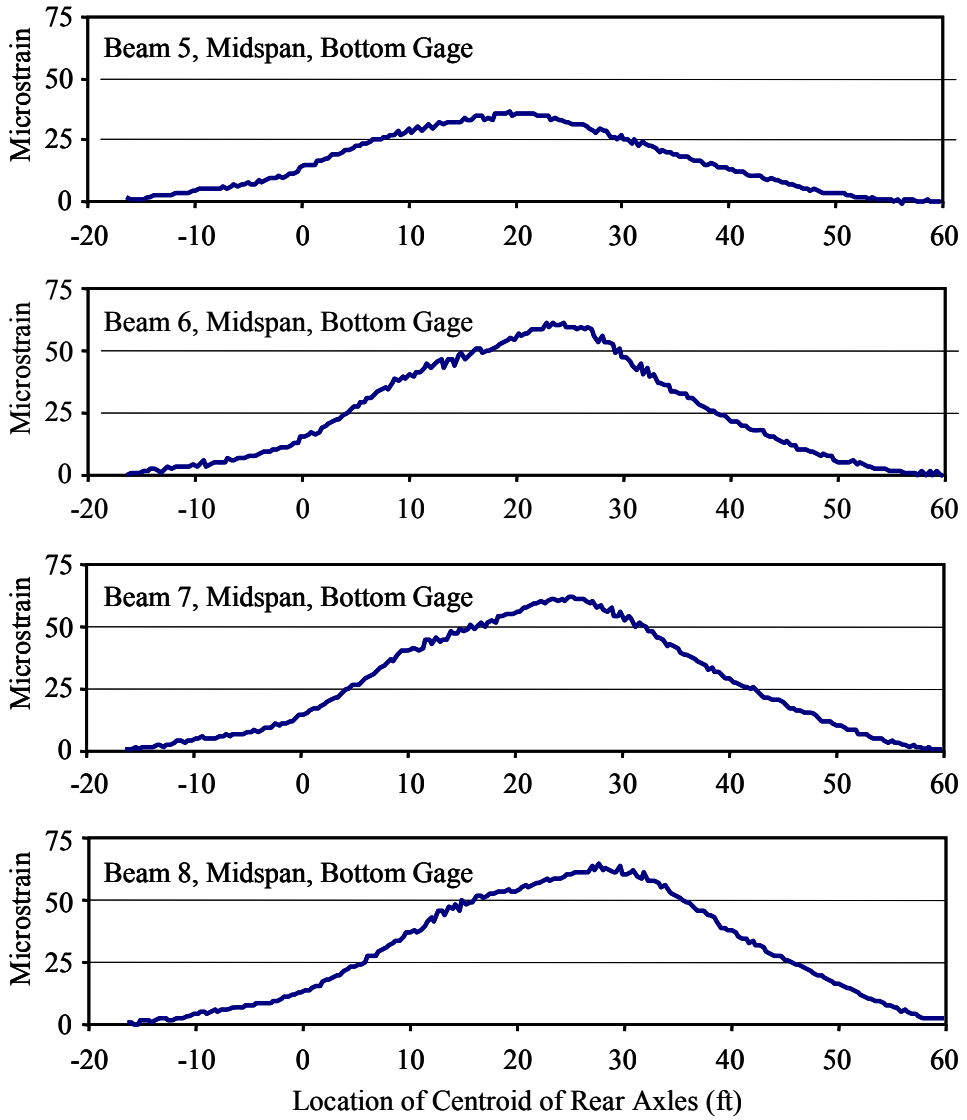

Figure 3.16 Chandler Creek Bridge (60-ft Span) – Side-by-Side Truck Configuration (Run 1)

Table 3.5 Maximum Tensile Strains Measured on Web at Midspan

Bridge Name	Beam 1	Beam 2	Beam 3	Beam 4	Beam 5
	$(\mu\varepsilon)$	$(\mu\varepsilon)$	$(\mu\varepsilon)$	$(\mu\varepsilon)$	$(\mu\varepsilon)$
Chandler Creek (40-ft Span)	28	26	26	28	—
Chandler Creek (60-ft Span)	39	32	30	37	—
Lake LBJ	32	46	56	48	—
Lampasas River (Span 1)	41	53	50	68	—
Lampasas River (Span 2)	39	42	47	69	—
Willis Creek	51	41	40	50	—
Wimberley (Span 1)	40	30	30	27	37
Wimberley (Span 2)	40	*	33	29	36

* Gage malfunctioned.

Table 3.6 Maximum Compressive Strains Measured along Top Flange at Midspan

Bridge Name	Beam 1	Beam 2	Beam 3	Beam 4	Beam 5
	$(\mu\varepsilon)$	$(\mu\varepsilon)$	$(\mu\varepsilon)$	$(\mu\varepsilon)$	$(\mu\varepsilon)$
Chandler Creek (40-ft Span)	-9	-9	-7	-6	—
Chandler Creek (60-ft Span)	-19	-16	-13	-15	—
Lake LBJ	-8	-10	-12	-10	—
Lampasas River (Span 1)	-18	-18	-25	-30	—
Lampasas River (Span 2)	-17	-19	-21	-25	—
Willis Creek	-26	-32	-31	-29	—
Wimberley (Span 1)	—	-11	-5	-11	—
Wimberley (Span 2)	—	-14	-16	-15	—

In most cases, the maximum live load strains recorded during the diagnostic load tests were symmetric with respect to the longitudinal axis of the bridge when the loading vehicles followed symmetric paths. The load paths corresponding to the maximum measured strains were not symmetric for the Lake LBJ and Lampasas River Bridges, and therefore, the measured live load strains in one exterior beam were significantly larger than in the other exterior beam.

3.4 SUMMARY

As discussed in Chapter 4, the diagnostic load tests provided valuable information about the condition of the prestressed concrete bridges considered in this investigation. However, a considerable amount of time is needed to instrument the bridges and to interpret the data. For those reasons, conducting diagnostic load tests as part of a regular inspection program is not recommended.

CHAPTER 4
Evaluation of Diagnostic Load Tests

The primary objective of the diagnostic load tests discussed in Chapter 3 was to obtain information about the condition of the prestressed concrete bridges. The procedure used to estimate the depth of the centroid of the composite cross section from the measured strains is discussed in Section 4.1 and the method used to calculate the girder moments is summarized in Section 4.2. Distribution factors calculated from the measured data are presented and compared with the design values from the AASHTO Standard and LRFD Specifications in Section 4.3. Detailed information about the live load distribution factors calculated using these design standards is discussed in Appendix A.

Throughout the chapter, the measured response of the bridges is compared with the results of linear, three-dimensional finite element analyses. BRUFEM (Bridge Rating Using Finite Element Modeling), which was developed at the University of Florida for the Florida Department of Transportation, was used for all calculations. Details of the finite element models are presented in Hagenberger (2004).

4.1 CENTROID OF COMPOSITE CROSS SECTION

As discussed in Chapter 3, strains were measured at two or three locations over the depth of the prestressed concrete girders at the instrumented sections. Strain profiles are typically assumed to vary linearly with depth, and the total strain at any location is the sum of four components (Figure 4.1): concentric precompression, eccentric precompression, noncomposite dead load, and the combination of superimposed dead load and live load.

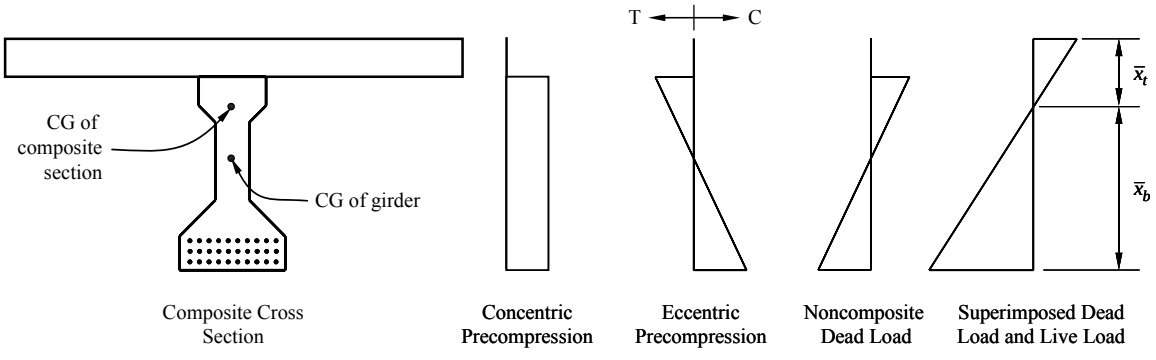

Figure 4.1 Assumed Distribution of Strains in Prestressed Concrete Bridge Girder

Because the strain gages were applied to the surface of the concrete with the precompression and dead loads acting, the measured strains represent the response to live loads only (Figure 4.2). The location of the centroid of the composite cross section, or the depth of zero strain due to live load, can then be approximated using each pair of strain gages:

$$\overline{x}_t = \frac{\varepsilon_t h + \varepsilon_b d_t}{\varepsilon_t + \varepsilon_b} \qquad \text{(top and bottom gages)} \qquad (4.1)$$

$$\overline{x}_t = \frac{\left(\varepsilon_w - \varepsilon_b\right) h + \varepsilon_b d_w}{\varepsilon_w - \varepsilon_b} \qquad \text{(web and bottom gages)} \qquad (4.2)$$

$$\overline{x}_t = \frac{\varepsilon_t \left(h - d_w\right) + \varepsilon_w d_t}{\varepsilon_t + \varepsilon_w} \qquad \text{(top and web gages)} \qquad (4.3)$$

where:

$\overline{x}_t$ = distance from top of slab to location of zero strain due to live load
$\overline{x}_b$ = distance from bottom of girder to location of zero strain due to live load = $\left(h - \overline{x}_t\right)$
ε_t = strain recorded by top gage
ε_w = strain recorded by web gage
ε_b = strain recorded by bottom gage
h = overall depth of composite section
d_t = distance from top of slab to top gage
d_w = distance from bottom of prestressed concrete girder to web gage

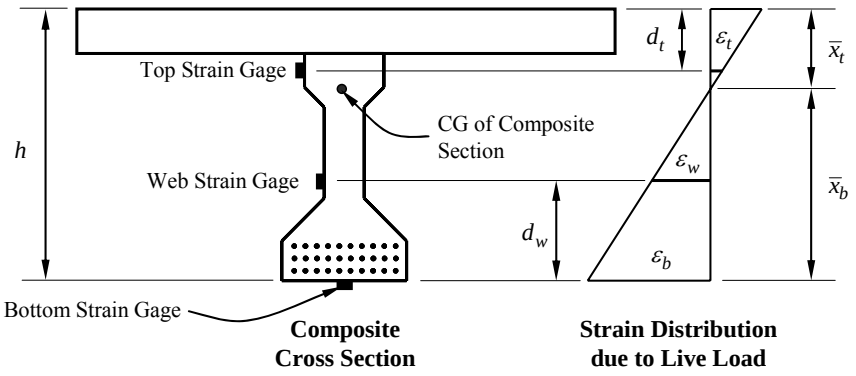

Figure 4.2 Assumed Strain Profile Due to Live Load

These calculations were performed for all possible pairs of gages for each diagnostic load test. Representative data are plotted as a function of the centroid of the rear axles of the loading vehicle in Figure 4.3. The scatter in the data at the beginning and end of the test is typical and occurs when the calculations are based on very small measured strains. To reduce the influence of the scatter, only the data between the vertical lines indicated in Figure 4.3 were considered. The distance between the vertical lines

corresponds to approximately one-third the span of the bridge and this region is centered on the location corresponding to the maximum total midspan moment for the bridge.

The average values of the distance from the top of the slab to the centroid of the composite section calculated for each type of bridge girder are plotted in Figure 4.4. Calculated values corresponding to the transformed composite sections calculated using the specified and estimated 28-day compressive strengths of the concrete (Table 2.17) are also shown. The distances calculated from the measured strains were consistently less than the values calculated using the properties of the transformed composite section. The maximum difference was approximately 20%.

The presence of flexural cracks is the most likely reason that the depth of zero live-load strain calculated from the measured strains is higher in the cross section than the centroid of the composite cross section. Each of the bridges had been in service more than 30 years at the time of the diagnostic load tests. Cracking may have occurred due to an overload or repeated loading at a level that creates a net tension at the bottom of the girder. Overman (1984) and Heller (2003) observed that cracks formed during fatigue tests of prestressed concrete beams when the tensile stress at the bottom fiber was less than half the modulus of rupture.

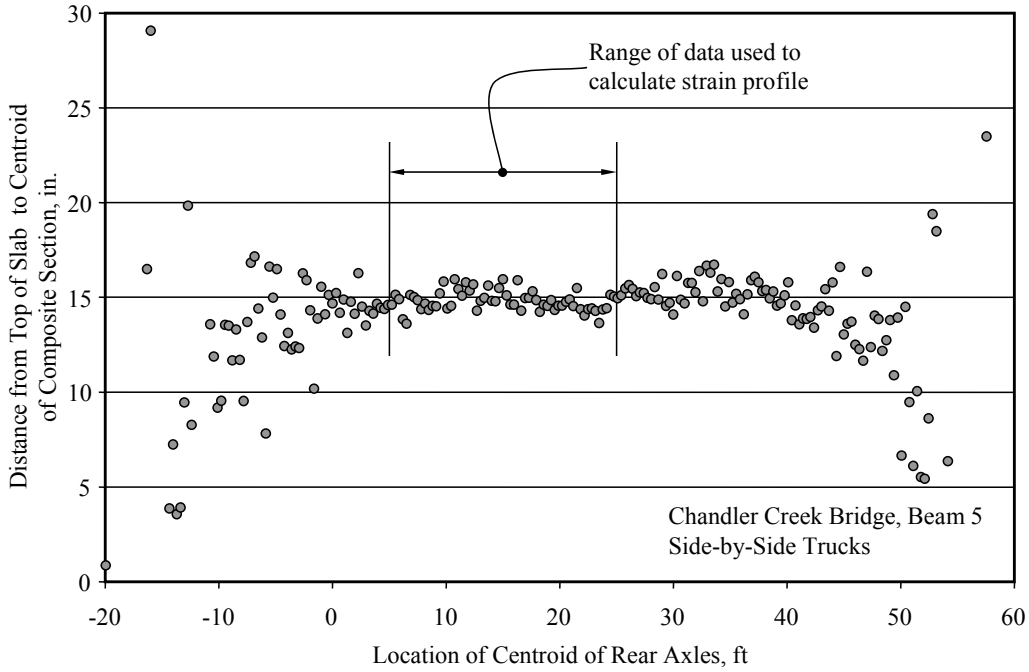

Figure 4.3 Distance from Top of Slab to Centroid of Composite Section Calculated from Measured Strain Data

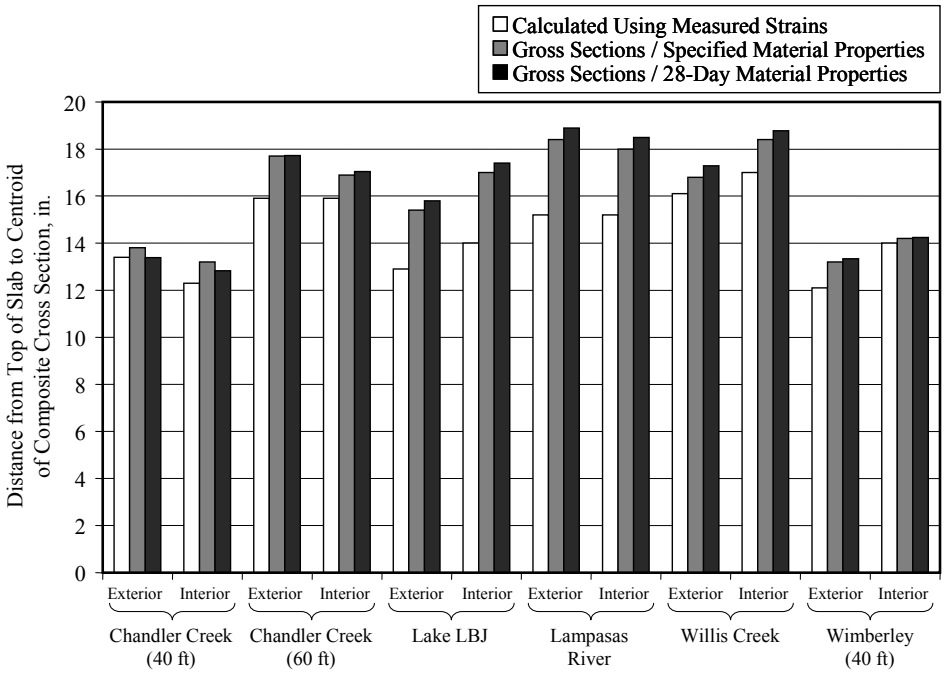

Figure 4.4 Average Depth of Centroid of Composite Cross Section

Based on the measured response of the bridges during the diagnostic load tests, it is reasonable to assume that the bridge girders were cracked. Because the loads applied to the bridges during the diagnostic load tests were low, the precompression in the girders would be sufficient to keep the cracks closed. This explains why the research team did not observe flexural cracks during their initial inspections of the bridges or during the diagnostic load tests.

4.2 MOMENTS IN GIRDERS

Live load moments were calculated from the measured strains by assuming a linear relationship between moment and curvature and a linear variation of live load strain with depth within each girder (Figure 4.5). The moment is directly related to the measured strain:

$$M = E_c I_c \phi_i = E_c I_c \frac{\varepsilon_i}{d_i} \tag{4.4}$$

where

M = moment due to live load in composite girder
E_c = modulus of elasticity of the concrete in the prestressed girder
I_c = gross moment of inertia of the transformed, gross, composite section
ϕ_i = curvature corresponding to measured strains
ε_i = measured strain (gage i)
d_i = distance from strain gage i to the location of zero shear due to live load

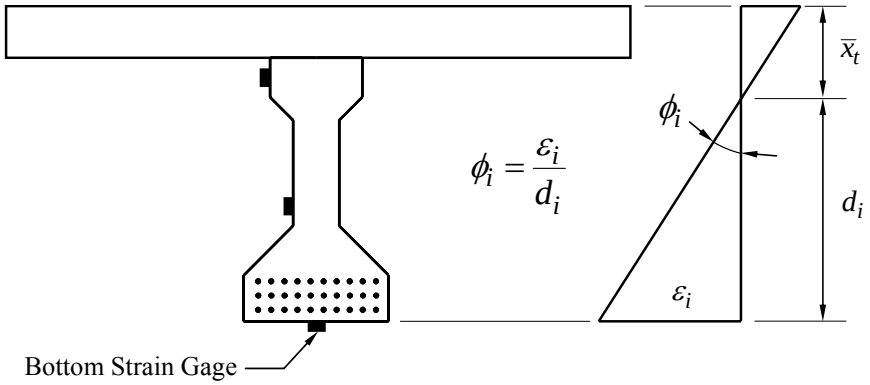

Figure 4.5 Curvature in Composite Girder due to Live Load

The calculated moment in each girder is sensitive to the distance from the top of the slab to the centroid of the composite section, $\bar{x}_t$, because d_i is the distance from the strain gage to the depth of zero live-load strain. Hagenberger (2004) concluded that the depth of zero live-load strain calculated from the measured data should be used to calculate the live load moment in the prestressed concrete girders.

The bottom and web strain gages were used to calculate the moment at midspan of each beam (Eq. 4.4) at each longitudinal vehicle position for each test run. The total moment at midspan of the bridge was then calculated by summing the moments at midspan of each beam:

$$M_t = \sum_{j=1}^{n} M_j \tag{4.5}$$

where

M_t = total moment at midspan of bridge
M_j = moment at midspan of beam j due to measured strains
n = number of beams

As indicated in Figure 4.6, the strain gages were positioned at midspan of each girder. Therefore, the section corresponding to midspan is parallel to the skew of the bridge.

A representative plot of the total moment at midspan as a function of the vehicle position is shown in Figure 4.7. The shapes of the curves calculated using the bottom and web strain gages are similar, but not identical. Of particular interest is the fact that the maximum total moments calculated using the two sets of gages do not occur at the same longitudinal position of the loading vehicle.

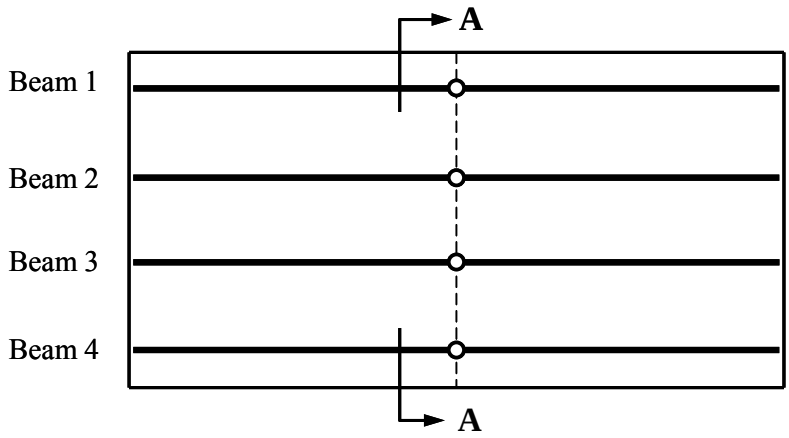

(a) Plan of Bridge without Skew

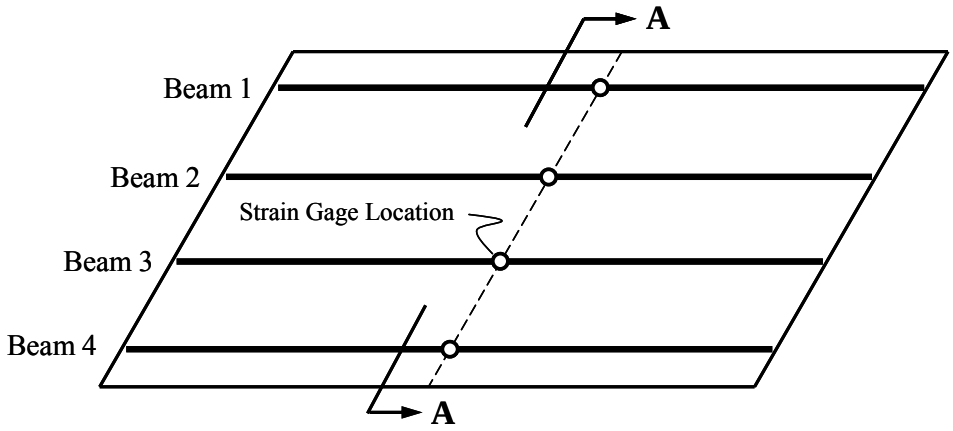

(b) Plan of Bridge with Skew

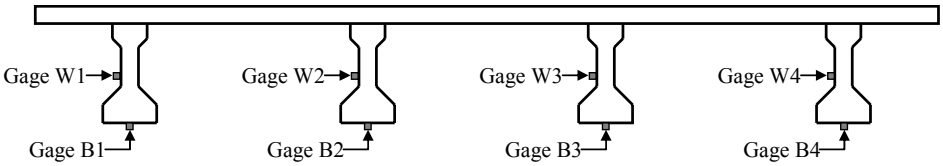

(c) Cross Section of Bridge (A-A)

Figure 4.6 Location of Strain Gages Used to Calculate Total Moment at Midspan

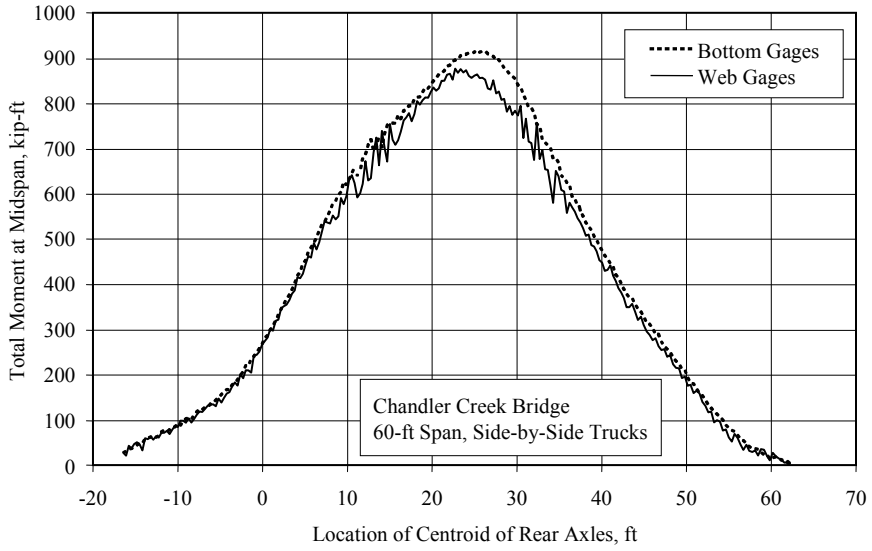

Figure 4.7 Variation of Total Moment at Midspan with Vehicle Location

The maximum total midspan moments for each combination of loading vehicle used in the diagnostic load tests are summarized in Figure 4.8 through Figure 4.12. The results of the finite element analyses are also shown.

For all bridges, the largest maximum total midspan moments were calculated when the two loading vehicles were positioned side by side (Figure 3.5 and Figure 3.6). The smallest maximum total midspan moments were calculated when one loading vehicle crossed the bridge at a time (Figure 3.4 and Figure 3.3). The maximum total midspan moments calculated using the web strain gages were within ±20% of the maximum total midspan moments calculated using the bottom strain gages. In most cases, however, the differences were within ±10%.

The maximum total midspan moments calculated using the finite element analyses were consistently larger than those calculated using the measured strains. The largest differences (approximately 20%) were observed for Span 2 of the Lampasas River Bridge (Figure 4.10) and the smallest differences (approximately 1%) were observed for Span 2 of the Chandler Creek Bridge (Figure 4.8).

The same values of the modulus of elasticity, E_c, and moment of inertia for the composite cross section, I_c, were used in the finite element analyses and to calculate moments from the measured strains. No indications of rotational restraint at the ends of the spans were observed from the measured strains. Therefore, variations in the maximum total midspan moment can not be attributed to differences in the material properties, cross-sectional properties, or boundary conditions. It is likely that the slabs carried a portion of the total moment during the diagnostic load tests, but the instrumentation was not sufficient to determine the magnitude of the moment carried directly by the slab.

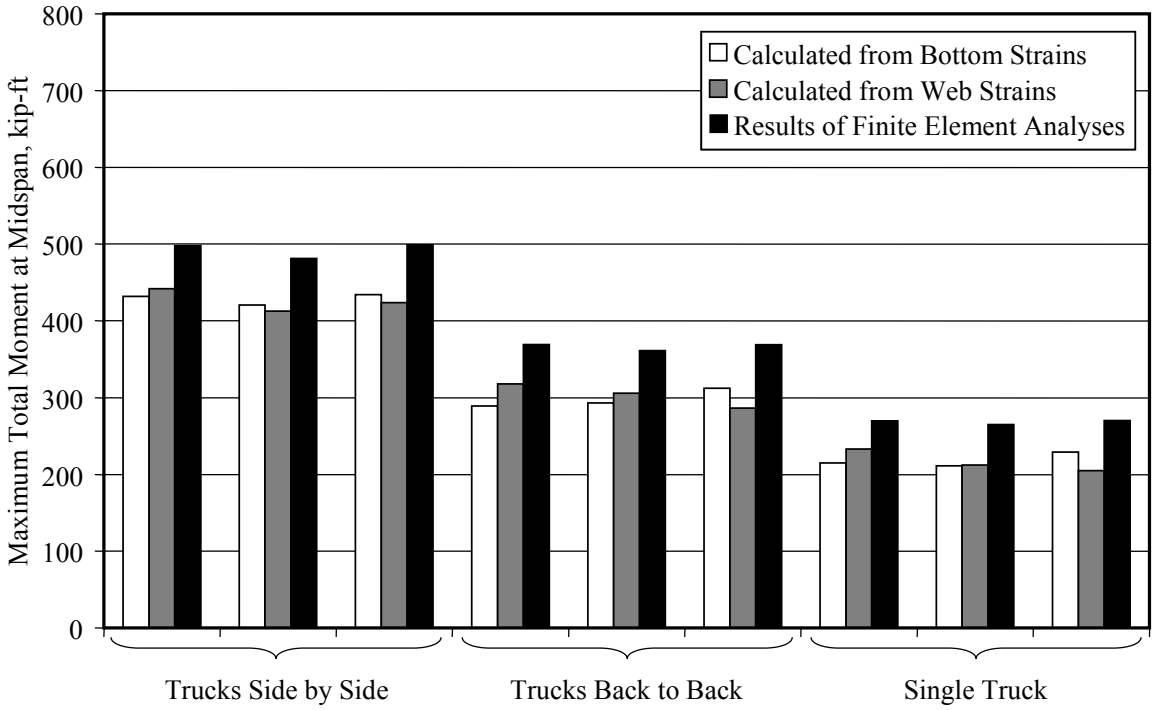

(a) Span 1 (40 ft)

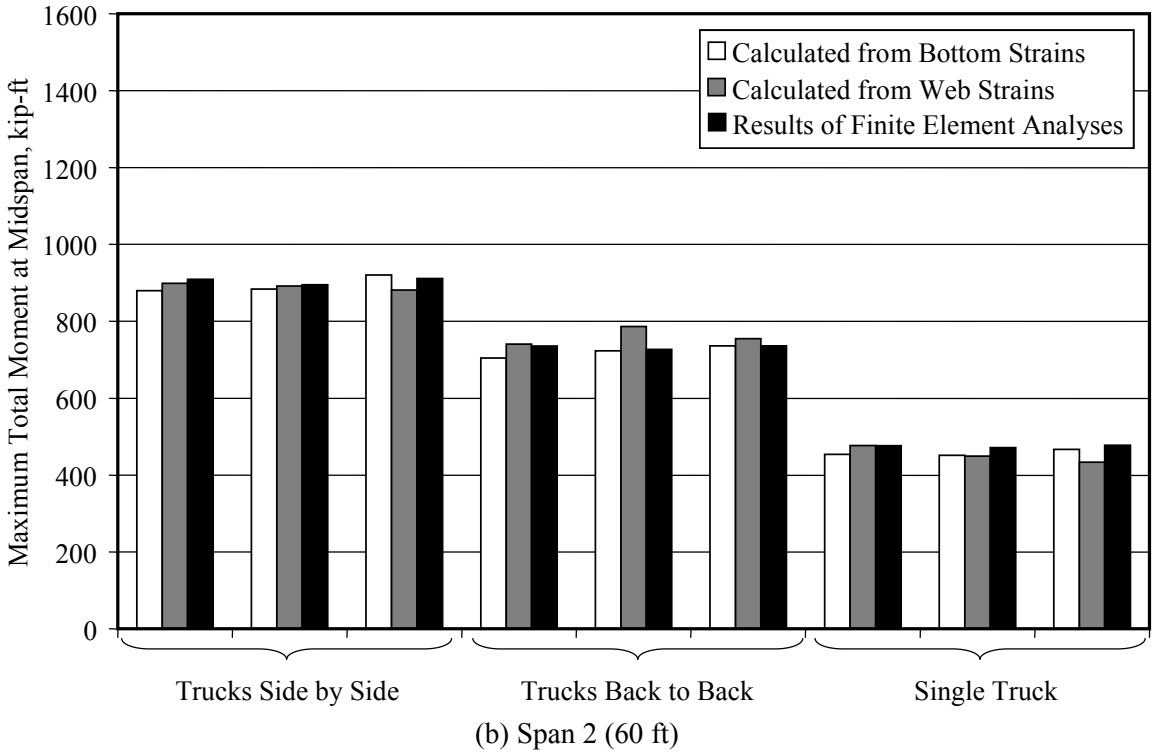

(b) Span 2 (60 ft)

Figure 4.8 Total Live Load Moments at Midspan – Chandler Creek Bridge

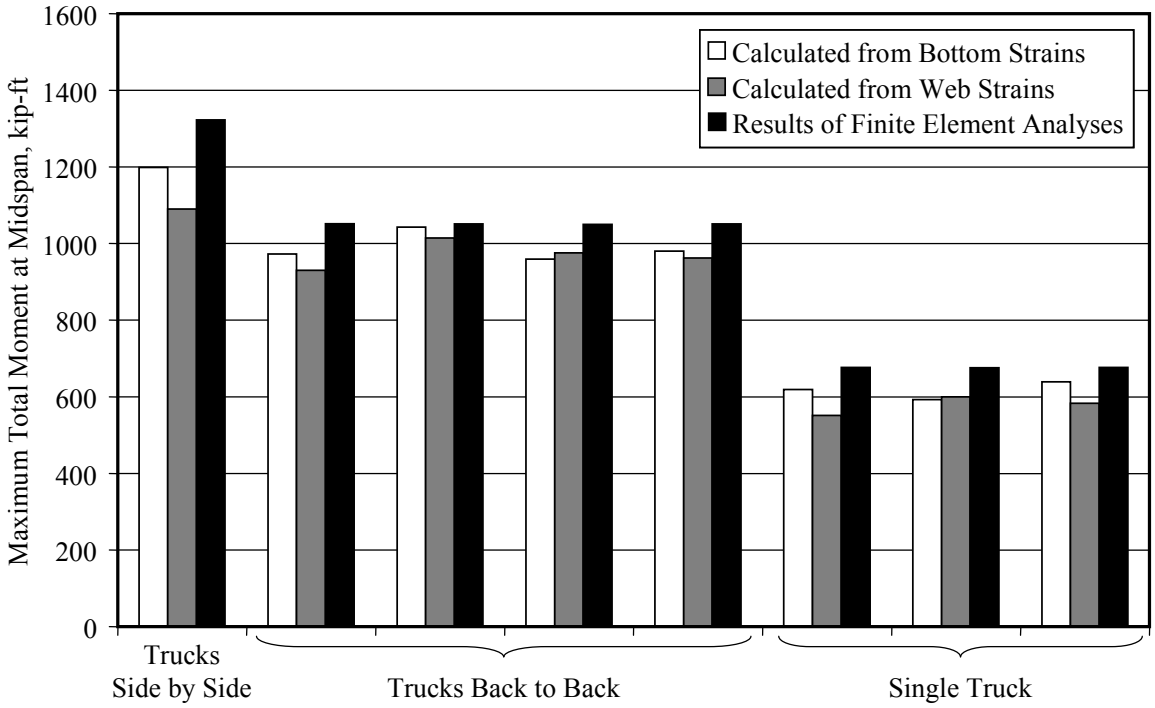

Figure 4.9 Total Live Load Moment at Midspan – Lake LBJ Bridge

4.3 DISTRIBUTION OF LIVE LOAD

Live load distribution factors calculated from the measured data, from the finite element analyses, and from the AASHTO Standard and LRFD Specifications are compared in this section.

4.3.1 Distribution of Live Load Moments Calculated from Measured Strains

As discussed in Section 4.2, the moment at midspan of each girder and the total moment at midspan were calculated from the measured strains for each run in the diagnostic load tests. The portion of the maximum total moment at midspan carried by each girder is represented by the factor γ:

$$\gamma = \frac{M_j}{(M_t)_{max}} \tag{4.6}$$

where

M_j = moment at midspan of beam *j* due to measured strains

$(M_t)_{max}$ = maximum total moment at calculated at midspan of bridge

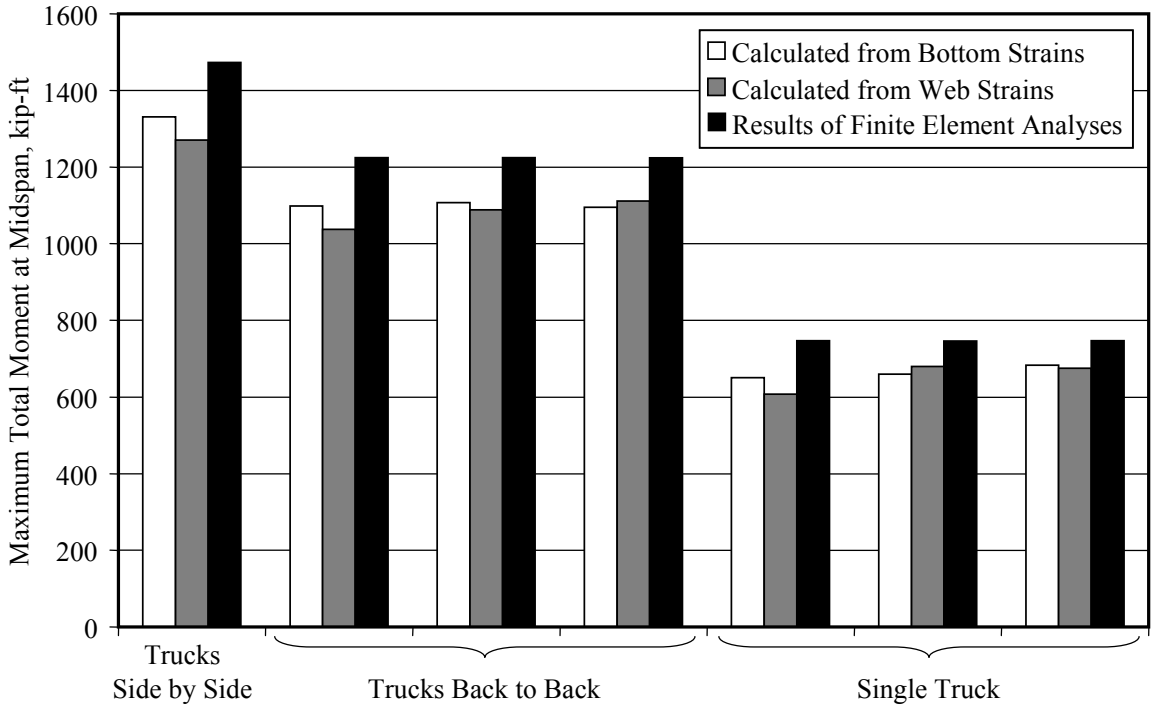

(a) Span 1

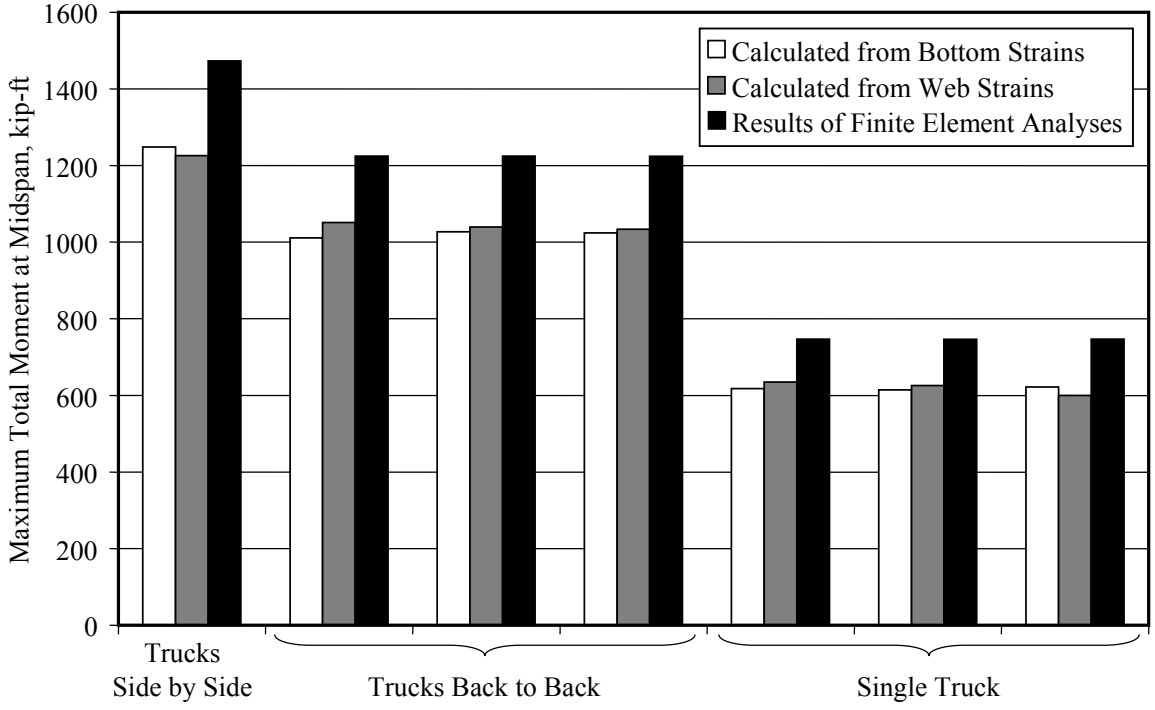

(b) Span 2

Figure 4.10 Total Live Load Moments at Midspan – Lampasas River Bridge

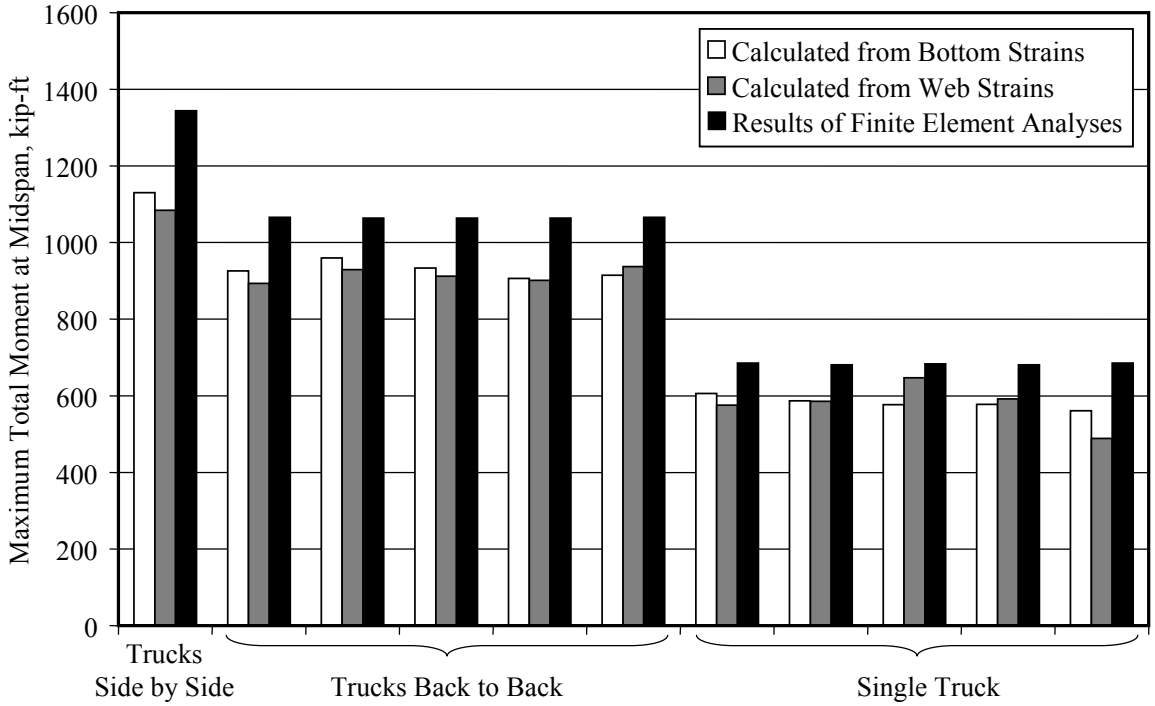

Figure 4.11 Total Live Load Moments at Midspan – Willis Creek Bridge

A representative plot is shown in Figure 4.13. At the vehicle location corresponding to the maximum moment in this girder, approximately 30% of the maximum total moment at midspan was distributed to this exterior girder. Hagenberger (2004) provided summaries of the maximum values of γ for each bridge girder and each run. Because the maximum moments in the girders do not occur at the same vehicle location, the sum of the maximum values of γ is typically between 1.0 and 1.1.

The values of the maximum total moment at midspan varied depending on the number and position of the loading vehicles (Figure 4.8 through Figure 4.12). Therefore, the values of γ can not be compared directly with the live load distribution factors. For consistency with the AASHTO LRFD Specifications, the live load distribution factors calculated from the measured strains were expressed in terms of a single design lane:

$$LLDF = \gamma \quad \text{(single truck and back-to-back trucks)} \tag{4.7}$$

$$LLDF = 2\gamma \quad \text{(side-by-side trucks)} \tag{4.8}$$

The resulting live load distribution factors, which represent the maxima from all the diagnostic load tests, are summarized in Table 4.1.

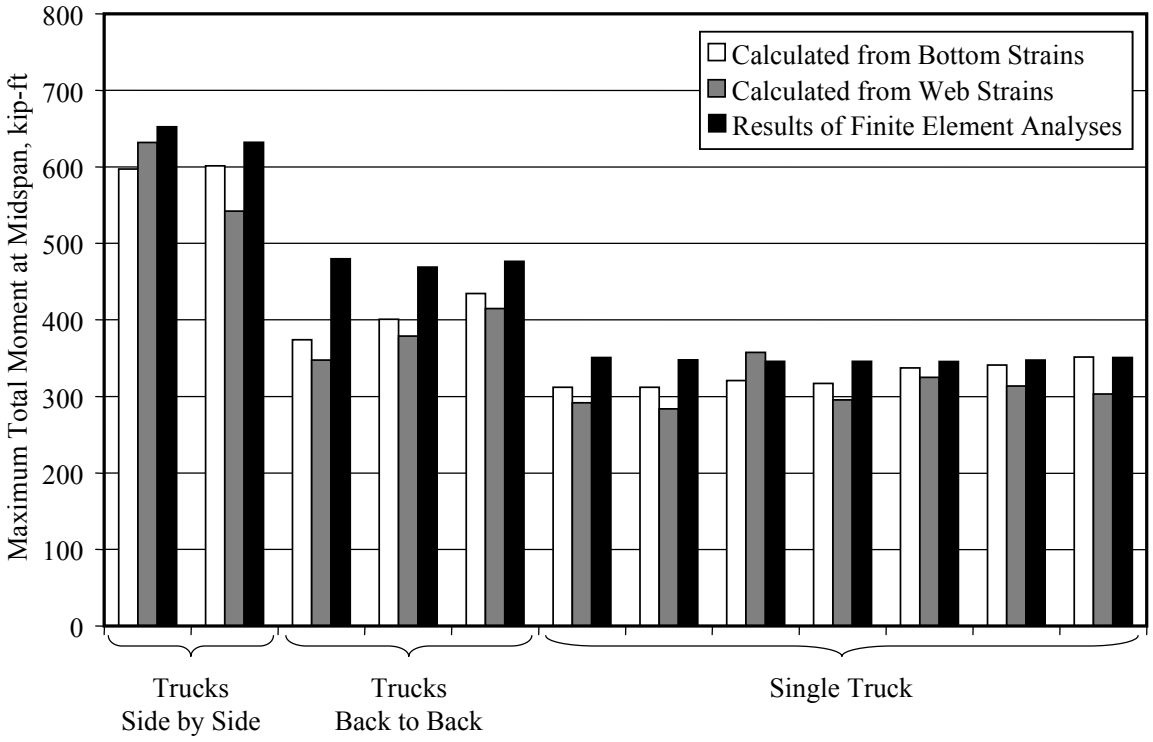

(a) Span 1

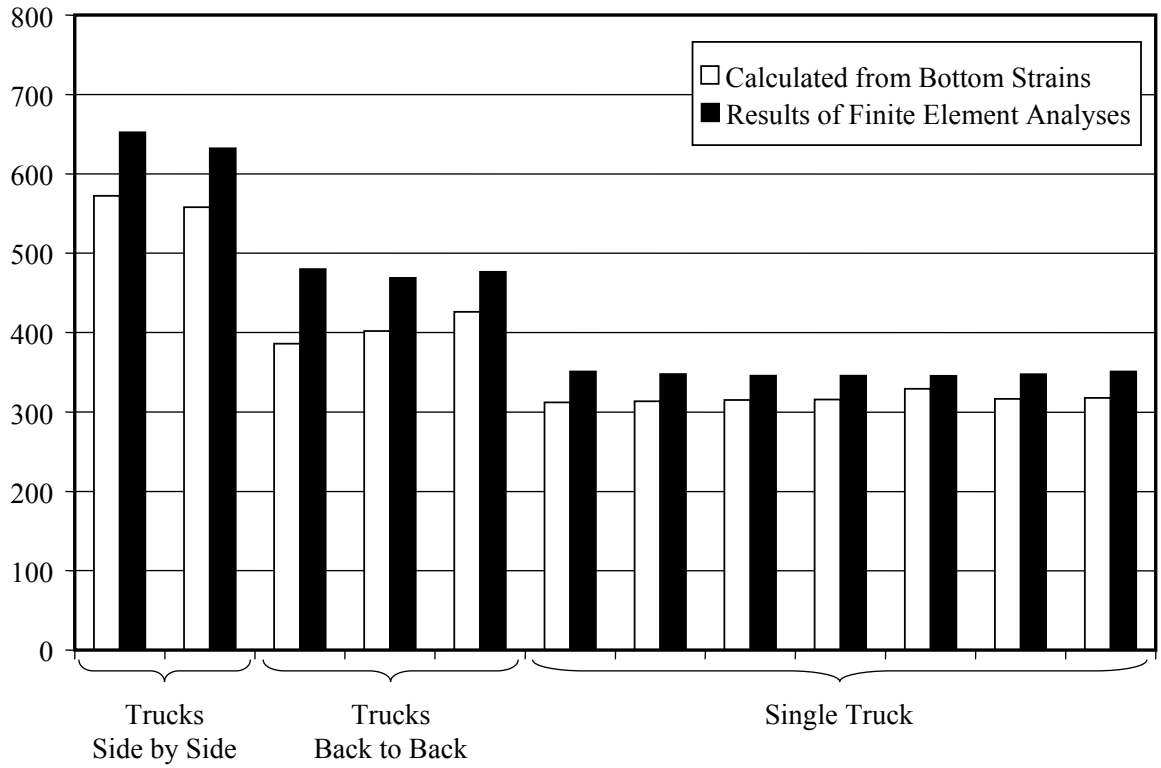

(b) Span 2

Figure 4.12 Total Live Load Moments at Midspan – Wimberley Bridge

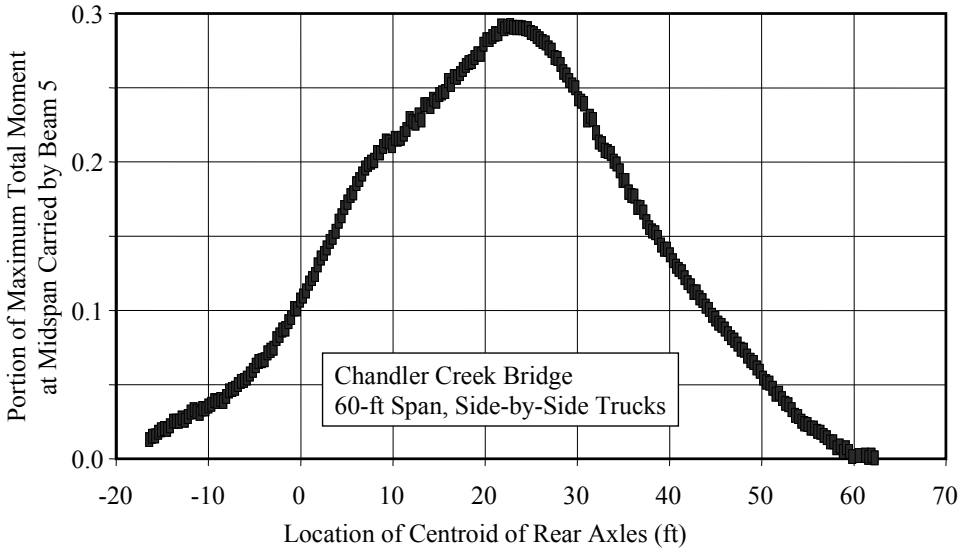

Figure 4.13 Portion of Maximum Total Moment at Midspan Carried by Exterior Girder

When side-by-side trucks were used to load two lanes, the distribution factors ranged from 0.50 to 0.64 for the interior girders and from 0.50 to 0.62 for the exterior girders. The live load distribution factors were lower when a single truck or back-to-back trucks were used, and the values ranged from 0.35 to 0.51 for interior girders and from 0.48 to 0.58 for the exterior girders. When two spans of the same length were tested on the same bridge, the differences in the live load distribution factors tended to be less than 5%.

Table 4.1 Maximum Live Load Distribution Factors Determined from Measured Strains

Bridge Name	Interior Beams		Exterior Beams	
	One Lane†	Two Lanes††	One Lane†	Two Lanes††
Chandler Creek, 40 ft Span	0.51	0.64	0.58	0.62
Chandler Creek, 60 ft Span	0.40	0.63	0.52	0.60
Lake LBJ	0.38	0.51	0.52	0.53
Lampasas River, Span 1	0.37	0.54	0.48	0.50
Lampasas River, Span 2	0.35	0.50	0.50	0.51
Willis Creek	0.38	0.50	0.51	0.55
Wimberley, Span 1	0.47	0.55	0.51	0.55
Wimberley, Span 2	0.46	0.59	0.48	0.55

† LLDF from tests with a single truck or back-to-back trucks.
†† LLDF from tests with side-by-side trucks.

4.3.2 Distribution of Live Load Moments from Finite Element Analyses

Each of the runs from the diagnostic load tests was reproduced using finite element analyses, with the loading vehicles moving along the same paths. Live load distribution factors were calculated from the results of these analyses using the same approach discussed in Section 4.3.1. The results are summarized in Table 4.2.

Table 4.2 Maximum Live Load Distribution Factors from Finite Element Analyses

Bridge Name	Interior Beams		Exterior Beams	
	One Lane†	Two Lanes††	One Lane†	Two Lanes††
Chandler Creek, 40 ft Span	0.38	0.64	0.49	0.69
Chandler Creek, 60 ft Span	0.35	0.60	0.46	0.59
Lake LBJ	0.34	0.50	0.45	0.51
Lampasas River	0.33	0.51	0.42	0.51
Willis Creek	0.34	0.50	0.44	0.50
Wimberley	0.39	0.49	0.49	0.52

† LLDF for single truck or back-to-back trucks.
†† LLDF for side-by-side trucks.

The results from the finite element analyses are compared with the results from the diagnostic load tests in Figure 4.14. In general, the live load distribution factors calculated using finite element analyses were less than those calculated from the measured strains. The differences were within 10% for both interior and exterior girders when the loading vehicles were positioned side by side. The differences tended to be between 10 and 20% when a single truck or back-to-back trucks were used.

4.3.3 Comparisons with AASHTO Design Specifications

The live load distribution factors calculated using the AASHTO Standard and LRFD Specifications are presented in Appendix A for the five bridges considered. Those values are compared with the live load distribution factors calculated from the measured data in Figure 4.15. As discussed in Appendix A, the LRFD live load distribution factors for a single loading lane have been divided by the multiple presence factor (m=1.2) to facilitate comparisons with the diagnostic load tests with one truck or back-to-back trucks.

The live load distribution factors calculated using the AASHTO Standard Specifications exceeded the measured response in all cases. The differences tended to be smallest for the bridges with the shorter spans (40-ft span of Chandler Creek Bridge and Wimberley Bridge).

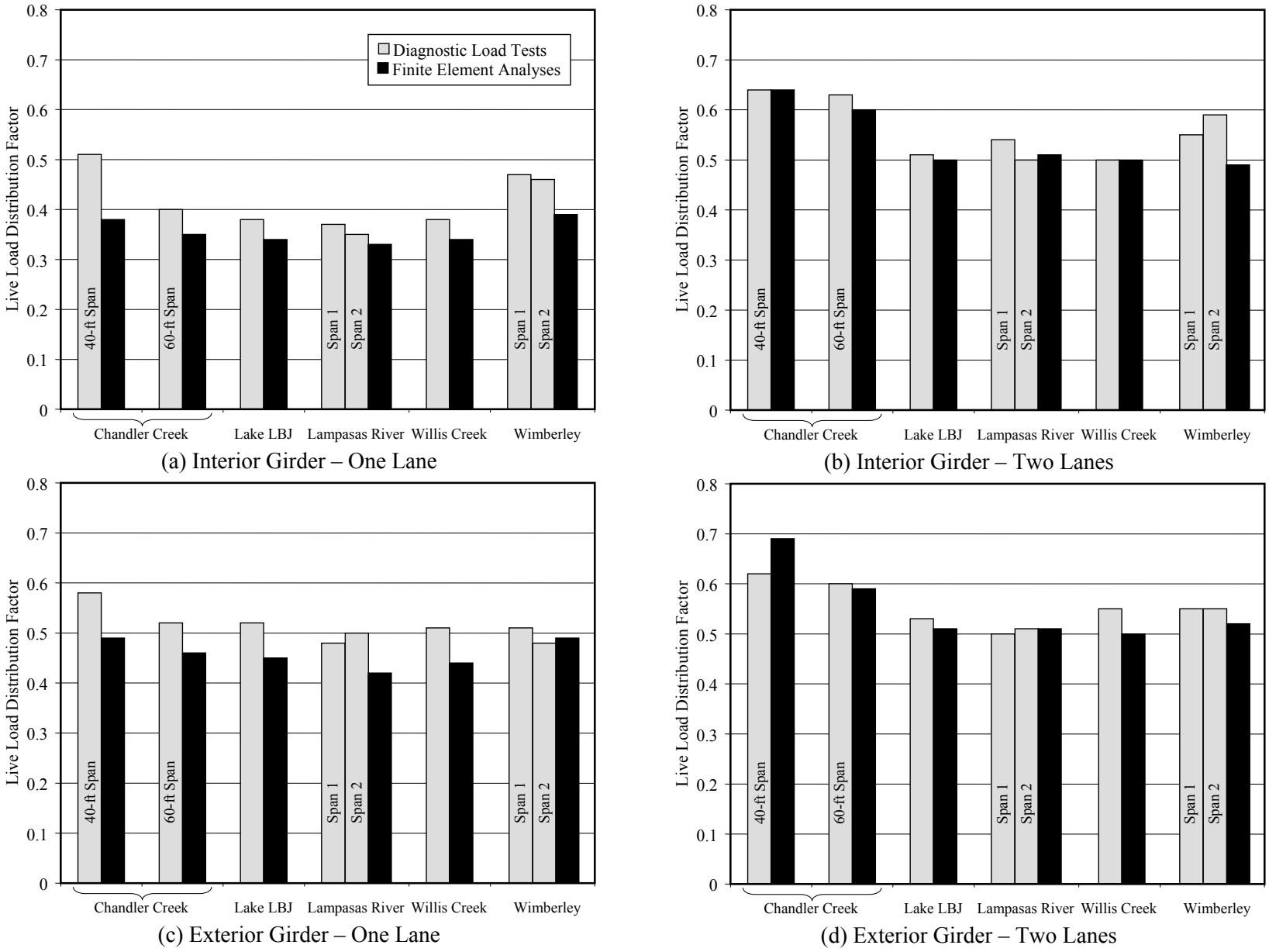

Figure 4.14 Comparison of Live Load Distribution Factors Calculated from Diagnostic Load Tests and Finite Element Analyses

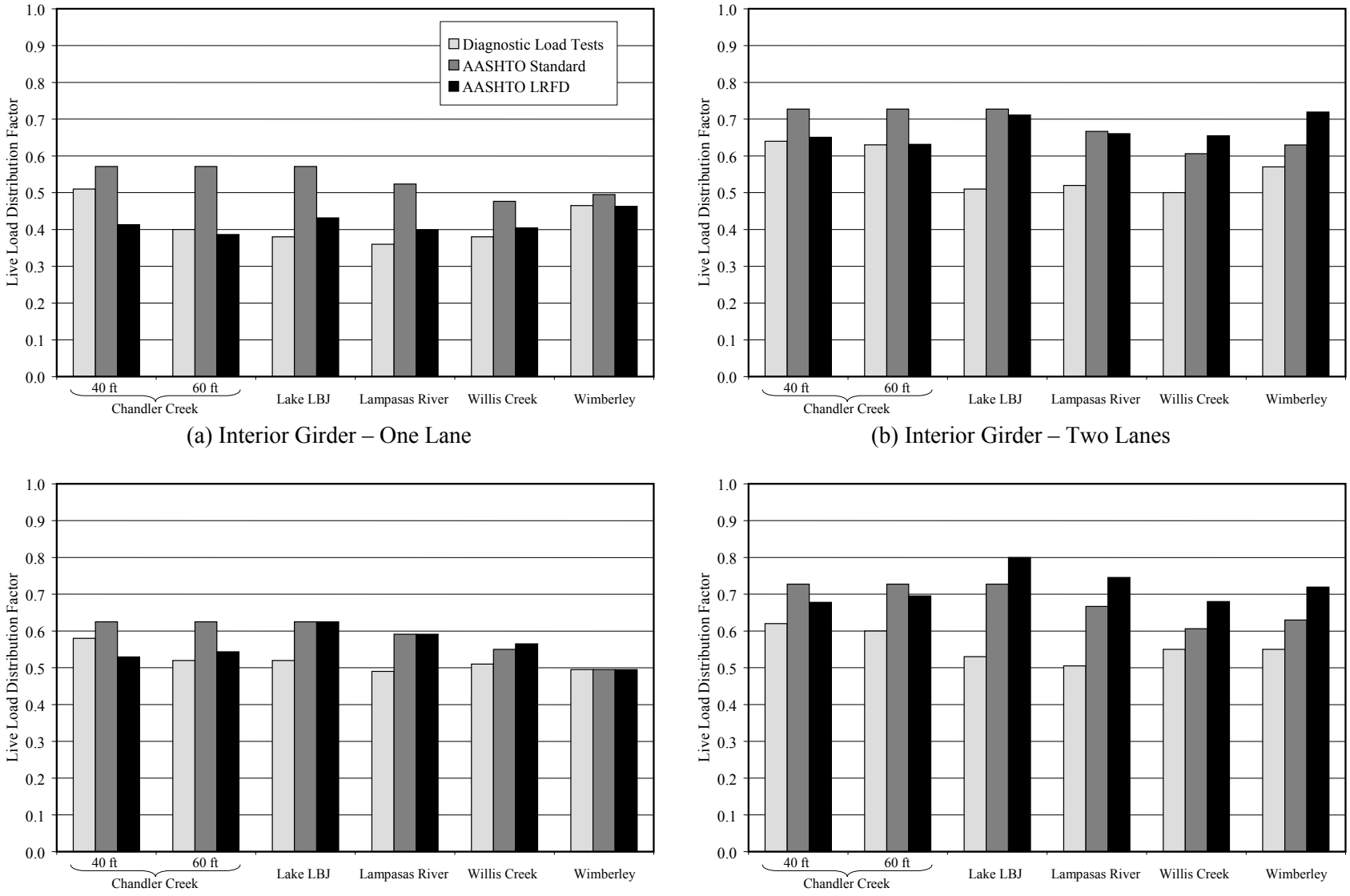

(a) Interior Girder – One Lane

(b) Interior Girder – Two Lanes

(c) Exterior Girder – One Lane

(d) Exterior Girder – Two Lanes

Figure 4.15 Comparison of Live Load Distribution Factors Calculated from Diagnostic Load Tests and AASHTO Specifications

Comparisons between the LRFD distribution factors and the results of the diagnostic load tests exhibited more variations. For cases with side-by-side loading vehicles, the LRFD distribution factors exceeded the measured response for all bridges. However, the differences were very small for the skewed spans (Chandler Creek Bridge) while the moment distributed to the exterior girders in the non-skewed bridges was overestimated by more than 50% in some cases (Lake LBJ Bridge). For skewed bridges with one loading vehicle, the LRFD distribution factors underestimated those from the diagnostic load tests for both interior and exterior girders. For non-skewed bridges with one loading vehicle, the LRFD provided a closer approximation to the measured response for the interior girders, while the Standard Specification provided a slightly better approximation for the exterior girders.

4.4 SUMMARY

The data recorded during the diagnostic load tests provided valuable information about the live load response of the five prestressed concrete bridges studied in this investigation. Although no visible evidence of cracking was observed, the depth of zero strain under live load was closer to the top surface of the slab than the calculated centroid of the composite cross section.

Although the bridges tested shared a number of important characteristics, the distribution of live load moments among the prestressed concrete girders varied from bridge to bridge. The live load distribution factors from the AASHTO Standard Specifications provided a conservative estimate of the measured response of the bridges. The live load distribution factors from the AASHTO LRFD Specifications were conservative in most cases, but underestimated the measured response for girders in skewed bridges with one lane loaded. The LRFD distribution factors were also more variable compared with the measured response than the distribution factors from the Standard Specifications.

CHAPTER 5
Laboratory Fatigue Tests

This chapter summarizes the design, fabrication, instrumentation, and testing program for six prestressed concrete beams. The one-quarter-scale specimens were designed to represent key features of the interior girder from the 60-ft span of the Chandler Creek Bridge, which was selected as the prototype for this investigation.

The initial objective of the fatigue tests was to evaluate the relationship between the maximum tensile stress in the concrete and the fatigue life of prestressed concrete beams. However, as discussed in Chapter 1, the fatigue life of prestressed concrete beams is controlled by the range of stress experienced by the prestressing strands due to the applied loads and the tensile stress in the concrete was found to be a poor indicator of the stress range in the strand. Therefore, stress range in the strand was used as the critical parameter for designing the laboratory fatigue tests.

The geometry of the laboratory specimens is discussed in Section 5.1 and the calculated ranges of strand stress in the prototype beam are summarized in Section 5.2. The construction of the test specimens is presented in Section 5.3, the set-up used for the fatigue tests is discussed in Section 5.4, and the procedures used to determine the effective prestress force in the test specimens are summarized in Section 5.5. The calculated ranges of strand stress in the test specimens are presented in Section 5.6, and the procedures used to test the specimens in fatigue are discussed in Section 5.7.

5.1 GEOMETRY OF TEST SPECIMENS

The test specimens were one-quarter scale representations of the prototype bridge girder. The cross-sectional geometry was simplified to facilitate construction, but key relationships between section properties were maintained. The dimensions of the test specimens are shown in Figure 5.1 and Figure 5.2, and the cross-sectional properties are summarized in Table 5.1. Ratios of section properties for both the prototype beam and test specimens are compared in Table 5.2. The differences in these geometrical parameters varied from 0 to 17%, with an average difference of 6%.

The compressive strengths of the concrete used for design were 6000 psi for the web concrete at release, 10,000 psi for the web concrete at the start of the fatigue tests, and 6000 psi for the slab concrete at the start of the fatigue tests. The measured compressive strengths of the concrete exceeded the specified values by up to 25%. While the geometry of the specimens was determined early in the design process, the loads applied during the fatigue tests could not be calculated until the actual material properties were known. Therefore, the differences between the measured and specified strengths were incorporated into the design process.

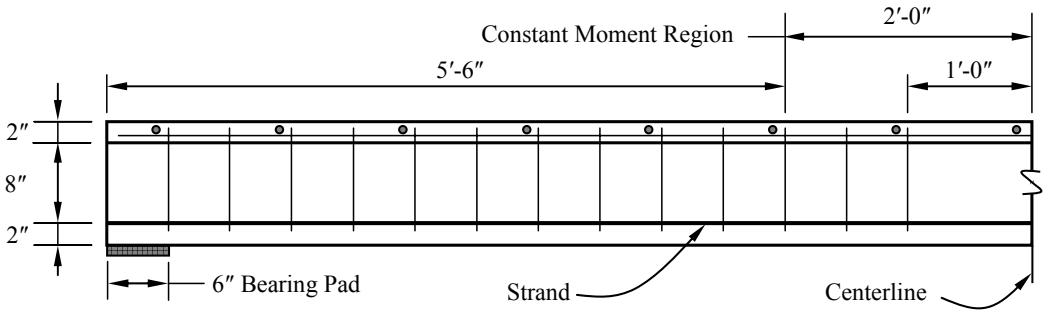

Figure 5.1 Elevation of Test Specimens

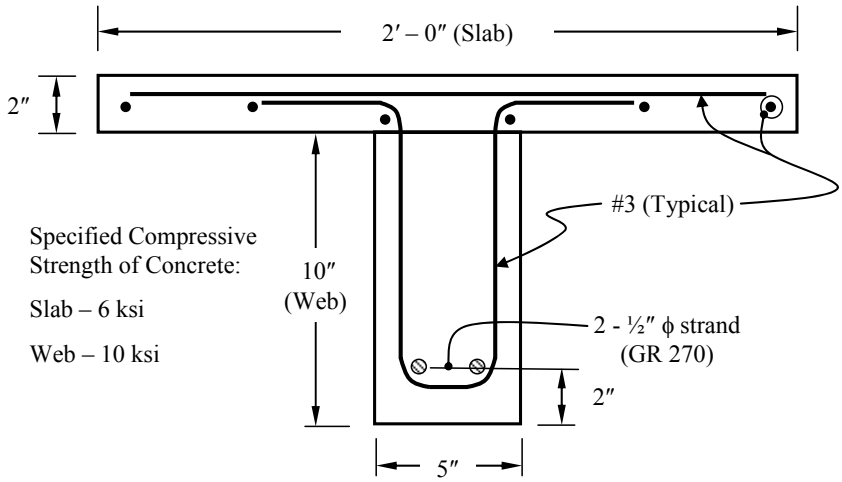

Figure 5.2 Cross Section of Test Specimens

Table 5.1 Properties of Prototype Bridge Beam and Fatigue Test Specimens

Property		Prototype Bridge*	Test Specimen†
Beam Length	L	60 ft	15 ft
Composite Beam Depth	h_{bc}	47.25 in.	12 in.
Effective Slab Width	b_e	94 in.	24 in.
Beam Moment of Inertia	I_b	82,800 in.^{4}	417 in.^{4}
Composite Beam Moment of Inertia	I_c	272,000 in.^{4}	1200 in.^{4}
Area of Beam	A_g	496 in.^{2}	50 in.^{2}
Transformed Area of Composite Beam	$A_{g,tr}$	1020 in.^{2}	90 in.^{2}
Area of Prestressing Steel	A_{ps}	3.24 in.^{2}	0.306 in.^{2}
Neutral Axis of Composite Beam	y_{bc}	30.42 in.	7.48 in.

* Cross-sectional properties based on estimated 28-day compressive strength of concrete for the Chandler Creek 60-ft span.

† Cross-sectional properties based on specified compressive strength of concrete for test specimens.

Table 5.2 Parameters from Prototype Bridge Beam and Fatigue Test Specimens

Parameter	Prototype Bridge	Test Specimen	Difference
L/h_{bc}	15	15	0 %
b_e/h_{bc}	2	2	0 %
I_c/I_b	3.3	2.9	12 %
A_g/A_{ps}	153	163	6 %
$A_{g,tr}/A_g$	2.1	1.8	17 %
$A_{g,tr}/A_{ps}$	321	294	8 %
h_{bc}/y_{bc}	1.56	1.63	2 %

5.2 ANALYSIS OF PROTOTYPE BRIDGE GIRDER

The prototype bridge girder was analyzed to determine the relationship between live load moment and change in stress in the strand induced by the live load. Five live load conditions were used to generate each relationship and are defined in Table 5.3. The resulting relationship between live load moment and strand stress range for estimated in situ material properties is shown in Figure 5.3.

Table 5.3 Definition of Analysis Points for Prototype Beam

Point	Description
1	Full dead load state
2	Decompression of bottom fiber
3	Neutral axis at bottom of web
4	Neutral axis at top of web
5	Flexural capacity
A	Maximum tensile stress of $6\sqrt{f_c'}$
B	Maximum tensile stress of $7.5\sqrt{f_c'}$
C	Maximum tensile stress of $12\sqrt{f_c'}$

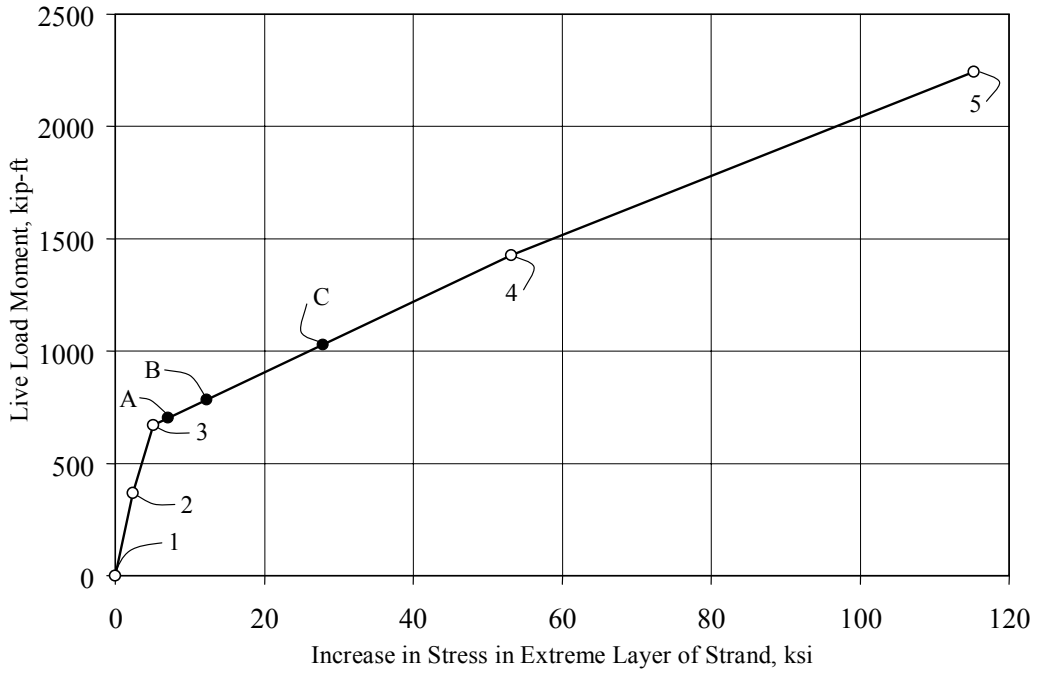

Figure 5.3 Calculated Live Load Response of Prototype Beam

Data point 1 represents the condition of zero live load. The effects of prestress losses and dead load are considered. Prestress losses were estimated using the procedures in the AASHTO LRFD Specifications. Dead loads include the weights of the beam, deck, diaphragms, overlay, and an allowance for miscellaneous dead load. The prestressed beams were assumed to be unshored during the placement of the deck. Data point 2 corresponds to the live load that results in zero net stress at the bottom fiber of the cross section, and is called the decompression point. Data points 3 and 4 were determined by specifying the neutral axis of the composite section and calculating the moment corresponding to equilibrium. Data point 5 corresponds to the flexural capacity of the composite cross section.

Data points 1, 2, and 3 were calculated using compatibility and equilibrium. Stress and strain were assumed to be linearly related in both the concrete and the prestressing steel. Data points 4 and 5 were calculated using strain compatibility and the stress-block factors (Collins and Mitchell, 1997) to estimate the nonlinear stress-strain relationship in the concrete. A detailed discussion of the methods used to analyze the bridge girders at each level of applied load is presented in Hagenberger (2004), and the results are summarized in Appendix B for all five bridges.

The stress range in the strand was also determined for each level of limiting tensile stress in the concrete. The total moments corresponding to tensile stress levels of $6\sqrt{f_c'}$, $7.5\sqrt{f_c'}$, and $12\sqrt{f_c'}$ in the precompressed tension zone were calculated using the gross, transformed cross-sectional properties. The cross sections were assumed to be uncracked in these calculations for consistency with typical practice. The dead load moment was then subtracted from the total moment, and the resulting live load moment was used to determine the stress range in the strand from the five data points plotted in Figure 5.3. Table 5.4 summarizes the results of the analyses of the prototype beam.

The results from the analyses of the other bridges studied in this investigation are summarized in Table 5.5. The strand stress range varies from 4 to 40 ksi, 5 to 45 ksi, and 15 to 65 ksi at tensile stress levels of $6\sqrt{f_c'}$, $7.5\sqrt{f_c'}$, and $12\sqrt{f_c'}$, respectively. These data indicate that as the maximum tensile stress in the concrete increases, the strand stress range increases, but there is no direct relationship between the tensile stress in the concrete and the variation in the strand stress due to live load. The data do indicate, however, that for a given value of maximum tensile stress in the concrete, the range in strand stress decreases with an increase in the span length of the bridges (Figure 5.4).

Table 5.4 Estimated Live Load Response of Prototype Bridge Girder

Maximum Tensile Stress in Concrete	Calculated Strand Stress Range (ksi)	Calculated Median Strand Stress (ksi)	M_L (kip-ft)
$6\sqrt{f_c'}$	7.1	138	703
$7.5\sqrt{f_c'}$	12.3	141	784
$12\sqrt{f_c'}$	27.9	149	1029

Table 5.5 Calculated Relationships between Maximum Tensile Stress in Concrete and Variation of Tensile Stress in Strand

Bridge	Interior Girder		Exterior Girder	
	Calculated Strand Stress Range (ksi)	M_L (kip-ft)	Calculated Strand Stress Range (ksi)	M_L (kip-ft)
Maximum Tensile Stress in Concrete = $6\sqrt{f_c'}$				
Chandler Creek (40-ft Span)	15.3	496	16.9	518
Chandler Creek (60-ft Span)	7.1	703	8.6	751
Lake LBJ	5.7	715	8.1	752
Lampasas River	3.9	451	4.2	497
Willis Creek	5.1	544	5.7	537
Wimberley (40-ft Span)	23.3	714	38.7	820
Wimberley (60-ft Span)	6.0	662	9.3	702
Maximum Tensile Stress in Concrete = $7.5\sqrt{f_c'}$				
Chandler Creek (40-ft Span)	20.2	548	22.1	568
Chandler Creek (60-ft Span)	12.3	784	14.0	832
Lake LBJ	7.9	797	13.7	844
Lampasas River	4.6	531	4.9	576
Willis Creek	8.6	619	11.7	618
Wimberley (40-ft Span)	29.1	763	45.5	876
Wimberley (60-ft Span)	10.7	737	14.9	779
Maximum Tensile Stress in Concrete = $12\sqrt{f_c'}$				
Chandler Creek (40-ft Span)	44.3	701	46.0	720
Chandler Creek (60-ft Span)	27.9	1029	30.1	1073
Lake LBJ	22.9	1045	30.7	1119
Lampasas River	16.8	769	17.9	813
Willis Creek	25.2	742	29.6	862
Wimberley (40-ft Span)	46.2	909	65.7	1041
Wimberley (60-ft Span)	27.9	960	31.8	1009

During the preliminary design of the test specimens, the goal was to design test specimens that experienced the same values of maximum tensile stress in the concrete and stress range in the strand as the prototype beam. However, based on the analyses of all beams, it is clear that there is no direct link between a particular level of tensile stress in the concrete and stress range in the strand. In addition, as discussed in Chapter 1, the fatigue life of prestressed beams is directly related to the strand stress range. Therefore, stress range in the strand was selected as the primary criterion for selecting the loading levels for the test specimens.

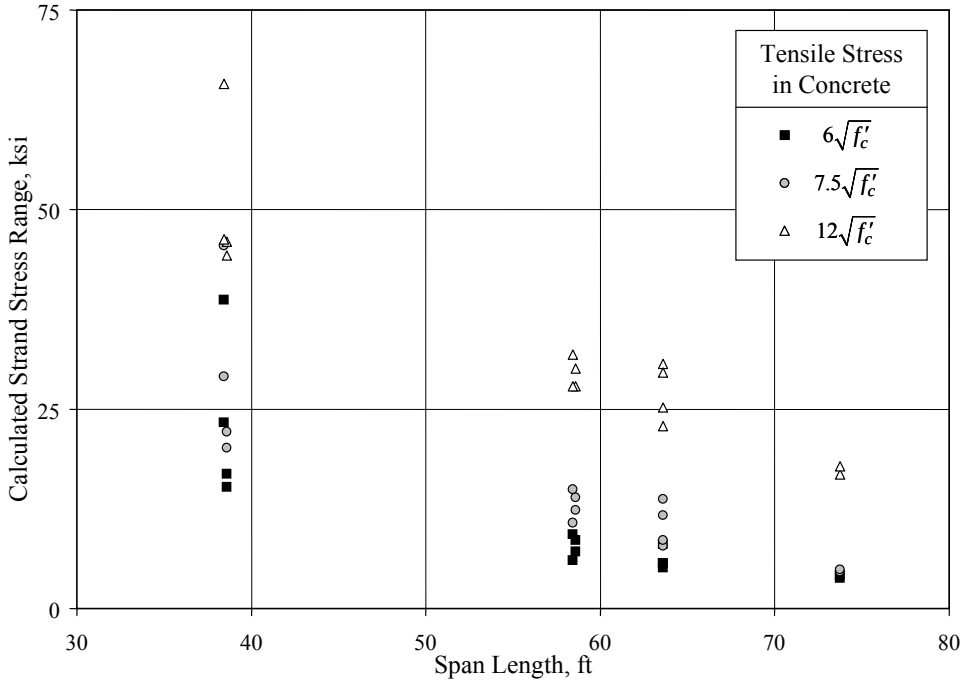

Figure 5.4 Calculated Range of Strand Stress for Prestressed Concrete Bridges

5.3 CONSTRUCTION OF TEST SPECIMENS

The six fatigue test specimens were constructed simultaneously, using the same construction sequence and materials. By fabricating all the specimens at one time, the impact of variation in concrete material properties and differences due to variation in the construction process were limited. The construction process is summarized in Section 5.3.1 and the measured material properties are reported in Section 5.3.2.

5.3.1 Overview

The test specimens were constructed in the Ferguson Structural Engineering Laboratory at the University of Texas at Austin. The six beams were built in the prestressing bed pictured in Figure 5.5. The prestressing bed consisted of three beam lines and two beams were constructed along each line.

The strands were stressed after the formwork, stirrups, and strain gages on the strand were in place. Each strand was stressed individually. In order to verify the initial prestress force, load tests were performed on each strand, as discussed in Section 5.5.2.

After the initial prestress force was determined, concrete was placed in the web portion of the beam. Approximately twenty-four hours after placement of the web concrete, the stress in the strands was released. The concrete in the slab was placed approximately twenty-four hours after release of the prestressing strands.

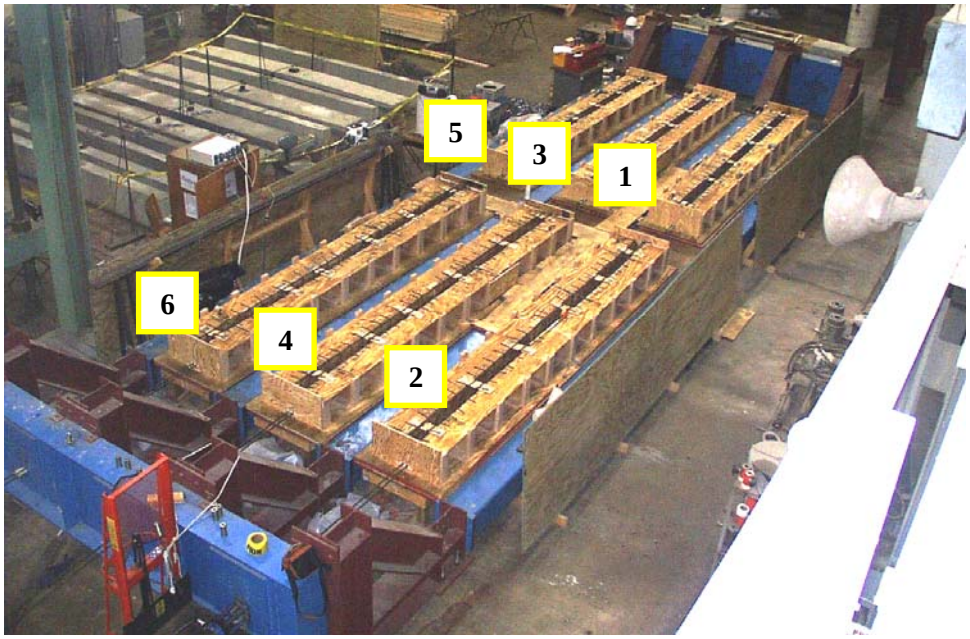

Figure 5.5 Prestressing Bed with Formwork Prior to Placement of Concrete

5.3.2 Material Properties

The materials used to construct the test specimens were evaluated during both the construction and testing phases. Concrete cylinders were tested in compression to determine the compressive strength and modulus of elasticity at various ages. Samples of the prestressing strand were tested in tension to determine the yield stress, tensile strength, and fatigue properties. A summary of the measured material properties is presented in Table 5.6. Detailed information about the measured material properties is presented in Hagenberger (2004) and Heller (2003).

The measured compressive strengths of the concrete agreed reasonably well with the values assumed during design. The largest deviation was in the strength of the web concrete at the beginning of the fatigue tests, which was approximately 25% larger than the assumed value of 10,000 psi. The measured values of the modulus of elasticity also exceeded the values assumed for design. In most cases, the measured values were 10 to 15% higher than the assumed values.

Table 5.6 Measured Material Properties

Property		Measured Value
Concrete (Web)	Compressive stress at release, f_{ci} (psi)	6100*
	Modulus at release, E_{ci} (ksi)	5200*
	Compressive strength at test, f_c' (psi)	12,000-12,800†
	Modulus at test, E_c (ksi)	6100-6200†
Concrete (Slab)	Compressive strength at test, f_{cs}' (psi)	6300-6800†
	Modulus, E_{cs} (ksi)	4900-5100†
Strand	Yield stress, f_y (ksi)	245
	Tensile strength, f_{pu} (ksi)	275
	Modulus, E_p (ksi)	29,400
	Apparent modulus, E_{pa} (ksi)‡	31,200

* Stress in strand was released approximately 24 hours after placement of concrete in web.
† Age of concrete at start of fatigue tests varied.
‡ Apparent modulus was used to convert the measured strains to axial stress in the strand.

5.4 TEST SET-UP

The test beams were simply supported and loaded near the center of the span (Figure 5.6). The ends of the beams were supported on elastomeric bearing pads on top of concrete piers. Each beam was loaded symmetrically with point loads located 2 ft from the beam centerline. The total length of the beam was 15 ft, and the distance between the centerline of the bearing pads was 14.5 ft.

A single hydraulic ram was used to apply the load to the beam (Figure 5.7). This load was distributed to two equal loads through a spreader beam. The load was transferred from the spreader beam to the test specimen through two, 1-in. thick elastomeric bearing pads. This loading configuration created a 4-ft constant moment region.

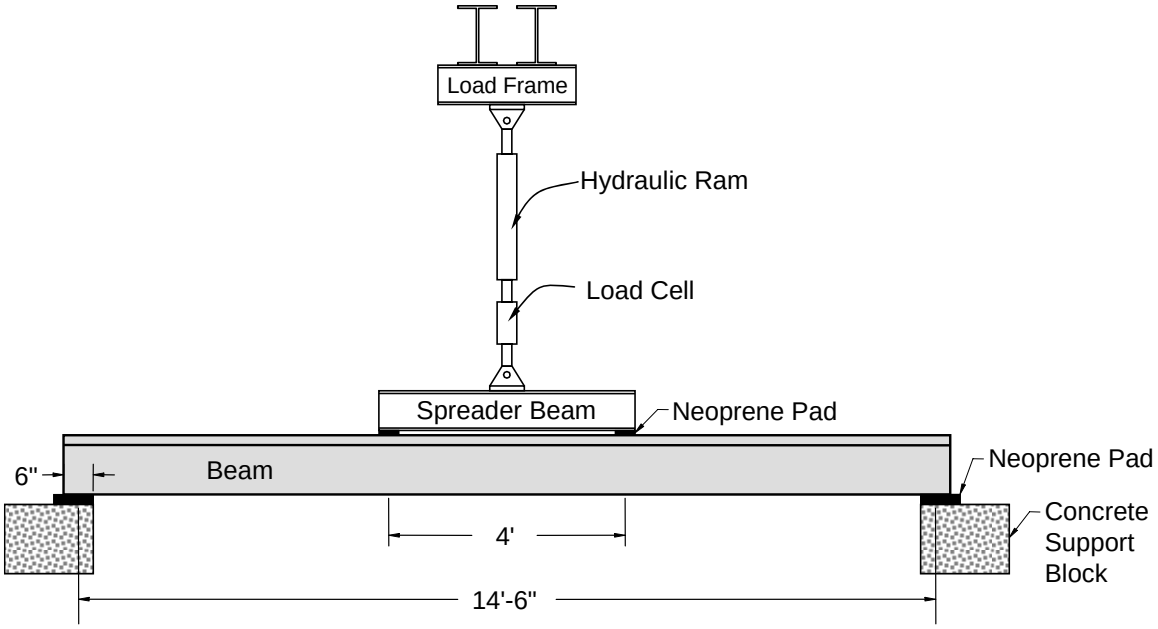

Figure 5.6 Geometry of Fatigue Test Specimens

Figure 5.7 Photograph of Test Specimen

5.5 EFFECTIVE PRESTRESS FORCE

The stress experienced by the strand during the fatigue tests depends on the effective prestress force. Therefore, detailed measurements were taken throughout the construction process to monitor losses. The instrumentation is discussed in Section 5.5.1, tests used to determine the initial prestress force are summarized in Section 5.5.2, and procedures used to estimate the effective prestress force at the time of the fatigue tests are described in Section 5.5.3.

5.5.1 Instrumentation

Two types of strain gages were used to evaluate the effective prestress force. Ten, 5-mm strain gages were attached to individual wires on the prestressing strand. The locations of the gages were staggered within 12 in. of the midspan of each beam. Six of the gages were installed before the strand was stressed. The remaining four gages were installed after the strands were stressed and prior to the placement of the concrete. One, 60-mm embedded concrete gage was positioned at the centroid of the prestressing strand and within 12-in. of midspan of each beam.

The strain gages on the strand and embedded in the concrete were monitored throughout the construction and testing phases of the investigation to evaluate the effective stress in the strand.

5.5.2 Initial Prestress Force

The initial prestress force in each strand was determined by conducting a load test, commonly called a lift-off test, after the strands were prestressed and before the concrete was placed. A schematic of the load test setup is shown in Figure 5.8. A load cell and hydraulic actuator were positioned outside the prestressing bed and pulled on the free end of the strand. During each load test, data were collected from the strain gages attached to the strand and from the load cell.

All strain gages were zeroed before the load tests; therefore, the measured strains correspond to increase in strain due to the applied load. Strains from the same strand were averaged to provide one reading per prestressing strand. The corresponding strand stress was calculated by dividing the applied load by the nominal area of the strand. The measured response of the two strands within Beams 1 and 2 are shown in Figure 5.9.

The idealized response of the strand is also shown in Figure 5.9. For stress less than the initial prestress of 150 ksi, no change in strain is expected. Above the initial prestress, the change in strain is expected to vary linearly with the change in stress.

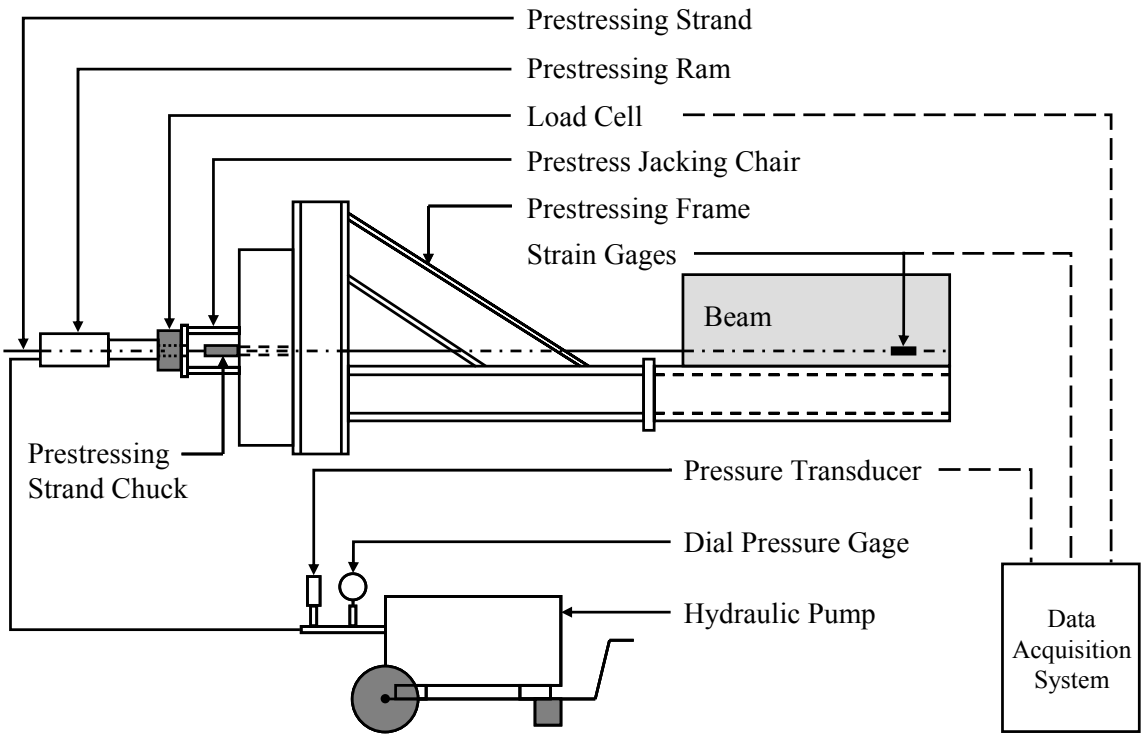

Figure 5.8 Setup for Lift-Off Test

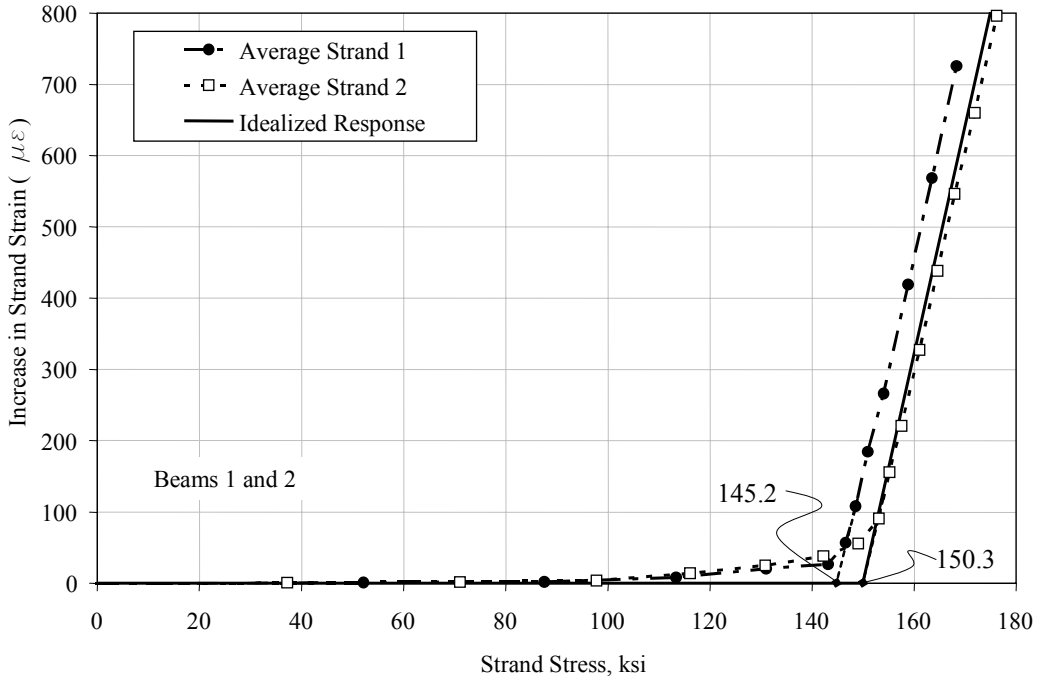

Figure 5.9 Variation of Strand Strain and Stress During Load Test

As shown in Figure 5.9, a small increase in strain was observed at prestress levels between 100 and 150 ksi. However, the strand strain did not increase appreciably until after the applied stress exceeded 150 ksi. As a result, the initial stress in the strand was determined by projecting the linearly varying portion of the data to the point of zero strain and assuming this point to be the initial prestress. These points are noted in Figure 5.9.

Results from all tests are reported by Hagenberger (2004). The maximum observed difference between the idealized and measured response was between 57 and 132 $\mu\varepsilon$, which corresponds to a difference in strand stress of 2 to 4 ksi.

5.5.3 Effective Prestress Force

The strain gages were monitored continuously between the time that the strands were released and the start of the fatigue tests. Representative data from Beam 1 is shown in Figure 5.10. The changes in strain include the immediate change at release and time dependent changes.

The variation in stress and strain in the strand with time was estimated using the method in the PCI Design Handbook (1992). The results are also plotted in Figure 5.10, and tended to overestimate the measured response of the test specimens. The measured change in strain for the six beams ranged from 75% to 90% of the calculated values. This corresponds to a difference of 105 to 201 $\mu\varepsilon$, or approximately 3 to 6 ksi in the strand. Additional information is provided in Hagenberger (2004).

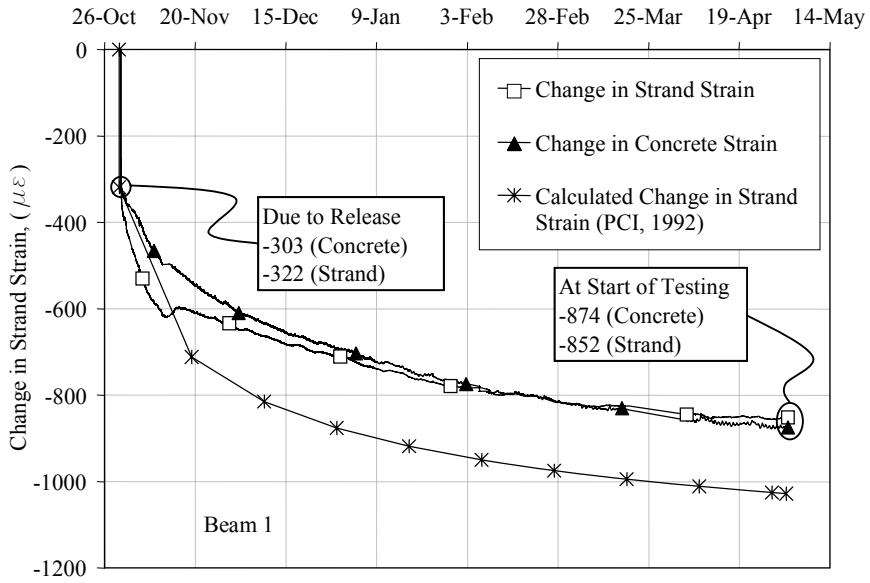

Figure 5.10 Typical Variation in Strand and Concrete Strain with Time

5.6 FORCE LIMITS FOR FATIGUE TESTS

Before each fatigue test, the specimens were analyzed to determine the required load range that would produce the desired strand stress range and median strand stress. All calculations were based on the measured concrete material properties (Table 5.6). The effective prestress force used for the analyses were based on measured strains. Table 5.7 summarizes the effective prestress at the start of each test. The effective prestress force at release was determined using the lift-off tests (Section 5.5.2), and prestress losses were calculated based on the measured change in strain (Section 5.5.3).

The beams were divided into three groups and the two beams in each group were subjected to the same nominal stress range in the strand. The three target stress ranges (10 ksi, 25 ksi, and 50 ksi) were selected to be representative of the variations observed within the group of five prestressed concrete bridges (Table 5.5). The fatigue life of the beams tested at the highest stress range was expected to be considerably shorter than that of the beams tested at the lowest stress range.

In order to relate the target stress ranges to the applied loads, the relationship between the strand stress and the live load must be determined. These analyses are similar to those described in Section 5.2 and Appendix C for the prototype beam, and five points were used to characterize the response of each beam (Table 5.8). Due to the shape of the cross section, the neutral axis for Point 3 was taken at the centroid of the strand. The other four points correspond to the limits used to analyze the prototype girder.

Details of these analyses are presented in Hagenberger (2004) and the calculated response is summarized in Table 5.9 through Table 5.10 and Figure 5.11 through Figure 5.12.

Table 5.7 Summary of Prestressing Data Used in Analyses of Beams

Beam ID	Number of Days Between Release and Testing	Average Measured Stress Prior to Release (ksi)	Average Measured Change in Strain at Release ($\mu\varepsilon$)	Average Total Measured Change in Strain ($\mu\varepsilon$)	Total Prestress Losses (ksi)	Effective Prestress at Start of Fatigue Test (ksi)
1	202	148	322	852	27	121
2	162	148	323	789	25	123
3	144	147	290	699	22	125
4	105	147	287	683	21	126
5	128	151	294	760	24	127
6	252	151	279	759	24	127

Table 5.8 Description of Analysis Points for Fatigue Specimens

Point	Description
1	Full dead load state
2	Decompression of bottom fiber
3	Neutral axis at center of gravity of strand
4	Neutral axis at top of web
5	Flexural Capacity
A	Minimum applied load for fatigue test
B	Maximum applied load for fatigue test

The stress range in the strand being investigated was then determined graphically using the five data points from the analysis and assuming the applied load varied linearly between each data point. Data points A and B correspond to the minimum and maximum applied load used for fatigue testing, respectively. The results are summarized in Table 5.15.

Beams 1 and 6 were subjected to the smallest variation in strand stress during the fatigue tests. The nominal stress range of 10 ksi is representative of the calculated live load stresses in the longer interior bridge girders for a maximum tensile stress of $6\sqrt{f_c'}$ in the concrete (Table 5.5). Beam 1 was the only test specimen where the neutral axis was calculated to be above the centroid of the strand at both the maximum and minimum applied force. In all other beams, the neutral axis was below the centroid of the strand at the minimum applied load and above the centroid of the strand at the maximum applied load.

Beams 2 and 3 were subjected to a nominal stress range of 25 ksi. This stress range is representative of the calculated live load stresses in the interior bridge girders for a maximum tensile stress between 7.5 $\sqrt{f_c'}$ and $12\sqrt{f_c'}$ in the concrete.

Beams 4 and 5 were subjected to a nominal stress range of 50 ksi. This range is larger than would be expected in the interior bridge girders under service loads, but was selected as an upper limit on the variations in strand stress

Table 5.9 Calculated Live Load Response of Beam 1

Point	Strand Stress, ksi	Strand Stress Range, ksi	Load, kip
1	121.2	0.0	0.0
2	129.4	8.2	9.2
3	129.6	8.4	9.4
4	145.7	24.5	11.5
5	275.0	153.8	24.7
Fatigue Loads			
A	138.1	7.1	10.5
B	145.2		11.4

Table 5.10 Calculated Live Load Response of Beam 6

Point	Strand Stress, ksi	Strand Stress Range, ksi	Load, kip
1	127.7	0.0	0.0
2	135.0	7.3	9.0
3	135.4	7.7	9.4
4	171.1	43.4	13.9
5	275.0	147.3	24.7
Fatigue Loads			
A	132.2	14.3	5.5
B	146.5		10.8

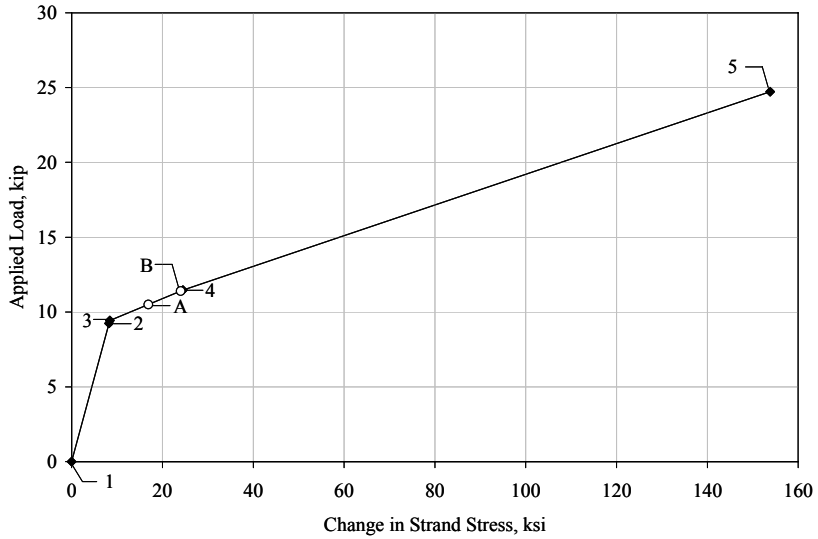

Figure 5.11 Variation in Strand Stress with Applied Load for Beam 1

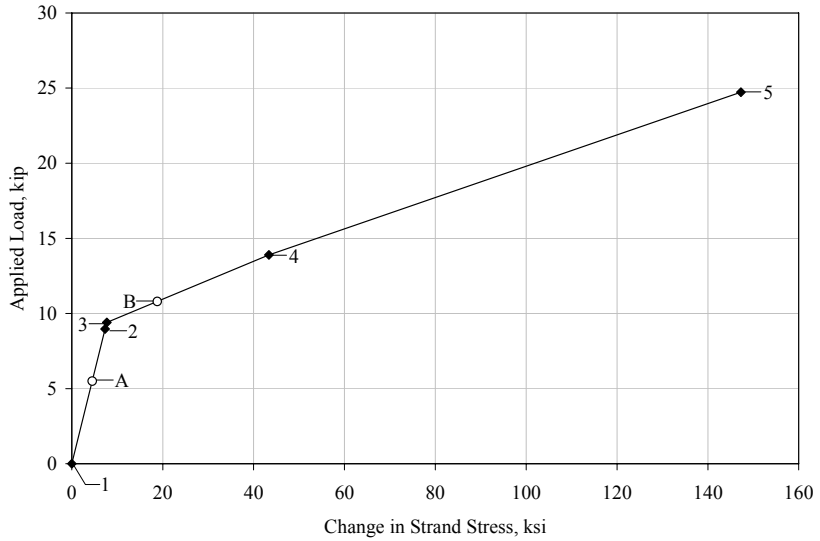

Figure 5.12 Variation of Strand Stress with Applied Load for Beam 6

Table 5.11 Calculated Live Load Response of Beam 2

Point	Strand Stress, ksi	Strand Stress Range, ksi	Load, kip
1	123.1	0.0	0.0
2	131.4	8.3	9.4
3	131.6	8.5	9.6
4	149.2	26.1	11.8
5	275.0	151.9	24.7
Fatigue Loads			
A	126.1	22.4	3.4
B	148.5		11.7

Table 5.12 Calculated Live Load Response of Beam 3

Point	Strand Stress, ksi	Strand Stress Range, ksi	Load, kip
1	125.6	0.0	0.0
2	133.2	7.6	9.3
3	133.4	7.8	9.5
4	158.2	32.6	12.7
5	275.0	149.4	24.7
Fatigue Loads			
A	127.5	24.8	2.3
B	152.2		11.9

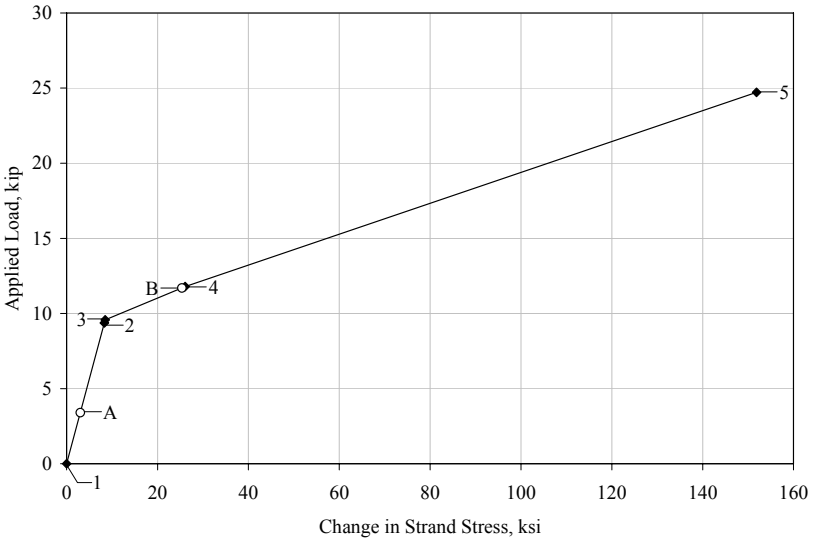

Figure 5.13 Variation in Strand Stress with Applied Load for Beam 2

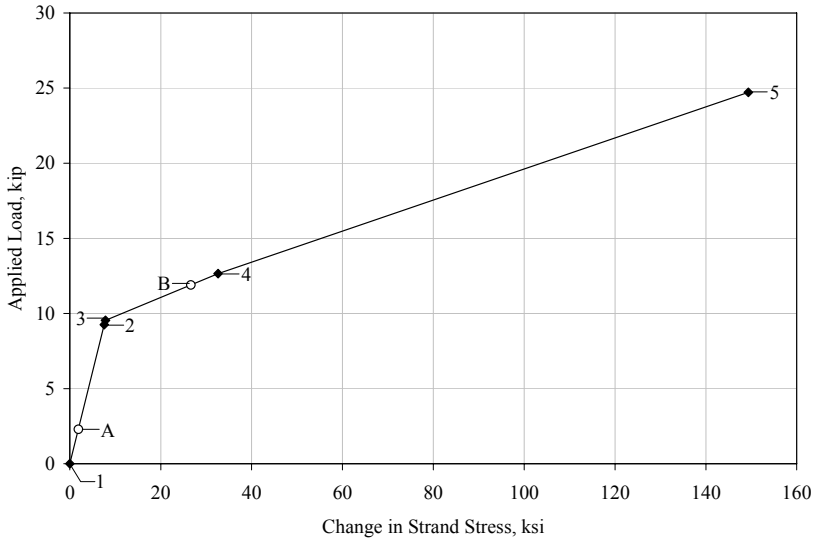

Figure 5.14 Variation of Strand Stress with Applied Load for Beam 3

Table 5.13 Calculated Live Load Response of Beam 4

Point	Strand Stress, ksi	Strand Stress Range, ksi	Load, kip
1	126.1	0.0	0.0
2	133.6	7.5	9.1
3	133.9	7.8	9.5
4	164.2	38.1	13.2
5	275.0	148.9	24.7
Fatigue Loads			
A	127.1	46.6	1.2
B	173.7		14.2

Table 5.14 Calculated Live Load Response of Beam 5

Point	Strand Stress, ksi	Strand Stress Range, ksi	Load, kip
1	123.7	0.0	0.0
2	131.1	7.4	9.1
3	131.5	7.8	9.5
4	165.4	41.7	13.7
5	271.0	147.3	24.7
Fatigue Loads			
A	124.2	46.7	0.6
B	170.9		14.3

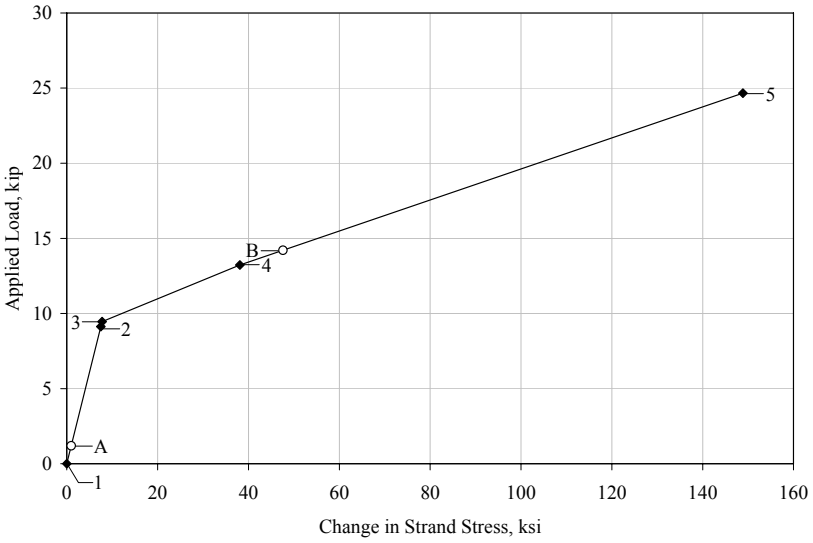

Figure 5.15 Variation of Strand Stress with Applied Load for Beam 4

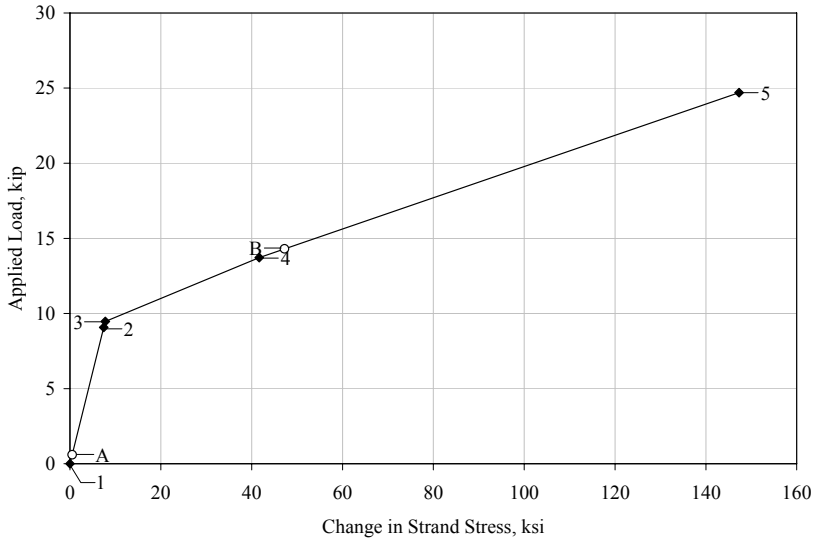

Figure 5.16 Variation of Strand Stress with Applied Load for Beam 5

Table 5.15 Summary of Analyses on Fatigue Test Specimens

Beam ID	Strand Stress at Minimum Load (ksi)	Strand Stress Range (ksi)	Median Strand Stress (ksi)
1	138	7	145
2	126	22	137
3	127	25	140
4	127	47	150
5	124	47	148
6	132	14	139

5.7 TEST PLAN

The primary objective of the experimental phase of this project was to evaluate the fatigue performance of the composite prestressed concrete beams. Each beam was also subjected to a series of static tests during the fatigue tests. Both the static and fatigue test procedures are discussed in the following sections.

5.7.1 Fatigue Tests

The fatigue tests were run under load control. The maximum and minimum loads used during the tests are reported in Table 5.9 through Table 5.14. Four error limits were set to ensure that each specimen was tested at the desired load levels:

- Input to output error signal – the output from the load cell was continuously compared with the command signal. If the difference exceeded the threshold, the test would stop. These differences indicated changes in the response of the specimens, such as cracking of the concrete or fracture of the wires.
- High load error signal – an error was triggered if the maximum output from the load cell exceeded a set range. This prevented the specimen from being damaged due to erroneously high command signals.
- Low load error signal – an error was also triggered if the minimum output from the load cell was less than a set range. This prevented erroneous fatigue cycles from being counted if the hydraulic pressure to the ram was lost.
- Displacement limit – a limit switch was positioned below the specimen at midspan. If the beam deflection exceeded the travel length of the limit switch (approximately 1/16 in.), a signal was sent to the controller to stop the fatigue test. The limit switch was an effective means of detecting changes in stiffness due to cracking of the concrete or fracture of wires.

Additional information about the procedures used to control the fatigue tests and the testing frequencies is provided in Heller (2003).

5.7.2 Static Tests

Static tests were performed periodically during the fatigue tests. The specimens were subjected to a static test before the fatigue tests were started and each time that an error signal stopped the tests.

a. Initial Static Tests

The purpose of the initial static tests was to define the baseline behavior of the beams for comparison with data collected during the fatigue tests. The response of the specimen was monitored using four vertical displacement transducers (two at midspan and one at the center of each bearing pad at the ends of the beam), strain gages on the prestressing strand, and an embedded concrete strain gage located at the center of gravity of the prestressing strand. Data were recorded during the loading and unloading phases of the initial static tests.

The load during the initial static test was typically applied in 1-kip increments. In the vicinity of the decompression load, the load increment was reduced to approximately 0.25 to 0.5 kip to capture the nonlinear beam behavior.

Beams 1, 2, 4, and 5 cracked during the initial static test. After unloading, a horizontal displacement transducer was installed across the most prominent crack (Figure 5.17) and two surface concrete strain gages were installed, one on each side of the prominent crack. After this instrumentation was installed, the static test was repeated.

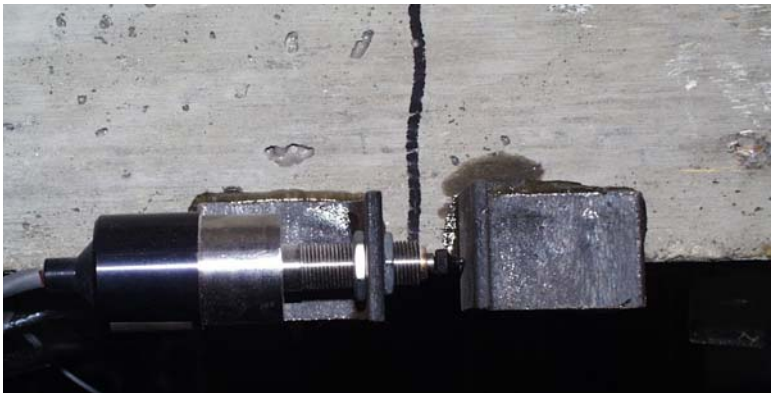

Figure 5.17 Displacement Transducer used to Opening and Closing of Flexural Crack

Beams 3 and 6 did not crack during the initial static test. As a result, a small number of fatigue cycles were performed until the first crack formed. After the crack appeared, the additional instrumentation was placed on these beams and an additional static test was performed.

Additional information about the instrumentation used during the static tests is presented in Heller (2003).

b. Periodic Static Tests

Additional static tests were performed periodically during the fatigue tests on each beam. In some cases, the fatigue loading was interrupted because the beam had sustained a predetermined number of cycles. In other cases, the displacement of the beam increased suddenly, typically due to the fracture of a wire. Each time the fatigue tests were interrupted for a static test, data were collected from all the instruments.

Similarly to the initial static test, data were collected during the loading and unloading portion of the tests. The load increments for these tests were the same as described for the initial static tests.

5.7.3 Post Mortem Investigation

The fatigue tests were run until the beams resisted 10,000,000 loading cycles or a significant decrease in the stiffness of the beam was observed. The stiffness decreased each time that a wire fractured, and at least four wire breaks were suspected before the tests were concluded for each specimen with a finite fatigue life.

After the beams were removed from the test setup, the concrete around the prestressing strands was removed within the region defined by the cracks furthest from midspan. Once the strand was exposed, it was possible to determine the number of fractured wires.

5.8 SUMMARY

Six prestressed concrete beams were designed, constructed, and subjected to fatigue loads in the experimental phase of this research. The fatigue loads applied to the specimens were established such that the nominal strand stress ranges were approximately 10 ksi, 25 ksi, or 50 ksi. These ranges were considered to be representative of the live load stresses expected in the interior girders from the five bridges considered in this investigation. The results of the fatigue tests are reported in Chapter 6.

CHAPTER 6
Results of Fatigue Tests

The results of the laboratory fatigue tests of six beams are summarized in this chapter. Detailed information about the response of the specimens is presented in Heller (2003) for Beams 2, 3, 4, and 5 and in Hagenberger (2004) for Beams 1 and 6.

All fatigue tests were conducted between February and August 2003 in the Ferguson Structural Engineering Laboratory at the University of Texas (Table 6.1). The beams were grouped in pairs and the calculated stress range in the strand was approximately the same in each pair of beams. Beams 1 and 6 were subjected to the lowest fatigue loads. Both beams survived 10 million loading cycles without experiencing a wire break. Beams 4 and 5 were subjected to the highest fatigue loads. The first wire breaks were detected in these beams after 300,000 to 550,000 cycles. Beams 2 and 3 sustained more than 2 million cycles before experiencing the first wire break.

The data presented in this chapter are divided into five sections. The results of the initial static tests are presented in Section 6.1. After flexural cracks formed, the measured response was used to estimate the decompression load. The values estimated from the measured response are compared with the calculated values in Section 6.2. The variations in the measured displacements and strains as the number of loading cycles increased are discussed in Section 6.3. These data provided evidence of accumulation of fatigue damage. Observed crack patterns at the end of the fatigue tests and the locations of the wire breaks are presented in Section 6.4. The variation of strand stress achieved during the fatigue tests is compared with the ranges calculated in Chapter 5 in Section 6.5, and the measured fatigue response of the beams is compared with the AASHTO fatigue life model for Detail Category C in Section 6.6.

Table 6.1 Overview of Fatigue Tests

Beam	Dates of Fatigue Tests		Calculated Stress Range (ksi)	No. of Cycles to First Wire Break	Total No. of Cycles	No. of Wire Breaks
	Start	Conclude				
1	19 May 03	9 Jun 03	7	—	10,000,000	—
2	10 Apr 03	5 May 03	22	5,293,700	5,778,700	7
3	22 Mar 03	8 Apr 03	25	2,424,120	3,142,800	6
4	17 Feb 03	27 Feb 03	47	519,800	642,960	7
5	10 Mar 03	19 Mar 03	47	318,960	365,580	4
6	8 Jul 03	5 Aug 03	14	—	10,000,000	—

6.1 INITIAL STATIC TESTS

During the initial static tests, the applied load was increased from zero to the maximum load used in the fatigue tests. Beams 1, 2, 4, and 5 cracked during the initial static tests, while beams 3 and 6 did not. The measured relationship between the applied load and the average strain in the strand for Beam 4 is shown in Figure 6.1. A distinct change in the stiffness may be observed at the load corresponding to the formation of the first flexural crack. As indicated in Table 6.2, the cracking loads estimated from the measured strains tended to be approximately 80% of the values calculated using gross cross-sectional properties and a modulus of rupture of $7.5\sqrt{f_c'}$, where f_c' is the measured compressive strength of the web concrete.

Beams 3 and 6 were subjected to a limited number of fatigue cycles (25 for Beam 3 and 1000 for Beam 6) before the static test was repeated. Flexural cracks were observed during this second static test for both beams. The observed crack patterns after the initial static tests are shown in Figure 6.2.

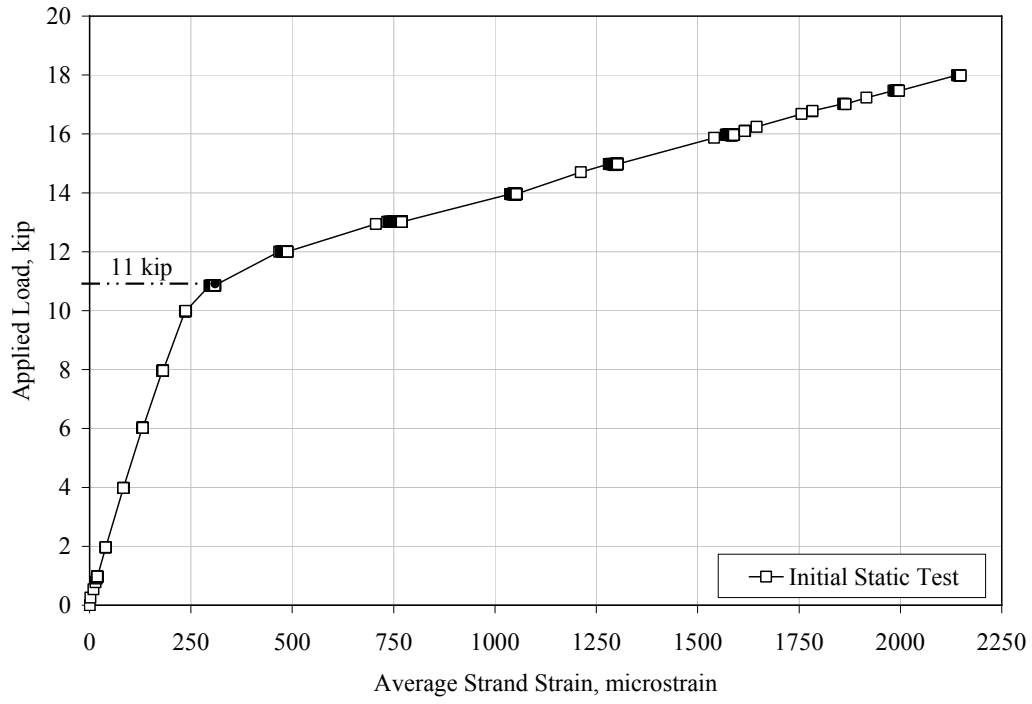

Figure 6.1 Measured Response of Beam 4 during Initial Static Test

Table 6.2 Response during Initial Static Tests

Beam ID	Calculated Cracking Load*	Cracking Load Inferred from Strand Data	Maximum Load during Initial Static Test
	(kip)	(kip)	(kip)
1	14.4	11.5	12.0
2	14.5	11.0	11.7
3	13.6	—	11.9
4	13.4	11.0	18.0
5	13.4	10.5	14.5
6	13.4	—	10.8

* Cracking load calculated using modulus of rupture corresponding to measured compressive strength of concrete.

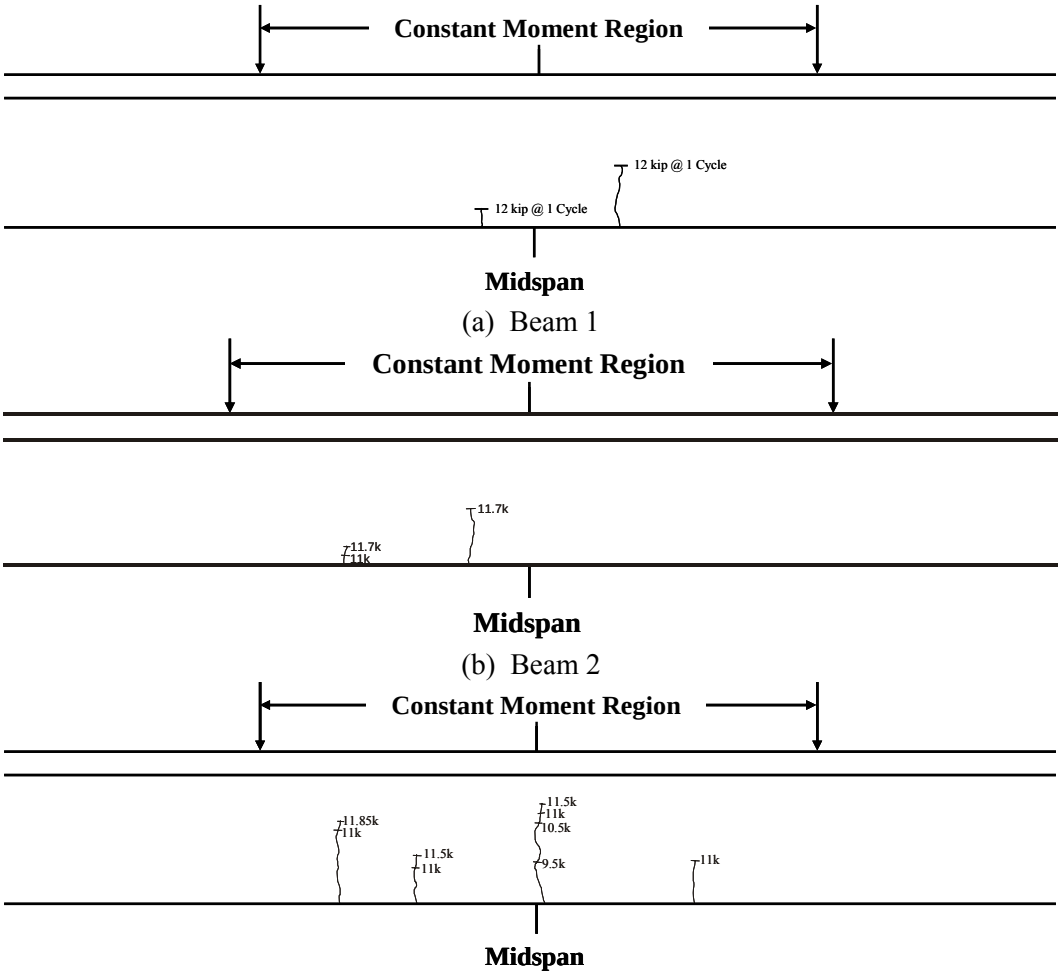

Figure 6.2 Observed Crack Patterns Following Initial Static Tests

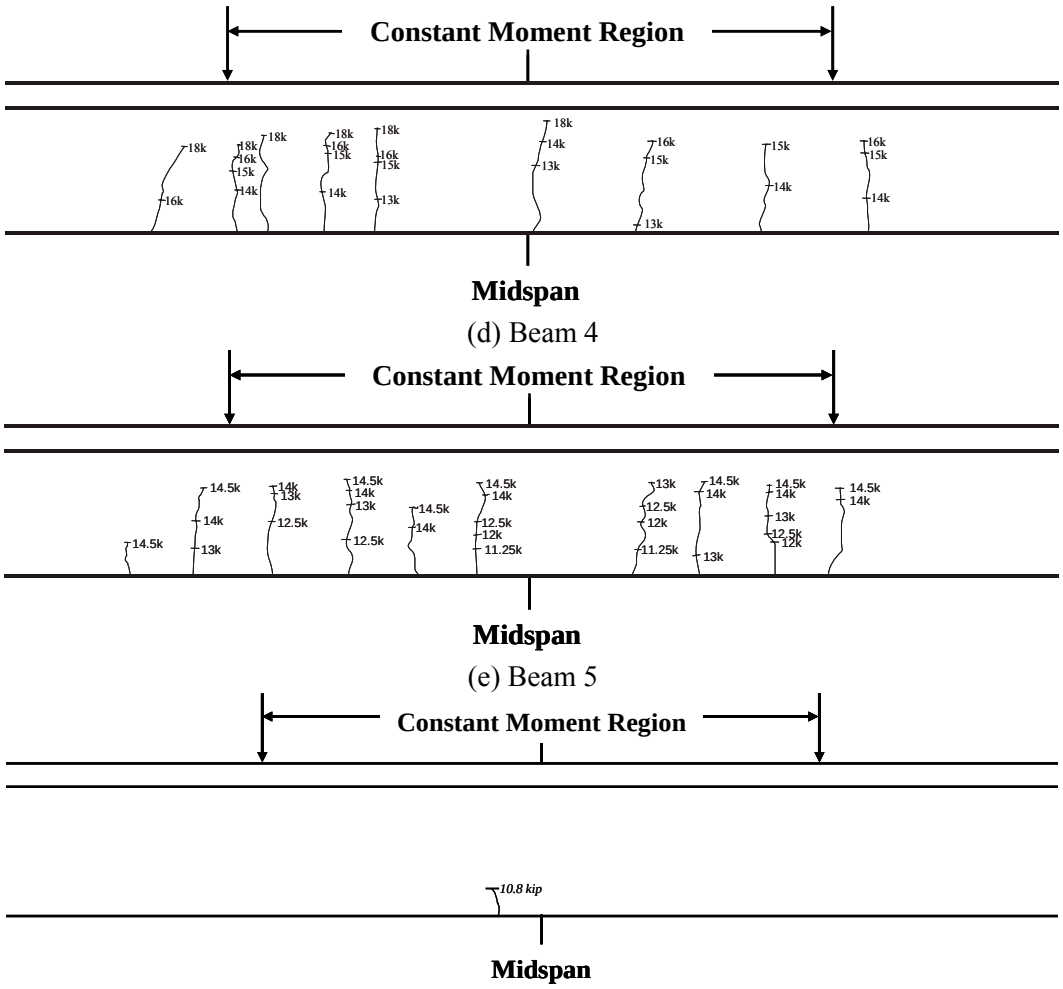

(d) Beam 4

(e) Beam 5

(7) Beam 6 (after 1000 Cycles)

Figure 6.2 (cont.) Observed Crack Patterns Following Initial Static Tests

6.2 DECOMPRESSION LOAD

The decompression load is the applied load at which the flexural tensile stress at the bottom fiber overcomes the net compressive stress due to combined prestressing and dead load. The calculated values (Point 2 in Tables 5.9 through Table 5.14) were based on the gross cross-sectional properties and the prestress losses calculated from the measured strains.

The decompression load could also be estimated from the measured response of the beams. After the initial cracks formed, the strain data from the prestressing strand, the midspan deflection data, and the data from the displacement gage across the most prominent crack were repeatable in successive static tests. Near the decompression load, a change in the effective stiffness of the cross section occurred. This change in stiffness occurred gradually, and a distinct decompression load can not be clearly identified from the data. However, the decompression load was approximated as the intersection of the best-fit lines

at loads above and below the nonlinear transition region. A typical example using strain data from Beam 1 is shown in Figure 6.3. Hagenberger (2004) includes the complete set of data.

Decompression loads estimated from the measured response are summarized in Table 6.3. In general the decompression loads estimated from the measured data are within ±10% of the calculated values.

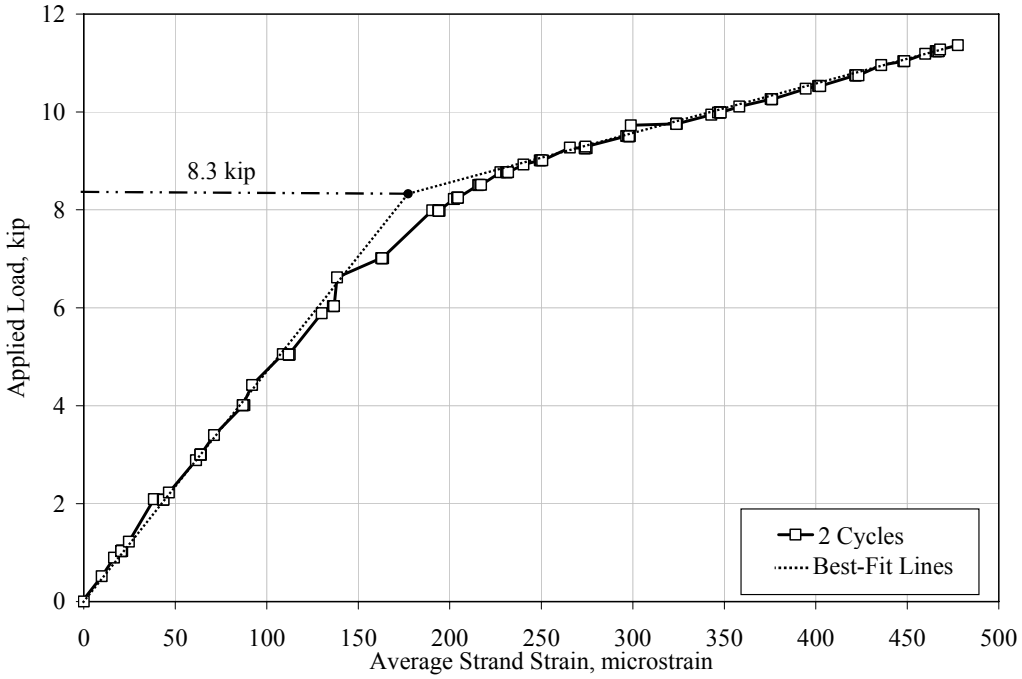

Figure 6.3 Estimated Decompression Load for Beam 1 Using Average Strand Strain

Table 6.3 Summary of Decompression Loads

Beam ID	Decompression Load (kip)			
	Calculated* (kip)	Estimated from Strand Strain (kip)	Estimated from Midspan Displacement (kip)	Estimated from Crack Opening (kip)
1	9.2	8.3	8.2	8.3
2	9.4	9.3	8.9	9.1
3	9.2	8.2	7.8	8.1
4	9.1	9.1	9.5	9.6
5	9.1	9.1	9.1	9.1
6	9.0	8.2	7.8	8.1

* Calculations summarized in Section 5.6.

6.3 FATIGUE TESTS

As discussed in Section 5.7, the fatigue tests were stopped periodically and the beams were subjected to additional static tests. Data were not recorded during the fatigue tests, so the periodic static tests provided the only means of evaluating changes in the response of the specimens due to the cyclic loading. Beams 1 and 4 will be used to compare the response of the specimens subjected to lowest and highest fatigue loads. Complete data sets are presented in Heller (2003) and Hagenberger (2004).

Applied load is plotted as a function of the midspan displacement in Figure 6.4. In both cases, significant changes in stiffness were observed between the first two static tests. Flexural cracks were not present in the beams before the initial static test, so this change in stiffness was expected. The stiffness continued to decrease as the number of fatigue cycles increased. After 10 million cycles, the maximum displacement at midspan of Beam 1 corresponding to the maximum fatigue load had increased by approximately 5% compared with the initial static test. After 500,000 cycles the maximum displacement at midspan of Beam 4 was approximately 35% larger than that measured during the initial static test. The stiffness decreased rapidly with increasing number of loading cycles in the subsequent static tests. These changes were attributed to fractures of the wires in the strand.

Applied load is plotted as a function of the average strain in the strand in Figure 6.5. The trends are similar to those observed in the midspan displacement data (Figure 6.4). However, it was not possible to evaluate the strain response for Beam 4 (or Beams 2, 3, and 5) during the later static tests, because all strain gages malfunctioned before the completion of the fatigue tests.

Applied load is plotted as a function of the width of the most prominent initial crack in Figure 6.6. The observed trends are very similar to those discussed for the midspan displacement.

Maximum midspan displacements from all six test specimens are plotted as a function of the number of loading cycles in Figure 6.7. The rapid increases in midspan displacement at the end of the fatigue tests for Beams 2, 3, 4, and 5 correspond to the failure of individual wires in the strand.

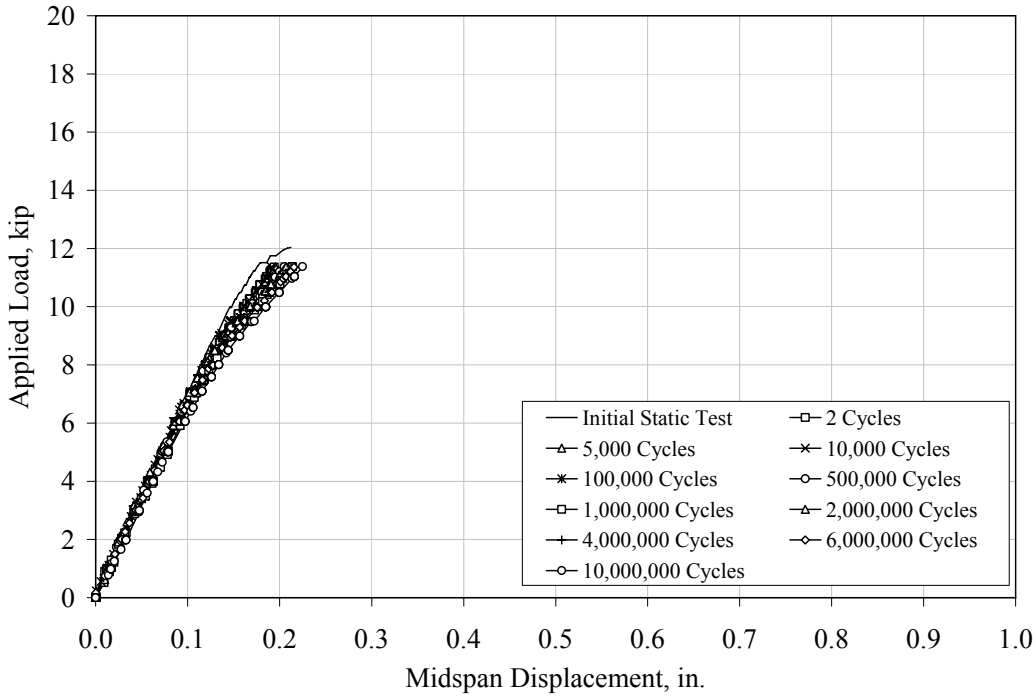

(a) Beam 1 (Strand Stress Range = 7 ksi)

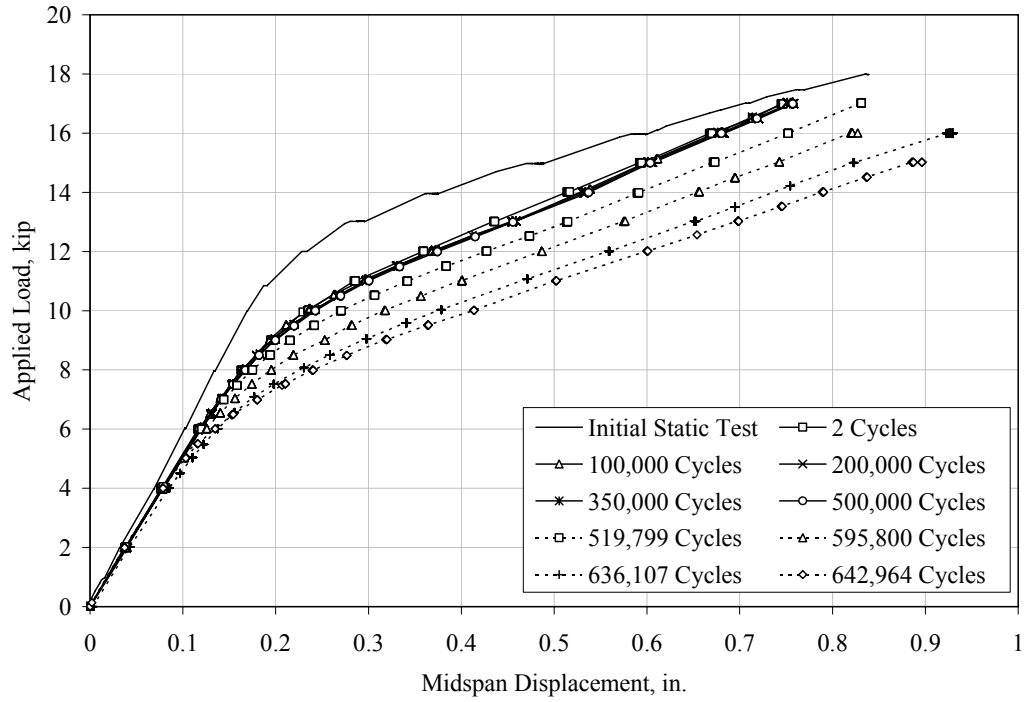

(b) Beam 4 (Strand Stress Range = 47 ksi)

Figure 6.4 Variation of Midspan Deflection during Fatigue Tests

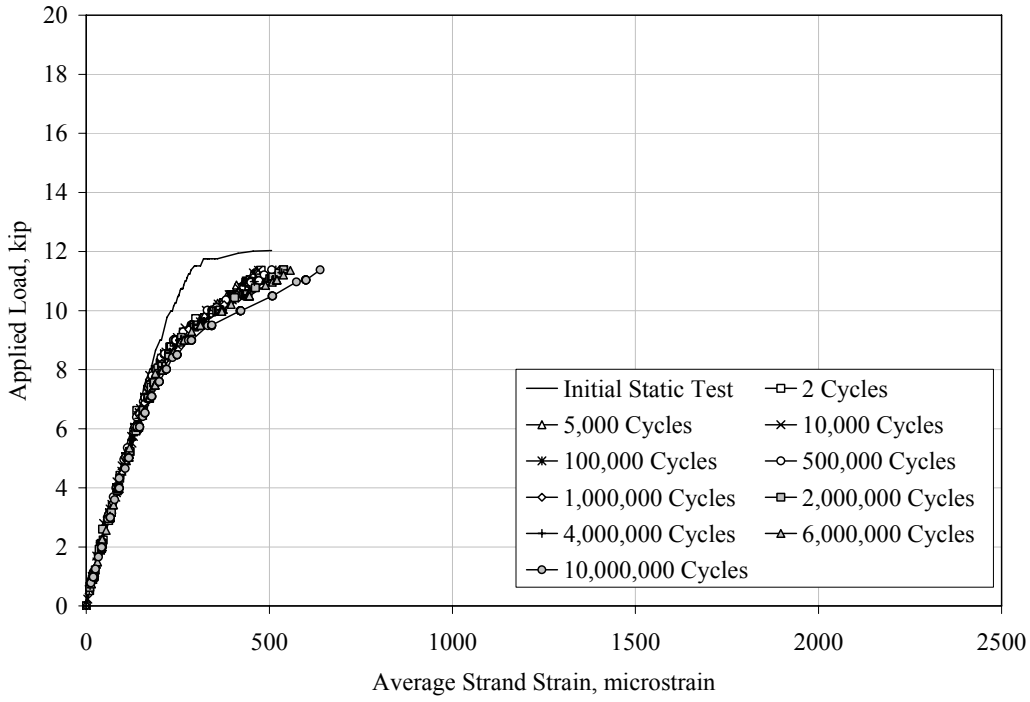

(a) Beam 1 (Strand Stress Range = 7 ksi)

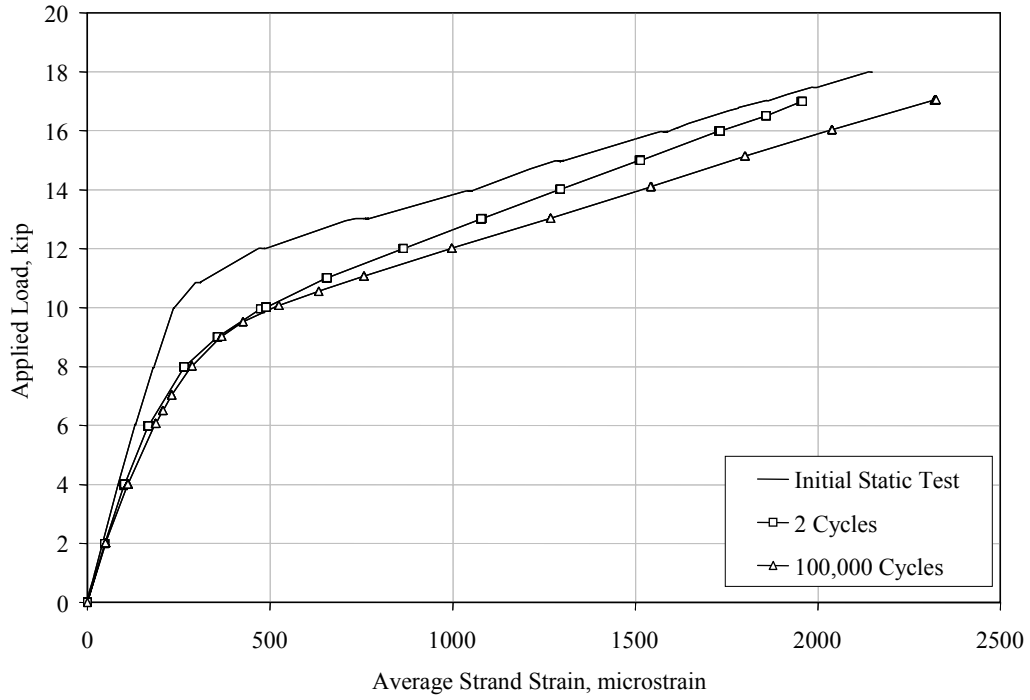

(b) Beam 4 (Strand Stress Range = 47 ksi)

Figure 6.5 Variation of Average Strand Strain during Fatigue Tests

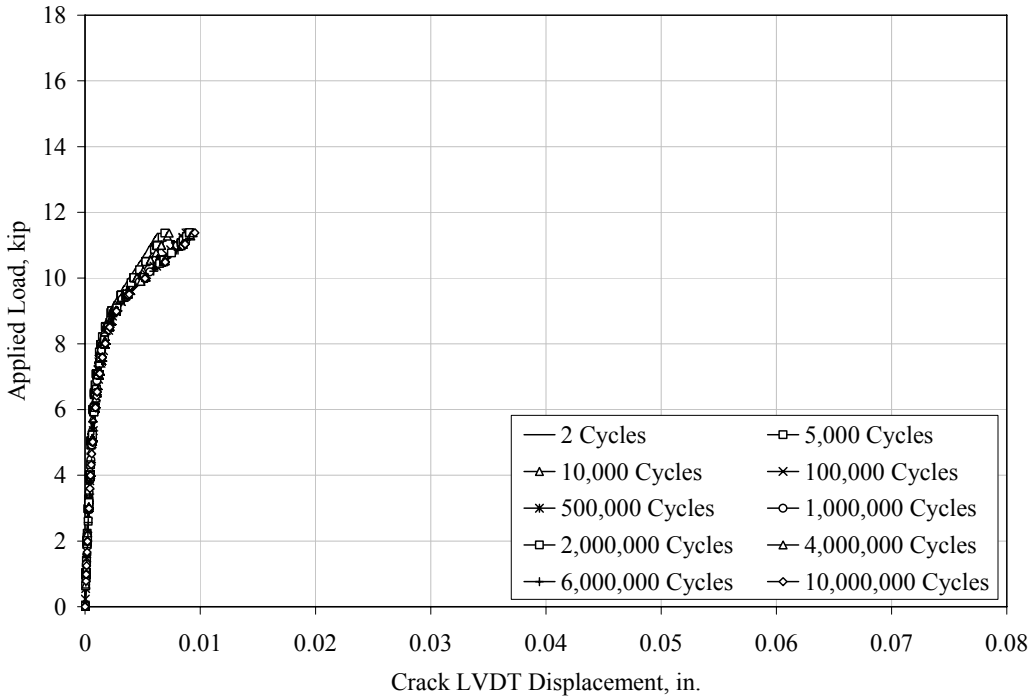

(a) Beam 1 (Strand Stress Range = 7 ksi)

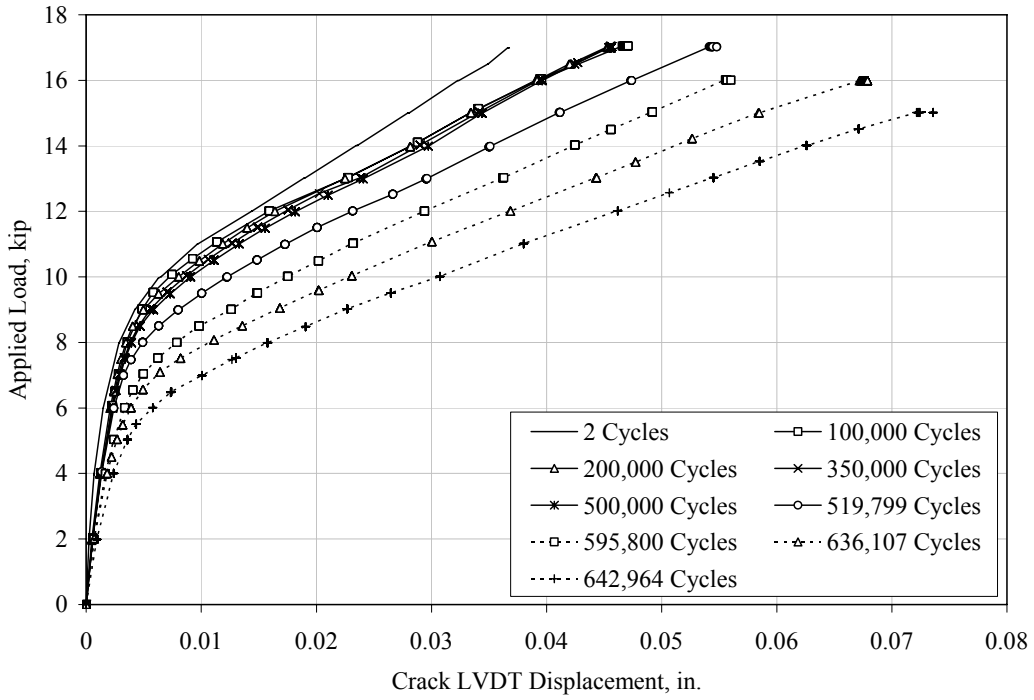

(b) Beam 4 (Strand Stress Range = 47 ksi)

Figure 6.6 Variation of Crack Gage Displacement during Fatigue Tests

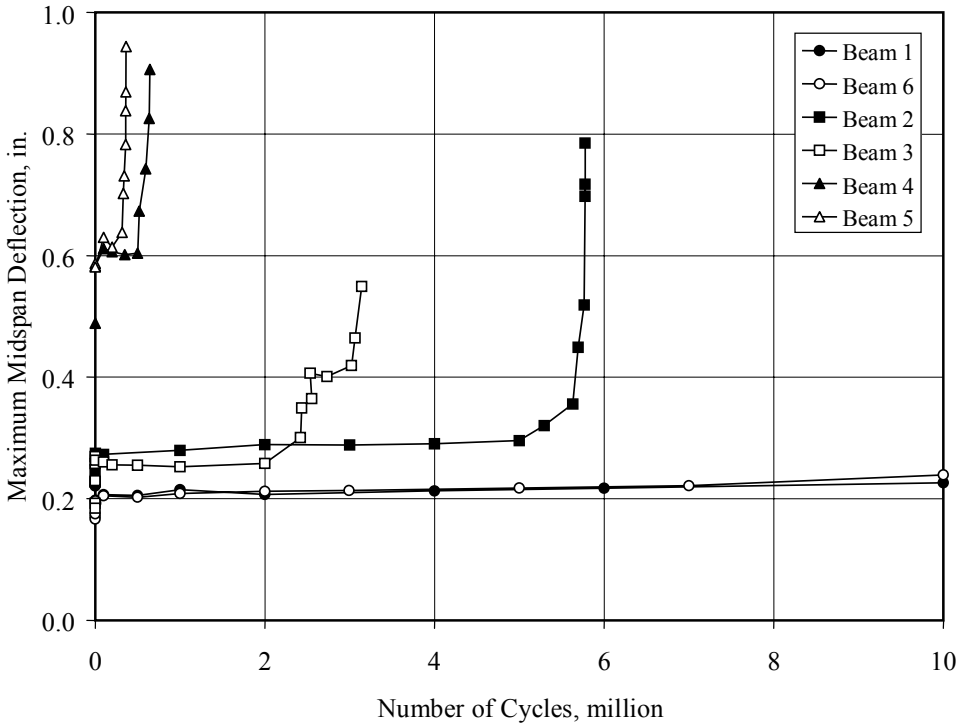

Figure 6.7 Comparison of Maximum Midspan Displacement with Number of Loading Cycles

6.4 CONDITION OF BEAMS AT END OF FATIGUE TESTS

The crack patterns observed at the completion of the fatigue tests are shown in Figure 6.8. The number and height of the cracks had increased, relative to the condition after the initial static test, in all beams. As expected, Beams 1 and 6 experienced fewer cracks than the beams tested with higher fatigue loads. The cracks extended the entire height of the web in Beams 2, 3, 4, and 5.

Horizontal cracks were observed at the level of the strand in Beams 3 and 5. Wire failures in these beams were located in the vicinity of the horizontal cracks. The wire breaks were distributed within ±12 in. of midspan in Beam 2 and all four wire breaks in Beam 4 were located 8 in from midspan. The locations of the wire breaks in Beam 4 were the only ones that did not coincide with the locations of flexural cracks.

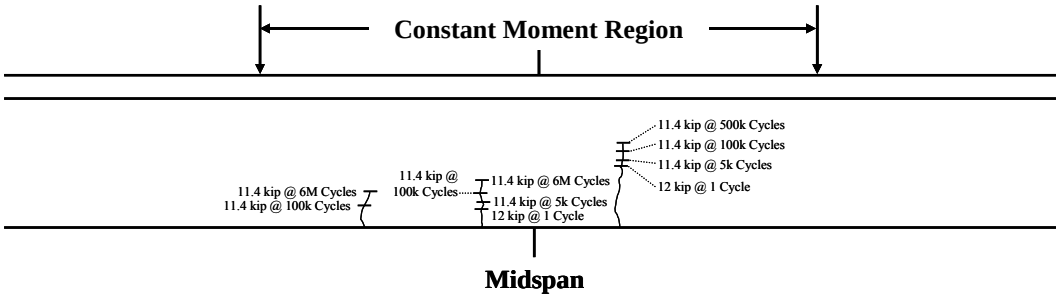

(a) Beam 1 – 10,000,000 Cycles

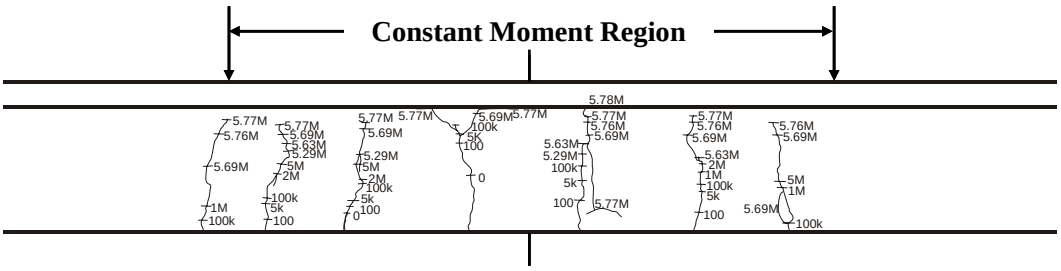

(b) Beam 2 – 5,778,700 Cycles

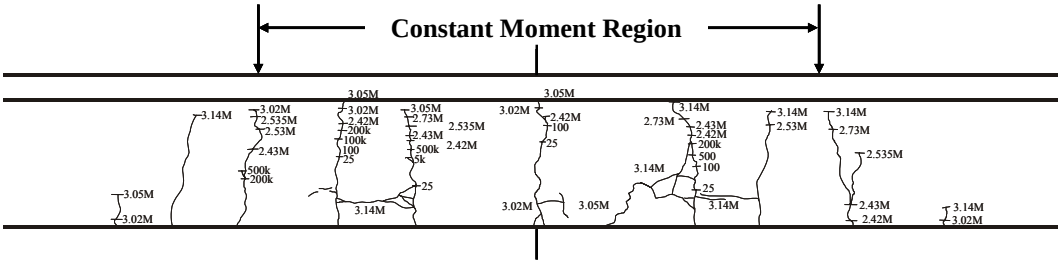

(c) Beam 3 – 3,142,800 Cycles

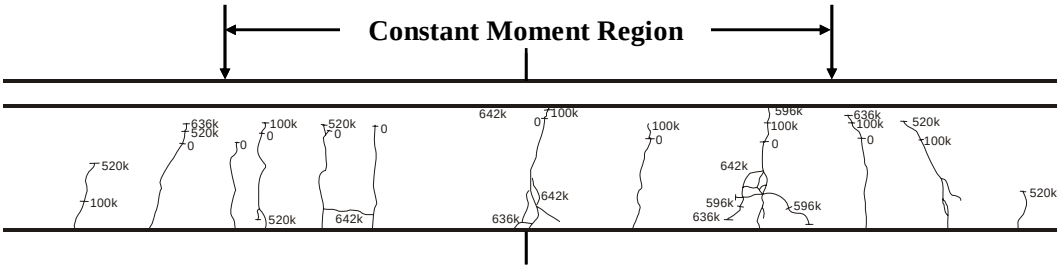

(d) Beam 4 – 642,960 Cycles

Figure 6.8 Observed Crack Patterns at Completion of Fatigue Tests

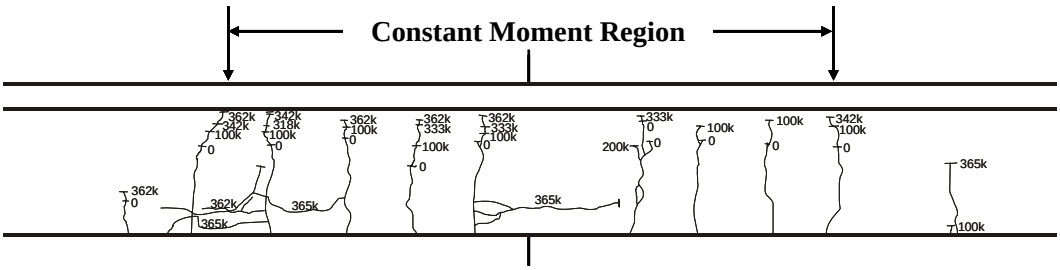

(e) Beam 5 – 365,580 Cycles

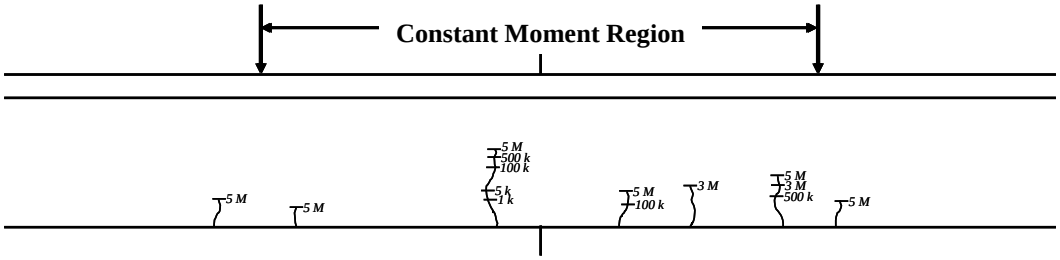

(f) Beam 6 – 10,000,000 Cycles

Figure 6.8 (cont.) Observed Crack Patterns at Completion of Fatigue Tests

6.5 STRAND STRESS

During the design of the test specimens, the range of strand stress was identified as the critical parameter for controlling the fatigue life of the prestressed concrete girder. Calculating the variation in strand stress due to live load requires detailed, strain compatibility calculations and detailed information about the prestress losses and .

Determining the variation in strand stress from the measured strains presents another set of challenges. As discussed in Chapter 5, ten strain gages were attached to individual wires on the prestressing strand in a staggered pattern and within 12 in. of the midspan of each beam. As a result of the staggered pattern, the location of each gage relative to flexural cracks in the beam varied. In the vicinity of a flexural crack, the strand will experience an increase in strain due to the discontinuity caused by the crack. In addition, as the number of loading cycles increases, the debonded length of strand from the crack will increase. Therefore, strains will be highest at gages located near a crack and will decrease as the distance between the crack and gage increases and at locations where the strand has debonded from the surrounding concrete in the vicinity of the crack.

To further complicate matters, all of the strain gages in Beams 2, 3, 4, and 5 malfunctioned before the completion of the fatigue tests. However, the available data were used to estimate the range of stress in the strand due to the fatigue loads. Maximum strain data from two static tests for each beam were used

to plot in Figure 6.9 through Figure 6.14. The first set of data was taken from a static test at the beginning of the fatigue tests (Static Test A), but after significant cracks had formed in the concrete. The second set of data was taken from the last test before wire breaks were detected (Static Test B). Because the strain gages malfunctioned early in the fatigue tests for some specimens, the number of cycles that had accumulated before Static Test B varied significantly.

The calculated response of the test specimens is also plotted in Figure 6.9 through Figure 6.14, as are the load limits used in the fatigue tests. In most cases, the stresses calculated from the measured strains are within 1 or 2 ksi of the calculated response. Beam 2 is an exception because the range of stress at the maximum load in both static tests exceeded the calculated response by 4 to 6 ksi. For Beams 4 and 5, the stresses corresponding to Static Test A were less than or equal to the calculated response, but the stresses corresponding to Static Test B were considerably larger. The average of the stress ranges from the two static tests is summarized Table 6.4.

Table 6.4 Variations in Strand Stress at Load Limits from Fatigue Tests

Beam	Minimum Fatigue Load (kip)	Maximum Fatigue Load (kip)	Variation in Strand Strain (ksi)	
			Calculated	Measured Strains
1	10.5	11.4	7	4
2	3.4	11.7	22	27
3	2.3	11.9	25	26
4	1.2	14.2	47	48
5	0.6	14.3	47	48
6	5.5	10.8	14	13

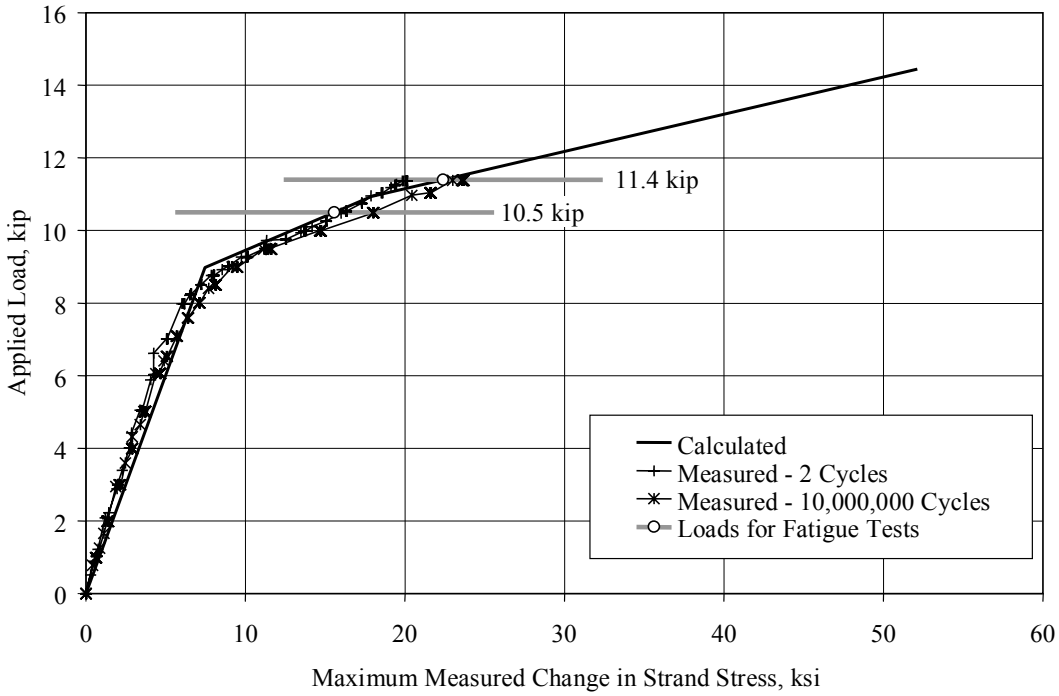

Figure 6.9 Comparison of Calculated and Measured Response of Beam 1

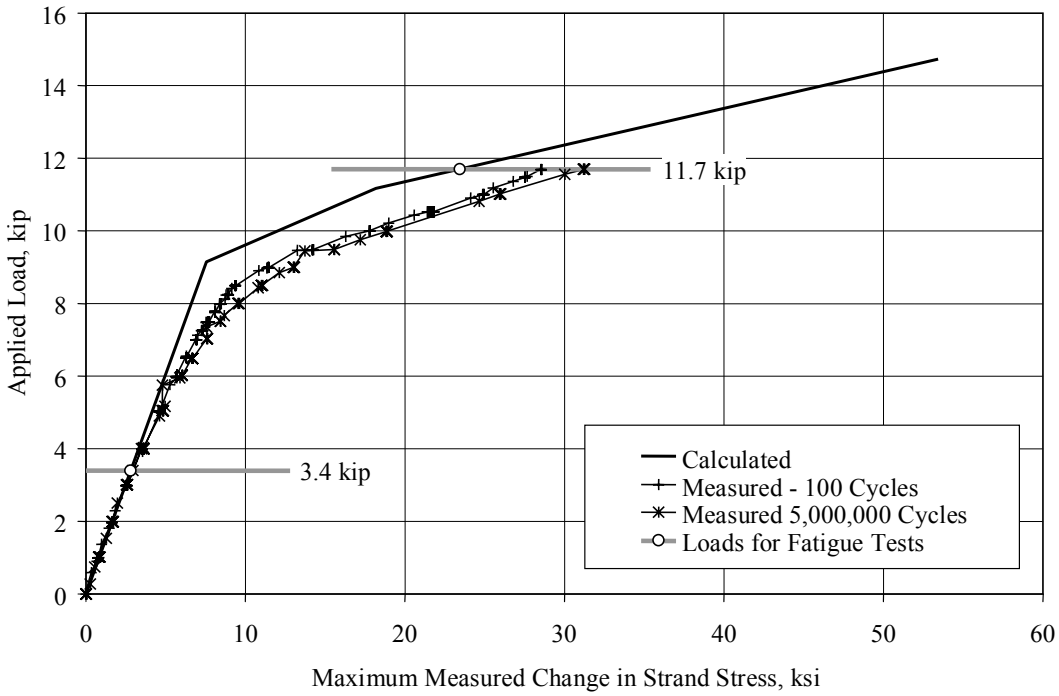

Figure 6.10 Comparison of Calculated and Measured Response of Beam 2

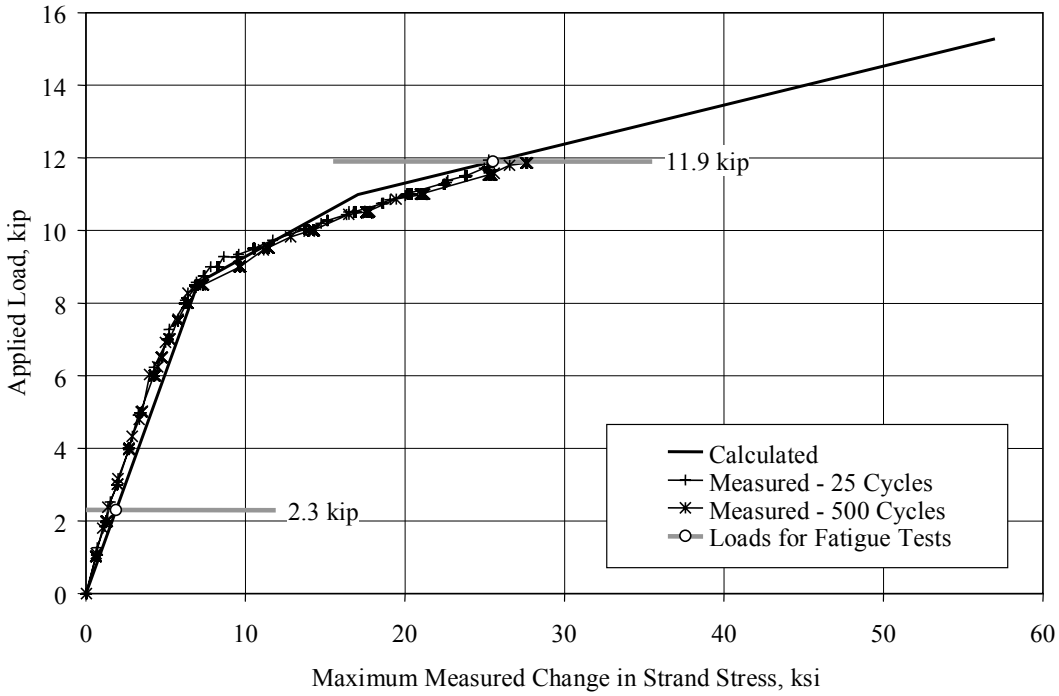

Figure 6.11 Comparison of Calculated and Measured Response of Beam 3

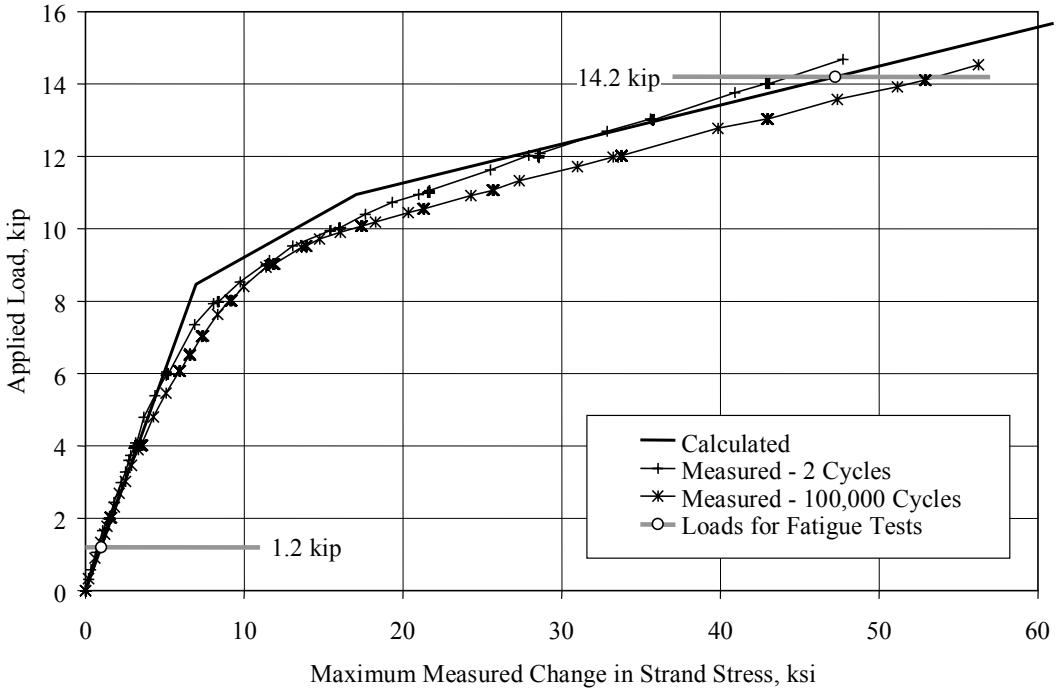

Figure 6.12 Comparison of Calculated and Measured Response of Beam 4

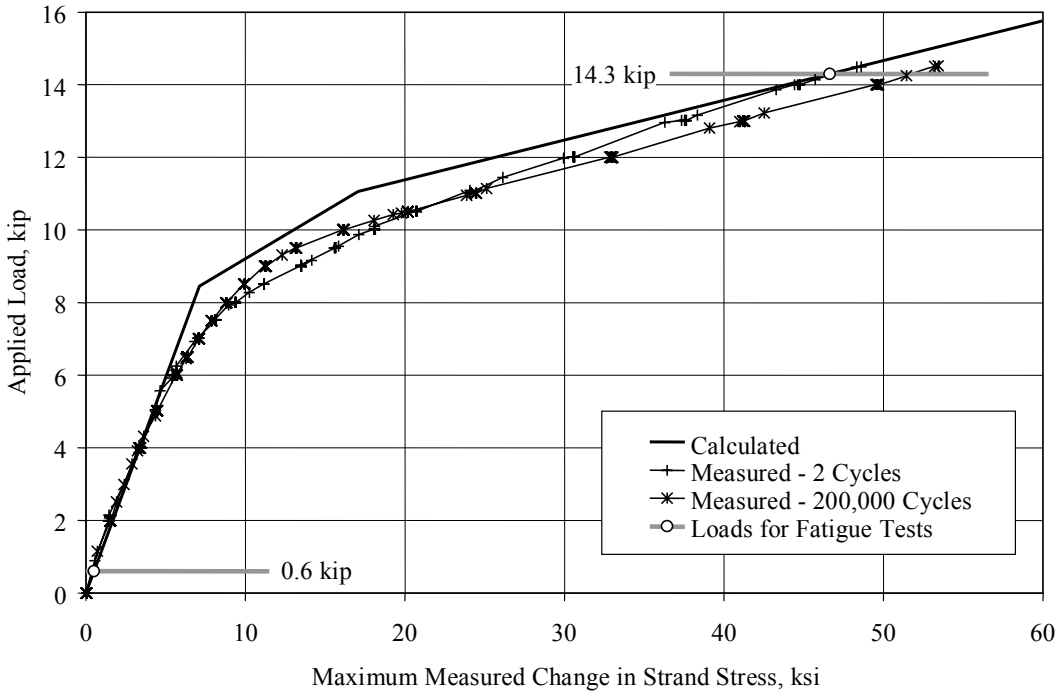

Figure 6.13 Comparison of Calculated and Measured Response of Beam 5

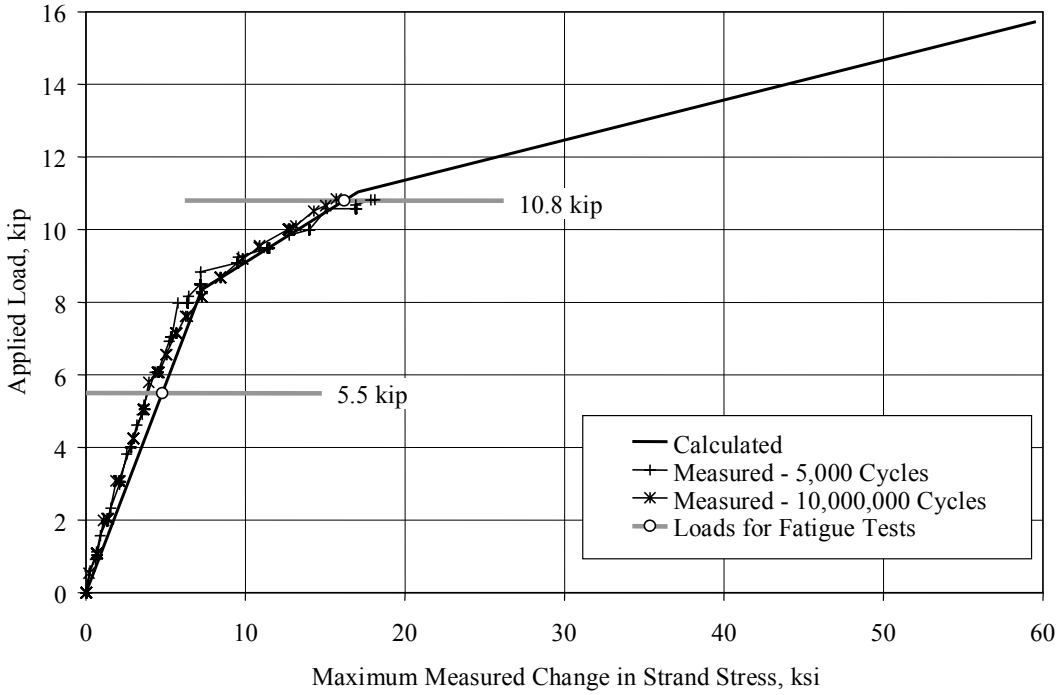

Figure 6.14 Comparison of Calculated and Measured Response of Beam 6

6.6 SUMMARY OF FATIGUE TESTS

Generally the trends in the measured response of the test specimens were as expected. As the stress range in the strand increased, the fatigue life decreased significantly. Beams 1 and 6, which were tested at the lowest strand stress range, survived 10,000,000 cycles with no signs of significant deterioration. Beams 2 and 3 survived an average of 3,900,000 cycles at a stress range of approximately 26 ksi after which significant deterioration began. Beams 4 and 5 survived an average of 420,000 cycles at a stress range of approximately 48 ksi before wires fractured in the strand.

The results from these six fatigue tests are compared with data from previous studies in Figure 6.15. The maximum measured range in stress of the strand was used in the plot. The measured fatigue lives of the beams tested in this experiment tended to be longer than those measured by previous researchers. The fatigue model for Detail Category C in the AASHTO LRFD Specifications is also plotted for reference.

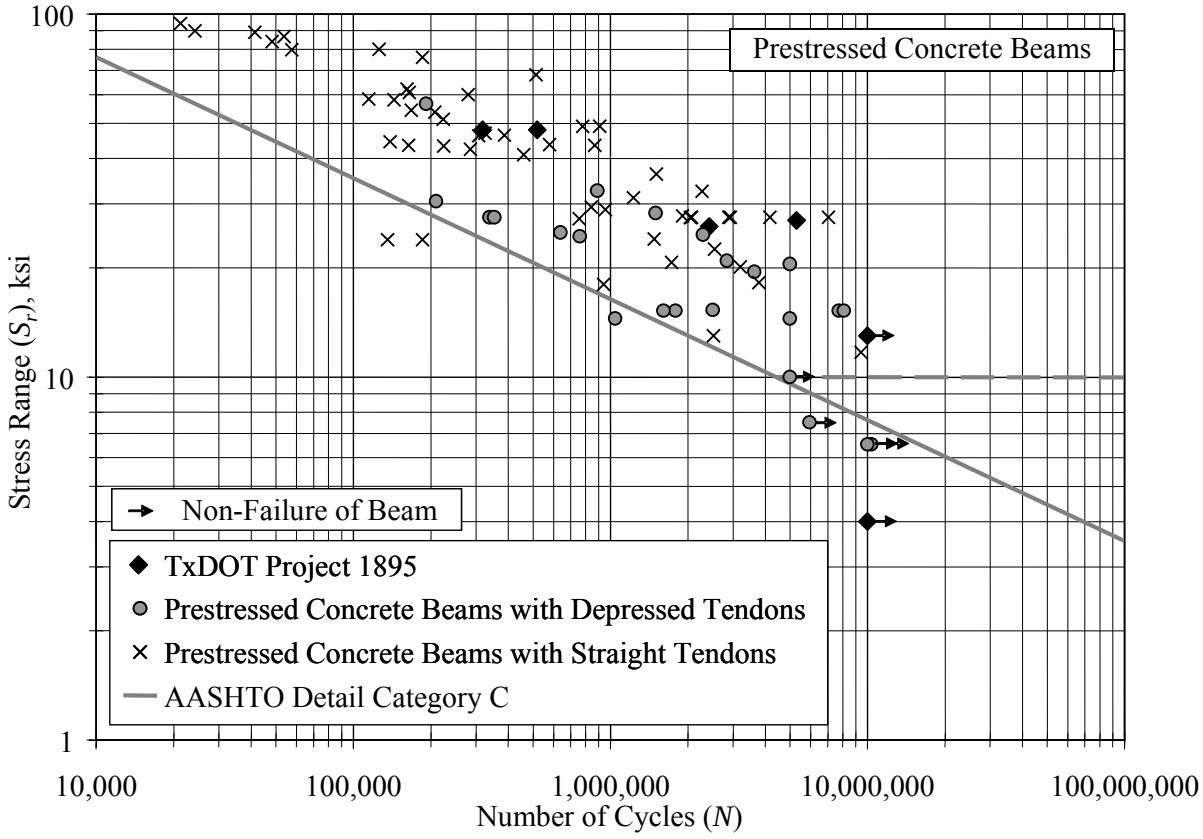

Figure 6.15 Comparison of Measured Response of Test Specimens with Previous Investigations

CHAPTER 7
Evaluation of Current Load Rating Procedures

The procedures in the AASHTO Manual for Condition Evaluation of Bridges are currently used by TxDOT to determine the load rating for existing bridges. A total of nine criteria (six at the inventory level and three at the operating level) must be evaluated for prestressed concrete bridges. These requirements are summarized in Section 7.1. As discussed in Chapter 2, the inventory-level rating is typically controlled by the serviceability limit state for the older prestressed concrete bridges considered in this investigation, and the load ratings tend to be less than 1.0. These ratings are not consistent with the results of visual inspections conducted by TxDOT and the project team, because no signs of deterioration have been observed.

Because the MCEB gives the engineer some flexibility in selecting material properties and distributing live load when evaluating a bridge, a range of rating factors may be calculated. Eight sets of inventory-level ratings are presented in Section 7.2. By increasing the limiting tensile stress in the concrete to $12\sqrt{f_c'}$, the inventory-level rating factors exceeded 1.0 for four of the five bridges considered. However, evaluation of fatigue data from prestressed concrete beams (Heller, 2003) confirmed that flexural cracks will be present in the bridge girders under repeated loadings to this level.

The stress range in the strand due to live load corresponding to a rating factor of 1.0 is calculated in Section 7.3. The results indicate that the fatigue limit state should be considered explicitly in the load rating process. Recommended changes to the load rating procedures in the MCEB for prestressed concrete bridges are summarized in Section 7.4. New procedures for evaluating the fatigue limit state are given in Chapter 8.

7.1 LOAD RATING PROCEDURES

Load rating is a method for determining the allowable live load for a bridge. Bridges are rated at both the inventory level and the operating level. The inventory-level rating corresponds to the live load that a bridge can resist for an infinite number of loading cycles. In contrast, the operating-level rating provides the maximum live load that a bridge can carry, but loading cycles at this level may shorten the life of the bridge.

7.1.1 Inventory-Level Rating

Both capacity and serviceability limit states are considered when determining the inventory-level rating for prestressed concrete bridges. The general form of the rating factor (*RF*) for the capacity limit state is:

$$RF = \frac{\phi R_n - A_1 D}{A_2 L(1+I)} \tag{7.1}$$

where:

R_n = nominal capacity of the member
ϕ = strength reduction factor
D = dead load effect
L = live load effect
A_1 = dead load factor
A_2 = live load factor
I = impact factor

The MCEB defines A_1 = 1.3 and A_2 =2.17 for inventory level ratings at the capacity limit state. The impact factor, *I*, is defined as $50/(L+125) \le 0.30$ in the AASHTO Standard Specifications, where L refers to the span length in ft. The HS-20 design vehicle (Figure 7.1) is used to calculate the live load response. A rear axle spacing of 14 ft produced the maximum moment in all spans.

Both the flexural and shear strengths of the prestressed concrete member must be evaluated using Eq. 7.1. For the bridges considered in this study, the flexural capacity controlled the inventory-level load rating at the capacity limit state (Wagener 2002).

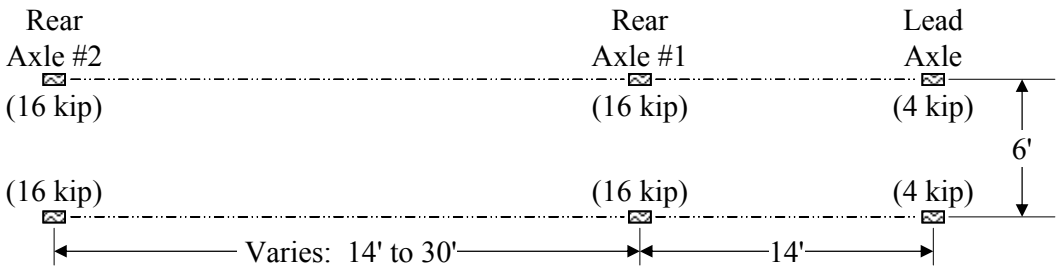

Figure 7.1 Axle Loads and Spacings for HS-20 Design Vehicle

The general form of the rating factor at the inventory level for the serviceability limit state is given in Eq. 7.2. Secondary stresses are not included in Eq. 7.2 because all bridges considered in this investigation are simply supported.

$$RF = \frac{f_{\lim} - \alpha\left(f_D + f_P\right)}{f_L} \tag{7.2}$$

where:

$f_{\lim}$ = limiting stress in concrete or prestressing steel
f_D = unfactored dead load stress
f_P = unfactored stress due to prestress force after all losses
α = reduction factor for sustained loads
f_L = unfactored live load stress including impact

The MCEB defines one limiting stress for tension in the concrete ($6\sqrt{f_c'}$), two for compression in the concrete ($0.6\,f_c'$ and $0.4\,f_c'$), and one for tension in the prestressing steel ($0.8\,f_y$). All stresses are calculated using gross cross-sectional properties. The value of α is taken as 0.5 when the limiting compressive stress in the concrete is $0.4\,f_c'$ and 1.0 for all other cases. A consistent sign convention must be used in Eq. 7.2. When evaluating tensile stresses in the concrete at the bottom fiber of the composite cross section, f_D and f_L are positive (indicating tensile stress), while f_P is negative (indicating compressive stress).

The tensile stress in the concrete controlled the inventory-level load rating for the serviceability limit state for all bridges considered in this investigation (Wagener 2002). The minimum rating factor from Eq. 7.1 and Eq. 7.2 determines the load rating for the bridge. If the governing rating factor is less than 1.0, the bridge must be posted to limit the live load that may cross the bridge.

7.1.2 Operating-Level Rating

Both capacity and serviceability limit states are also considered when determining the operating-level rating. For the capacity limit state, the general form of the rating equation is the same as Eq. 7.1. The value of A_2, however, is taken as 1.3 for the operating level. The values of A_1 and I remain unchanged. Both the flexural and shear strengths of the prestressed concrete member must be evaluated at the operating level.

Only one serviceability limit state is defined at the operating level, and it corresponds to the tensile stress in the prestressing steel. The rating factor has the same form as Eq. 7.2, but $f_{\lim}$ is taken as $0.9\,f_y$ and α is taken as 1.0.

The flexural capacity controlled the operating-level load rating for all bridges considered in this investigation (Wagener 2002).

7.2 CALCULATED LOAD RATINGS

Load ratings are typically calculated using the material properties specified on the structural drawings and the design procedures in the AASHTO Standard Specifications. The results of these analyses at the inventory and operating levels are presented in Section 7.2.1. The MCEB also allows the engineer to use the measured material properties and the live load distribution factors determined from diagnostic load tests or advanced structural analysis methods in the load rating analyses. Two parametric studies are discussed in this section to demonstrate the range of load ratings that can be calculated for older prestressed concrete bridges by taking advantage of the flexibility in the MCEB provisions. The sensitivity of the inventory-level load ratings to the choice of limiting tensile stress in the concrete is discussed in Section 7.2.2, and the sensitivity of the inventory-level load ratings to the choice of live load distribution factors is discussed in Section 7.2.3.

The values of parameters A_1, A_2, and I were not varied in the analyses and are defined in Section 7.1. The cross-sectional properties corresponding to the specified material properties were used in all analyses.

7.2.1 Evaluation using Baseline Assumptions

The rating factors discussed in this section were calculated using the baseline assumptions in the MCEB: the limiting tensile stress in the concrete was taken as $6\sqrt{f_c'}$, where f_c' corresponds to the specified compressive strength of the concrete, and live load distribution factors were taken from the AASHTO Standard Specifications. These results will be used as the baseline for evaluating the parametric studies presented in Sections 7.2.2 and 7.2.3, and will be referenced as Analysis A throughout this section.

Two rating factors are reported at the inventory level (serviceability limit state corresponding to the tensile stress in the concrete and capacity limit state corresponding to the flexural capacity of the composite cross section) and one is reported at the operating level (flexural capacity). Although other limit states are defined in the MCEB for the evaluation of prestressed concrete bridge, the corresponding rating factors were significantly larger and did not control for any of the bridges considered (Wagener, 2002). The results are summarized in Table 7.1 for the inventory level and in
Table 7.2 for the operating level. The results are also plotted in Figure 7.2. When the lengths of the spans are not constant along a bridge, the rating factors for both spans are reported. However, the governing rating factor for the entire bridge is also identified.

As expected, the inventory-level ratings were controlled by the tensile stress in the concrete at the serviceability limit state for all bridges. The corresponding rating factors were less than 1.0 for all bridges except the Wimberley Bridge. The rating factor was less than 0.5 for the Lampasas River Bridge, and ranged between 0.70 to 0.96 for the Chandler Creek, Lake LBJ, and Willis Creek Bridges.

The inventory-level ratings corresponding to the flexural capacity exceeded 1.0 for all five bridges. The operating-level ratings were approximately 60% larger than the inventory-level ratings, due to the different values of A_2 used in the calculations.

These results of the baseline analyses are consistent with TxDOT calculations. The fact that none of these bridges exhibits any signs of deterioration is a strong indicator that using a limiting tensile stress of $6\sqrt{f_c'}$ to evaluate the serviceability limit state is overly conservative. Approaches for increasing the inventory-level load rating are discussed in the following sections. Operating-level ratings are not addressed explicitly because any change in the rating factor will be directly proportional to the change in the inventory-level rating factor corresponding to the flexural capacity limit state.

Table 7.1 Results of Load Rating Analysis A: Inventory-Level Rating

Bridge		Rating Factor			
		Tensile Stress Criterion		Flexural Strength Criterion	
		Interior Girder	Exterior Girder	Interior Girder	Exterior Girder
Chandler Creek	40-ft Span	1.23	1.28	1.17	1.18
	60-ft Span	0.96*	1.03	1.25	1.26
Lake LBJ		0.88*	0.92	1.31	1.27
Lampasas River		0.49*	0.55	1.04	1.05
Willis Creek		0.72	0.70*	1.16	1.12
Wimberley	40-ft Span	2.02	2.32	2.00	1.94
	60-ft Span	1.04*	1.09	1.43	1.37

* Controls load rating at inventory level.

Table 7.2 Results of Load Rating Analysis A: Operating-Level Rating

Bridge		Rating Factor Flexural Strength Criterion	
		Interior Girder	Exterior Girder
Chandler Creek	40-ft Span	1.95*	1.97
	60-ft Span	2.08	2.11
Lake LBJ		2.18	2.11*
Lampasas River		1.74*	1.76
Willis Creek		1.94	1.88*
Wimberley	40-ft Span	3.35	3.26
	60-ft Span	2.38	2.28*

* Controls load rating at operating level.

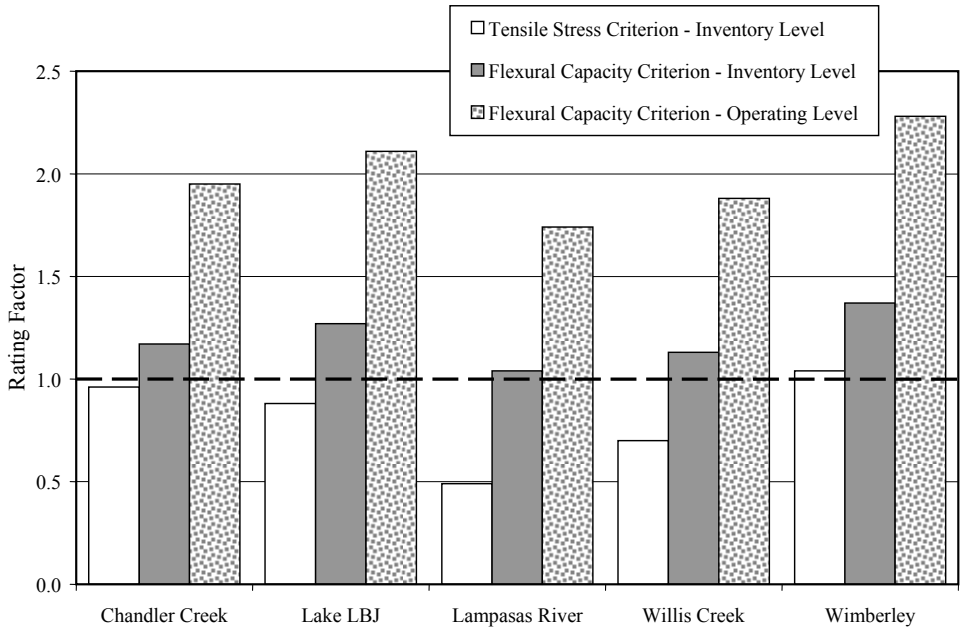

Figure 7.2 Summary of Baseline Load Ratings

7.2.2 Sensitivity to Limiting Tensile Stress in Concrete

The first parameter study was designed to investigate the sensitivity of the inventory-level ratings to the choice of limiting tensile stress in the concrete. Four values were selected for investigation (Table 7.3). As discussed in Section 7.2.1, Analysis A corresponds to the MCEB limit of $6\sqrt{f_c'}$. The value was increased to $7.5\sqrt{f_c'}$ in Analysis B, which corresponds to the limit often used by TxDOT for load rating older prestressed concrete bridges. A value of $12\sqrt{f_c'}$ was used in Analysis C, which corresponds to the upper limit used by TxDOT.

As discussed in Chapter 2, results from the quality control tests are often available in the TxDOT archives. The limiting tensile stress of $6\sqrt{f'_{c_{28}}}$ was selected for Analysis D to represent the strength of the concrete at the time of construction.

The results of the load rating Analyses B through D are summarized in Table 7.4 through Table 7.6, respectively. The results are also shown graphically in Figure 7.3.

When the limiting tensile stress was increased to $7.5\sqrt{f'_c}$ (Analysis B), the rating factors were still controlled by the tensile stress criterion for all five bridges. However, the rating factors increased by 10 to 20% compared with the results from Analysis A, and exceeded 1.0 for both the Chandler Creek and Wimberley Bridges. Using a limiting tensile stress of $6\sqrt{f'_{c_{28}}}$ (Analysis D) increased the rating factors by another 5 to 10%, and the governing rating factor for the Lake LBJ Bridge exceeded 1.0.

The rating factors calculated in Analysis C ($12\sqrt{f'_c}$) were 20 to 70% larger than those calculated in Analysis A. For this level of limiting tensile stress in the concrete, the flexural capacity limit state controlled the inventory-level load rating for all bridges except the Lampasas River Bridge, and the Lampasas River Bridge was the only bridge with a rating factor less than 1.0.

Table 7.3 Parameters used to Evaluate Sensitivity of Rating Factors to Limiting Tensile Stress

Load Rating Analysis	Live Load Distribution Factors	Limiting Tensile Stress in Concrete
A	AASHTO Standard	$6\sqrt{f'_c}$
B	AASHTO Standard	$7.5\sqrt{f'_c}$
C	AASHTO Standard	$12\sqrt{f'_c}$
D	AASHTO Standard	$6\sqrt{f'_{c_{28}}}$

Note:

f'_c = specified compressive strength of concrete

$f'_{c_{28}}$ = estimated compressive strength of concrete at 28 days

Table 7.4 Results of Load Rating Analysis B

Bridge		Inventory-Level Rating Factor			
		Tensile Stress Criterion		Flexural Strength Criterion	
		Interior Girder	Exterior Girder	Interior Girder	Exterior Girder
Chandler Creek	40-ft Span	1.35	1.41	1.17	1.18
	60-ft Span	1.08*	1.14	1.25	1.26
Lake LBJ		0.99*	1.04	1.31	1.27
Lampasas River		0.58*	0.64	1.04	1.05
Willis Creek		0.83	0.82*	1.16	1.12
Wimberley	40-ft Span	2.16	2.48	2.00	1.94
	60-ft Span	1.16*	1.22	1.43	1.37

* Controls load rating at inventory level.

Table 7.5 Results of Load Rating Analysis C

Bridge		Inventory-Level Rating Factor			
		Tensile Stress Criterion		Flexural Strength Criterion	
		Interior Girder	Exterior Girder	Interior Girder	Exterior Girder
Chandler Creek	40-ft Span	1.73	1.79	1.17*	1.18
	60-ft Span	1.41	1.47	1.25	1.26
Lake LBJ		1.29	1.38	1.31	1.27*
Lampasas River		0.85*	0.91	1.04	1.05
Willis Creek		1.16	1.18	1.16	1.12*
Wimberley	40-ft Span	2.59	2.96	2.00	1.94
	60-ft Span	1.52	1.59	1.43	1.37*

* Controls load rating at inventory level.

Table 7.6 Results of Load Rating Analysis D

Bridge		Inventory-Level Rating Factor			
		Tensile Stress Criterion		Flexural Strength Criterion	
		Interior Girder	Exterior Girder	Interior Girder	Exterior Girder
Chandler Creek	40-ft Span	1.36	1.42	1.17	1.18
	60-ft Span	1.13*	1.19	1.25	1.26
Lake LBJ		1.01*	1.07	1.31	1.27
Lampasas River		0.63*	0.68	1.04	1.05
Willis Creek		0.87	0.86*	1.16	1.12
Wimberley	40-ft Span	2.17	2.49	2.00	1.94
	60-ft Span	1.17*	1.23	1.43	1.37

* Controls load rating at inventory level.

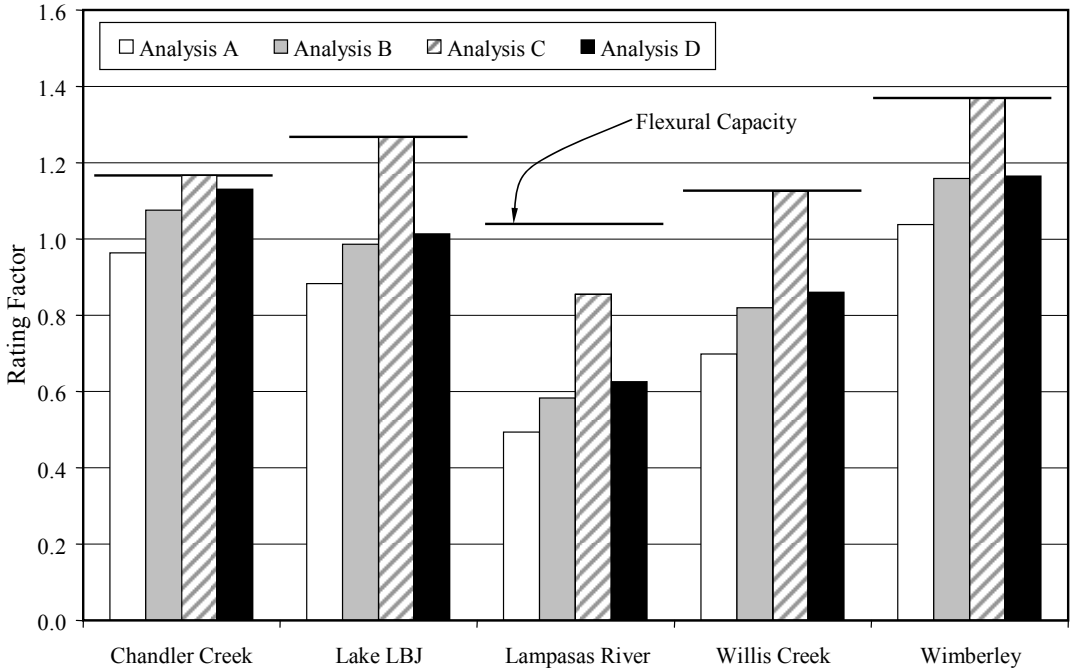

Figure 7.3 Variation of Inventory-Level Rating Factors with Limiting Tensile Stress in Concrete

7.2.3 Sensitivity to Live Load Distribution Factors

The second parameter study was designed to investigate the sensitivity of the inventory-level load ratings to the choice of live load distribution factors. Five sets of distribution factors were selected for investigation (Table 7.7). As discussed in Section 7.2.1, Analysis A corresponds to the default parameters within the MCEB. The live load distribution factors from the AASHTO LRFD Specifications (Appendix A) were selected for Analysis E. Finite element analyses (Chapter 4) were used to determine the live load distribution factors for Analyses F and G. In Analysis F, the loading vehicles were placed transversely to maximize the live load response, while the loading vehicles were centered in the traffic lanes in Analysis G. The maximum live load distribution factors from the diagnostic load tests (Chapter 4) were used in Analysis H. The live load distribution factors corresponding to two design lanes were used in all analyses.

The results of the load rating analyses E through H are summarized in Table 7.8 through Table 7.11, respectively. The results are also shown graphically in Figure 7.4.

Table 7.7 Parameters used to Evaluate Sensitivity of Rating Factors to Distribution of Live Load

Load Rating Analysis	Live Load Distribution Factors	Limiting Tensile Stress in Concrete
A	AASHTO Standard	$6\sqrt{f_c'}$
E	AASHTO LRFD	$6\sqrt{f_c'}$
F	Finite Element Analyses (Maximum Response)	$6\sqrt{f_c'}$
G	Finite Element Analyses (Centered in Lanes)	$6\sqrt{f_c'}$
H	Diagnostic Load Tests	$6\sqrt{f_c'}$

Table 7.8 Results of Load Rating Analysis E

Bridge		Inventory-Level Rating Factor			
		Tensile Stress Criterion		Flexural Strength Criterion	
		Interior Girder	Exterior Girder	Interior Girder	Exterior Girder
Chandler Creek	40-ft Span	1.38	1.37	1.31	1.27
	60-ft Span	1.12	1.07*	1.44	1.32
Lake LBJ		0.91	0.83*	1.34	1.16
Lampasas River		0.50	0.49*	1.06	0.94
Willis Creek		0.66	0.62*	1.07	1.00
Wimberley	40-ft Span	1.77	2.03	1.75	1.70
	60-ft Span	1.02*	1.09	1.41	1.37

* Controls load rating at inventory level.

Table 7.9 Results of Load Rating Analysis F

Bridge		Inventory-Level Rating Factor			
		Tensile Stress Criterion		Flexural Strength Criterion	
		Interior Girder	Exterior Girder	Interior Girder	Exterior Girder
Chandler Creek	40-ft Span	1.38	1.64	1.31	1.51
	60-ft Span	1.13*	1.14	1.47	1.40
Lake LBJ		1.06*	1.21	1.56	1.68
Lampasas River		0.57*	0.60	1.20	1.16
Willis Creek		0.78	0.74*	1.26	1.19
Wimberley	40-ft Span	2.21	2.68	2.18	2.22
	60-ft Span	1.13*	1.25	1.55	1.57

* Controls load rating at inventory level.

Table 7.10 Results of Load Rating Analysis G

Bridge		Inventory-Level Rating Factor			
		Tensile Stress Criterion		Flexural Strength Criterion	
		Interior Girder	Exterior Girder	Interior Girder	Exterior Girder
Chandler Creek	40-ft Span	1.69	1.64	1.61	1.51
	60-ft Span	1.33*	1.39	1.72	1.71
Lake LBJ		1.29*	1.31	1.91	1.81
Lampasas River		0.65*	0.72	1.37	1.38
Willis Creek		0.87	0.85*	1.41	1.36
Wimberley	40-ft Span	2.60	2.81	2.58	2.35
	60-ft Span	1.33*	1.33*	1.84	1.66

* Controls load rating at inventory level.

Table 7.11 Results of Load Rating Analysis H

Bridge		Inventory-Level Rating Factor			
		Tensile Stress Criterion		Flexural Strength Criterion	
		Interior Girder	Exterior Girder	Interior Girder	Exterior Girder
Chandler Creek	40-ft Span	1.40	1.50	1.33	1.39
	60-ft Span	1.12*	1.25	1.44	1.54
Lake LBJ		1.26*	1.26*	1.87	1.74
Lampasas River		0.61*	0.72	1.29	1.38
Willis Creek		0.87	0.77*	1.41	1.24
Wimberley	40-ft Span	2.16	2.66	2.14	2.22
	60-ft Span	1.11*	1.25	1.52	1.57

* Controls load rating at inventory level.

As discussed in Appendix A, the live load distribution factors in the LRFD Specifications were lower for the interior girders and higher for the exterior girders compared with those in the Standard Specifications for four of the five bridges considered. The live load distribution factors for the Chandler Creek Bridge were lower in the LRFD Specifications for all girders due to the skew reduction factor. As a result of these differences, the rating factors corresponding to the LRFD distribution factors (Analysis E) were 0 to 10% lower than those corresponding to Standard Specifications distribution factors (Analysis A) for the non-skewed bridges. The rating factor from Analysis E was 10% larger than that from Analysis A for the Chandler Creek Bridge.

When the distribution factors from the finite element analyses were used, the rating factors increased 5 to 20% relative to Analysis A for the loading vehicles positioned to maximize the live load response (Analysis F) and 20 to 45% for loading vehicles centered in the traffic lanes (Analysis G). The rating factors were 10 to 40% larger than those from Analysis A when the results of the diagnostic load tests (Analysis H) were used.

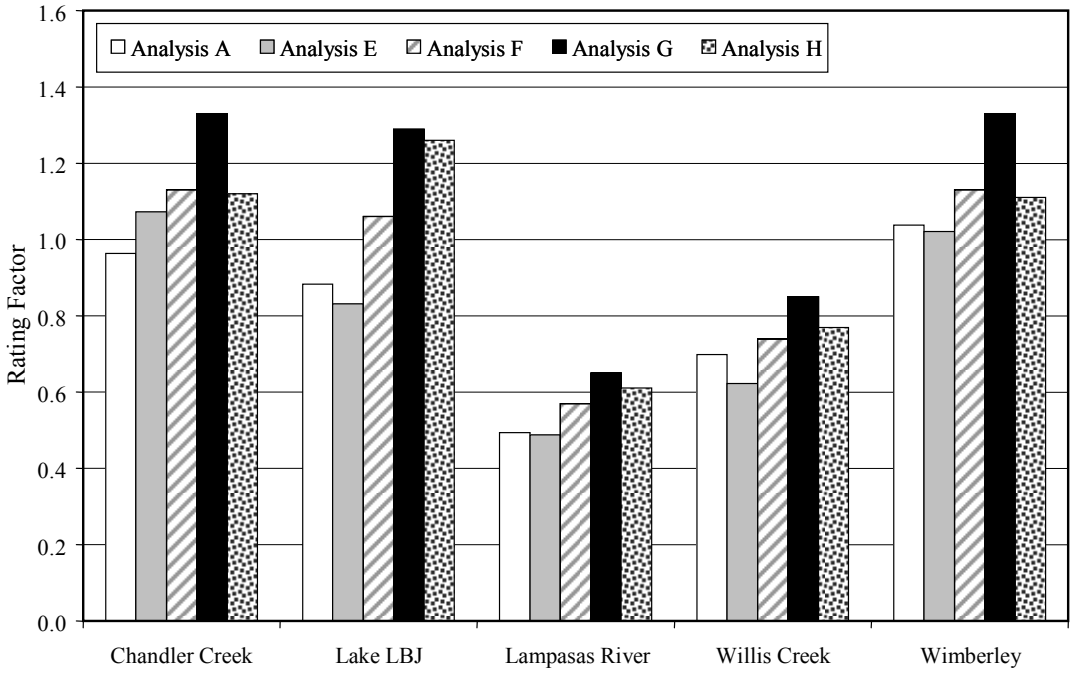

Figure 7.4 Variation of Inventory-Level Rating Factors with Live Load Distribution Factors

7.3 IMPLICATIONS OF INVENTORY-LEVEL LOAD RATINGS

A fundamental inconsistency exists in the process used to determine the inventory-level load rating for a prestressed concrete bridge. The serviceability limit state related to the tensile stress in the concrete is only valid for an uncracked cross section. The diagnostic load tests (Chapter 4) indicated that flexural cracks are likely to be present in most of the girders tested, yet no evidence of structural deterioration was detected. The presence of flexural cracks means that the possibility of fatigue damage is greater, it does not necessarily mean that the live load crossing the bridge must be reduced.

As a simple means of evaluating the likelihood that the fatigue limit state will control the inventory-level load rating, the variation of stress in the strand was estimated from the rating factors discussed in Section 7.2. For each girder, the maximum moment corresponding to an HS-20 design vehicle was multiplied by the impact amplification factor, $(1+I)$; the applicable live load distribution factor from the AASHTO Standard Specifications for two lanes of traffic; and the inventory-level rating factor for the bridge. The resulting moment represents the live-load moment distributed to the girder under the inventory-level live load. The nonlinear relationships between live load moment and stress range in the strand (Appendix B) were then used to estimate the variation of stress in the strand due to the inventory-level live load.

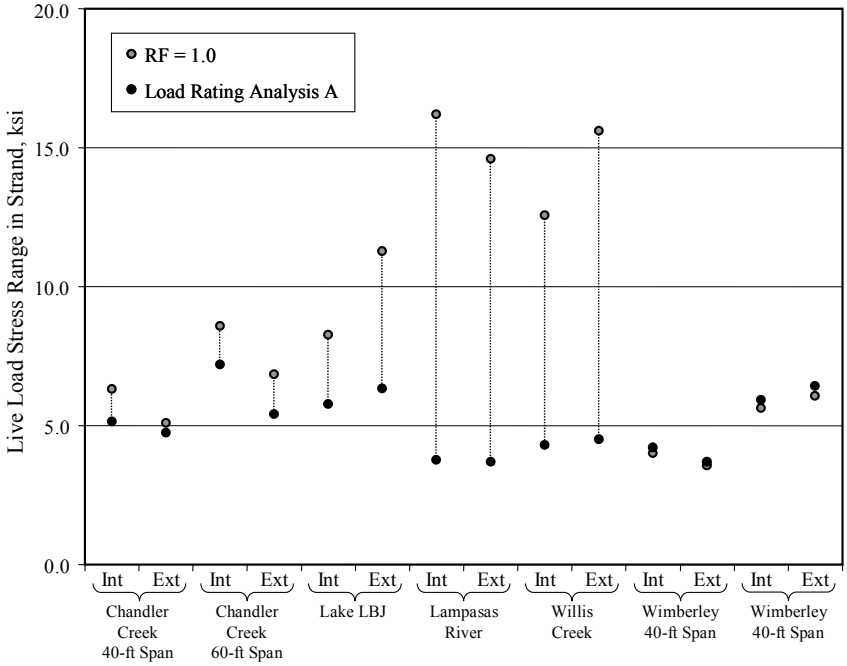

Figure 7.5 Variation of Strand Stress Range for Inventory-Level Live Load

The results of these analyses are plotted in Figure 7.5 for two cases: the default parameters in the MCEB (Analysis A) and a rating factor of 1.0. The variation of strand stress due to live load in Analysis A ranged from 3 to 8 ksi, while the variation corresponding to a rating factor of 1.0 ranged from 3 to 16 ksi. As indicated in Figure 6.15, no evidence of fatigue failures in prestressed concrete beams has been observed at a stress range of 3 ksi; however, the fatigue life of prestressed concrete beams ranged from 1 to 10 million cycles for stress ranges between 10 and 20 ksi.

Assuming a design life of 75 years, a fatigue life of 1 million cycles corresponds to approximately 40 loading cycles per day and a fatigue life of 10 million cycles corresponds to approximately 400 loading cycles per day. The average daily truck traffic exceeds this lower limit for all five bridges considered in this investigation (Table 2.2).

Although the analyses presented in this section do not correspond to a fatigue limit state, the results indicate that the fatigue life of the prestressed concrete bridges must be considered in more detail when determining the inventory-level load rating. Recommendations for evaluating the fatigue limit state are presented in Chapter 8.

7.4 RECOMMENDED CHANGES TO LOAD-RATING PROCEDURES IN MCEB

Based on the analyses discussed in this chapter, the following changes are recommended to the MCEB for existing prestressed concrete girder bridges that were designed in the 1950s and 1960s and exhibit no signs of deterioration during visual inspections:

(1) Use the capacity limit state provisions in the MCEB to determine the inventory-level and operating-level load ratings. The serviceability limit states do not need to be considered.

(2) Evaluate the fatigue limit state directly using the procedures defined in Chapter 8.

For the class of bridges considered in this investigation, the serviceability limit state defined in the MCEB corresponding to the maximum tensile stress in the concrete at the inventory level is overly conservative and is not a valid indicator of the fatigue limit state. A much better indication of the condition of the bridge is obtained by considering fatigue directly.

The rating factors corresponding to the over serviceability limit states do not influence the load rating, and can be safely ignored.

CHAPTER 8
Fatigue Life of Prestressed Concrete Bridges

As discussed in Chapter 7, the calculated inventory-level load ratings for all five prestressed concrete bridges considered in this investigation were controlled by the serviceability limit state for concrete in tension. It is recommended that the fatigue limit state be evaluated directly during the evaluation process, rather than using the serviceability limit states defined in the MCEB. The fatigue response of the five bridges is evaluated in detail in this chapter, and simplified procedures are introduced in Chapter 9.

When evaluating an existing bridge for the fatigue limit state, a spectrum of loading vehicles must be defined. Ideally, site-specific traffic data would be used, but this information is rarely available. Therefore, vehicle data from an interstate highway was used to evaluate all five bridges. The vehicle spectrum is presented in Section 8.1, and the corresponding spectra of moments induced in the bridges are discussed in Section 8.2. Procedures used to determine evaluate the fatigue life are discussed in Section 8.3.

8.1 SPECTRUM OF LOADING VEHICLES

A spectrum of loading vehicles was used to evaluate the fatigue response of prestressed concrete bridges. As part of TxDOT Project 0-4096, 50 days of weigh-in-motion data were evaluated from I-35 south of San Antonio (station 516 in Lytle). Nearly a quarter million trucks were detected by the weigh-in-motion station during this period. Trucks with five axles represented more than 80% of the total population, and trucks with three, four, or five axles represented approximately 99% of the total. The maximum number of axles recorded was nine.

The gross weights of the vehicles were grouped in 2-kip increments as shown in Figure 8.1, and a detail of the heavier vehicles is shown in Figure 8.2. The maximum recorded vehicle weight was 182 kip. The effective gross vehicle weight was calculated using Eq. 8.1 (AASHTO Guide Specifications, 1990):

$$GVW_{eff} = \left[\sum_{i=1}^{n} \left(\gamma_i \cdot GVW_i^3 \right) \right]^{1/3} \tag{8.1}$$

where

GVW_{eff} = effective gross vehicle weight of the entire spectrum of vehicles
γ_i = frequency of trucks in load range i within the entire spectrum of vehicles
GVW_i = mean gross vehicle weight in load range i
n = number of vehicles in entire spectrum

For this set of weigh-in-motion data, the effective gross vehicle weight is 56.8 kip, which is approximately 80% of the gross weight of the HS-20 design vehicle.

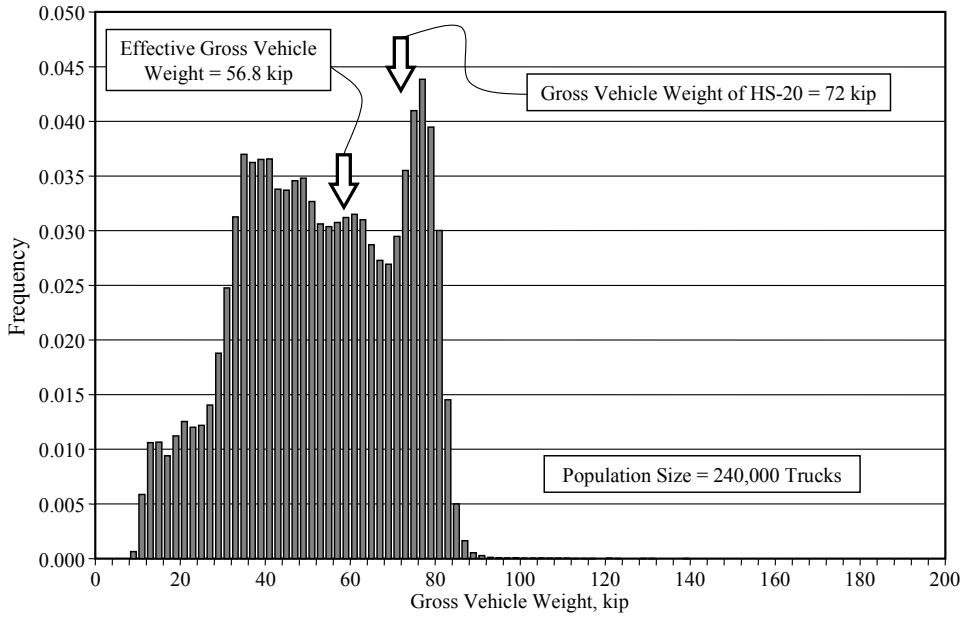

Figure 8.1 Spectrum of Trucks Corresponding to Interstate Traffic

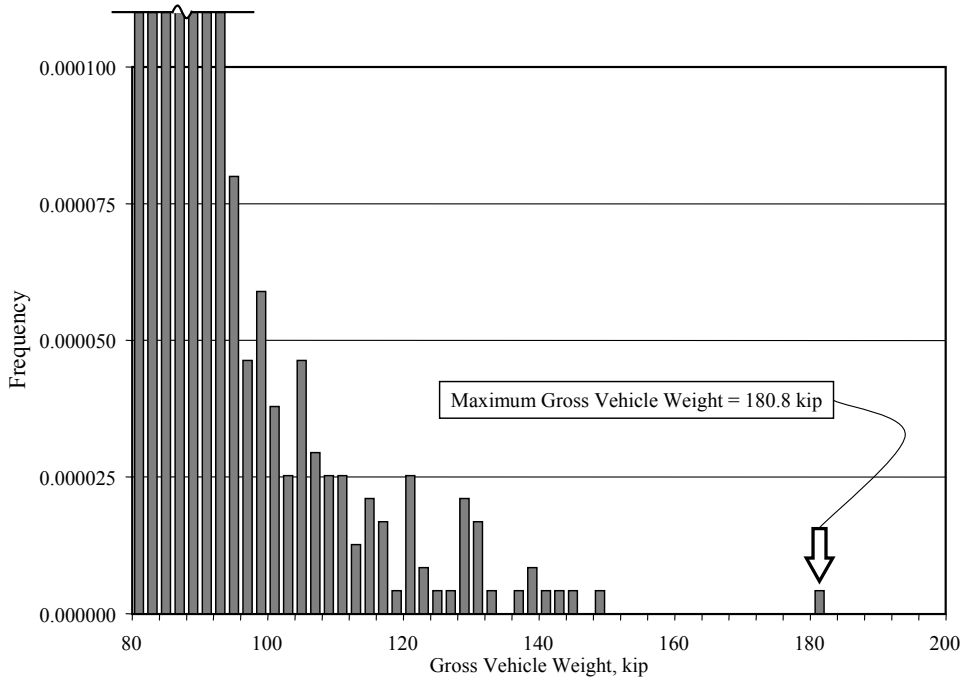

Figure 8.2 Detail of Truck Spectrum

8.2 SPECTRA OF LIVE LOAD MOMENTS

Because the maximum live load moment induced in a bridge by a vehicle depends on the span of the bridge and the configuration of the vehicle (number, weight, and spacing of axles), it is not possible to calculate the moment spectrum directly from the vehicle spectrum. Therefore, a series of line girder analyses were conducted and the maximum moment at midspan of each bridge was calculated for each vehicle within the population. The resulting moment spectra for the Chandler Creek, Lake LBJ, and Lampasas River Bridges are shown in Figure 8.3 through Figure 8.5. The spectra for the Willis Creek and Wimberley Bridges are essentially the same as those for the Lake LBJ and Chandler Creek Bridges, respectively.

The maximum live load moments at midspan were grouped in bins of 10 kip-ft, and the effective maximum moment at midspan was calculated using the same approach used to calculate the effective gross vehicle weight Eq. (8.1). The values of effective maximum moment and maximum moment at midspan corresponding to the entire spectrum of loading vehicles are listed in Table 8.1.

Table 8.1 Live Load Moments at Midpsan of Bridge

Bridge	Effective Maximum Moment at Midspan of Bridge (kip-ft)	Maximum Moment at Midspan of Bridge (kip-ft)
Chandler Creek (40-ft Span)	227	586
Chandler Creek (60-ft Span)	388	1023
Lake LBJ	432	1158
Lampasas River	529	1433
Willis Creek	432	1158
Wimberley (40-ft Span)	221	582
Wimberley (60-ft Span)	387	1018

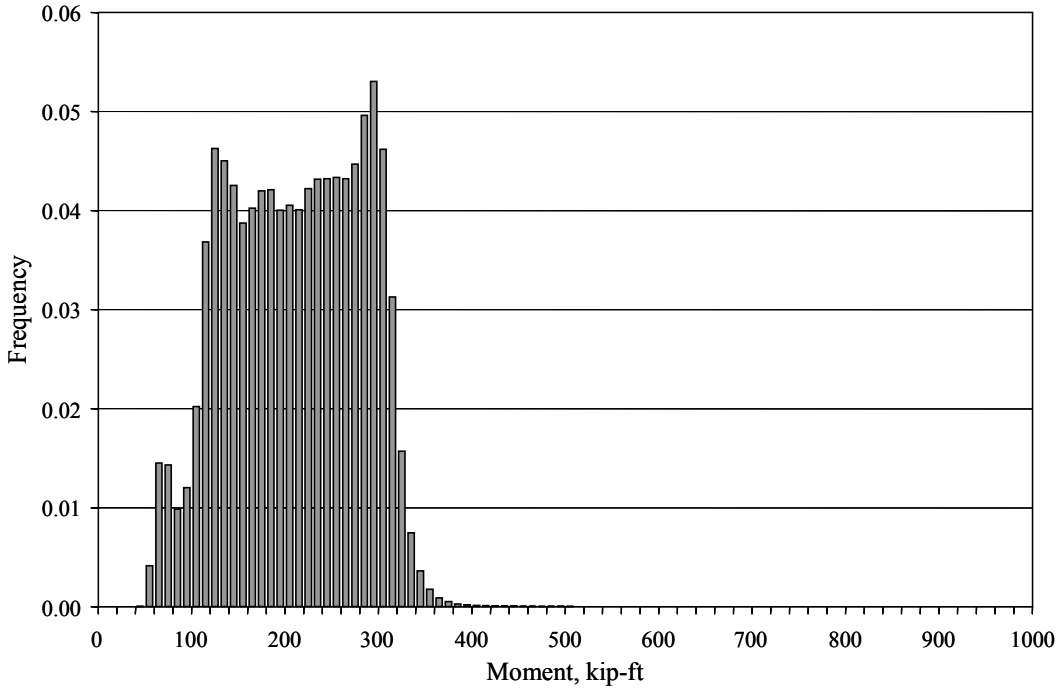

(a) 40-ft Span

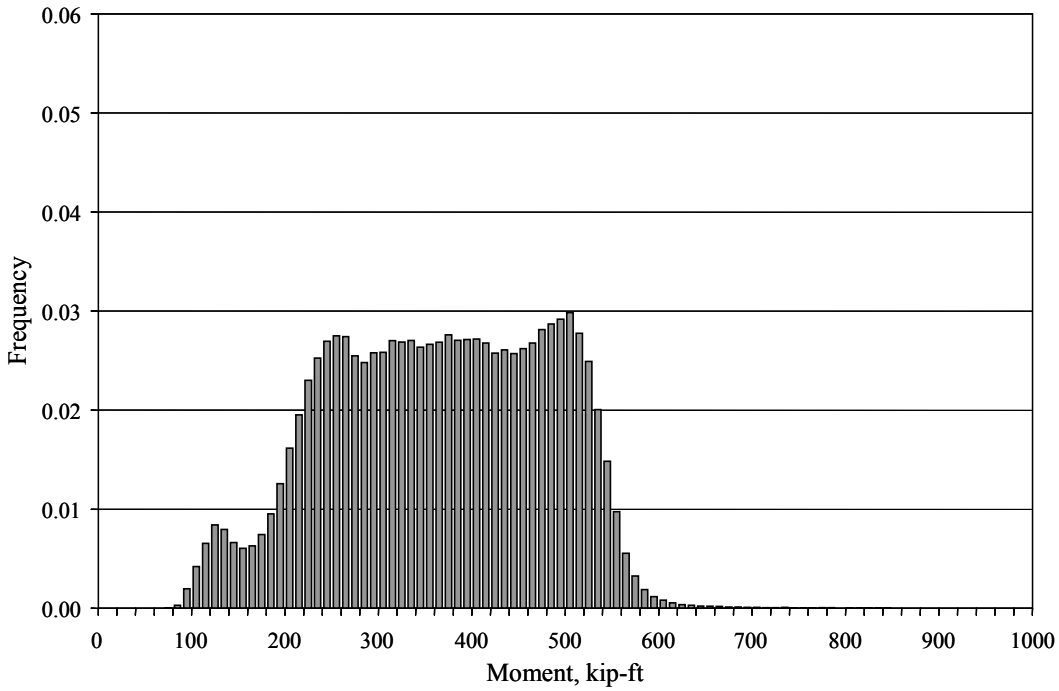

(b) 60-ft Span

Figure 8.3 Live Load Moment Spectra for Chandler Creek Bridge

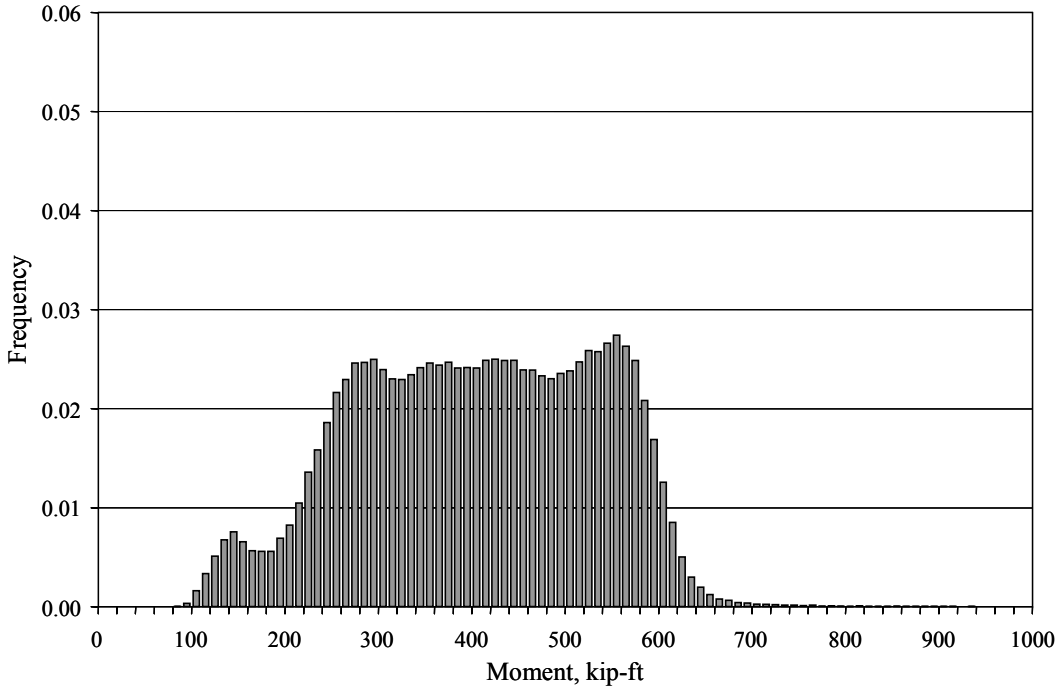

Figure 8.4 Live Load Moment Spectra for Lake LBJ Bridge

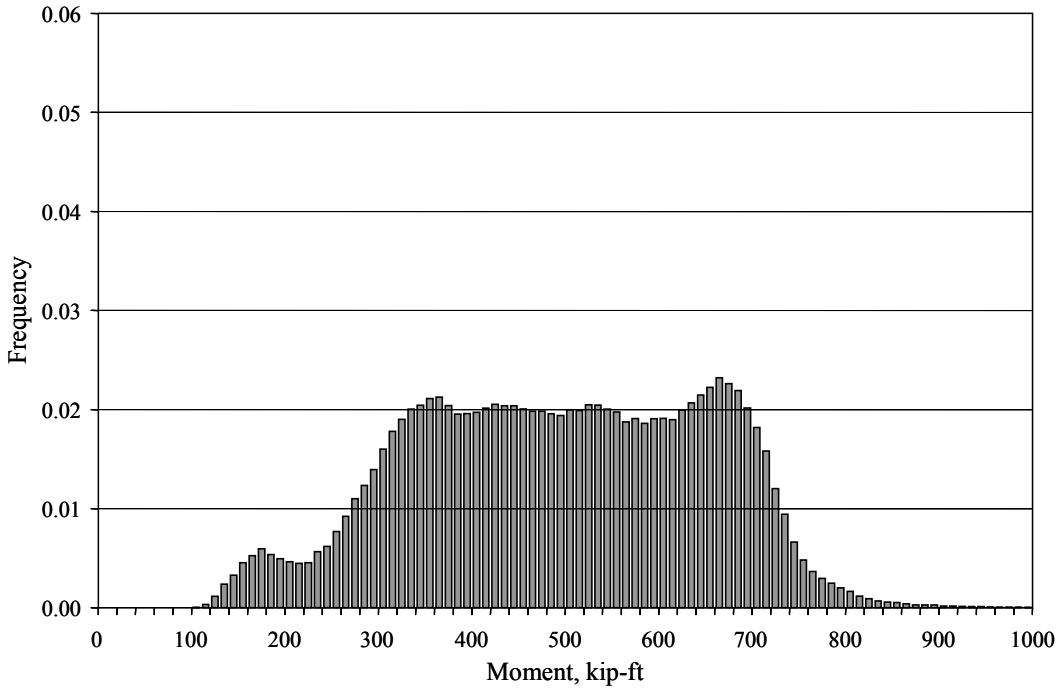

Figure 8.5 Live Load Moment Spectra for Lampasas River Bridge

8.3 FATIGUE LIFE OF BRIDGE GIRDERS

As discussed in Chapter 6, the fatigue life model for Detail Category C from the AASHTO LRFD Specifications (Figure 8.6) was adopted for prestressed concrete girders. If the stress induced in the strand by the maximum live load moment is less than the threshold stress, the girder is assumed to have an infinite fatigue life. However, if the live load stress in the strand under the maximum moment exceeds the threshold stress, the girder is assumed to have a finite fatigue life. For detail category C, the threshold stress is 10 ksi.

The maximum moments reported in Table 8.1 correspond to the maximum moment induced in the bridge for the spectrum of loading vehicles. In order to evaluate the stress in the strand, the moment must be distributed to the individual girders. For the fatigue limit state, the AASHTO LRFD Specifications use live load distribution factors corresponding to one lane of traffic and the impact factor, I, is taken as 0.15. The live load distribution factors from the AASHTO Standard Specifications were used in all calculations for consistency with the load rating procedures in the MCEB.

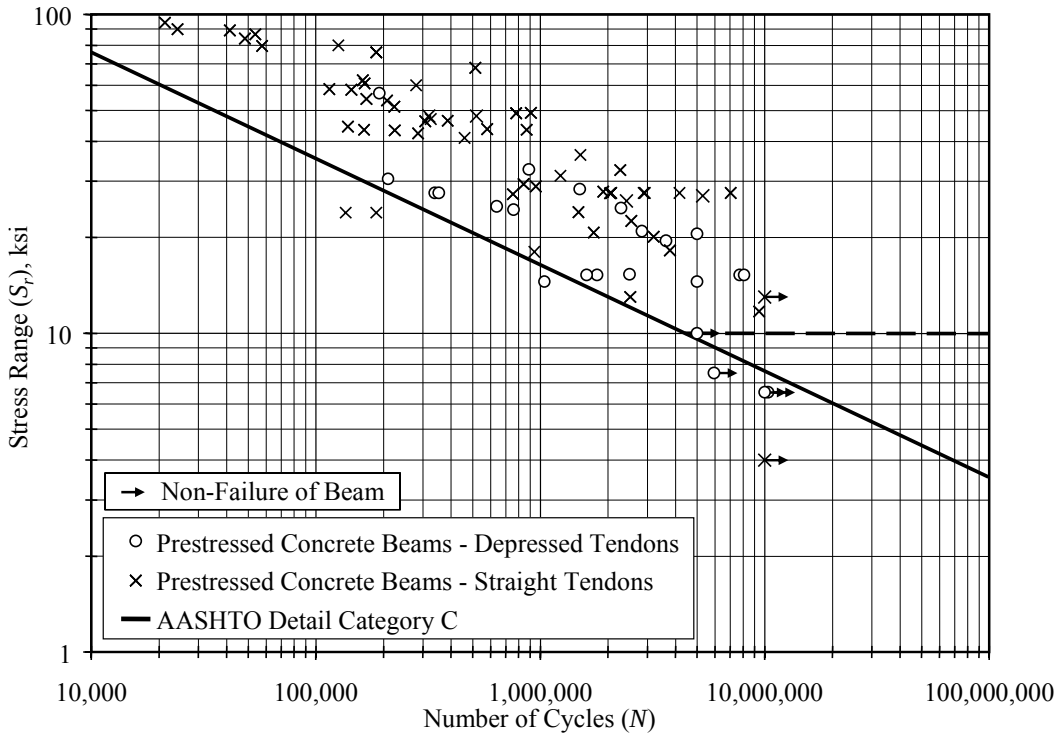

Figure 8.6 Idealized Fatigue Model for Prestressed Concrete Girders

Table 8.2 Maximum Live Load Moments in Bridge Girders

Bridge		Interior Girder		Exterior Girder	
		$M_{\max}$	$S_{r,\max}$	$M_{\max}$	$S_{r,\max}$
Chandler Creek	40-ft Span	384	4.7	424	7.3
	60-ft Span	671	5.1	741	7.9
Lake LBJ		759	6.1	839	13.4
Lampasas River		856	22.1	972	27.5
Willow Creek		639	10.1	732	20.0
Wimberley	40-ft Span	335	4.2	335	3.4
	60-ft Span	586	5.2	586	5.6

Maximum live load moments distributed to each girder, $M_{\max}$ are summarized in Table 8.2. The corresponding stress range in the strand, $S_{r,\max}$, was estimated from the nonlinear live load relationships for each girder (Appendix B). Based on these results, both spans of the Chandler Creek Bridge and both spans of the Wimberley Bridge are considered to have an infinite fatigue life because $S_{r,\max} \le S_{r,TH}$, where $S_{r,TH}$ is the threshold stress (10 ksi). The interior girders of the Lake LBJ Bridge were also considered to have an infinite fatigue life. This check for infinite fatigue life is the same as that used in the AASHTO Manual for Condition Evaluation and Load and Resistance Factor Rating of Highway Bridges (LRFR).

Because the Lampasas River Bridge, the Willow Creek Bridge, and exterior girders of the Lake LBJ Bridge do not satisfy the criterion for infinite fatigue life, the fatigue life must be determined and compared with the number of loading cycles expected during the 75-year design life of the bridge. However, an important difference exists between prestressed concrete bridges and steel bridges. For steel bridges, each loading vehicle induces stress cycles which reduce the fatigue life of the bridge. For prestressed concrete bridges, the accumulation of fatigue damage is assumed to be negligible if the maximum applied moment is less than the decompression moment in the girder. Therefore, only vehicles that induce moments above the decompression moment are considered when evaluating the fatigue life of a prestressed concrete bridge.

For example, the live load moment spectrum corresponding to vehicles that contribute fatigue cycles in the exterior girder of the Lake LBJ Bridge is shown in Figure 8.7. The total number of vehicles that that induce moments above the decompression moment in these girders is approximately 30% of the total population (Figure 8.1). Because the decompression moments in the girders depend on many factors, including the number and arrangement of strand, different spectra must be used to evaluate each girder of each bridge.

Once the fatigue spectrum is determined for each girder, the effective maximum moment at midspan is determined using Eq. 8.2:

$$M_{eff} = \left[\sum_{i=1}^{m} \left(\gamma_i' \cdot M_i^3 \right) \right]^{1/3} \tag{8.2}$$

where

M_{eff} = effective maximum moment at midspan of girder for fatigue spectrum
γ_i' = frequency of moments in range i within the fatigue spectrum
M_i = mean maximum moment at midspan in range i
m = number of vehicles in fatigue spectrum

The parameter β_{cr} represents the fraction of the total population of loading vehicles that exceed the critical moment, which is also the number of vehicles in the fatigue spectrum divided by the number of vehicles in the entire traffic spectrum, m/n.

The live load stress range at midspan of each girder was calculated from the maximum live load moment for each vehicle and the appropriate nonlinear live load relationship in Appendix B. The fatigue spectrum of live load stresses for the exterior girders of the Lake LBJ Bridge is shown in Figure 8.8. The effective live load stress corresponding to the fatigue spectrum is then calculated using Eq. 8.3:

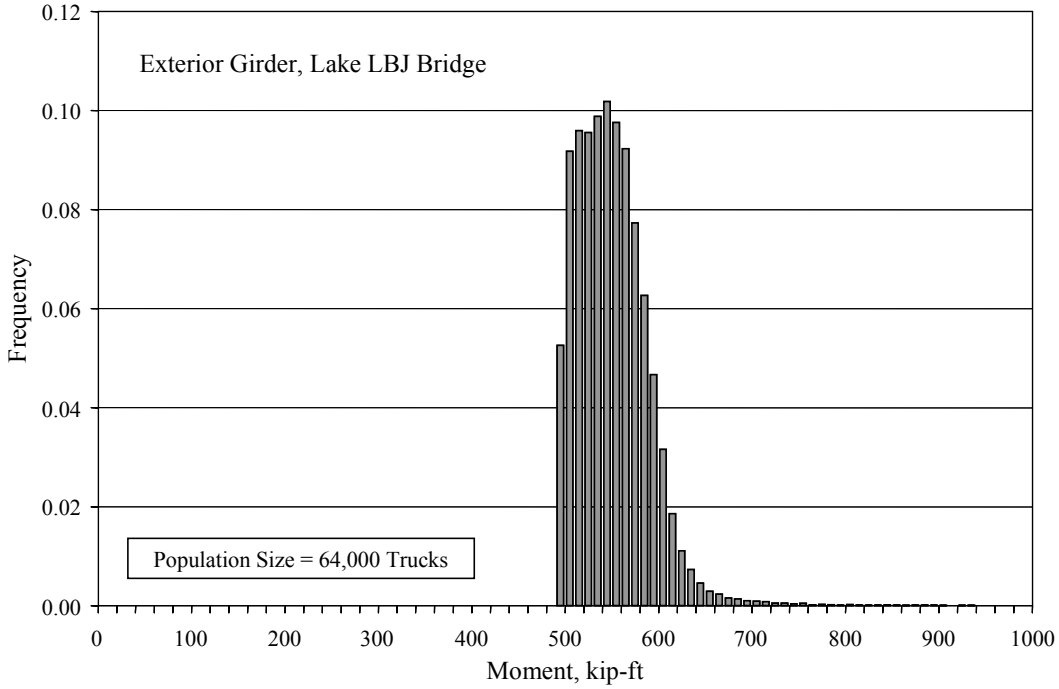

Figure 8.7 Fatigue Spectrum of Live Load Moments at Midspan of Exterior Girders for Lake LBJ Bridge

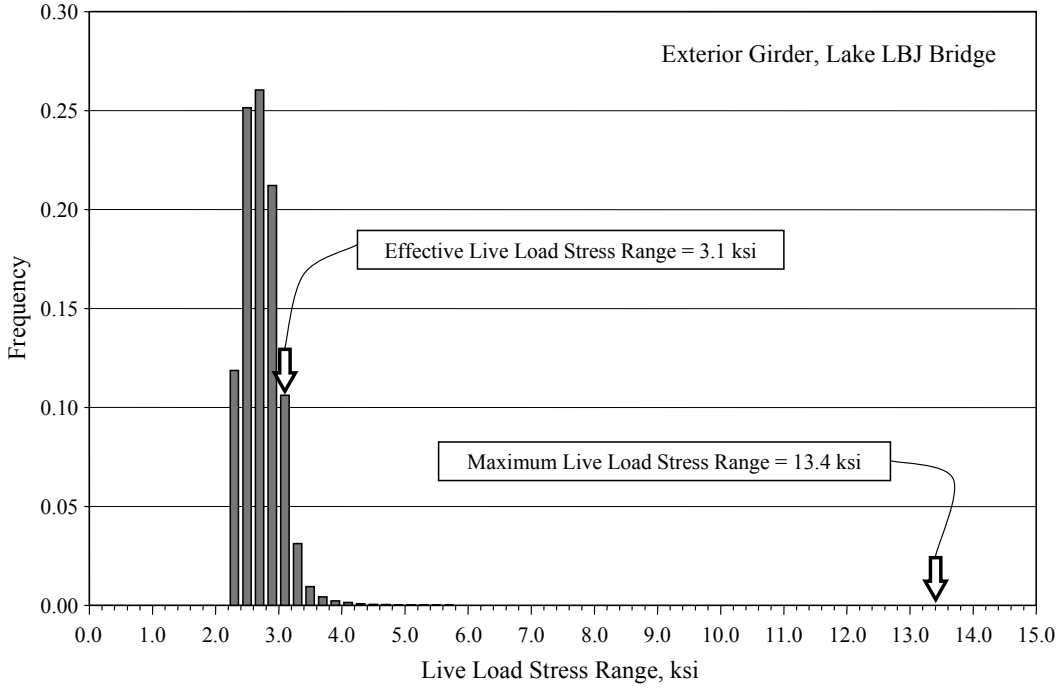

Figure 8.8 Fatigue Spectrum of Live Load Stress Range at Midspan of Exterior Girders for Lake LBJ Bridge

$$S_{r,eff} = \left[\sum_{i=1}^{m} \left(\gamma_i' \cdot S_{r,i}^3 \right) \right]^{1/3} \tag{8.3}$$

where

$S_{r,eff}$ = effective live load stress range midspan of girder for fatigue spectrum
γ_i' = frequency of stress range in range i within the fatigue spectrum
$S_{r,i}$ = live load stress range at midspan in range i
m = number of vehicles in fatigue spectrum

The effective live load moment and effective live load stress range are reported for all girders, including those with infinite fatigue lives, are reported in Table 8.3. It is interesting to note that no vehicles generated moments in the 40-ft span of the Wimberley Bridge that exceeded the decompression moment. Therefore, regardless of the traffic volume, fatigue cycles will not accumulate in this span. In contrast, approximately 95% of the total spectrum of vehicles contributes fatigue cycles to the Lampasas River Bridge.

Table 8.3 Effective Maximum Live Load Moments in Bridge Girders and Corresponding Fatigue Life

Bridge	Girder	Fraction of Population β_{cr}	M_{eff} (kip-ft)	$S_{r,eff}$ (ksi)	N (Cycles)
Chandler Creek 40-ft Span	Interior	0.0002	314	3.6	72,000,000
	Exterior	0.0003	340	4.0	51,000,000
Chandler Creek 60-ft Span	Interior	0.0085	395	2.7	176,000,000
	Exterior	0.0045	456	3.1	115,000,000
Lake LBJ	Interior	0.084	391	2.8	151,000,000
	Exterior	0.27	401	2.8	156,000,000
Lampasas River	Interior	0.96	321	2.7	174,000,000
	Exterior	0.93	367	3.1	115,000,000
Willow Creek	Interior	0.42	290	2.3	272,000,000
	Exterior	0.70	302	2.6	199,000,000
Wimberley 40-ft Span	Interior	0.0	—	—	—
	Exterior	0.0	—	—	—
Wimberley 60-ft Span	Interior	0.0012	402	3.1	107,000,000
	Exterior	0.0005	436	3.5	78,000,000

As expected, the effective stress ranges in the strand are considerably less than the stress range corresponding to the maximum moment. The fatigue life of each girder, N, was then determined using Eq. 8.4:

$$N = A\left(R_f S_{r,eff}\right)^{-3} \tag{8.4}$$

where $A = 44 \times 10^8$ (ksi^3) as defined in the AASHTO LRFD Specifications, $S_{r,eff}$ is the effective stress range in the strand (ksi), and R_f is an amplification factor to account for the increase in strain due to crack growth under repeated loading. A value of 1.10 was considered to be appropriate for R_f based on the results of the fatigue tests discussed in Chapter 6. The corresponding fatigue life for each girder is reported in Table 8.3, and ranged from approximately 50 million for the exterior girders of the 40-ft span of the Chandler Creek Bridge to more than 250 million for the interior girders of the Willow Creek Bridge.

The prestressed concrete bridges considered in this investigation (Table 2.1) were placed in service between 25 and 60 years ago. Traffic patterns have changed considerably during that period. Both the legal vehicle weight and traffic volume have increased. For the purpose of estimating the number of fatigue cycles experienced by each bridge during its service life, the distribution of vehicle

weights in the population (Figure 8.1) is assumed to be constant, and the number of trucks is assumed to grow at the same rate as the total traffic volume.

During the service life, the traffic volume is assumed to increase by a constant percentage annually. The projected increase in traffic volume over the 75-year design life of a typical highway bridge is shown in Figure 8.9 for annual growth rates of 2%, 4%, and 6%. The total traffic volume during the design life may be expressed as:

$$T_{total} = T_i \sum_{i=0}^{75} (1+u)^i \tag{8.5}$$

where

T_{total} = total traffic volume over 75-year service life of bridge
T_i = initial traffic volume
u = annual rate of traffic growth

As indicated in Table 2.2, traffic volume data are reported on a periodic basis. If T reflects the most current traffic volume information, it can be related to the initial traffic volume by:

$$T = T_i (1+u)^k \tag{8.6}$$

where k is the age of bridge in years at the time the traffic volume information was collected.

The ratio of the average annual traffic volume over the design life to the current traffic volume, Ω, provides a convenient means of estimating the total number of loading cycles during the design life:

$$\Omega = \frac{(T_{total}/75)}{T} = \frac{T_i \sum_{i=0}^{75} (1+u)^i}{75 T_i (1+u)^k} = \frac{\sum_{i=0}^{75} (1+u)^i}{75(1+u)^k} \tag{8.7}$$

The ratio Ω is plotted in Figure 8.10 for annual growth rates of 2%, 4%, and 6%. For bridges in service 50 or more years, $\Omega \le 1.0$ regardless of the assumed rate of traffic growth. For bridges in service 30 to 50 years, $1.0 \le \Omega \le 3.0$. Most of the bridges considered in this investigation are within this range.

Once the ratio Ω is known, the expected number of fatigue cycles over the 75-year service life of the bridge, N_{75}, may be calculated:

$$N_{75} = \Omega \beta (ADTT)(365)(75) \tag{8.8}$$

where $ADTT$ is the current average daily volume of truck traffic.

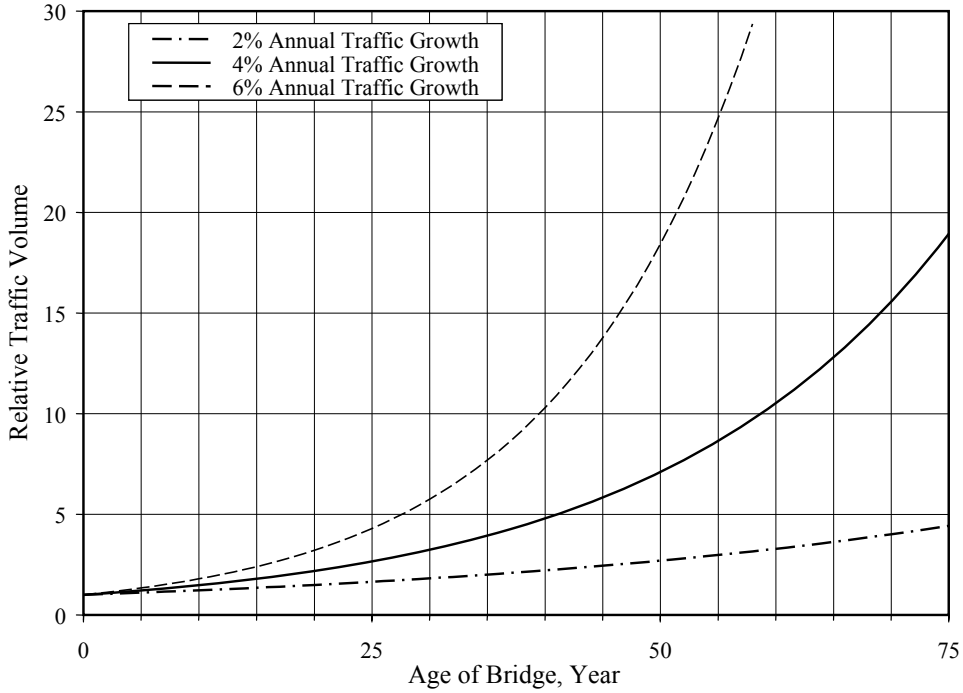

Figure 8.9 Assumed Increase in Traffic Volume with Time

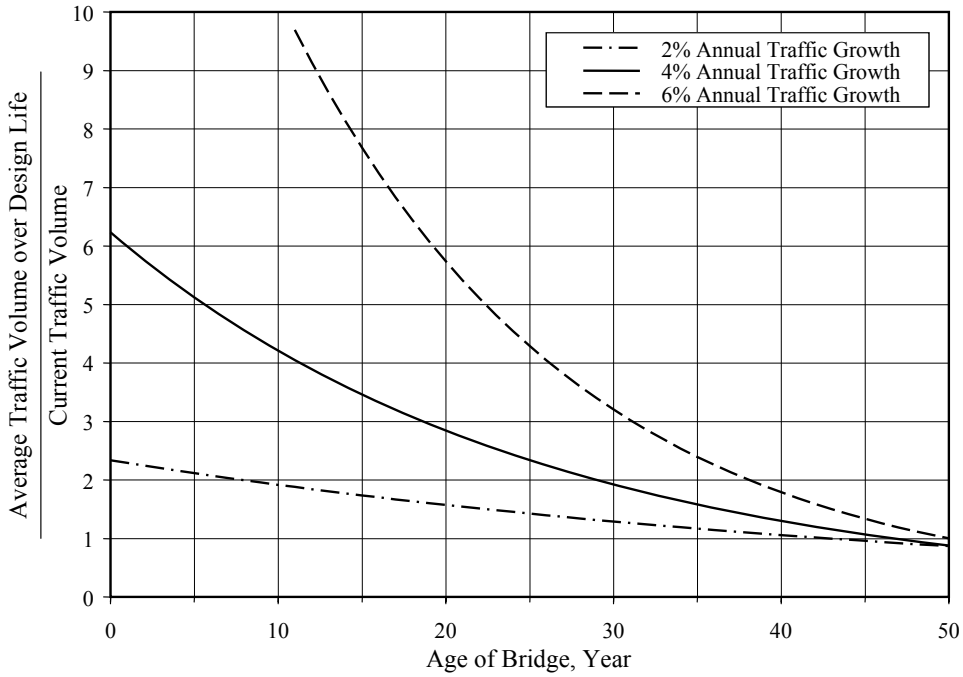

Figure 8.10 Ratio of Average Traffic Volume over Design Life to Current Traffic Volume

Table 8.4 Expected Number of Fatigue Cycles during 75-Year Design Life

Bridge	Girder	k^* (year)	$\Omega^\dagger$	ADTT*	$N_{75}{}^\dagger$ (Cycles)
Chandler Creek – 40-ft Span	Interior	34	2.5	2000	30,000
	Exterior	34	2.5	2000	40,000
Chandler Creek – 60-ft Span	Interior	34	2.5	2000	1,100,000
	Exterior	34	2.5	2000	550,000
Lake LBJ	Interior	35	2.4	420	2,200,000
	Exterior	35	2.4	420	7,400,000
Lampasas River	Interior	29	3.4	250	22,500,000
	Exterior	29	3.4	250	21,600,000
Willow Creek	Interior	38	2.0	130	3,000,000
	Exterior	38	2.0	130	4,900,000
Wimberley – 40-ft Span	Interior	40	1.8	510	0
	Exterior	40	1.8	510	0
Wimberley – 60-ft Span	Interior	40	1.8	510	30,000
	Exterior	40	1.8	510	10,000

* Traffic data recorded between 1999 and 2000.
† Assumed annual rate of traffic growth = 6%

The number of fatigue cycles expected during the 75-year design life of each girder, assuming an annual rate of traffic growth of 6%, is listed in Table 8.4. The Lampasas River Bridge was expected to experience more than 20 million fatigue cycles over the 75-year design life, while the Chandler Creek and Wimberley Bridges are likely to experience less than 1 million fatigue cycles. In all cases, the fatigue life, N, was considerably larger than the expected number of loading cycles, N_{75}. Therefore, fatigue did not limit the design life of any of the bridges considered in this investigation.

8.4 SUMMARY

Although the current requirements in the MCEB indicate that four of the five bridges considered in this investigation do not satisfy the serviceability limit state criteria at the inventory level, detailed analyses of the bridges indicates that two have an infinite fatigue life and that fatigue does not limit the design life of the remaining three. Because all five bridges satisfy the capacity limit state criteria at the inventory level and were evaluated using a traffic spectrum representative of interstate traffic along a major transportation corridor, posting of the legal live load is not required for any of these bridges.

CHAPTER 9
Recommended Procedures for Including Fatigue in the Load Rating Process

The detailed analyses discussed in Chapter 8, indicated that fatigue did not limit the service life of any of the five bridges considered in this investigation. However, the calculations required to reach this conclusion were too extensive to be recommended for use in the load rating process. A series of conservative assumptions are made in this chapter to develop recommended procedures for evaluating the fatigue life of prestressed concrete girder bridges. These procedures are intended to replace the serviceability limit state criteria in the MCEB. Unlike the serviceability limit states defined in the MCEB; however, a specific load rating will not be tied directly to the fatigue limit state. Rather, the calculations will indicate if the spectrum of loading vehicle limits the fatigue life of the bridge.

Three fatigue categories have been defined: (1) the bridge has an infinite fatigue life (Category PC1), (2) the bridge has a finite fatigue life that exceeds the design life (Category PC2), and (3) the bridge has a finite fatigue life that is shorter than the design life (Category PC3). If the bridge satisfies the requirements for either Category PC1 or PC2, fatigue does not limit the service life of the bridge. If inventory-level load rating – ignoring the serviceability limit state criteria – exceeds 1.0, then no restrictions would need to be placed on the bridge. Bridges in Category PC2, however, would need to be evaluated on a periodic basis, because larger than anticipated increases in the volume of traffic crossing the bridge could cause the structure to be reclassified in Category PC3.

If the bridge is classified as Category PC3, the service life of the bridge is limited by fatigue. But TxDOT has two options to address this situation: (1) the bridge can remain open with no limit on the live load, recognizing the fact that the bridge would need to be replaced before the end of the 75-year design life, or (2) the bridge could be posted to limit the live load, and the expected life of the bridge would be maintained. The flexibility of not restricting the live load during the planning and construction of a replacement structure may be important in some situations.

The proposed method is summarized in Section 9.1. The parameters used throughout the fatigue limit state evaluation are discussed in Section 9.2, and the procedures used to approximate the live load moment spectra for each bridge are presented in Section 9.3.

The stress range in the strand is not related linearly to the live load moment, and calculations based on strain compatibility (Appendix B) are considered to be too detailed for load rating purposes. A simpler procedure is proposed in Section 9.4 to approximate the nonlinear response of the prestressed concrete bridge girders.

The details of the simplified method recommended for evaluating the fatigue life of a prestressed concrete bridge are discussed in Section 9.5 and the five bridges are evaluated in Section 9.6. Using the proposed procedures, the inventory-level ratings were not limited by fatigue for any of the bridges considered, and therefore, posting to limit the live load is not required.

9.1 OVERVIEW OF METHOD

The procedure used to evaluate the fatigue response of a prestressed concrete bridge is summarized in Figure 9.1 and includes three basic steps. The overall concept is similar to the approach used in the LRFR procedures for steel bridges, but the details differ. In the first step, the susceptibility to fatigue damage is evaluated. In the second step, the distinction between an infinite fatigue life and a finite fatigue life is made. The finite fatigue life is evaluated in the third step. Each of the steps is described briefly below.

The likelihood of cracking is used to determine if a bridge is susceptible to fatigue damage. The existence of flexural cracks has a significant impact on the fatigue behavior, because the live-load stress range in the strand is extremely small in an uncracked beam. Therefore, if a prestressed concrete girder is calculated to be uncracked, the fatigue life is assumed to be infinite, and no additional calculations are required.

The criterion used to determine the presence of flexural cracks is based on gross cross-sectional properties, but differs from the approach used in the MCEB to evaluate the serviceability limit state in two ways:

(1) An overload vehicle is used to evaluate cracking. Prestressed concrete bridges experience millions of loading cycles during their design life, and a single heavy vehicle is sufficient to crack the girders. Once a crack forms, it may close in the absence of live load due to the precompression, but the stress range in the strand due to live load in a cracked girder always exceeds that in an uncracked girder.

(2) A limiting tensile stress of $3\sqrt{f_c'}$ is used to evaluate cracking. Experimental evidence has demonstrated that cracks will form at stress levels considerably less than the static modulus of rupture under repeated loading, and this value was selected to be conservative.

These assumptions may seem overly conservative relative to the design calculations. However, the results of the diagnostic load tests (Chapter 3) demonstrated that the centroid of the composite cross section was closer to the top of the slab than calculated using gross cross-sectional properties in most of the girders. Therefore, flexural cracks are assumed to be present unless the bridge was designed very conservatively.

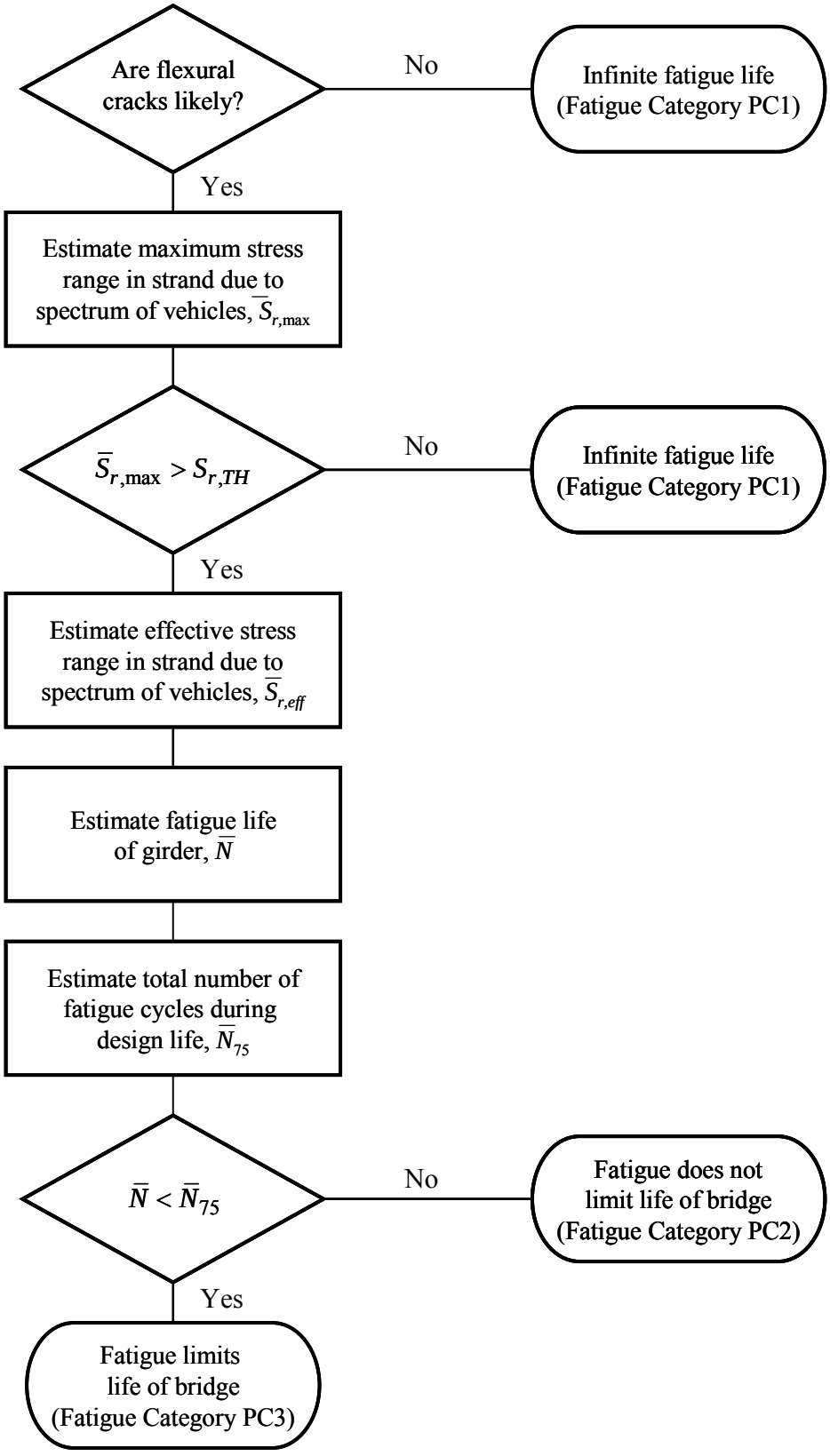

Figure 9.1 Overview of Process to Evaluate Fatigue Life of Prestressed Concrete Bridges

After determining that flexural cracks are likely to be present in a prestressed concrete girder, the maximum live load stress range in the strand due to the spectrum of loading vehicles is estimated. A simple method is introduced to estimate the maximum moment in each girder, but a nonlinear relationship must be used to determine the corresponding maximum stress range in the strand. This stress range is then compared with the threshold stress from the fatigue life model (Figure 8.6). If the maximum stress range in the strand is less than the threshold stress of 10 ksi, the girder is assumed to have an infinite fatigue life (Category PC1).

Only if the maximum stress range exceeds the threshold stress is the fatigue life of the girder determined. The effective stress range for only the portion of the moment spectrum that exceeds the decompression moment in the girder is used to determine the finite fatigue life. As discussed in Chapter 8, unique fatigue spectra must be developed for each girder to determine the effective stress range. However, a conservative approximation has been developed to estimate of the effective stress range.

The descending branch of the S-N curve (Figure 8.6) is then used to determine the finite fatigue life of the girder. The expected number of fatigue cycles during the 75-year design life of the bridge is also calculated. The number of fatigue cycles depends on the current age of the bridge, the assumed annual rate of traffic growth, the average daily truck traffic, and the weight of the vehicle needed to exceed the decompression moment in the girder.

If the fatigue life of the bridge exceeds the number of fatigue cycles expected in 75 years, the bridge is classified in Category PC2 and the fatigue life has no influence on the inventory-level rating. However, if the fatigue life of the bridge is less than the number of cycles expected in 75 years, the bridge is classified in Category PC3 and some form of corrective action is required.

9.2 PARAMETERS USED TO EVALUATE FATIGUE LIMIT STATE

As discussed in Chapter 7, a number of parameters must be defined to evaluate an existing bridge. For the fatigue limit state, the loading vehicle, impact factor, and live load distribution factors defined in Table 9.1 were used in all analyses discussed in this chapter. The choice of loading vehicle, impact factor, and number of lanes of traffic for the live load distribution factors are consistent with the design provisions for fatigue in the AASHTO LRFD Specifications. The HS-20 vehicle with a rear axle spacing of 30 ft will be called the HS-20 fatigue vehicle throughout this chapter to avoid confusion with the HS-20 design vehicle (14-ft rear axle spacing) that was used in Chapter 7 for load rating.

The values of live load distribution factors from the AASHTO Standard Specifications were selected for consistency with the provisions in the MCEB for the capacity limit state and because these values were conservative for all bridges considered in this investigation (Section 4.3.3). The value of the

live load factor is higher than that used in the fatigue provisions in the AASHTO LRFD Specifications, but was selected to be conservative. The specified material properties were used in all calculations and prestress losses were estimated using the procedures in the AASHTO LRFD Specifications.

Moments at midspan for each bridge considered in this investigation due to the HS-20 fatigue vehicle are summarized in Table 9.2

Table 9.1 Parameters used to Evaluate Fatigue Limit State

Parameter	Value
Loading vehicle	HS-20 fatigue vehicle (30-ft rear axle spacing)
Impact factor, I	0.15
Live load distribution factors, DF	One lane from AASHTO Standard Specifications
Dead load factor, A_1	1.0
Live load factor, A_2	1.0

Table 9.2 Maximum Moments at Midspan Induced by HS-20 Fatigue Vehicle

Bridge	Maximum Moment at Midspan (kip-ft)
Chandler Creek – 40-ft Span	329
Chandler Creek – 60-ft Span	529
Lake LBJ	608
Lampasas River	791
Willis Creek	608
Wimberley – 40-ft Span	328
Wimberley – 60-ft Span	528

Throughout this chapter, a series of approximations are introduced to evaluate the fatigue response of prestressed concrete girders. Most of the parameters used in the detailed analyses discussed in Chapter 8 must also be estimated in this chapter. To avoid confusion, a slightly different set of notation has been introduced for the approximate analyses: a bar is used to identify the estimated parameters. For example, $S_{r,eff}$ represents the effective live load stress range in the strand calculated from the girder-specific fatigue spectrum, while $\overline{S}_{r,eff}$ represents the approximate value of the effective live load stress estimated using the procedures in this chapter.

9.3 IDEALIZED SPECTRUM OF LIVE LOAD MOMENTS

As discussed in Chapter 8, a spectrum of live load moments is required to evaluate the fatigue life of a bridge. However, calculating a unique spectrum for each prestressed concrete bridge in Texas is too time consuming. Therefore, procedures are discussed in this section to estimate the spectrum of live load moments from the spectrum of gross vehicle weights.

In the evaluation process outlined in Figure 9.1, two moments must be determined for each bridge girder: the maximum moment induced at midspan due to the total population of loading vehicles, $M_{\max}$, and the effective moment at midspan due to loading vehicles that induce moments larger than the decompression moment, M_{eff}. Procedures used to estimate the maximum moment at midspan of the girder are presented in Section 9.3.1. The approximate moment spectrum for the entire population of loading vehicles is discussed in Section 9.3.2, and the effective moment corresponding to loading vehicles that exceed the decompression moment is discussed in Section 9.3.3.

9.3.1 Maximum Live Load Moment

A series of line-girder analyses were conducted to evaluate the maximum moment at midspan of bridges with spans between 40 and 80 ft. This range of spans was considered to be representative of older prestressed concrete bridges in Texas. The complete vehicle spectrum (Figure 8.1) was used to determine the maximum moment for each span, and the values are compared with two times the moment corresponding to the HS-20 fatigue vehicle in Figure 9.2. The moment induced by two times the HS-20 fatigue vehicle provided a conservative approximation of the maximum moment at midspan for all span lengths considered in this investigation. This simple approximation over-estimated the maximum moment at midspan of the bridge by 3 to 12% (Figure 9.2).

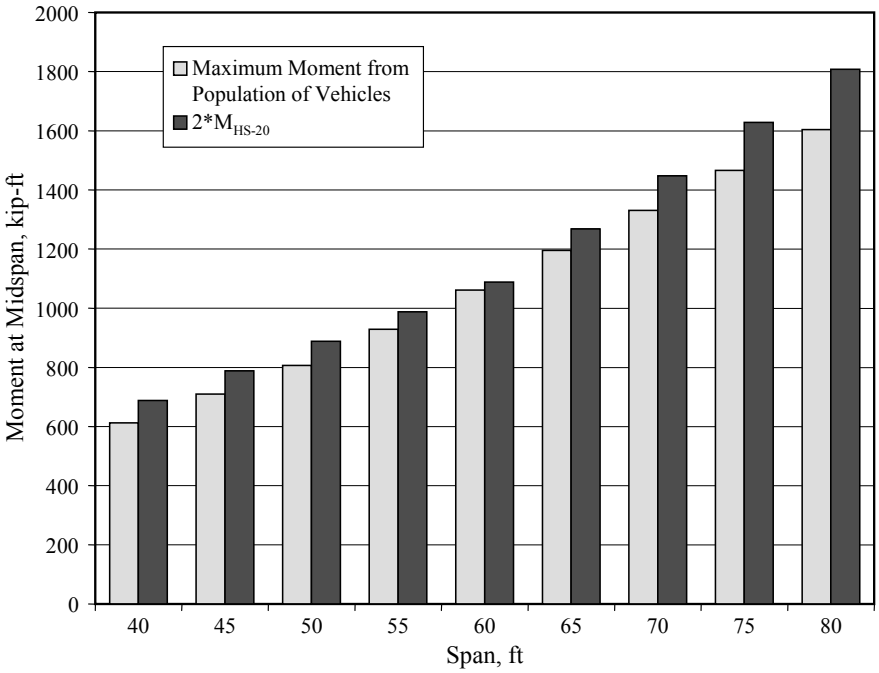

Figure 9.2 Maximum Live Load Moment at Midspan

9.3.2 Idealized Moment Spectrum

As shown in Figure 8.3 through Figure 8.5, the spectra for live load moment at midspan vary with the span. Individual live load moment spectra for spans of 40, 50, 60, 70, and 80 ft are plotted in Figure 9.3 where the moments have been normalized by the maximum moment at midspan induced by the HS-20 fatigue vehicle. The general shapes of the normalized spectra are the same, but the amplitudes are larger for the shorter spans.

The normalized spectrum for gross vehicle weight is shown in Figure 9.4. This spectrum has the same general shape as the normalized live load moment spectra shown in Figure 9.3 The amplitude of the normalized gross vehicle weight spectrum is approximately the same as that for a 50-ft span, but the spectrum of normalized gross vehicle weight is shifted to the right compared with the spectra of the normalized live load moments. With the exception of the 40-ft span, the normalized gross vehicle weight spectrum provides a conservative estimate of the normalized live load moment spectra. Therefore, the normalized gross vehicle spectrum will be used to approximate the normalized live load moment spectra for each bridge.

When the normalized effective live load moments for the entire spectra are compared with the normalized effective vehicle weight (Figure 9.5), the normalized effective gross vehicle weight is a conservative estimate of the normalized effective live load moments for all span lengths.

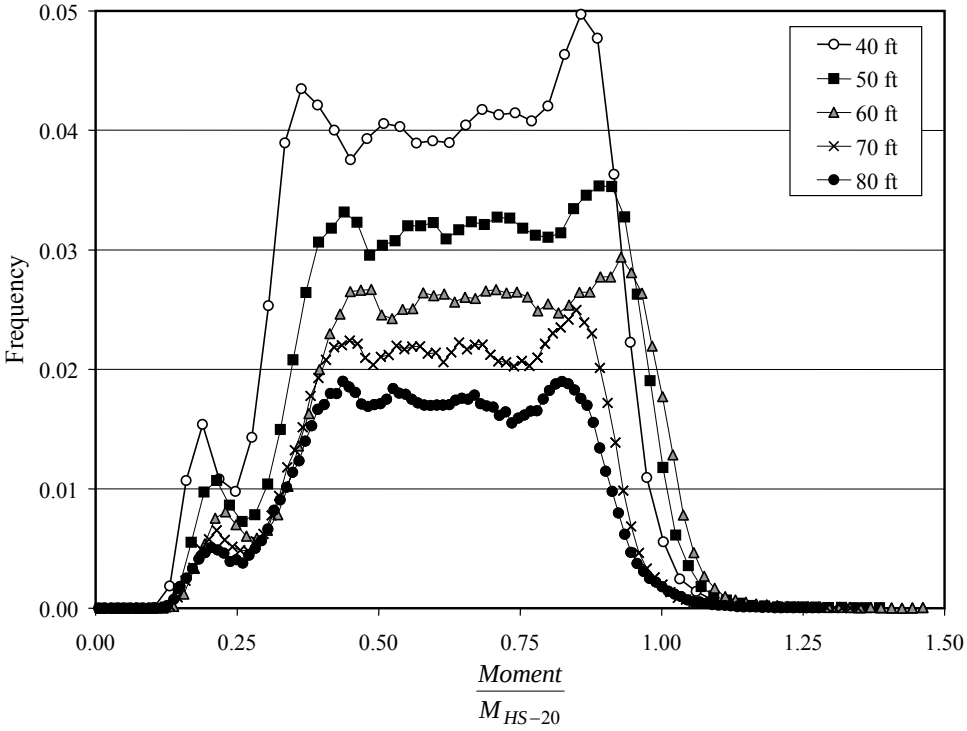

Figure 9.3 Normalized Live Load Moment Spectra

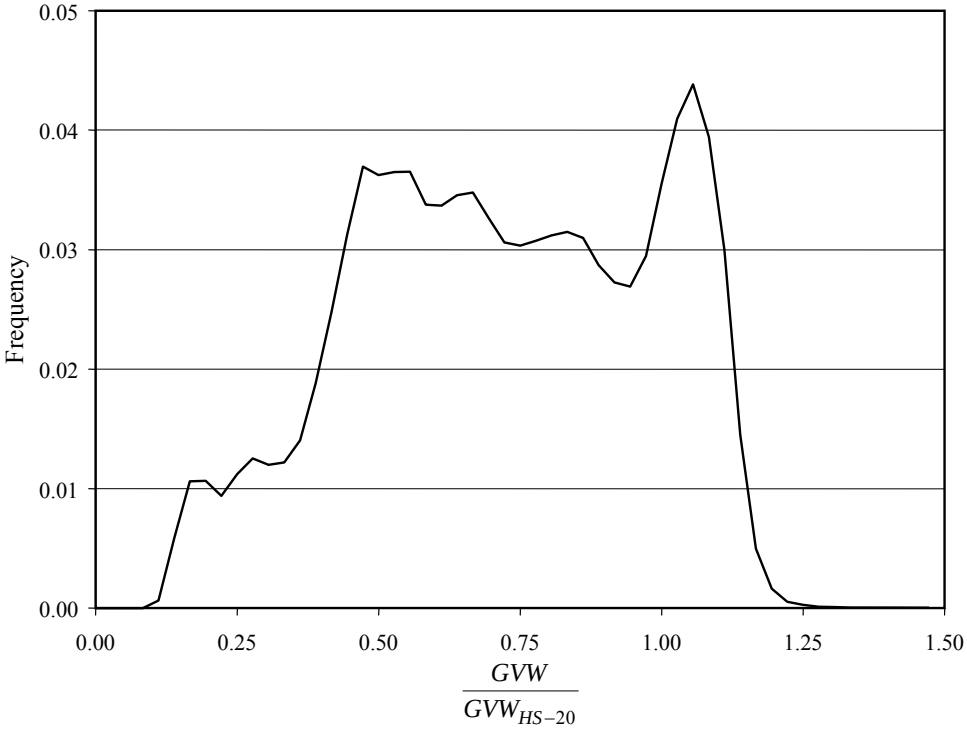

Figure 9.4 Normalized Gross Vehicle Weight Spectrum

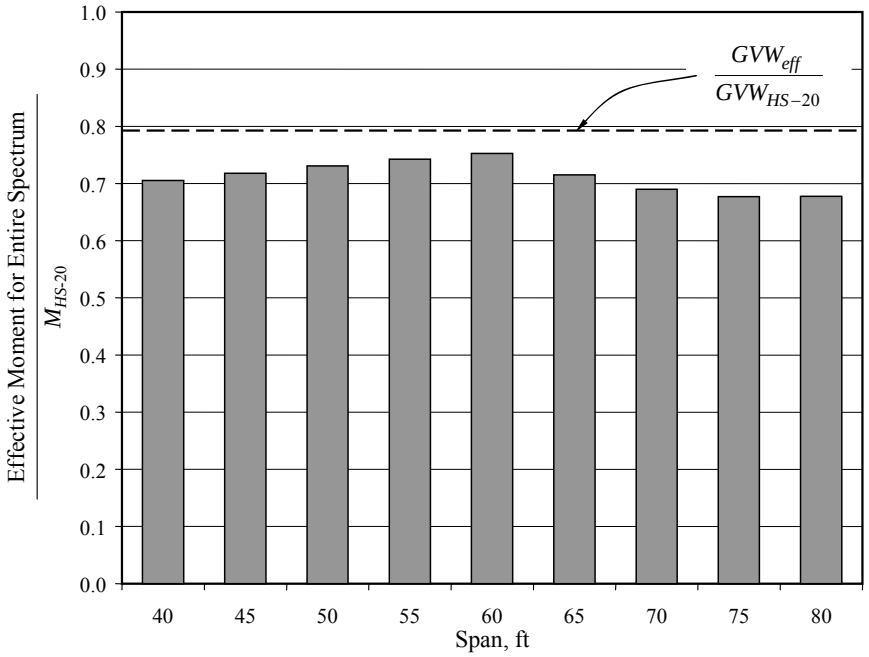

Figure 9.5 Variation of Effective Live Load Moment with Span Length

The parameter ζ will be used in the following discussion to refer to the normalized gross vehicle weight:

$$\zeta = \frac{GVW}{72 \text{ kip}} = \text{normalized gross vehicle weight} \tag{9.1}$$

Based on the comparisons discussed above, the parameter ζ will also be assumed to be equal to the normalized live load moment:

$$\zeta = \frac{M}{M_{HS-20}} = \text{normalized live load moment at midspan} \tag{9.2}$$

While the normalized gross vehicle weight and normalized live load moment spectra are not identical, using the gross vehicle weight spectrum to approximate the normalized live load moment spectra is a convenient simplification, because the gross vehicle weight spectrum does not vary with the span of the bridge. In essence, this simplification assumes that all vehicles have the same axle configuration and relative axle weights as the HS-20 fatigue vehicle.

To illustrate the appropriateness of this assumption, influence line analyses were conducted using approximately 5000 vehicles that were detected by the weigh-in-motion station on a typical day. The maximum moment at midspan is plotted as a function of the gross vehicle weight for a 60-ft span in Figure 9.6. The same analyses were conducted for span lengths of 40, 50, 70, and 80 ft, and the observed trends were similar.

The line shown in Figure 9.6 corresponds to the moment induced by the axle configuration of the HS-20 fatigue vehicle for a given gross vehicle weight:

$$M\left(GVW\right) = M_{HS-20}\left(\frac{GVW}{72\text{ kip}}\right) \tag{9.3}$$

In general, the HS-20 fatigue vehicle configuration provides a reasonable estimate of the mean moment induced by the spectrum of actual vehicles. The approximation becomes more conservative as the number of axles and gross vehicle weight increase.

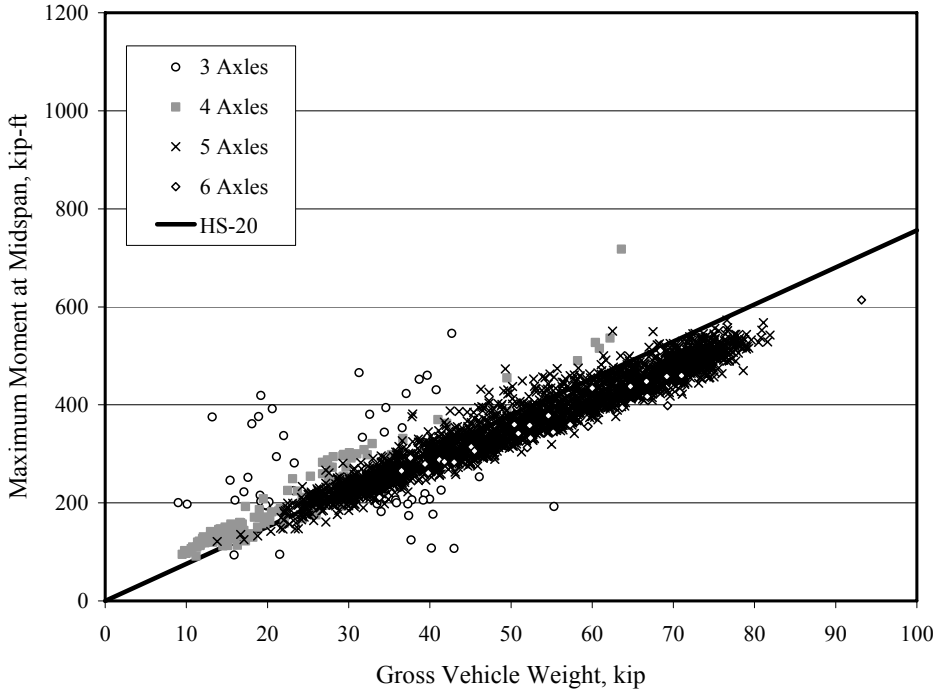

Figure 9.6 Maximum Moments at Midspan for 60-ft Span

9.3.3 Fatigue Spectrum

For the evaluation of prestressed concrete bridges, only those vehicles that induce moments above the decompression moment are assumed to represent a loading cycle for individual girders. The decompression moment depends on the length of the span, the dead load, the number of strands, and the layout of the strands. Therefore, the portion of the vehicle spectrum that must be considered varies for each bridge.

To facilitate these calculations, the effective gross vehicle weight of heavier vehicles was calculated for each group of vehicle weights within the total population:

$$GVW_{eff,i} = \left[\sum_{j=i}^{n} \left(\gamma'_j \cdot GVW_j^3 \right) \right]^{1/3} \tag{9.4}$$

where $GVW_{eff,i}$ is the effective gross weight of vehicles that are equal to or heavier than load range *i*, and γ'_j is the frequency of trucks in load range *j* within the population of vehicles that are equal to or heavier than load range *i*. The values of $GVW_{eff,i}$ ranged from 181 kip, representing the heaviest vehicle in the population, to 56.8 kip, representing the effective gross vehicle weight of the entire population (Figure 9.7).

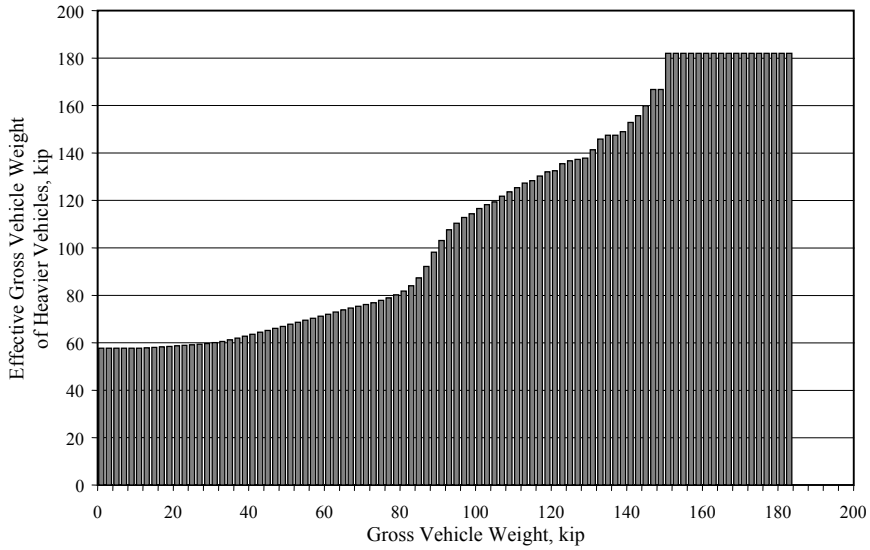

Figure 9.7 Variation of Gross Effective Weight of Heavier Vehicles with Gross Vehicle Weight

A smoothed function was selected to represent the distribution of effective vehicle weights of heavier vehicles, as shown in Figure 9.8:

$$\lambda = 0.4\zeta^2 + 0.8 \leq 2.4 \tag{9.5}$$

where ζ is the normalized gross vehicle weight and λ is the normalized gross vehicle weight of heavier vehicles:

$$\lambda = \frac{GVW_{eff,i}}{72 \text{ kip}} \tag{9.6}$$

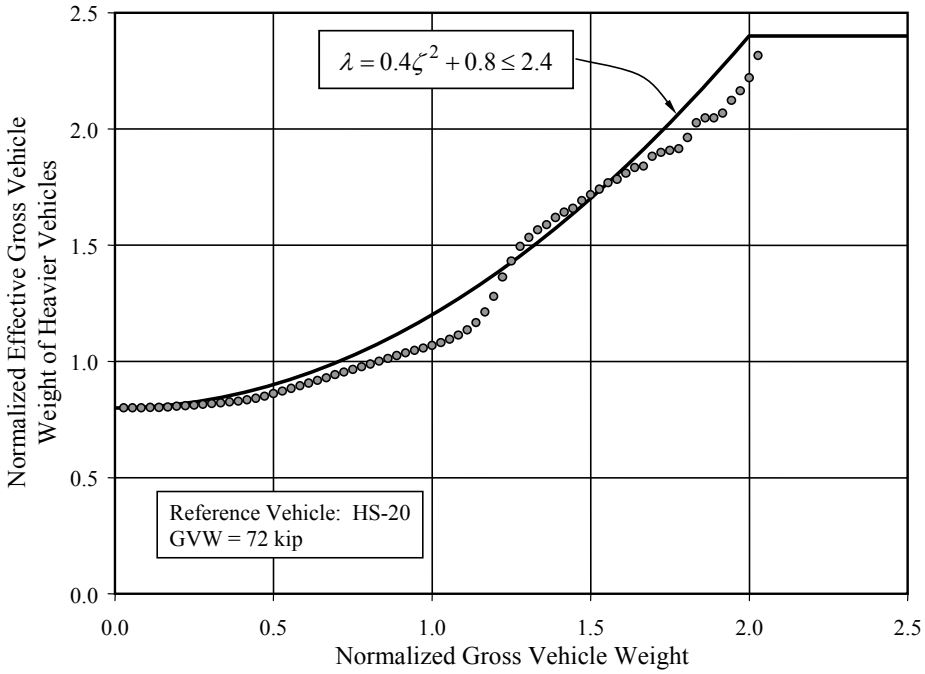

Figure 9.8 Idealized Variation of Gross Effective Weight of Heavier Vehicles

As shown in Figure 9.8, Eq. 9.5 provides a conservative estimate of the weigh-in-motion data for station 516. This spectrum was developed for an interstate highway along a major transportation corridor near a large metropolitan area, but is considered to be conservative for highways throughout Texas.

The cumulative percentage of heavier vehicles must also be calculated to determine the number of loading cycles experienced by a bridge during its design life. These data are plotted in Figure 9.9. As expected, all vehicles exceeded a gross vehicle weight of 0 kip and very few exceeded a gross vehicle weight of 90 kip. Approximately 20% of the population exceeded the gross weight of the HS-20 fatigue vehicle.

The factor β is defined as the fraction of heavier trucks within the population:

$$\beta = 1.0 - 0.8\zeta^2 \ge 0.005 \tag{9.7}$$

The approximate value of β given by Eq. 9.7 is slightly unconservative for gross vehicle weights less than 36 kip (ζ =0.5), but is conservative between 36 kip and 72 kip ($0.5 \le \zeta \le 1.0$).

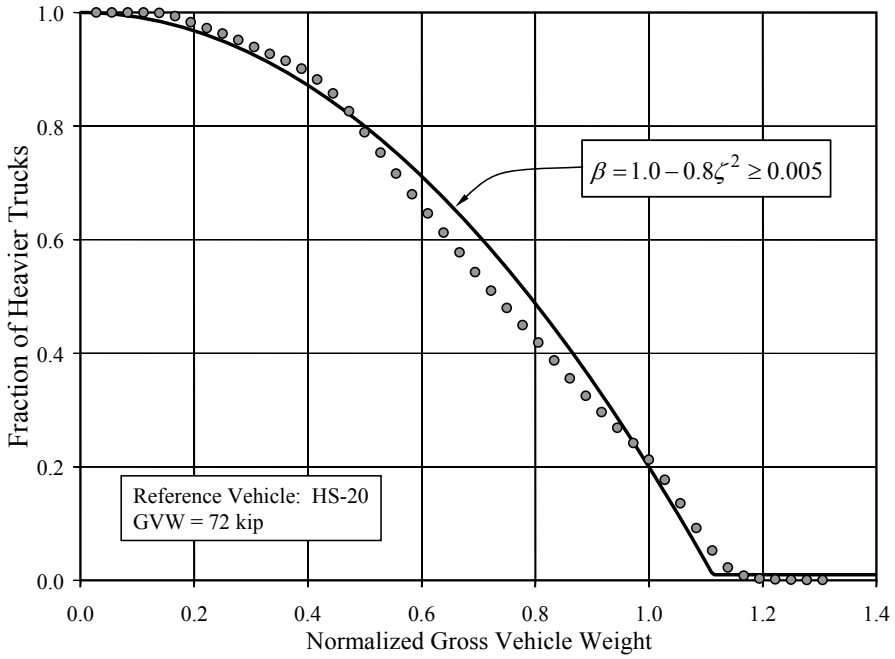

Figure 9.9 Fraction of Heavier Trucks in Total Population

9.4 RELATIONSHIP BETWEEN STRESS RANGE AND LIVE LOAD MOMENT

As discussed in Chapter 5, the relationship between live load moment and stress range in the strand is nonlinear. A procedure for calculating this relationship based on strain compatibility is presented in Hagenberger (2004) and the results are summarized in Appendix B. However, this approach is considered to be too complex for load rating. Therefore, a simpler procedure was developed.

Two points are used to idealize the nonlinear live load response of a prestressed concrete girder (Figure 9.10). The first point $\left(\Delta f_{s,br}, M_{br}\right)$ represents the transition from the initial response that is dominated by the uncracked properties of the composite section to the post-cracking response of the section. The second point $\left(\Delta f_{sn}^{*}, M_{n}^{*}\right)$ corresponds to the nominal capacity of the girder. These four parameters are defined below. The specified material properties were used in all calculations.

$$M_{br} = 0.45M_n - M_D \tag{9.8}$$

$$M_n^{*} = M_n - M_D \tag{9.9}$$

where

M_n = nominal flexural capacity of the composite girder
M_D = unfactored moment due to dead load

$$\Delta f_{s,br} = \frac{M_{br}\left(y_{bc} - c_b\right)n}{I_c} \tag{9.10}$$

where

y_{bc} = distance from centroid of composite section to bottom fiber of beam
c_b = distance from bottom fiber of beam to centroid of extreme layer of strand (typically 2 in.)
n = modular ratio = E_p / E_c
E_p = modulus of elasticity of strand
E_c = modulus of elasticity of concrete
I_c = moment of inertia of composite cross section

$$\Delta f_{sn}^{*} = f_u - f_{se} \tag{9.11}$$

where

f_u = tensile strength of strand
f_{se} = effective tensile stress in strand after losses

It should be noted that the change in stress in the strand is evaluated at the centroid of the extreme layer of strand, rather than the centroid of all strands, which is commonly used to determine the flexural capacity of the cross section.

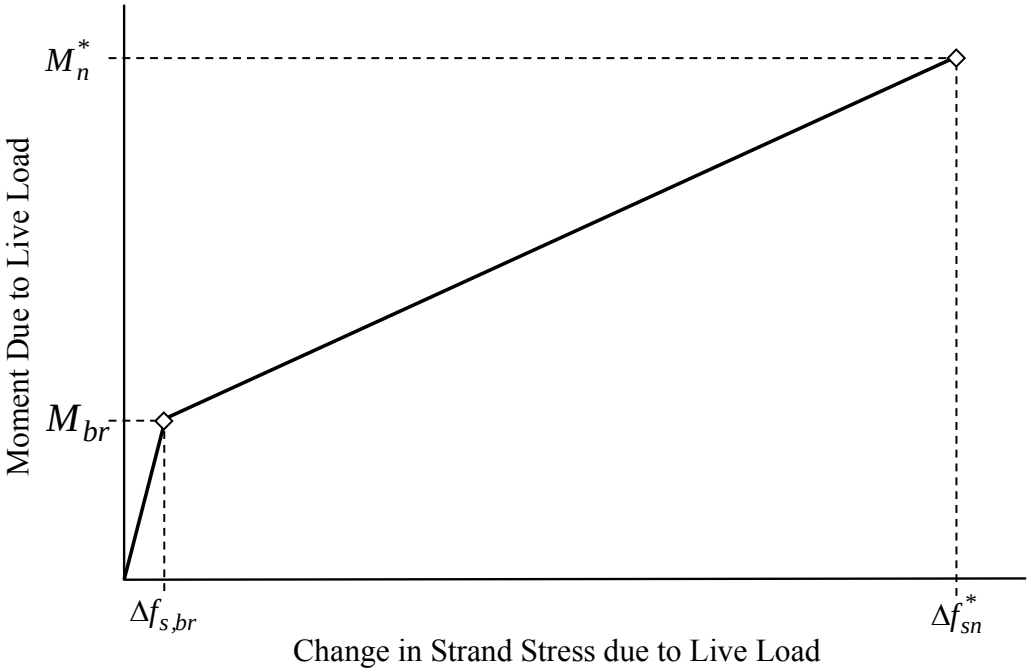

Figure 9.10 Idealized Bilinear Relationship between Live Load Moment and Strand Stress Range

The bilinear approximation is compared with the nonlinear calculations for two representative beams in Figure 9.11 and data for all beams are plotted in Appendix B. In all cases, the stress ranges calculated using the bilinear approximation at a given moment are slightly larger than those calculated using the results of the nonlinear analysis.

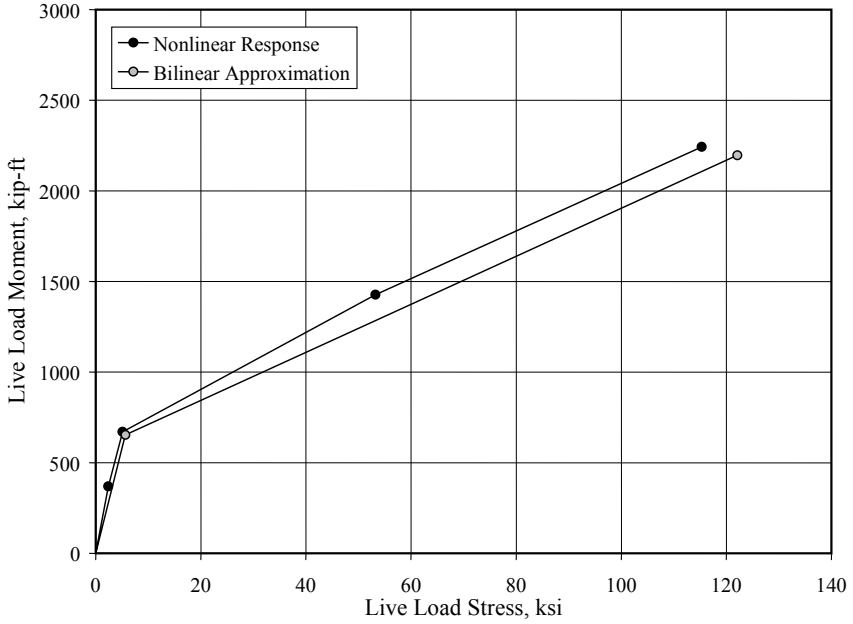

(a) Interior Girder, 60-ft Span, Chandler Creek Bridge

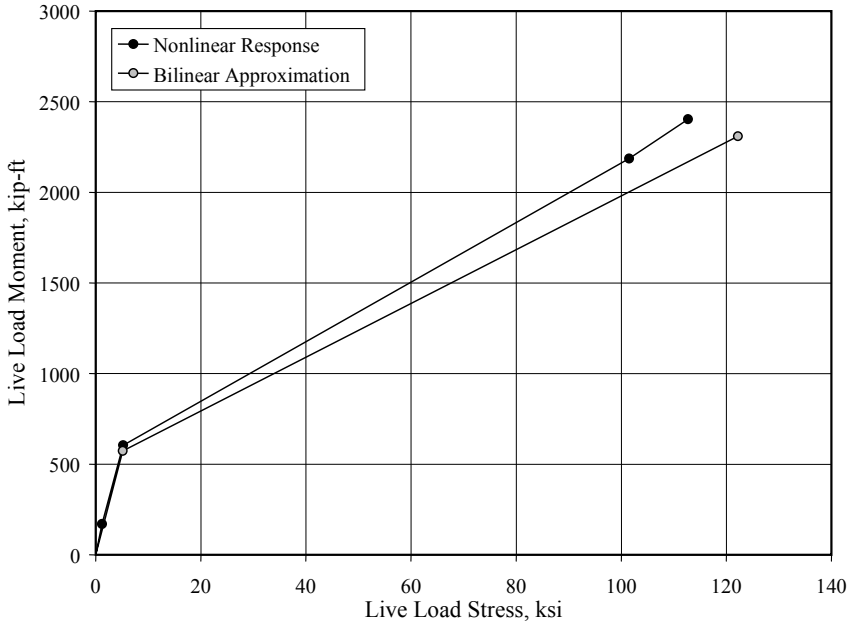

(b) Exterior Girder, Lampasas River Bridge

Figure 9.11 Bilinear Approximation of Nonlinear Live Load Response

9.5 FATIGUE LIFE OF PRESTRESSED CONCRETE BRIDGES

The process used to evaluate the fatigue response of prestressed concrete girders was outlined in Figure 9.1, and the calculations are summarized in this section. Four sets of calculations are required. Detecting the presence of flexural cracks is summarized in Section 9.5.1. The procedures used to estimate the maximum stress range in the strand are discussed in Section 9.5.2, and those used to estimate the effective stress range in the strand for girders with a finite fatigue life are discussed in Section 9.5.3. The fatigue life and number of expected fatigue cycles for a prestressed concrete girder are estimated in Section 9.5.4.

9.5.1 Presence of Flexural Cracks

As discussed in Section 9.1, flexural cracks are assumed to be present in a prestressed concrete girder if the tensile stress in the precompressed tension zone exceeds $3\sqrt{f_c'}$ due to an overload vehicle. This criterion is written in the same form as the rating factors for serviceability limit states in the MCEB as:

$$FF = \frac{3\sqrt{f_c'} - \left(f_D + f_P\right)}{2 f_L} \tag{9.12}$$

where:

FF = fatigue factor
f_D = unfactored dead load stress in concrete at bottom fiber of cross section
f_P = unfactored stress in concrete at bottom fiber of cross section due to prestress force after all losses
f_L = unfactored live load stress including impact in concrete at bottom fiber of cross section due to a single HS-20 fatigue vehicle

Note that the values of f_D, f_P, and f_L are taken as positive for tensile stresses and negative for compressive stresses.

If $FF \geq 1.0$, the girder is assumed to be uncracked and the fatigue life of the girder is assumed to be infinite (Category PC1). No additional calculations are required. If $FF < 1.0$, the maximum stress range in the strand due to live load must be calculated.

When evaluating the five bridges considered in this investigation, only the 40-ft span of the Wimberley Bridge satisfied the flexural cracking criterion. As discussed in Section 8.3, this span was unique among those considered because none of the vehicles within the spectrum of loading vehicles (Figure 8.1 and Figure 8.2) induced moments that exceeded the decompression moment.

9.5.2 Maximum Stress Range

As discussed in Section 9.3.1, the maximum live load moment at midspan of the bridge due to the spectrum of loading vehicles is approximated as two times the moment induced by the HS-20 fatigue vehicle. The total moment in the bridge is then distributed among the girders using the live load factor, live load distribution factors, and impact factor discussed in Section 9.2 to estimate the maximum live load moment at midspan of each girder:

$$\bar{M}_{\max} = A_2 \cdot DF \cdot (1 + I) \cdot 2.0 \cdot M_{HS-20} \tag{9.13}$$

where:

$\bar{M}_{\max}$ = approximate maximum live load moment at midspan of girder
A_2 = live load factor = 1.0
DF = live load distribution factor for one traffic lane (AASHTO Standard Specifications)
I = impact factor = 0.15
M_{HS-20} = maximum moment at midspan of bridge due to HS-20 fatigue vehicle

The approximate value of maximum stress range in the strand, $\bar{S}_{r,max}$, can then be estimated from $\bar{M}_{\max}$ and the idealized bilinear live load relationship for the girder (Figure 9.11). The approximate values of maximum moment at midspan of the girders, $\bar{M}_{\max}$, and the corresponding values of maximum live load stress range, $\bar{S}_{r,max}$, are summarized in Table 9.3 for the spans in which Eq. 9.12 indicated that flexural cracks were likely to be present under service loads. The maximum moments estimated using Eq. 9.13 were 4 to 13% larger than the maximum moments calculated using the unique moment spectra for the bridges (Table 8.2). The approximate maximum live load stress ranges were also conservative. For the 60-ft span of the Wimberley Bridge, the estimated stress ranges were within 10% of those calculated in Chapter 8. However, the approximate values were 2 to 3 times larger than the stress ranges calculated in Chapter 8 for the 40-ft span of the Chandler Creek Bridge.

The estimated values of $\bar{S}_{r,max}$ are used to determine if the girders have an infinite fatigue life. If $\bar{S}_{r,max}$ is less than the threshold stress of 10 ksi (Figure 8.6), the girder is assumed to have an infinite fatigue life (Category PC1). No additional calculations are required in this case. However, if $\bar{S}_{r,max}$ exceeds 10 ksi, the fatigue life of the girder is assumed to be finite. Only the interior girders of Chandler Creek Bridge (60-ft span), the interior girders of Lake LBJ Bridge, and the interior and exterior girders of the Wimberley Bridge (60-ft span) satisfied the criterion for infinite fatigue life using the approximate values of the maximum live load stress range.

Table 9.3 Approximate Values of Maximum Moment and Stress Range

Bridge	Girder	Maximum Moment at Midspan†		Maximum Live Load Stress Range†	
		$\bar{M}_{\max}$ (kip-ft)	$\frac{\bar{M}_{\max}}{M_{\max}}$	$\bar{S}_{r,\max}$ (ksi)	$\frac{\bar{S}_{r,\max}}{S_{r,\max}}$
Chandler Creek (40 ft)	Interior	432	1.13	15.0	3.2
	Exterior	477	1.13	20.3	2.8
Chandler Creek (60 ft)	Interior	694	1.04	8.7*	1.7
	Exterior	767	1.04	12.9	1.6
Lake LBJ	Interior	798	1.05	9.5*	1.6
	Exterior	881	1.05	17.3	1.3
Lampasas River	Interior	946	1.11	31.4	1.4
	Exterior	1074	1.11	38.9	1.4
Willis Creek	Interior	672	1.05	13.8	1.4
	Exterior	770	1.05	24.3	1.2
Wimberley (60 ft)	Interior	607	1.04	5.7*	1.1
	Exterior	607	1.04	5.5*	1.0

† $\bar{M}_{\max}$ calculated using Eq. 9.13 and $\bar{S}_{r,\max}$ calculated using idealized bilinear live load relationships, $M_{\max}$ and $S_{r,\max}$ reported in Table 8.2.

* Girders with infinite fatigue life.

9.5.3 Effective Stress Range

Only vehicles that induce moments that exceed the decompression moment in a girder are considered when evaluating the finite fatigue life. The live load moment in the girder corresponding to decompression, M_{dc}^{*}, may be calculated as:

$$M_{dc}^{*} = \frac{\left(f_D + f_P\right) I_c}{y_{bc}} \tag{9.14}$$

where

I_c = moment of inertia of composite cross section

y_{bc} = distance from centroid of composite section to bottom fiber of beam

The critical moment, M_{cr}, is defined as the moment at midspan of the bridge corresponding to the decompression moment in the girder:

$$M_{cr} = \frac{M_{dc}^{*}}{A_2 \cdot DF \cdot \left(1 + I\right)} \tag{9.15}$$

The critical live load moment ratio, ζ_{cr}, is then calculated by dividing the critical moment by the moment corresponding to the HS-20 fatigue vehicle:

$$\zeta_{cr} = \frac{M_{cr}}{M_{HS-20}} \tag{9.16}$$

The corresponding effective moment ratio for heavier vehicles, λ_{cr}, is calculated from the idealized gross vehicle weight spectrum (Figure 9.8) using Eq. 9.5 with $\zeta = \zeta_{cr}$. And the effective moment at midspan of the girder, $\bar{M}_{eff}$, is approximated as:

$$\bar{M}_{eff} = \lambda_{cr} \cdot A_2 \cdot DF \cdot (1 + I) \cdot M_{HS-20} \tag{9.17}$$

The approximate value of effective stress range in the strand, $\bar{S}_{r,eff}$, is then calculated from the idealized bilinear live load relationship for the girder (Figure 9.11) using $\bar{M}_{eff}$.

The approximate values of the effective moment at midspan of the girders, $\bar{M}_{eff}$, and the corresponding values of effective stress range, $\bar{S}_{r,eff}$, are summarized in Table 9.4 for the spans that did not satisfy the infinite fatigue life criterion. The effective moments approximated using Eq. 9.17 were 3 to 22% larger than the moments calculated using the unique moment spectra for the bridge (Table 8.3) and the corresponding values of effective live load stress range exceeded the values calculated in Chapter 8 by 19 to 40%.

The approximate value of critical live load moment ratio, $\bar{\beta}_{cr}$, which represents the fraction of heavier vehicles in the total population (Figure 9.9), is calculated using Eq. 9.7 with $\zeta = \zeta_{cr}$. Values of $\bar{\beta}_{cr}$ are also reported in Table 9.4. With the exception of the 40-ft span of the Chandler Creek Bridge, the approximate fraction of heavier vehicles, $\bar{\beta}_{cr}$, provided a reasonable estimate of the individual moment spectra. The approximation was extremely conservative for the 40-ft span of the Chandler Creek Bridge because the number of vehicles that induced moments above the decompression moment was so small for this span.

Table 9.4 Approximate Values of Effective Moment and Stress Range

Bridge	Girder	Effective Moment at Midspan*		Effective Live Load Stress Range*		Fraction of Heavier Vehicles*	
		$\bar{M}_{eff}$ (kip-ft)	$\frac{\bar{M}_{eff}}{M_{eff}}$	$\bar{S}_{r,eff}$ (ksi)	$\frac{\bar{S}_{r,eff}}{S_{r,eff}}$	$\bar{\beta}_{cr}$	$\frac{\bar{\beta}_{cr}}{\beta_{cr}}$
Chandler Creek (40 ft)	Interior	330	1.05	4.5	1.26	0.005	27.0
	Exterior	357	1.05	4.9	1.23	0.005	19.8
Chandler Creek (60 ft)	Exterior	499	1.10	4.4	1.42	0.005	1.12
Lake LBJ	Exterior	487	1.21	3.7	1.35	0.39	1.45
Lampasas River	Interior	394	1.23	3.5	1.31	0.94	0.98
	Exterior	454	1.24	4.1	1.33	0.91	0.97
Willis Creek	Interior	341	1.18	3.2	1.39	0.57	1.36
	Exterior	354	1.17	3.1	1.20	0.76	1.09

* $\bar{M}_{eff}$ calculated using Eq. 9.17, $\bar{S}_{r,eff}$ calculated using idealized bilinear live load relationships, and $\bar{\beta}_{cr}$ calculated using Eq. 9.7. M_{eff}, $S_{r,eff}$, and β_{cr} reported in Table 8.3.

9.5.4 Finite Fatigue Life

The fatigue life model for a prestressed concrete girder is assumed to be the same as Detail Category C in the AASHTO LRFD Specifications. The approximate fatigue life of the girder, $\bar{N}$, is calculated from the estimated value of the effective stress range in the strand, $\bar{S}_{r,eff}$:

$$\bar{N} = A\left(\bar{S}_{r,eff}\right)^{-3} \tag{9.18}$$

where $A = 44 \times 10^8$ (ksi^3). The amplification factor, R_f, which appears in Eq. 8.2, is not used in Eq. 9.18 because the procedure used to approximate the effective stress range is conservative (Table 9.4). As discussed in Section 9.5.3, the values of effective stress range calculated using the approximate procedures are 20 to 40% larger than those calculated using the detailed procedures in Chapter 8.

The number of fatigue cycles experienced by the girder during the 75-year design life, $\bar{N}_{75}$, depends on the current average daily truck traffic crossing the bridge (*ADTT*), the current age of the bridge, the assumed annual rate of traffic growth, and the fraction of damaging vehicles (β_{cr}). The parameter Ω was introduced in Eq. 8.5 to represent the ratio of the average annual traffic volume over the design life of the bridge to the current traffic volume. Rather than using the equations in Chapter 8 to calculate Ω for each bridge, the approximate values in Table 9.5 are recommended.

The total number of loading cycles can then be expressed as:

$$\bar{N}_{75} = \bar{\beta}_{cr} \cdot \bar{\Omega} \cdot ADTT \cdot 365 \cdot 75 \tag{9.19}$$

If the estimated fatigue life of the girder, $\bar{N}$, exceeds the expected number of fatigue cycles, $\bar{N}_{75}$, fatigue does not limit the life of the bridge and no action is required (Category PC2). If $\bar{N} < \bar{N}_{75}$, the life of the bridge is limited by fatigue (Category PC3) and corrective action is required.

Table 9.5 Approximate Ratio of Average Annual Traffic Volume during Design Life to Current Traffic Volume, $\bar{\Omega}$

Current Age of Bridge (year)	Assumed Annual Rate of Traffic Growth			
	2%	4%	6%	8%
20	1.6	2.9	5.7	12.4
25	1.4	2.3	4.3	8.4
30	1.3	1.9	3.2	5.7
35	1.2	1.6	2.4	3.9
40	1.1	1.3	1.8	2.7
45	1.0	1.1	1.3	1.8
50	0.9	0.9	1.0	1.2

9.6 EVALUATION OF BRIDGES TESTED IN THIS INVESTIGATION

The calculations described in Section 9.5 are summarized in Table 9.6 and Table 9.7 for interior and exterior girders, respectively. Evaluation of the fatigue factor, FF, indicated that flexural cracks were likely to be present in all girders, except the interior and exterior girders of the 40-ft span of the Wimberley Bridge. The calculated values of $\bar{S}_{r,\max}$ were less than the threshold stress of 10 ksi for four girders: interior girders of 60-ft span of the Chandler Creek Bridge, interior girders of the Lake LBJ Bridge, and both interior and exterior girders of the 60-ft span of the Wimberley Bridge. These girders were assumed to have an infinite fatigue life. All other girders were assumed to have a finite fatigue life.

The values of ζ_{cr}, the critical live load moment ratio, ranged from 0.28 for the Lampasas River Bridge to 1.35 for the 40-ft span of the Chandler Creek Bridge. This means that trucks with a gross vehicle weight exceeding 20 kip generate fatigue cycles for the Lampasas River Bridge, while trucks heavier than 100 kip are needed to generate fatigue cycles for the 40-ft span of the Chandler Creek Bridge.

The calculated values of effective stress range in the strand, $\bar{S}_{r,eff}$, varied from 3.1 to 4.9 ksi. The calculated fatigue life exceeded the expected number of fatigue cycles, assuming an annual rate of traffic growth of 6%. Based on this evaluation, fatigue does not limit the service life of any of the

bridges, and because the inventory-level rating corresponding to the flexural capacity exceeds 1.0 for all five bridges (Table 7.2), no corrective action is required. This result is consistent with the observed condition of the bridges.

9.7 SUMMARY

When the five prestressed concrete bridges considered in this investigation were evaluated using the serviceability limit states in the MCEB at the inventory level, four failed the tensile stress criterion in the concrete but all five satisfied the flexural strength criterion (Table 7.2). Therefore, using the traditional approach of ignoring fatigue in prestressed concrete girders, these bridges would require posting to limit the legal vehicle loads.

However, a procedure has been developed to consider the fatigue life of prestressed girders directly in the load rating process. One of the unique features of this approach is that a spectrum of loading vehicles is considered, and only those vehicles that induce moments above the decompression moment in the girders are used to evaluate each bridge.

Using the procedures outlined in Figure 9.1, the Wimberley Bridge was found to have an infinite fatigue life. Fatigue did not limit the design life of the Chandler Creek, Lake LBJ, Lampasas River, or Willis Creek Bridges. Based on these results, posting was not required for any of the bridges. The results are also consistent with the fact that no damage has been observed in these bridges, and they have been in service between 35 and 50 years.

The analyses also provide a means of ranking the relative vulnerability of the bridges to fatigue damage. The fraction of the vehicle population that induce fatigue cycles, $\overline{\beta}_{cr}$, and the ratio of expected fatigue cycles during the design life to fatigue life, $\overline{N}_{75}/\overline{N}$, were highest for the Lampasas River Bridge. Therefore, if traffic patterns were to change suddenly and significantly more trucks crossed this bridge on a regular basis, the Lampasas River Bridge is the most likely of the bridges considered to be classified in Category PC3 and require posting or replacement.

Table 9.6 Summary of Fatigue Calculations for Interior Bridge Girders

Parameter		Chandler Creek		Lake LBJ	Lampasas River	Willis Creek	Wimberley	
		40 ft	60 ft				40 ft	60 ft
Geometry								
	L (ft)	38.6	58.6	63.6	73.8	63.6	38.4	58.4
	M_D (kip-ft)	238	609	717	877	603	202	526
	M_{HS-20} (kip-ft)	329	529	608	791	608	328	528
	$A_2 \cdot DF \cdot (1+I) \cdot M_{HS-20}$ (kip-ft)	216	347	399	473	336	188	303
Girder Live Load Response								
	M_n (kip-ft)	1345	2805	3261	3173	2595	1721	2622
	M_{br} (kip-ft)	367	654	561	551	564	573	654
	M_n^* (kip-ft)	1107	2196	2544	2296	1992	1519	2096
	$\Delta f_{s,br}$ (ksi)	5.0	5.6	6.4	4.9	5.3	8.2	6.1
	Δf_{sn}^* (ksi)	119	122	125	122	119	123	120
Flexural Cracking Criterion								
	FF	0.91	0.77	0.68	0.29	0.50	1.60	0.81
Infinite Fatigue Life Criterion								
	$\overline{M}_{\max}$ (kip-ft)	432	694	798	946	672	—	607
	$\overline{S}_{r,\max}$ (ksi)	15.0	8.7	9.5	31.4	13.8	—	5.7
Finite Fatigue Life Criterion								
	M_{dc}^* (kip-ft)	292	—	—	133	246	—	—
	ζ_{cr}	1.35	—	—	0.28	0.73	—	—
	λ_{cr}	1.53	—	—	0.83	1.01	—	—
	$\overline{M}_{eff}$ (kip-ft)	330	—	—	394	341	—	—
	$\overline{S}_{r,eff}$ (ksi)	4.5	—	—	3.5	3.2	—	—
	$\overline{N}$ (cycles)	47,800,000	—	—	102,700,000	135,000,000	—	—
	$\overline{\beta}_{cr}$	0.005	—	—	0.94	0.57	—	—
	$\overline{\beta}_{cr} \cdot \overline{\Omega} \cdot ADTT$	32	—	—	1007	178	—	—
	$\overline{N}_{75}$ (cycles)	900,000	—	—	27,600,000	4,900,000	—	—
Fatigue Category								
		PC2	PC1	PC1	PC2	PC2	PC1	PC1
Inventory-Level Load Rating								
		1.17*	1.25	1.31	1.04*	1.16	2.00	1.43

* Controls load rating for bridge.

Table 9.7 Summary of Fatigue Calculations for Exterior Bridge Girders

Parameter		Chandler Creek		Lake LBJ	Lampasas River	Willis Creek	Wimberley	
		40 ft	60 ft				40 ft	60 ft
Geometry								
	L (ft)	38.6	58.6	63.6	73.8	63.6	38.4	58.4
	M_D (kip-ft)	224	576	743	847	637	197	514
	M_{HS-20} (kip-ft)	329	529	608	791	608	328	528
	$A_2 \cdot DF \cdot (1+I) \cdot M_{HS-20}$ (kip-ft)	239	383	441	537	385	188	303
Girder Live Load Response								
	M_n (kip-ft)	1342	2781	3218	3157	2578	1662	1529
	M_{br} (kip-ft)	380	675	705	574	523	551	624
	M_n^* (kip-ft)	1118	2205	2475	2310	1941	1466	2015
	$\Delta f_{s,br}$ (ksi)	5.2	5.9	5.4	5.1	4.5	7.0	5.7
	Δf_{sn}^* (ksi)	119	122	125	122	118	123	120
Flexural Cracking Criterion								
	FF	0.87	0.76	0.63	0.31	0.40	1.83	0.86
Infinite Fatigue Life Criterion								
	$\overline{M}_{\max}$ (kip-ft)	477	767	881	1074	770	—	607
	$\overline{S}_{r,\max}$ (ksi)	20.3	12.9	17.3	38.9	24.3	—	5.5
Finite Fatigue Life Criterion								
	M_{dc}^* (kip-ft)	315	430	384	182	212	—	—
	ζ_{cr}	1.32	1.12	0.87	0.34	0.55	—	—
	λ_{cr}	1.50	1.30	1.10	0.85	0.92	—	—
	$\overline{M}_{eff}$ (kip-ft)	357	499	487	454	354	—	—
	$\overline{S}_{r,eff}$ (ksi)	4.9	4.4	3.7	4.1	3.1	—	—
	$\overline{N}$ (cycles)	36,7000,000	53,100,000	84,400,000	65,400,000	154,500,000	—	—
	$\overline{\beta}_{cr}$	0.005	0.005	0.39	0.91	0.76	—	—
	$\overline{\beta}_{cr} \cdot \overline{\Omega} \cdot ADTT$	32	32	395	976	237	—	—
	$\overline{N}_{75}$ (cycles)	900,000	900,000	10,800,000	26,700,000	6,500,000	—	—
Fatigue Category								
		PC2	PC2	PC2	PC2	PC2	PC1	PC1
Inventory-Level Load Rating								
		1.17*	1.25	1.31	1.04*	1.16	2.00	1.43

* Controls load rating for bridge.

CHAPTER 10
Summary and Conclusions

Most of the prestressed concrete girder bridges in Texas that were constructed before 1970 fail to satisfy the serviceability limit state criterion related to the tensile stress in the concrete in the precompressed tensile zone when evaluated using the current procedures in the AASHTO Manual for Condition Evaluation of Bridges. As a result, the inventory-level rating factors for these bridges are less than 1.0. If the provisions in the MCEB were followed as written, these bridges would need to be posted to limit the legal live loads. TxDOT has not taken that step with most of the bridges because visual inspections have not identified any signs of deterioration. Instead, TxDOT has increased the limiting tensile stress used in the load rating calculations. The primary objective of this investigation was to determine if this increase in limiting tensile stress had a negative impact on the fatigue life of the bridges.

The investigation may be divided into three phases. In the first phase, diagnostic load tests were conducted on five prestressed bridges in the Austin District that were designed in the 1950s and 1960s. In the second phase, fatigue tests of prestressed concrete beams were conducted in the Ferguson Structural Engineering Laboratory. The load rating criteria were evaluated critically in the third phase, and recommendations were developed for including the fatigue limit state directly in the load rating process.

10.1 DIAGNOSTIC LOAD TESTS

Five prestressed concrete bridges were selected for evaluation using diagnostic load tests. All bridges supported two lanes of traffic. The spans of the simply-supported prestressed concrete girders ranged from 40 to 75 ft, roadway widths varied between 24 ft and 28 ft-8 in., beam spacing varied between 6 ft-8 in. and 8 ft, and skew angles varied between 0° and 30°.

A total of eight spans on the five bridges were visually inspected, instrumented and load tested. No signs of flexural cracking in the concrete or corrosion of the prestressing strand were observed during the visual inspections.

Two, standard, 10-yd^3 dump trucks were used for the diagnostic load tests. Several load paths and vehicle configurations were used to obtain a comprehensive view of the live load response of each bridge. Measured data collected during the load tests were used to estimate the depth of the centroid of the composite cross section and the live load distribution factors for each girder. The results indicated that flexural cracks are likely to be present in most of the bridge girders. The precompresssion was sufficient to close the cracks in the absence of live load, which is why the cracks were not detected during the visual inspections.

The live load distribution factors in the AASHTO Standard Specifications were found to be conservative compared with the measured response of the bridges. The live load distribution factors in the AASHTO LRFD Specifications were more variable. In some cases they were more conservative than those in the Standard Specifications, and in other cases they were unconservative compared with the measured response.

10.2 LABORATORY FATIGUE TESTS

An interior beam from the 60-ft span of the Chandler Creek Bridge was selected as the prototype for the laboratory fatigue tests. Initially, it was hoped that the specimens could reproduce the same level of tensile stress in the precompressed tension zone and stress range in the strand. However, the tensile stress in the concrete was found to be an unreliable indicator of the stress in the strand. Therefore, the stress range in the strand was selected as the primary experimental parameter in the laboratory tests. Nominal stress ranges of 10, 25, and 50 ksi were selected for investigation.

The two laboratory specimens tested with calculated strand stress ranges of 4 and 13 ksi survived 10 million loading cycles and exhibited no appreciable degradation beam behavior. The two specimens tested with calculated strand stress ranges of 26 and 27 ksi had fatigue lives of 2.4 and 5.3 million cycles, respectively. The two specimens tested with a calculated strand stress range of 48 ksi had fatigue lives of 0.3 and 0.5 million cycles, respectively. These results are comparable with those from previous experimental investigations.

10.3 LOAD RATING PROCEDURES FOR PRESTRESSED CONCRETE BRIDGES

Analyses of the bridges considered in this investigation, evaluation of the measured data, and the results of the laboratory fatigue tests confirmed the assumption that prestressed concrete bridges are likely to crack under service loads. Even at repeated cycles that induce tensile stresses in the concrete as low as $3\sqrt{f_c'}$, flexural cracks are expected to develop. Prestressed concrete beams with flexural cracks are assumed to be susceptible to fatigue damage, due to increased live load stress levels in the strand and stress concentrations in the vicinity of the cracks.

Because flexural cracks are expected, calculations based on the gross cross-sectional properties of the composite cross section are not considered to be representative of the response of prestressed concrete bridges. Therefore, the tensile stress criterion in the MCEB is not sufficient to ensure the fatigue does not limit the service life of these bridges. Recommendations were developed to consider the fatigue limit state of prestressed concrete girders explicitly in the load rating process.

10.3.1 Proposed Changes to MCEB

The current provisions in the MCEB define four serviceability limit state criteria at the inventory level and one at the operating level. Of these, the limit on the tensile stress in the concrete controlled the inventory-level rating for all five bridges considered in this investigation. By increasing the limiting tensile stress in the concrete, TxDOT was successful in increasing the inventory-level ratings, but the use of the increased tensile stress could not be justified from the laboratory data. In addition, it was demonstrated that the calculated tensile stress in the concrete is a very poor indicator of the live load stress range in the strand. The limiting tensile stress of $6\sqrt{f_c'}$ used in the MCEB is considered to be appropriate for identifying the girders that are not likely to experience flexural cracks, but is overly conservative when used as a metric for identifying bridges that are susceptible to fatigue damage.

The rating factors calculated using the other serviceability limit state criteria were typically 2 to 10 times larger than the rating factor for the capacity limit states. Therefore, it is recommended that TxDOT ignore the serviceability limit state criteria, and use the capacity limit state criteria in the MCEB to determine the inventory and operating-level ratings for prestressed concrete bridges. However, the fatigue limit state must also be evaluated to determine if fatigue limits the design life of these bridges.

10.3.2 Inclusion of Fatigue Limit State

Unlike the limit states defined in the MCEB, the recommended procedures for evaluating the fatigue limit state do not produce a rating factor for a prestressed concrete bridge. Rather the procedures may be used to determine if a spectrum of loading vehicles representative of interstate highway traffic along a major transportation corridor in Texas will limit the design life of the bridge. Fatigue categories corresponding to infinite life, finite fatigue life that exceeds the design life, and finite fatigue life that limits the design life have been defined. Corrective action, such as limiting the legal live load, is only required for bridges in the third category.

The proposed procedures for evaluating the fatigue limit state are similar in concept to those for steel bridges in the Manual for Condition Evaluation and Load and Resistance Factor Rating of Highway Bridges. Beams that are likely to experience flexural cracks under service loads are considered to be susceptible to fatigue damage. Provisions were developed to distinguish beams with infinite fatigue lives from those with finite fatigue lives. The fatigue life model for Detail Category C in the AASHTO LRFD Specifications was selected for prestressed concrete girders.

The proposed procedures differ from those in the LRFR in that fatigue cycles are only counted for vehicles that induce moments above the decompression moment in the prestressed concrete girders and a nonlinear relationship is used to relate the live load moment to the stress range in the strand.

The calculations required to evaluate the fatigue life are more complex than those used in the MCEB for the serviceability limit state, but are considered to be reasonable for load rating. Simple approximations for each parameter are discussed in Chapter 9 so that the calculations can easily be included in standard TxDOT spreadsheets.

The benefits of including the fatigue life directly in the load rating process are clear. Fatigue did not limit the design life for any of the five bridges considered based on the current traffic volume. However, if the Lampasas River Bridge were to experience the same level of truck traffic as the Chandler Creek Bridge, fatigue would limit its design life. As traffic volumes increase throughout the state, the information obtained by considering the fatigue limit state will be valuable for setting priorities for bridge replacements.

10.3.3 Limitations of Proposed Methods

A number of underlying assumptions were made to develop the recommended procedures for evaluating fatigue life discussed in Chapter 9. These assumptions limit the applicability of the proposed method and are discussed below.

- The spectrum of loading vehicles was developed from weigh-in-motion data collected on I-35 south of San Antonio. This spectrum was assumed to be representative of highway traffic throughout Texas. While the percentage of five-axle trucks is higher at this location than many rural highways, the distribution of gross vehicle weight is believed to be sufficiently broad to provide a reasonable estimate of the fatigue cycles induced by truck traffic. If a bridge is known to be in the immediate vicinity of a ready-mix concrete plant or source of aggregates, site specific traffic spectra should be developed and used in place of the spectrum shown in Figure 8.1. If the legal live load were to increase in Texas, a vehicle spectrum that is representative of the increased vehicle weights would also need to be developed.
- The procedures were developed for prestressed concrete beams that exhibited no evidence of deterioration under service loads. If evidence of damage, such as corrosion of the strand or flexural cracks in the absence of live load, is visible, corrective action should be taken regardless of the calculated fatigue life.
- The bilinear approximation used to estimate the live load response of the girders was developed for Type B and C prestressed concrete beams. These relationships must be evaluated before they are used to calculate the response of different types of girders.

- All bridges considered in this investigation were simply supported and none of the cast-in-place slabs was continuous over the supports. Therefore, the bridges were only subjected to positive moments due to the vehicle loads and each loading vehicle generated one cycle of stress. The influence of continuity and moment reversals has not been considered in the development of the method.

10.4 ADDITIONAL RESEARCH NEEDS

Based on the available data, the fatigue life model for Detail Category C in the AASHTO LRFD Specifications was adopted for prestressed concrete girders. However, all the test data corresponds to constant-amplitude loading cycles and no finite life fatigue data are available for stress ranges less than 10 ksi. Long-duration, fatigue tests of prestressed girders are required to confirm the applicability of this fatigue life model.

APPENDIX A
Live Load Distribution Factors

Live load distribution factors (LLDF) are used for the design of new bridges and to evaluate the capacity of existing bridges. Two approaches for calculating these factors are summarized in this appendix. The traditional approach in the AASHTO Standard Specifications for Highway Bridge Design is summarized in Section A.1 and the procedures in the AASHTO LRFD Bridge Design Specifications are summarized in Section A.2. Although all five bridges considered in this investigation carry two lanes of traffic, the live load distribution factors were calculated for both one and two lanes of traffic to facilitate comparisons with the results of the diagnostic load tests.

A.1 AASHTO STANDARD SPECIFICATIONS

The design wheel load, W, is distributed among the longitudinal beams using the procedures in the AASHTO Standard Specifications. For an interior prestressed concrete beam with a concrete deck, the design load, R_i, is given as:

$$R_i = \frac{S}{7.0} \text{ (single traffic lane)} \tag{A.1}$$

$$R_i = \frac{S}{5.5} \text{ (two or more traffic lanes)} \tag{A.2}$$

where

S = center-to-center spacing of girders (ft)

The lever rule is used to determine the distribution factor for the exterior girders. As shown in Figure A.1, the value of the distribution factor depends on the distance from the exterior girder to the inside face of the curb (d_e), the spacing of the girders (S), and the distance between the outermost wheel load and the inside face of the curb. For this investigation, the outermost wheel load was assumed to be 2 ft from the face of the curb and the spacing between wheel loads was taken as 6 ft.

For four of the five prestressed bridges considered, two wheel loads contributed to the design load for the exterior girder, R_e:

$$R_e = \frac{Wx_1 + Wx_2}{S} \tag{A.3}$$

where

x_1 = distance from outside wheel load to interior girder (ft)

x_2 = distance from inside wheel load to interior girder (ft)

Because the inside face of the curb was closer to the exterior girder for the Wimberley Bridge and the girders were closely spaced, only one wheel load contributed to the design load:

$$R_e = \frac{Wx_1}{S} \qquad \text{(A.4)}$$

The calculated design loads for interior and exterior girders for the five bridges are summarized in Table A.1, where the ratios R_i and R_e are expressed in terms of the wheel load W. To facilitate comparisons with the distributions factors calculated in the LRFD Specifications, the values are expressed in terms of the axle load in Table A.2 ($LLDF_i = R_i/2$ and $LLDF_e = R_e/2$).

The AASHTO Standard Specifications also require that the flexural capacity of the exterior girders be at least as large as the flexural capacity for the interior girders. This provision is reflected in Table A.2 and controlled the two-lane loading for all bridges and the one-lane loading for the Wimberley Bridge.

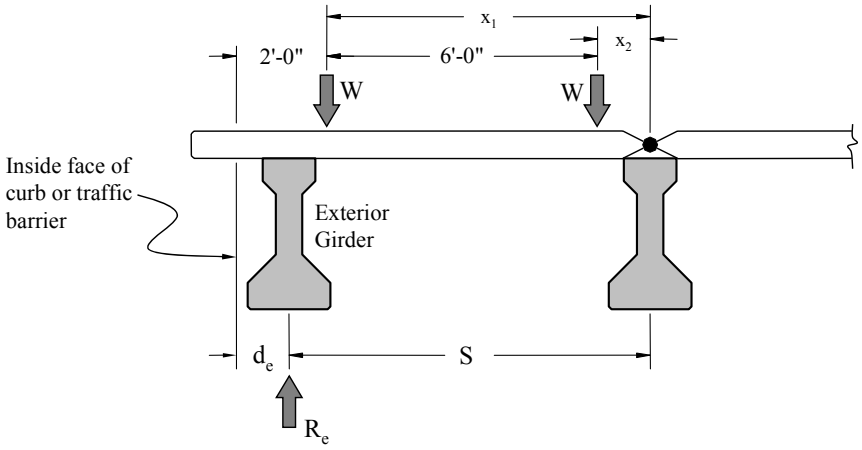

(a) Two Wheel Loads between Exterior and Interior Girder

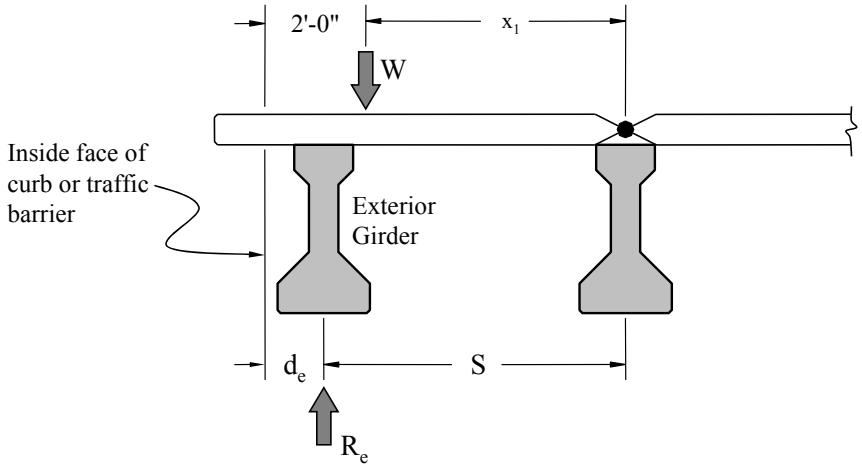

(b) One Wheel Load between Exterior and Interior Girder

Figure A.1 Lever Rule for Exterior Girder

Table A.1 Design Loads for Calculated using AASHTO Standard Specifications and Expressed in Terms of Wheel Load

Bridge Name	S (ft)	d_e (ft)	x_1 (ft)	x_2 (ft)	Interior Girder R_i		Exterior Girder R_e
					One Lane	Two Lanes	
Chandler Creek	8.0	2.0	8.0	2.0	1.14	1.45	1.25
Lake LBJ	8.0	2.0	8.0	2.0	1.14	1.45	1.25
Lampasas River	7.33	2.0	7.33	1.33	1.05	1.33	1.18
Willis Creek	6.67	2.0	6.67	0.67	0.95	1.21	1.10
Wimberley	6.92	1.0	5.92	—	0.99	1.26	0.86

Table A.2 Live Load Distribution Factors Calculated using AASHTO Standard Specifications

Bridge Name	Interior Girder $LLDF_i$		Exterior Girder $LLDF_e$	
	One Lane	Two Lanes	One Lane	Two Lanes
Chandler Creek	0.57	0.73	0.63	0.73
Lake LBJ	0.57	0.73	0.63	0.73
Lampasas River	0.52	0.67	0.59	0.67
Willis Creek	0.48	0.61	0.55	0.61
Wimberley	0.50	0.63	0.50	0.63

A.2 AASHTO LRFD SPECIFICATIONS

In the AASHTO LRFD Specifications, the lane load is distributed among the longitudinal girders. For an interior prestressed concrete girder with a concrete deck, the live load distribution factor, $LLDF_i$, is given as:

$$LLDF_i = 0.06 + \left(\frac{S}{14}\right)^{0.4}\left(\frac{S}{L}\right)^{0.3}\left(\frac{K_g}{12Lt_s^3}\right)^{0.1} \quad \text{(one design lane)} \qquad \text{(A.5)}$$

$$LLDF_i = 0.075 + \left(\frac{S}{9.5}\right)^{0.6}\left(\frac{S}{L}\right)^{0.2}\left(\frac{K_g}{12Lt_s^3}\right)^{0.1} \quad \text{(two design lanes)} \qquad \text{(A.6)}$$

where

S = center-to-center spacing of girders (ft), $\left(3.5 \le S \le 16\right)$

L = span length (ft), $\left(20 \le L \le 240\right)$

t_s = thickness of concrete slab (in.), $\left(4.5 \le t_s \le 12\right)$

$K_g = n\left(I + Ae_g^2\right)$

n = modulus of elasticity of the concrete in prestressed concrete girder divided by modulus of elasticity of concrete in the slab = E_{cg} / E_{cs}

I = moment of inertia of noncomposite beam (in.^{4})

A = area of noncomposite beam (in.^{2})

e_g = distance between centers of gravity of noncomposite beam and slab (in.)

The live load distribution factors calculated using Eq. (A.5) and Eq. (A.6) are summarized in Table A.3

Table A.3 Live Load Distribution Factors for Interior Girders Calculated using AASHTO LRFD Specifications

Bridge Name	S (ft)	L (ft)	t_s (in.)	n	I (in.^{4})	A (in.^{2})	e_g (in.)	K_g (in.^{4})	$LLDF_i$	
									One Lane	Two Lanes
Chandler Creek (40 ft)	8.0	38.6	7.25	1.3	43,300	360	22.7	295,900	0.59	0.77
Chandler Creek (60 ft)	8.0	58.6	7.25	1.3	82,800	496	26.5	557,400	0.53	0.73
Lake LBJ	8.0	63.6	7.25	1.3	82,800	496	26.5	557,400	0.52	0.71
Lampasas River	7.33	73.8	6.5	1.3	82,800	496	26.2	550,200	0.48	0.66
Willis Creek	6.67	63.6	6.0	1.3	82,800	496	25.9	536,400	0.49	0.66
Wimberley (40 ft)	6.93	38.4	6.25	1.3	43,300	360	22.2	285,500	0.56	0.72
Wimberley (60 ft)	6.93	58.4	6.25	1.3	82,800	496	26.0	540,600	0.51	0.68

For the exterior girders and one design traffic lane, the lever rule is used to determine the live load distribution factors (Figure A.1 and Table A.2). For two design lanes, the live load distribution factor for the exterior girder is related to the distribution factor for the interior girder:

$$LLDF_e = \lambda \cdot LLDF_i \tag{A.7}$$

$$\lambda = 0.77 + \frac{d_e}{9.1} \geq 1.0 \tag{A.8}$$

where

d_e = distance from center of exterior girder and inside face of curb or traffic barrier (ft), $\left(d_e \leq 3\right)$

For the five bridges considered, the value of λ was controlled by the lower limit of 1.0. Therefore, the live load distribution factors for the exterior girders were the same as the live load distribution factors for the interior girders when two design lanes were considered.

In addition, for bridges with diaphragms, the live load distribution factors for the exterior girders are also calculated by assuming that the bridge deflects and rotates as a rigid body (Figure A.2). The corresponding distribution factors are:

$$LLDF_e = \frac{N_L}{N_b} + \frac{x_{ext}\sum_{i=1}^{N_L} e_i}{\sum_{i=1}^{N_b} x_i^2} \quad \text{(A.9)}$$

where

N_L = number of design lanes
N_b = number of beams, $\left(N_b \geq 4\right)$
x_{ext} = horizontal distance between centers of gravity of pattern of girders and exterior girder (ft)
e_i = horizontal distance between center of gravity of loading lane *i* and pattern of girders (ft)
x_i = horizontal distance from center of gravity of pattern of girders to girder *i* (ft)

When using the lever rule or rigid body analysis to determine the live load distribution factors for one design traffic lane, the distribution factors must be multiplied by a multiple presence factor (m=1.2). The live load distribution factors calculated for the exterior girders are summarized in Table A.4.

Table A.4 Live Load Distribution Factors for Exterior Girders Calculated using AASHTO LRFD Specifications

Bridge Name	One Lane*		Two Lanes	
	Lever Rule	Rigid Body	Eq. A.7	Rigid Body
Chandler Creek (40 ft)	0.75	0.71	0.77	0.80
Chandler Creek (60 ft)	0.75	0.71	0.73	0.80
Lake LBJ	0.75	0.71	0.71	0.80
Lampas River	0.71	0.69	0.66	0.75
Willis Creek	0.66	0.68	0.66	0.68
Wimberley (40 ft)	0.59	0.58	0.72	0.68
Wimberley (60 ft)	0.59	0.58	0.68	0.68

* Live load distribution factor includes multiple presence factor (m = 1.2).

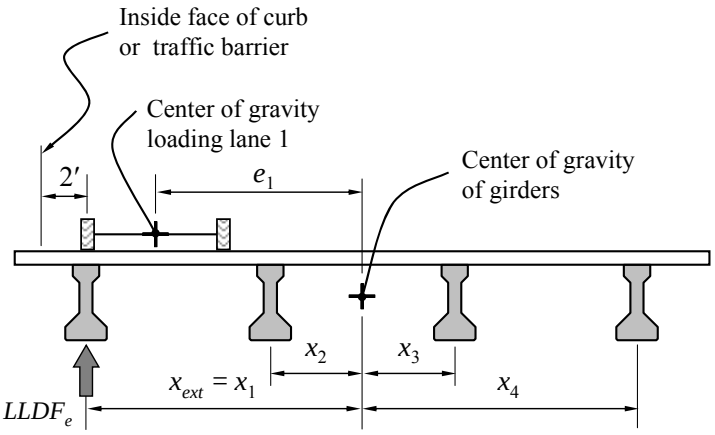

(a) One Design Traffic Lane

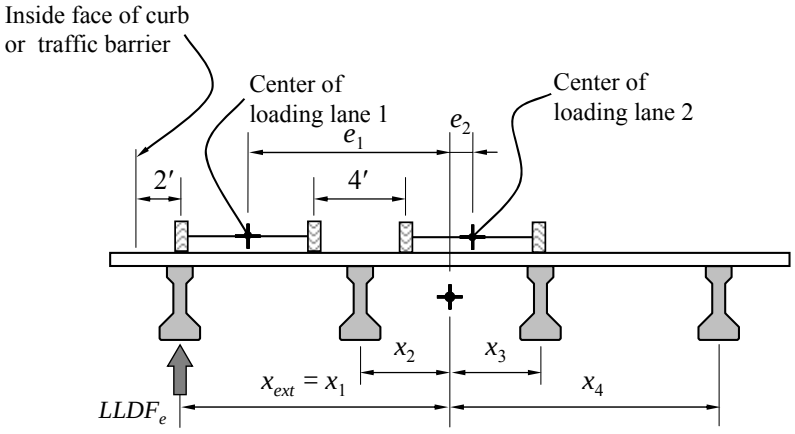

(b) Two Design Traffic Lanes

Figure A.2 Rigid Body Analysis of Prestressed Concrete Girder Bridge with Diaphragms

The AASHTO LRFD Specifications include a reduction factor for skewed prestressed concrete girder bridges. The design moments may be reduced by the factor γ if the angle of the skew, θ, is between 30° and 60°:

$$\gamma = 1 - c_1 \left(tan\theta \right)^{1.5} \tag{A.10}$$

$$c_1 = 0.25 \left(\frac{K_g}{12Lt_s^3} \right)^{0.25} \left(\frac{S}{L} \right)^{0.5} \tag{A.11}$$

Only the Chandler Creek Bridge satisfies the limits on skew angle. The values of γ are 0.85 for the 40-ft span and 0.87 for the 60-ft span.

The live load distribution factors calculated using the AASHTO LRFD Specifications are summarized in Table A.5.

Table A.5 Live Load Distribution Factors Calculated using AASHTO LRFD Specifications

Bridge Name	Interior Girder $LLDF_i$		Exterior Girder $LLDF_e$	
	One Lane	Two Lanes	One Lane	Two Lanes
Chandler Creek (40 ft)*	0.50	0.65	0.64	0.68
Chandler Creek (60 ft)*	0.46	0.63	0.65	0.70
Lake LBJ	0.52	0.71	0.75	0.80
Lampasas River	0.48	0.66	0.71	0.75
Willis Creek	0.49	0.66	0.68	0.68
Wimberley (40 ft)	0.56	0.72	0.59	0.72
Wimberley (60 ft)	0.51	0.68	0.59	0.69

* Reduction factor for skew is included in live load distribution factors for Chandler Creek Bridge.

In Chapter 4, live load distribution factors are calculated from the strain data measured during the diagnostic load tests. Two types of tests were conducted: (1) one or two trucks in a single lane, and (2) one truck in each of two lanes. For cases with trucks positioned in two lanes, the measured data were compared directly with the live load distribution factors for two lanes in Table A.5. However, for cases with trucks in one lane only, the live load distribution factors in Table A.5 were divided by the multiple presence factor, *m,* because no vehicles were present in the second lane. The live load distribution factors used to compare with the measured data are summarized in Table A.6.

Table A.6 Live Load Distribution Factors Based on using AASHTO LRFD Specifications used to Compare with Measured Response

Bridge Name	Interior Girder $LLDF_i$		Exterior Girder $LLDF_e$	
	One Lane	Two Lanes	One Lane	Two Lanes
Chandler Creek (40 ft)	0.41	0.65	0.53	0.68
Chandler Creek (60 ft)	0.39	0.63	0.54	0.70
Lake LBJ	0.43	0.71	0.63	0.80
Lampasas River	0.40	0.66	0.59	0.75
Willis Creek	0.40	0.66	0.55	0.68
Wimberley (40 ft)	0.46	0.72	0.50	0.72
Wimberley (60 ft)	0.42	0.68	0.50	0.68

A.3 COMPARISON OF LIVE LOAD DISTRIBUTION FACTORS

The live load distribution factors calculated using the AASHTO Standard and LRFD Specifications are compared in Figure A.3. The following trends were observed for interior girders:

- The LRFD distribution factors were 10 to 20% lower than the Standard distribution factors for the Chandler Creek Bridge due to the reduction factor for skewed bridges.
- The LRFD distribution factors were up to 10% lower than the Standard distribution factors for the Lake LBJ and Lampasas River Bridges.
- The LRFD distribution factors were up to 15% higher than the Standard distribution factors for the Willis Creek and Wimberley Bridges.

The following trends were observed for exterior girders:

- For a single traffic lane, the LRFD distribution factors were approximately 20% larger than the Standard distribution factors due to the multiple presence factor, m. The skew reduction factor offset the multiple presence factor for the Chandler Creek Bridge. In all cases, the LRFD distribution factors exceeded the Standard distribution factors.
- For two traffic lanes, the LRFD distribution factors were 10 to 15% larger than the Standard distribution factors for the non-skewed bridges. The LRFD distribution factors were less than 10% lower than the Standard distribution factors for the Chandler Creek Bridge.

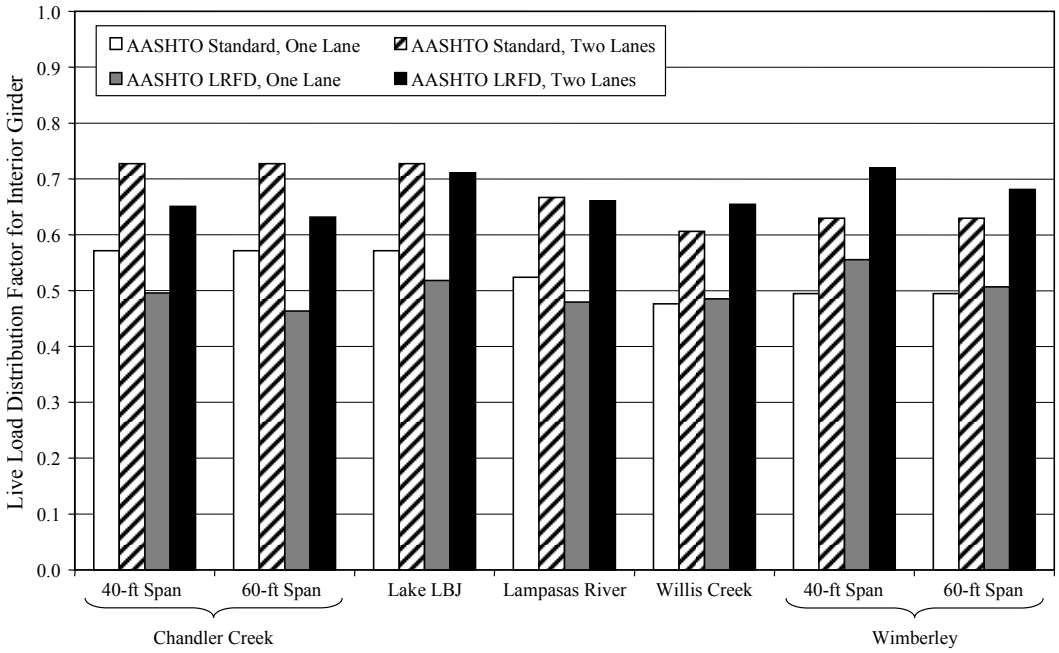

(a) Interior Girders

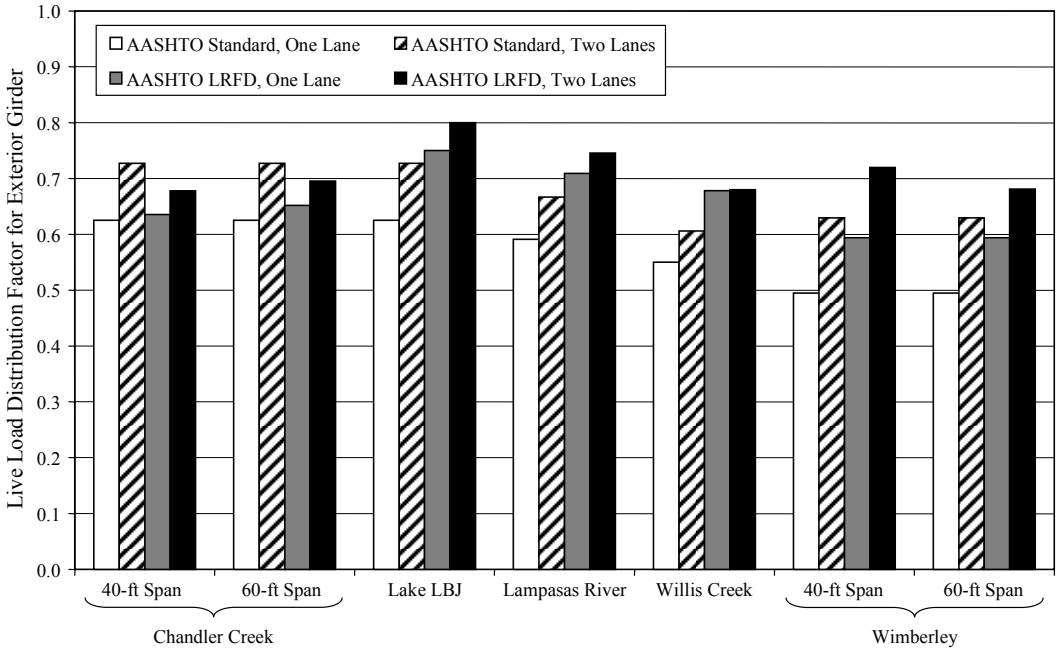

(b) Exterior Girders

Figure A.3 Comparison of Live Load Distribution Factors Calculated Using AASHTO Standard and LRFD Specifications

APPENDIX B
Variation in Strand Stress Due to Live Load

Bridge engineers typically do not calculate the stress in the strand at service load levels. However, the range of stress experienced by the strand under fatigue loads has a significant impact on the fatigue performance of the prestressed concrete girder. The results of two methods for estimating the variation of stress in the strand is summarized in this appendix. In the first method, five points are used to define the relationship between the increase in tensile stress in the extreme layer of the strand and the live load moment (Figure B.1). The live load conditions corresponding to each point are defined in Table B.1. Nonlinear relationships between stress and strain in both the concrete and the prestressing strand were assumed in these calculations. Details of this procedure are presented in Hagenberger (2004) and the results are presented in Section B.1.

Table B.1 Definition of Points in Nonlinear Analysis

Point	Description
1	Full dead load state
2	Decompression of bottom fiber
3	Neutral axis at bottom of web
4	Neutral axis at top of web
5	Flexural capacity

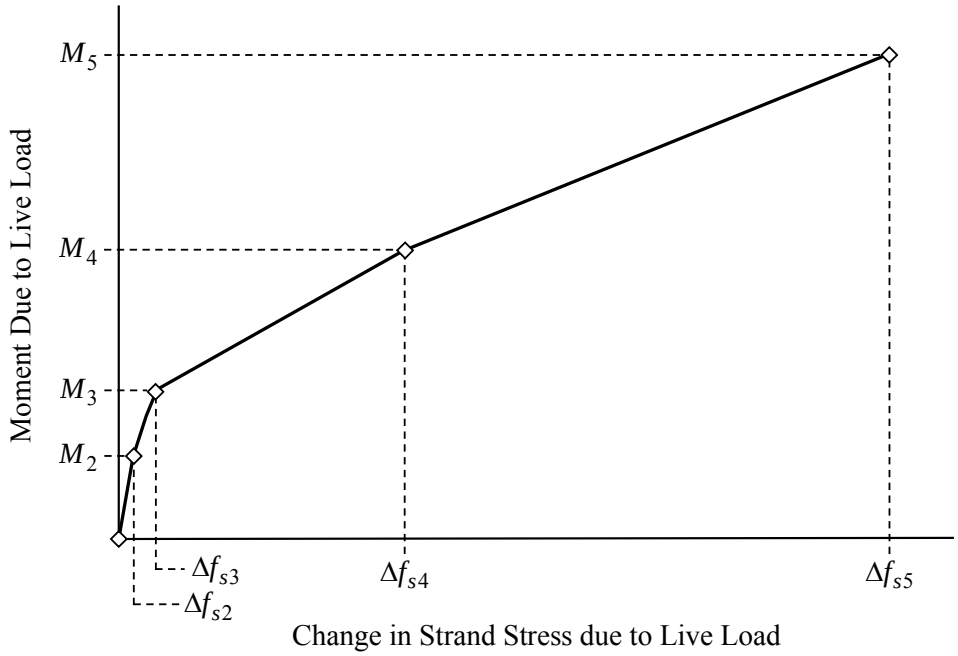

Figure B.1 Idealized Relationship between Live Load Moment and Change in Strand Stress

A simple, bilinear approach for approximating the nonlinear response is discussed in Section 8.4, and those results are compared with the nonlinear approximation in Section B.2.

All calculations in Section B.1 are based on the estimated compressive strength of the concrete 28 days after casting, while the specified material properties are used in the bilinear approximation. Prestress losses were estimated using the procedures in the AASHTO LRFD Specifications in all cases.

B.1 NONLINEAR RELATIONSHIP BETWEEN STRAND STRESS AND MOMENT

The nonlinear response of each bridge girder is summarized in this section. Critical values are listed in Table B.2 through Table B.8, and the data are plotted in Figure B.2 through Figure B.6.

Table B.2 Calculated Live Load Response of Wimberley Bridge (40-ft Span)

Level of Live Load	Interior Girder		Exterior Girder	
	Strand Stress Range (ksi)	Live Load Moment (kip-ft)	Strand Stress Range (ksi)	Live Load Moment (kip-ft)
1	0	0	0	0
2	3.2	290	3.5	313
3	4.7	386	4.9	401
4	22.5	572	25.0	596
5	114.5	1117	115.0	1129

Table B.3 Calculated Live Load Response of Wimberley Bridge (60-ft Span)

Level of Live Load	Interior Girder		Exterior Girder	
	Strand Stress Range (ksi)	Live Load Moment (kip-ft)	Strand Stress Range (ksi)	Live Load Moment (kip-ft)
1	0	3	0	0
2	2.4	369	2.7	420
3	5.1	671	5.4	704
4	53.2	1427	609	1533
5	115.3	2243	116.0	2271

Table B.4 Calculated Live Load Response of Lake LBJ Bridge

Level of Live Load	Interior Girder		Exterior Girder	
	Strand Stress Range (ksi)	Live Load Moment (kip-ft)	Strand Stress Range (ksi)	Live Load Moment (kip-ft)
1	0	0	0	0
2	2.6	371	2.3	358
3	6.2	770	6.1	720
4	80.9	2001	94.9	2162
5	116.7	2624	117.0	2570

Table B.5 Calculated Live Load Response of Lampasas River Bridge

Level of Live Load	Interior Girder		Exterior Girder	
	Strand Stress Range (ksi)	Live Load Moment (kip-ft)	Strand Stress Range (ksi)	Live Load Moment (kip-ft)
1	0	0	0	0
2	0.8	123	1.2	170
3	5.0	574	5.2	605
4	99.0	2128	101.5	2187
5	112.2	2392	112.7	2404

Table B.6 Calculated Live Load Response of Willis Creek Bridge

Level of Live Load	Interior Girder		Exterior Girder	
	Strand Stress Range (ksi)	Live Load Moment (kip-ft)	Strand Stress Range (ksi)	Live Load Moment (kip-ft)
1	0	0	0	0
2	1.7	238	1.3	201
3	5.5	577	5.2	530
4	101.2	1864	102.3	1853
5	111.7	2072	111.4	2022

Table B.7 Calculated Live Load Response of Wimberley Bridge (40-ft Span)

Level of Live Load	Interior Girder		Exterior Girder	
	Strand Stress Range (ksi)	Live Load Moment (kip-ft)	Strand Stress Range (ksi)	Live Load Moment (kip-ft)
1	0	0	0	0
2	5.2	443	5.3	515
3	7.6	580	7.9	569
4	71.2	1121	102.5	1341
5	118.6	1561	117.4	1524

Table B.8 Calculated Live Load Response of Wimberley Bridge (60-ft Span)

Level of Live Load	Interior Girder		Exterior Girder	
	Strand Stress Range (ksi)	Live Load Moment (kip-ft)	Strand Stress Range (ksi)	Live Load Moment (kip-ft)
1	0	0	0	0
2	2.7	363	2.9	395
3	6.2	677	6.6	665
4	99.5	1898	106.3	2025
5	113.4	2171	111.3	2106

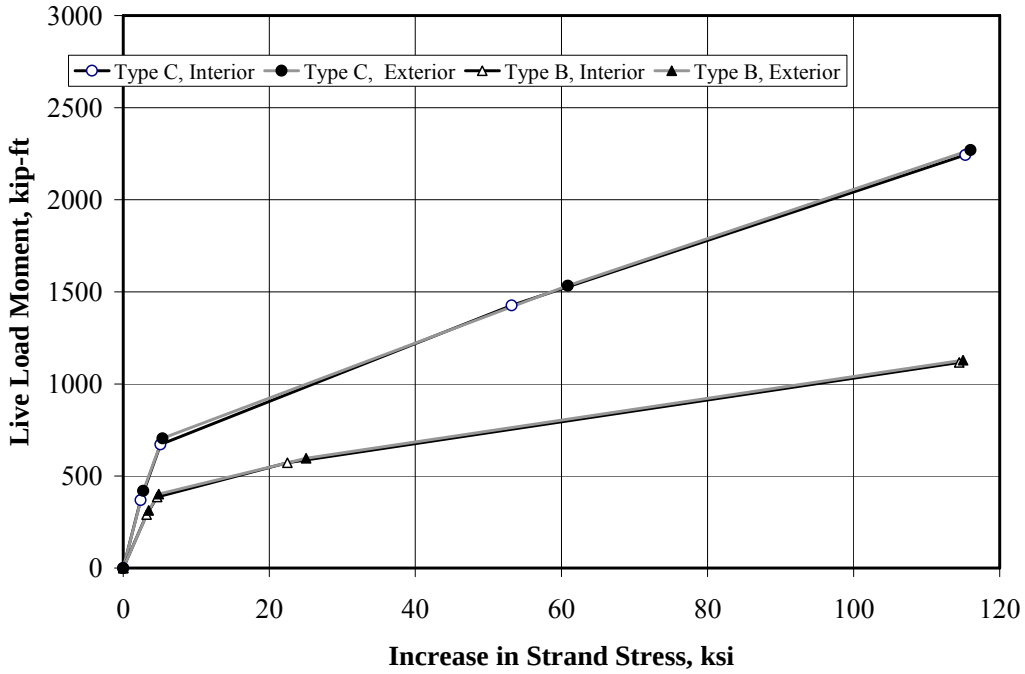

Figure B.2 Calculated Live Load Response of Chandler Creek Bridge

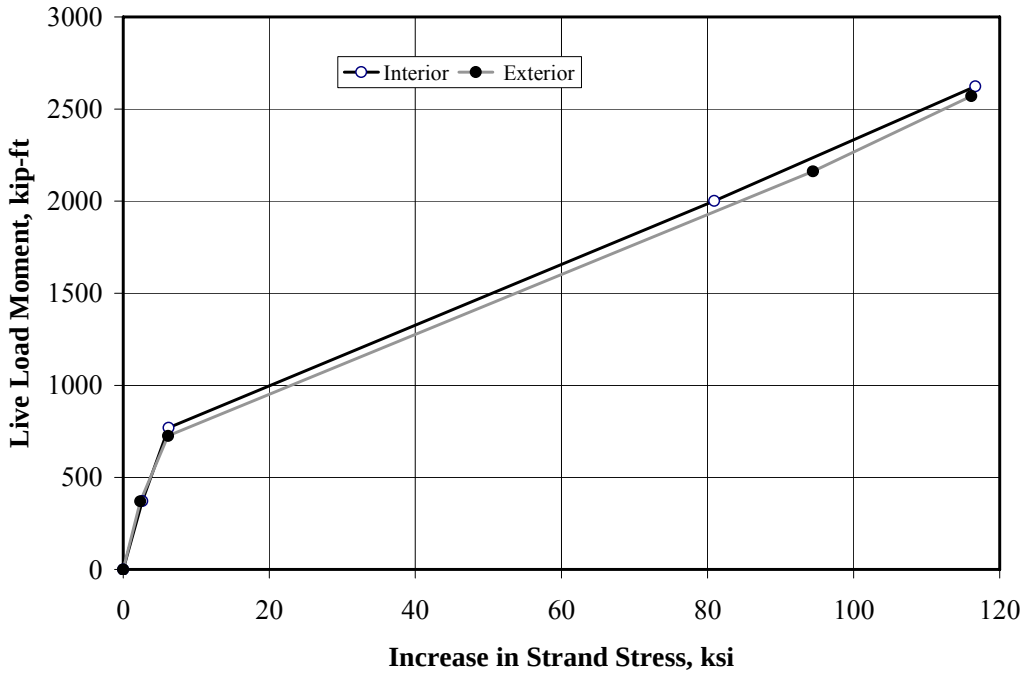

Figure B.3 Calculated Live Load Response of Lake LBJ Bridge

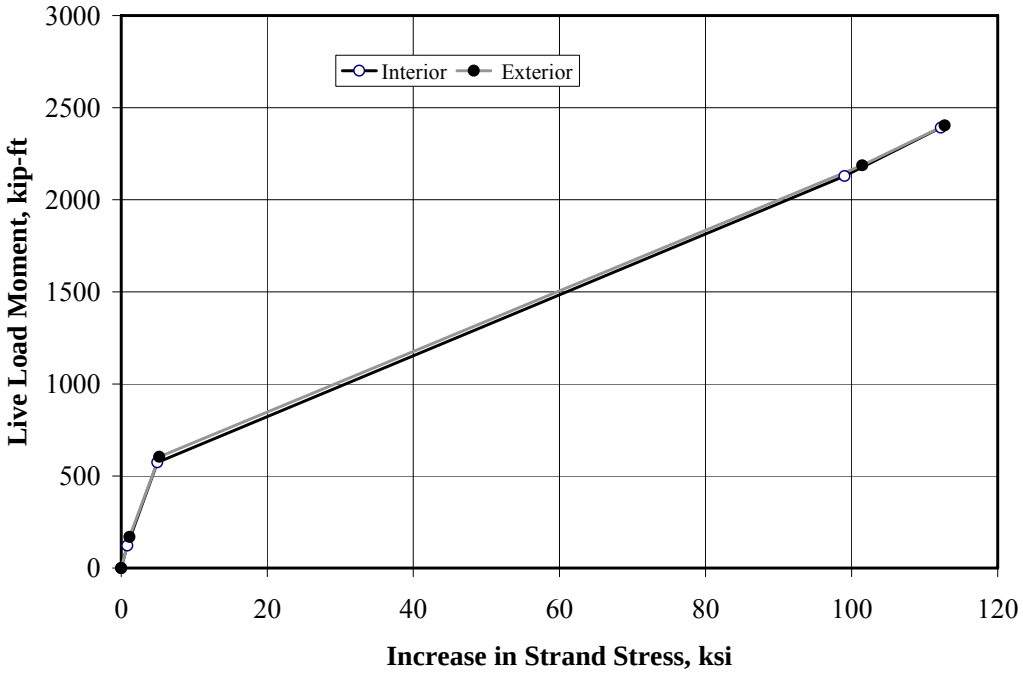

Figure B.4 Calculated Live Load Response of Lampasas River Bridge

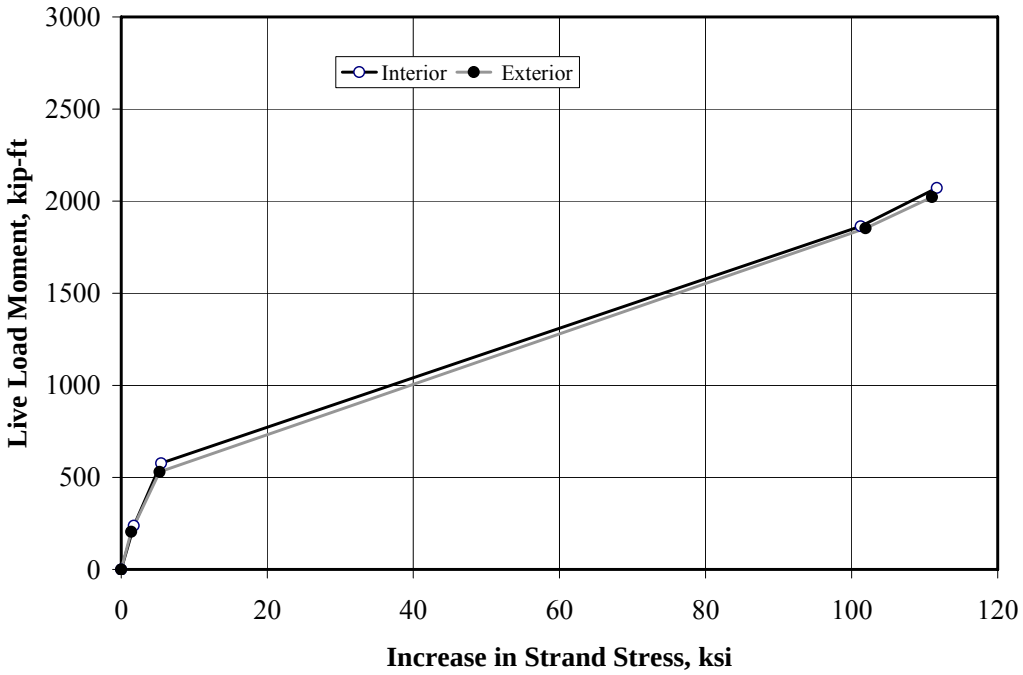

Figure B.5 Calculated Live Load Response of Willis Creek Bridge

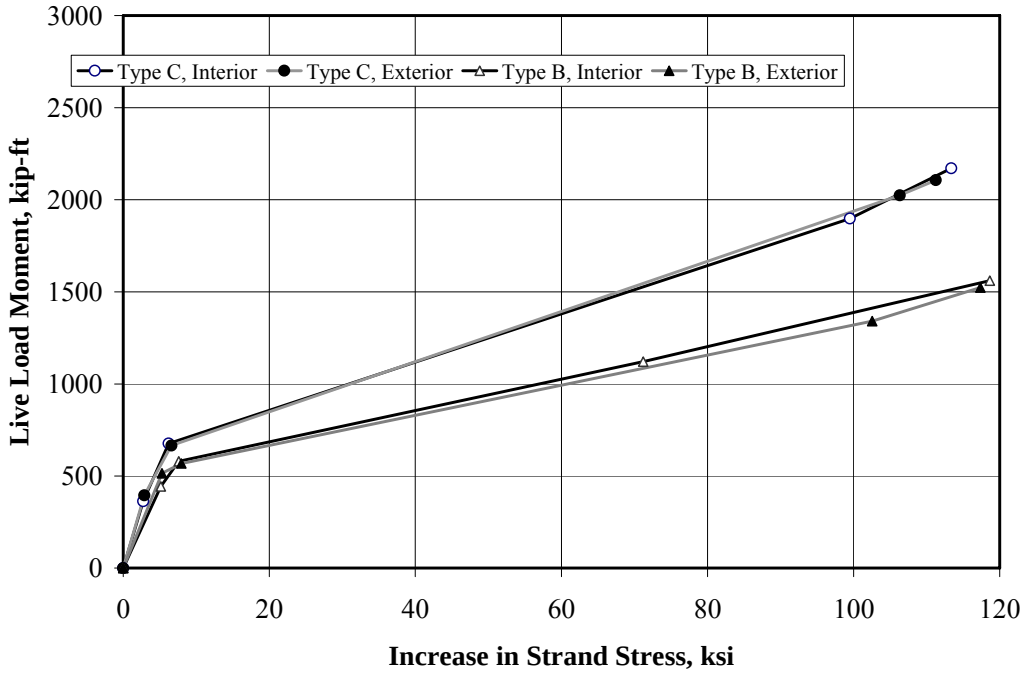

Figure B.6 Calculated Live Load Response of Wimberley Bridge

B.2 BILINEAR APPROXIMATION OF NONLINEAR RESPONSE

As discussed in Section 8.4, the bilinear approximation was developed to simplify the calculations required to determine the variation of stress in the strand due to live load. Critical values are reported in Table 8.2 and plotted in Figure B.7 through Figure B.20.

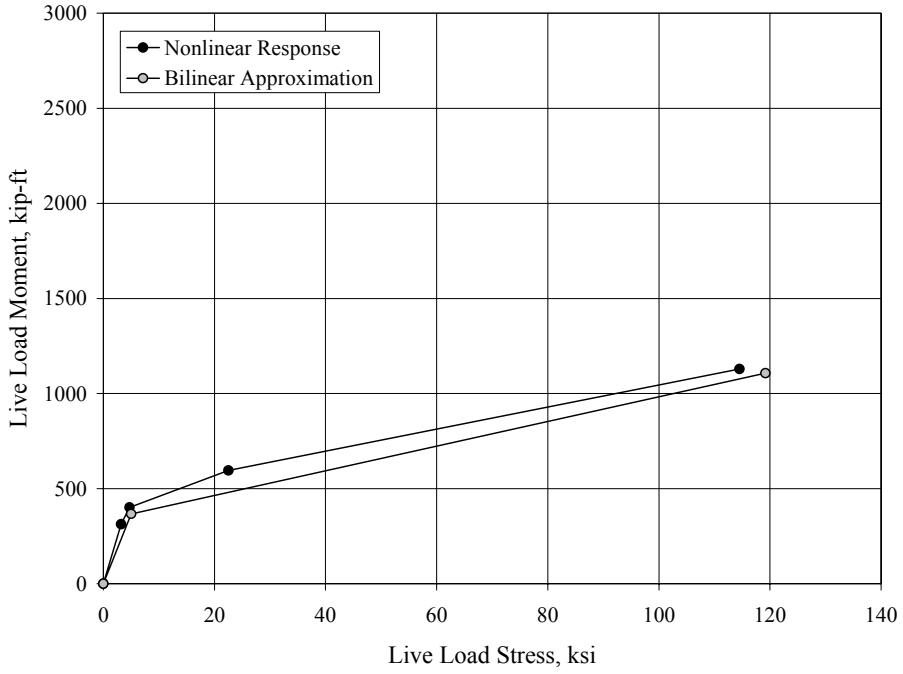

Figure B.7 Idealized Response of Interior Girder, Chandler Creek Bridge, 40-ft Span

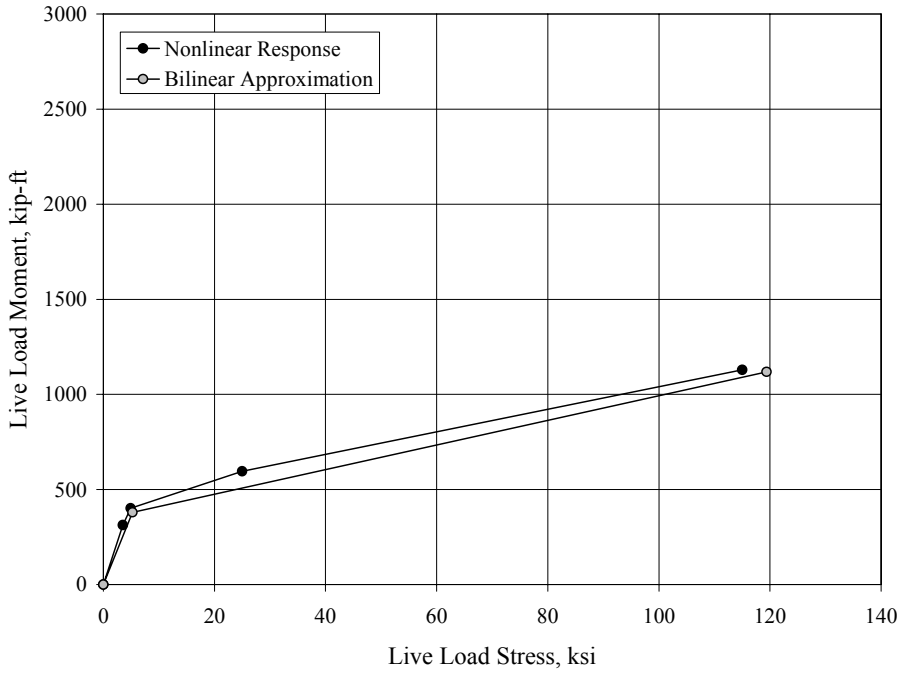

Figure B.8 Idealized Response of Exterior Girder, Chandler Creek Bridge, 40-ft Span

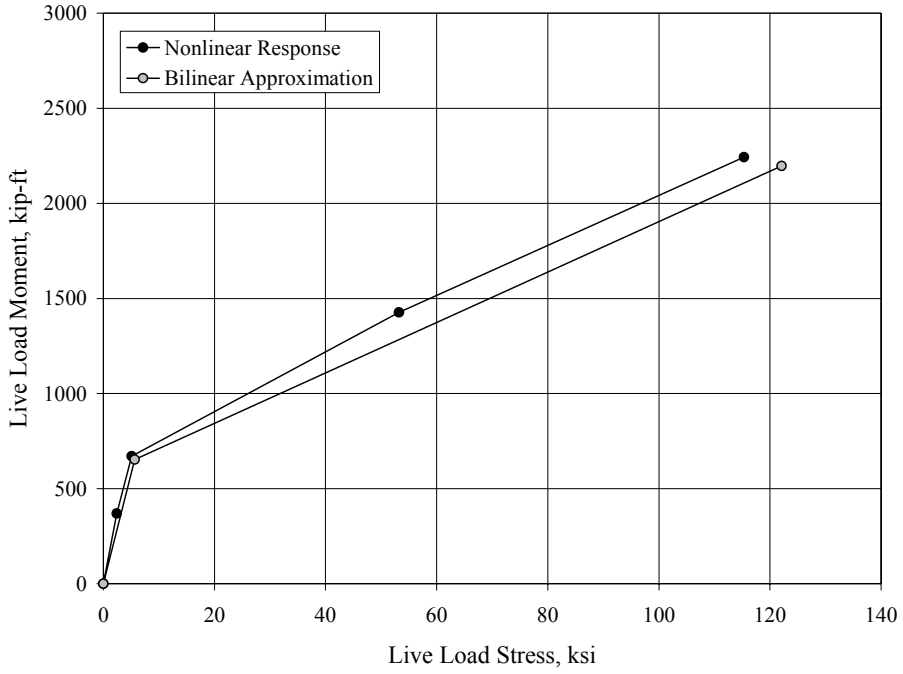

Figure B.9 Idealized Response of Interior Girder, Chandler Creek Bridge, 60-ft Span

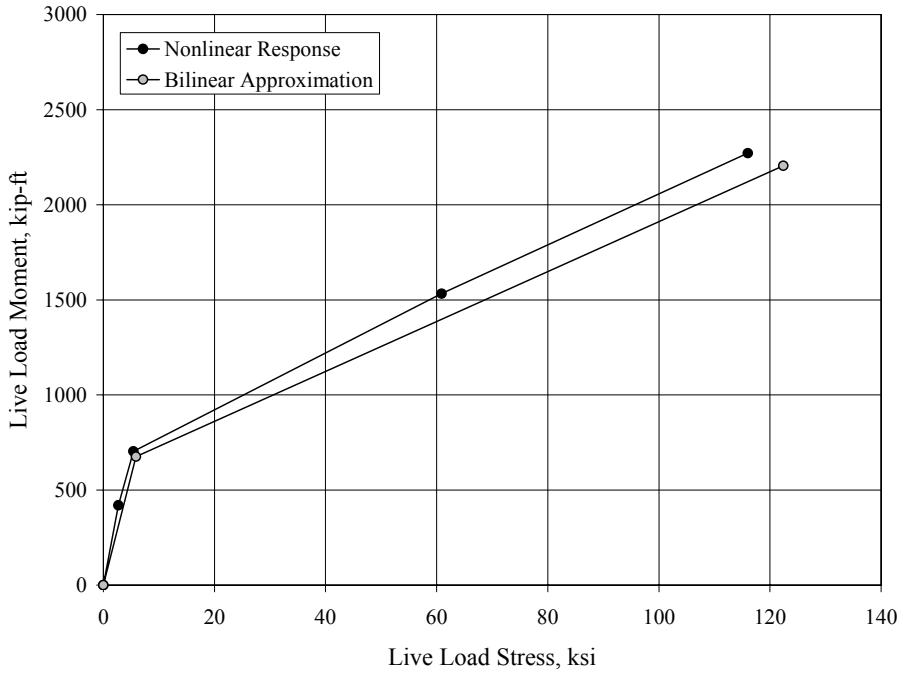

Figure B.10 Idealized Response of Exterior Girder, Chandler Creek Bridge, 60-ft Span

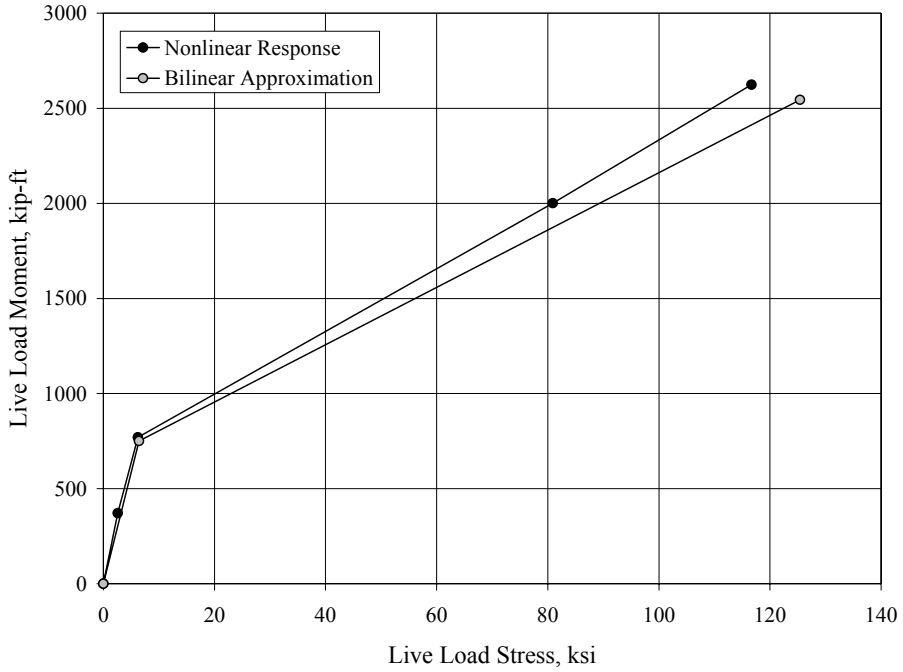

Figure B.11 Idealized Response of Interior Girder, Lake LBJ Bridge

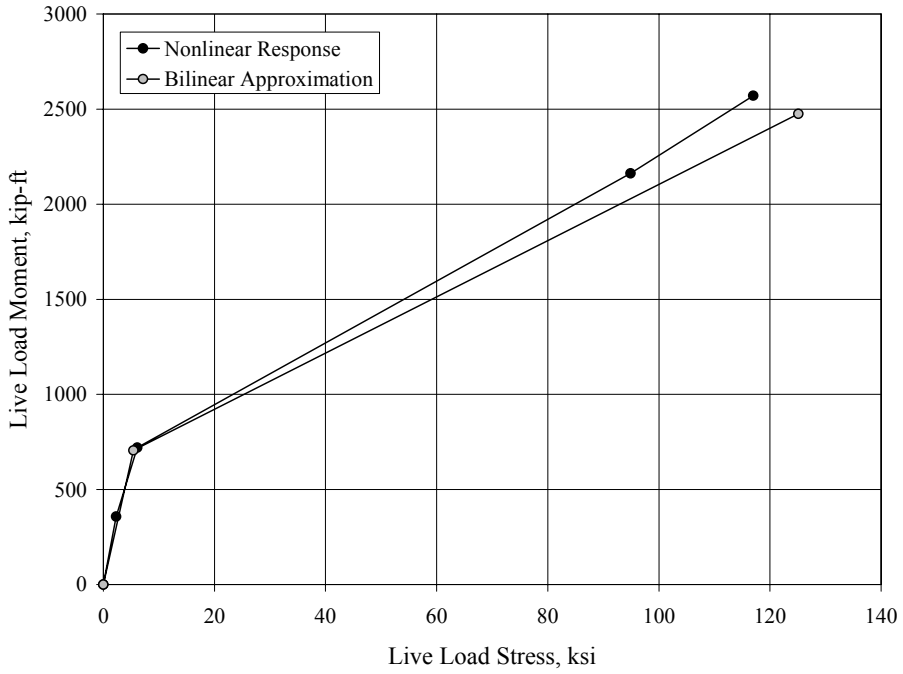

Figure B.12 Idealized Response of Exterior Girder, Lake LBJ Bridge

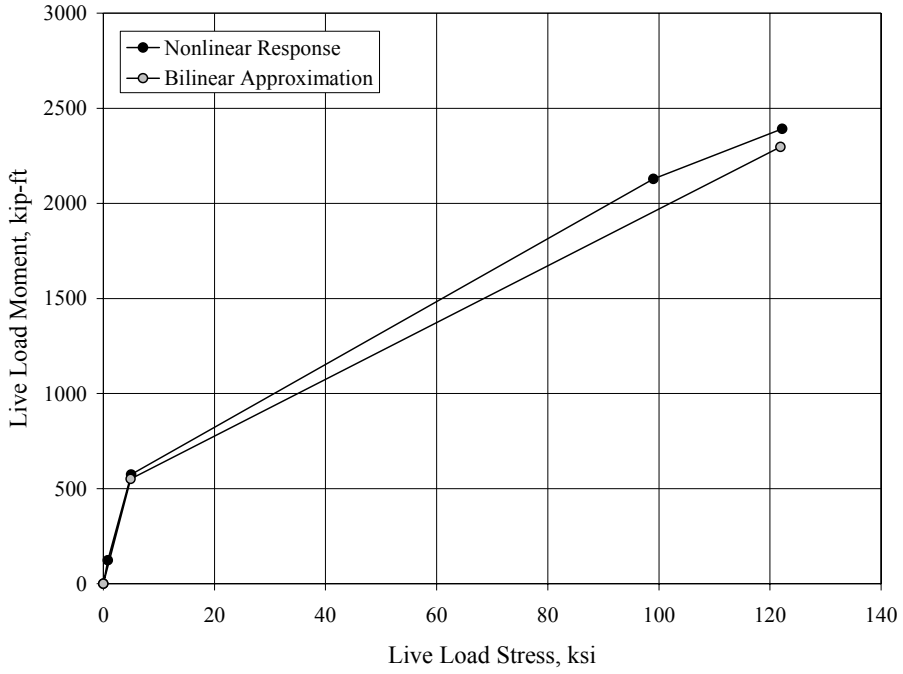

Figure B.13 Idealized Response of Interior Girder, Lampasas River Bridge

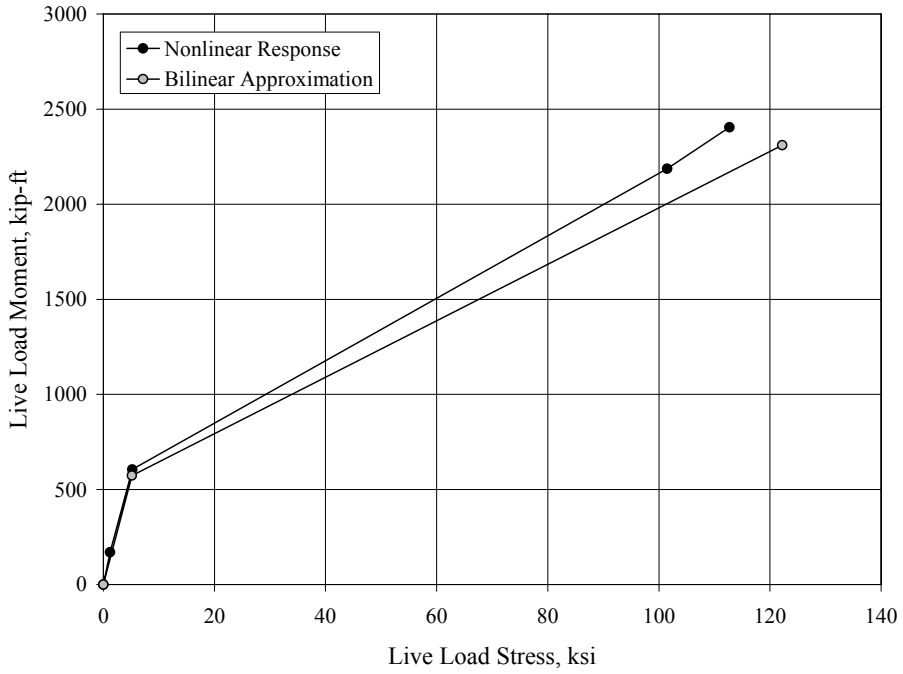

Figure B.14 Idealized Response of Exterior Girder, Lampasas River Bridge

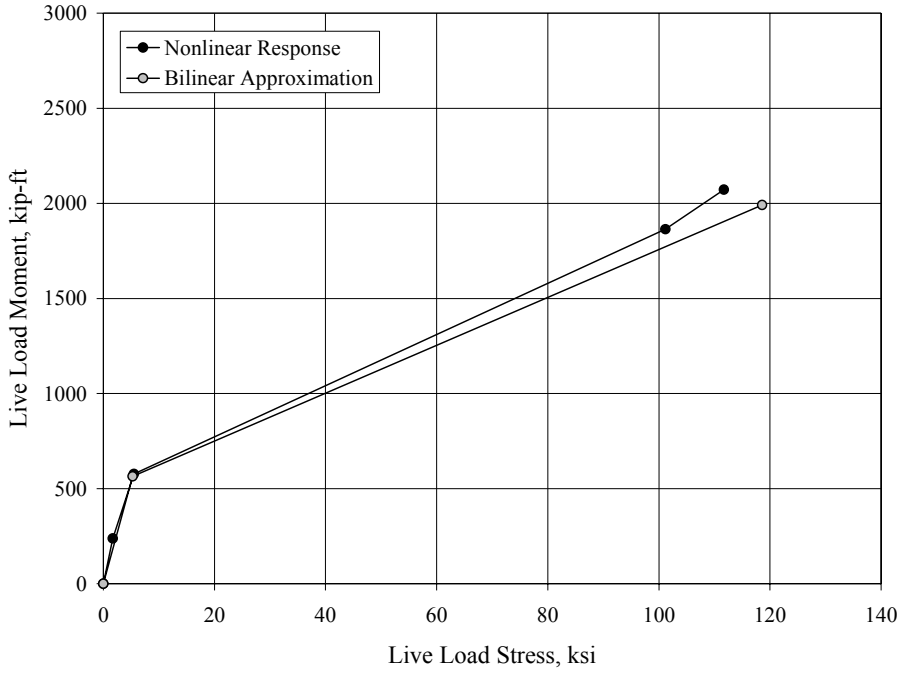

Figure B.15 Idealized Response of Interior Girder, Willis Creek Bridge

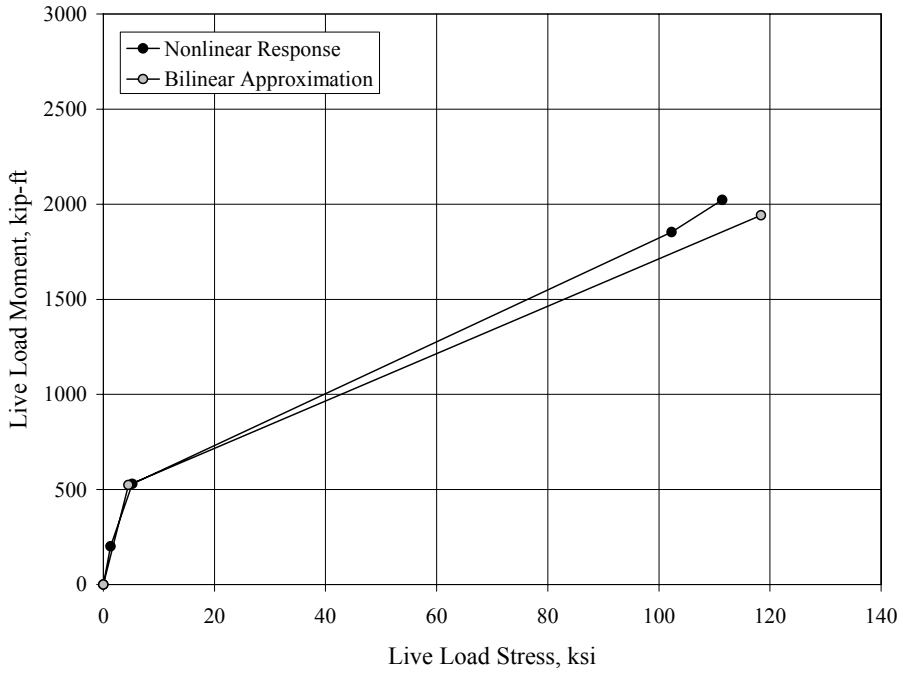

Figure B.16 Idealized Response of Exterior Girder, Willis Creek Bridge

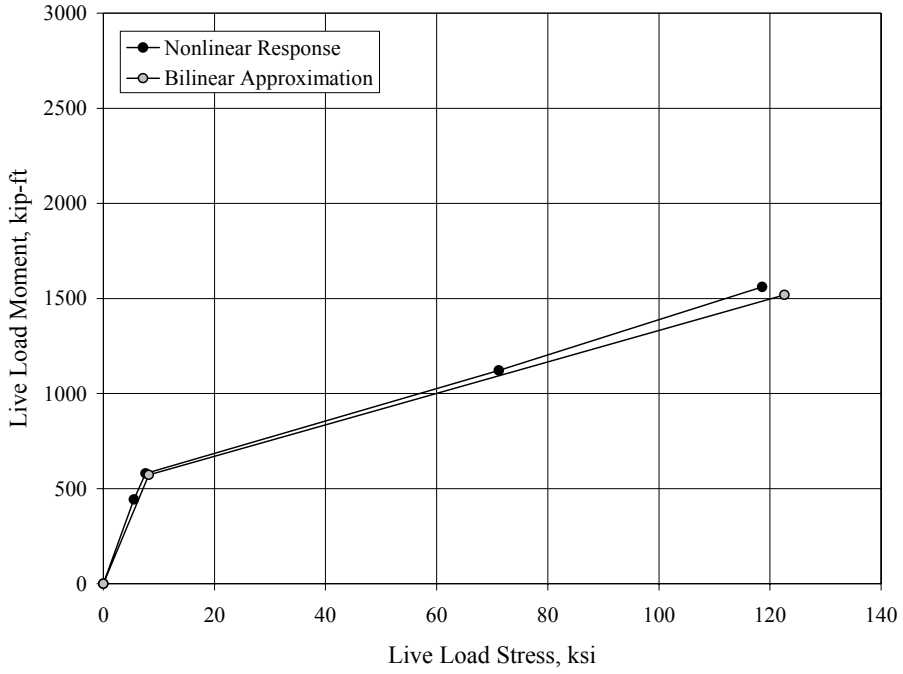

Figure B.17 Idealized Response of Interior Girder, Wimberley Bridge, 40-ft Span

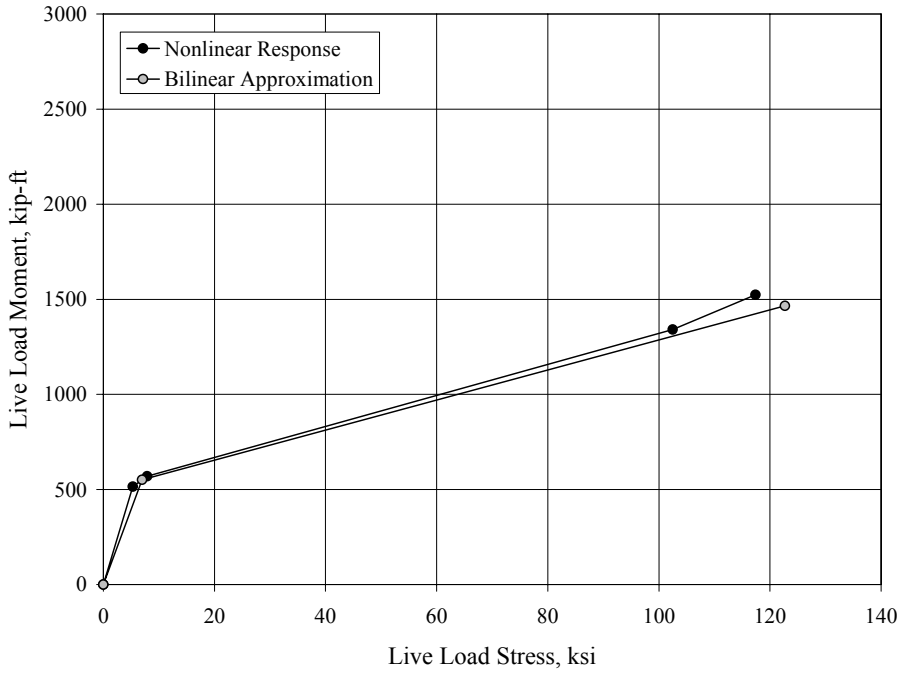

Figure B.18 Idealized Response of Exterior Girder, Wimberley Bridge, 40-ft Span

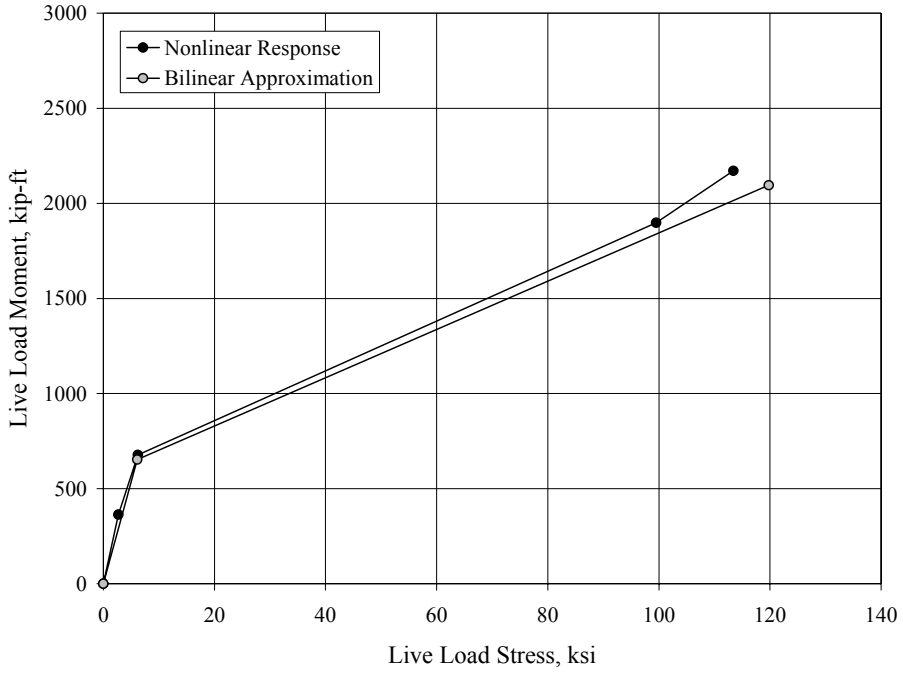

Figure B.19 Idealized Response of Interior Girder, Wimberley Bridge, 60-ft Span

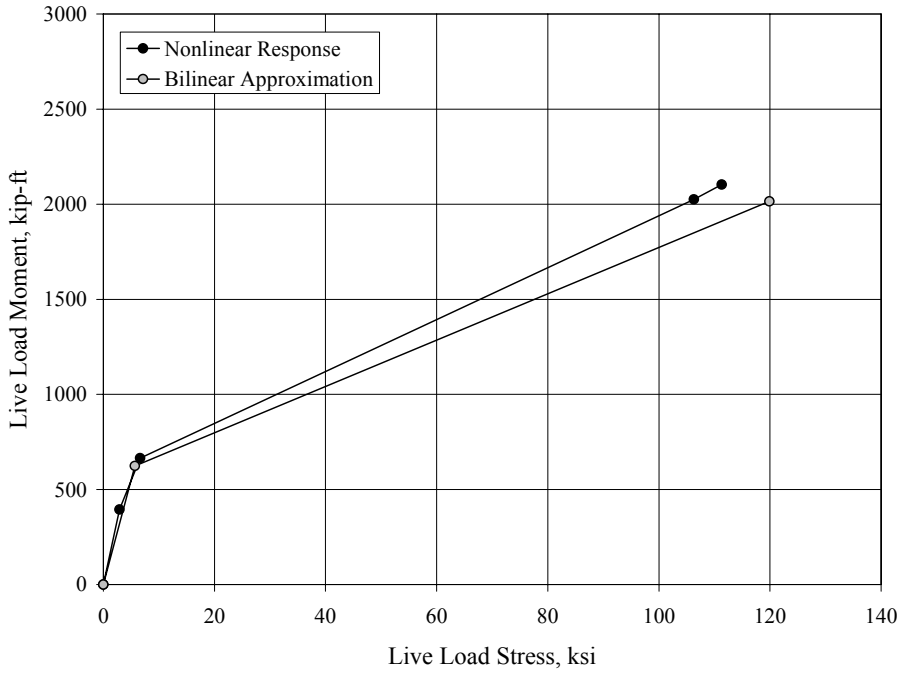

Figure B.20 Idealized Response of Exterior Girder, Wimberley Bridge, 60-ft Span

References

Abeles, P.W., Brown, E.I, II, and Hu, C.H. (1974). "Behavior of Under-Reinforced Prestressed Concrete Beams Subjected to Different Stress Ranges." *Abeles Symposium on Fatigue of Concrete, SP-41, American Concrete Institute,* Detroit, MI, pp. 279-299.

ACI Committee 209 (1992). "Prediction of Creep, Shrinkage, and Temperature Effects in Concrete Structures." American Concrete Institute, Farmington Hills, MI.

ACI Committee 215 (1974). "Considerations for Design of Concrete Structures Subjected to Fatigue Loading." Revised 1992, American Concrete Institute, Farmington Hills, MI.

ACI Committee 318 (2005). "Building Code Requirements for Structural Concrete and Commentary," American Concrete Institute, Farmington Hills, MI.

American Association of State Highway and Transportation Officials (1990). *Guide Specifications for Fatigue Evaluation of Existing Steel Bridges*, with 1995 Interim Revisions. Washington, D.C.

American Association of State Highway and Transportation Officials (2000). *Manual for Condition Evaluation of Bridges,* Second Edition with 2003 Interim Revisions. Washington, D.C.

American Association of State Highway and Transportation Officials (2002). *Standard Specifications for Highway Bridges,* 17th Edition with 2005 Errata. Washington, D.C.

American Association of State Highway and Transportation Officials (2003). *Manual for Condition Evaluation and Load and Resistance Factor Rating (LRFR) of Highway Bridges*, with 2005 Interim Revisions. Washington, D.C.

American Association of State Highway and Transportation Officials (2004). *LRFD Bridge Design Specifications,* Third Edition with 2005 Interim Revisions. Washington, D.C.

Bean, M.J. (2006). "Bending Fatigue Performance of Small-Scale Stay Cables." M.S. Thesis, Department of Civil, Architectural, and Environmental Engineering, University of Texas at Austin.

Collins, M.P. and Mitchell, D. (1997). *Prestressed Concrete Structures*. Response Publications, Toronto, Canada.

Hagenberger, M.J. (2004). "Consideration of Strand Fatigue for Load Rating Prestressed Concrete Bridges." Ph.D. Dissertation, Department of Civil Engineering, University of Texas at Austin.

Hays, Jr., C.O., Consolazio, G.R., Hoit, M.I., and Kakhandiki, A., (1994). "Bridge Rating of Girder – Slab Bridges Using Automated Finite Element Technology," Final Report, Department of Civil Engineering, University of Florida, Gainsville.

Heller, B. (2003). "Fatigue Response of Pretensioned Concrete Beams." M.S. Thesis, Department of Civil Engineering, University of Texas at Austin.

Laman, J.A. and Nowak, A.S. (1996). "Fatigue-Load Models for Girder Bridges." *Journal of Bridge Engineering*, American Society of Civil Engineers, Vol. 122, No. 7, pp. 726-733.

Muller, J.F., and Dux, P.F. (1994). "Fatigue of Prestressed Concrete Beams with Inclined Strands." *Journal of Structural Engineering*, American Society of Civil Engineers, Vol. 120, No. 4, April, 1994, pp. 1122-1139.

Nordby, G.M., and Venuti, W.J. (1957). "Fatigue and Static Tests of Steel Strand Prestressed Beams of Expanded Shale Concrete and Conventional Concrete." *Journal*, American Concrete Institute, August 1957, pp. 141-160.

Overman, T.R. (1984). "Flexural Fatigue Behavior of Pretensioned Concrete Girders." M.S. Thesis, Department of Civil Engineering, University of Texas at Austin.

Ozell, A.M. (1962). "Fatigue Tests of Prestressed Concrete I-Beams with Depressed Strands." Fourth Congress, Federation Internationale de la Precontrainte, pp. 128-135.

Ozell, A.M., and Ardaman, E. (1956). "Fatigue Tests of Pre-Tensioned Prestressed Beams." *Journal*, American Concrete Institute, Vol. 53, pp. 413-424.

Ozell, A.M., and Diniz, J.F. (1958). "Composite Prestressed Concrete Beams under Repetitive Loading." *Journa*l, Prestressed Concrete Institute, Vol. 3, pp. 19-27.

Paulson, C., Frank, K.H., and Breen, J.E. (1983). "A Fatigue Study of Prestressing Strand." Research Report 300-1, Center for Transportation Research, University of Texas at Austin.

Rabbat, B.G., Karr, P.H., Russel, H.G., and Bruce, N.G. (1978). "Fatigue Tests of Full Size Prestressed Girders." Research Report 113, Portland Cement Association, Skokie, IL.

Roller, J.J., Russell, H.G., Bruce, R.N., and Martin, B.T. (1995). "Long-Term Performance of Prestressed, Pretensioned High Strength Concrete Bridge Girders." *Journal*, Precast/Prestressed Concrete Institute, Vol. 40, No. 6, pp. 48-59.

Texas Department of Transportation (2002). "Bridge Inventory, Inspection, and Appraisal Program (BRINSAP) Database."

Wagener, P. (2002). "Load Testing of Prestressed Concrete Girder Bridges in Texas." M.S. Thesis, Department of Civil Engineering, University of Texas at Austin.

Warner, R.F., and Hulsbos, C.L. (1966). "Probable Fatigue Life of Prestressed Concrete Beams." *Journal*, Prestressed Concrete Institute, Vol. 11, No. 2, pp. 16-39.